



DEEP SEATED MAGMATISM, Its sources and plumes

Глубинный магматизм, его источники и плюмы



**IRKUTSK
2014**

*Russian Academy of Sciences
Vinogradov Institute of Geochemistry
Siberian Branch
Russian Foundation of Basic Research*



Deep-seated magmatism, its sources and plumes

(Глубинный магматизм, его источники и плюмы)

PROCEEDING
of XIII International Workshop
«Deep-seated magmatism, its
sources and plumes »

Edited by Dr. N.V. Vladykin

IRKUTSK

2014

Deep-seated magmatism, its sources and plumes

Proceedings of the XIII International Conference. Publishing House of the Institute of Geography SB RAS, 2014, 232 p., Vol.3, ISBN 978-5-94797-198-9

The given book presents the articles of leading scientists studying the problems of the deep-seated magmatism. The geodynamics of Pz-Mz magmatism of the Central Asia, geochemical features of radioactive elements of the Guli complex (Arctic Siberia), deep-seated structure of magmatic systems of Kola alkaline province are considered in the reports. The present issue also discusses the composition of kimberlites and deep-seated xenoliths from them, composition of the low-mantle sources of diamonds, isotope trace-element composition of the primitive mantle, nature of D'' layer, Os isotope systematics of platinum deposits. The articles on melt inclusions of salt (carbonatite) melts and sulfide-silicate immiscibility in the upper mantle are of particular interest.

The book is of great importance for petrologists, geochemists, and specialists studying deep alkaline and kimberlite magmatism, students and teaching staff of Universities.

*Published following the decision of the Scientific Council
of Vinogradov Institute of Geochemistry SB RAS*

Editor: Prof. N.V. Vladykin

*Reviewers: Prof. V.S. Antipin
Original-model: V.I. Andrievska, T.A. Radomska*

Institute of Geography SB RAS
664033, Irkutsk, Ulanbatorskaja str. 1

Published in Glazkovskaya printing House

Irkutsk, Gogol str., 53.

Order № 1283. Edition 100 copies.

ISBN 978-5-94797-198-9

© Institute of Geochemistry SB RAS, 2014

© Irkutsk Geography SB RAS, 2014

TABLE OF CONTENTS

Foreword	4
Chakhmouradian A.R, Cooper M.A, Ball N, Reguir E.P, Medici L, Abdu Y. , Antonov A.A Vladykinite, $\text{Na}_3\text{Sr}_4(\text{Fe}^{2+}\text{Fe}^{3+})\text{Si}_8\text{O}_{24}$: a new complex sheet silicate from peralkaline rocks of the Murun complex, Eastern Siberia, Russia	5
Kogarko L. N. Geochemical features of radioactive elements in ultramafic-alkaline rocks (example –largest in the globe Guli complex)	22
Ryabchikov I. D. and Kaminsky F. V. The Composition of the Lower Mantle: Source of Diamonds with High-Pressure Mineral Inclusions	32
Kostitsyn Yu. A. Trace element composition of primitive Mantle – non-chondrite model	39
Yarmolyuk V.V., Kuzmin M.I., and Kozlovsky A. M. Late paleozoic-early mesozoic within-plate magmatism in North Asia: traps, rifts, giant batholiths, and the geodynamics of their origin	66
Pushkarev Y.D. Fundamental problems of the Earth evolution and the nature of D'' layer as one of them	104
Arzamastsev A. A., Arzamastseva L. V., Zhirova A. M., and Glaznev V. N. Model of formation of the Khibiny-Lovozero orebearing volcanic-plutonic complex	124
Andreeva I.A., Salt (carbonatite) melts of the Bol'shaya Tagna massif, the eastern Sayan region: evidence from melt inclusions	148
Solovova I.P., Girnits A.V., Behavior of F and Cl in agpaitic acid melts	155
Spetsius Z.V., Polyanchko V.V., Xarlamova E.I., Tarskix O.V Ivanov A.S. Geology, petrography and mineralogy of the Zarya pipe kimberlites	160
Sablukov S.M., Sablukova L.I., Stegnitskiy Yu.B., Karpenko M.A Origin of the mantle xenoliths with green garnets from kimberlites (dike Newlands, Southern Africa and Nyurbinskaya pipe, Yakutia)	178
Ashchepkov I.V., Vladykin N.V., Ntaflos T. ,Yudin D.S. , Karpenko M.A. , Palesskiy V.S. , Alymova N.V., Khmel'nikova O.S Deep-seated xenoliths and xenocrysts from Sytykanskaya pipe: evidence for the evolution of the mantle beneath Alakit, Yakutia	203

FOREWORD

Proceedings of the XIII International Conference “Deep-seated magmatism, its sources and plumes” is devoted to the 70th anniversary of the permanent Chairman of the Organizing Committee of the Conference and the chief editor of the Proceedings of the Conference Nikolai V. Vladykin.

N.V. Vladykin is a well-known scientist in the area of geochemistry, petrology and mineralogy of alkaline rocks both in Russia and abroad. After graduating the Mineralogy Department of the Leningrad University in 1966 he started his work at the Institute of Geochemistry, SB RAS, Irkutsk in 1968.

He has been studying geochemistry, mineralogy and ore potential of rare-metal alkaline and granite rocks from a vast area covering Siberia and Mongolia for 50 years. Together with the Academician V.I. Kovalenko he discovered: 1) South-Gobi belt of alkaline rocks; 2) Luningol alkaline complex containing TR deposit in carbonatites; 3) the largest Khan-Bogdo complex of alkaline rocks with large Zr-Nb-TR deposit; 4) new province of carbonatites in Gobi with large TR and Mushugai-Khuduk apatite deposits; 5) ongonite, a new rock variety which is a volcanic analogue of rare-metal Li-F granites. He discovered three new minerals: MONGOLITE, KOVALENKOITE, ARMSTRONGITE, named in honor of the first astronaut N. Armstrong, setting foot on the Moon. In 1978 he defended the candidate thesis entitled “Mineralogical-geochemical features of rare-metal granitoids of Mongolia” which was published as a monograph. Later he studied magmatism, geochemistry and petrology of K-alkaline rocks of Siberia and Aldan shield. He developed a new scheme of magmatism for the whole alkaline Aldan province. He was the first in the former USSR who discovered LAMPROITES and distinguished the Aldan province of lamproites, discovered lamproites in the Eastern Anabar region and Tomtor complex. On the Murun he discovered apatite and synnyrite deposits and gave a new interpretation for the genesis of unique charoite-carbonatite rocks. A prominent contribution into the petrology of alkaline rocks is a complete series of differentiates of potassium alkaline magmatites from ultramafic rocks to alkaline granites discovered by N.V. Vladykin for the Bilibin and Murun complexes. In 1997 he defended the doctor thesis “Petrology and ore potential of K-alkaline complexes of Mongol-Okhotsk magmatic area”. In 2006 Dr. N.V. Vladykin was proposed for the title of the Corresponding Member of RAS.

N.V. Vladykin is an author of over 400 articles and 5 monographs. He is a chief of Russian and International projects. In his laboratory he created the museum – a scientific collection “Alkaline complexes”, which contains samples for over 300 alkaline massifs throughout the world. N. V. Vladykin has joint research grants and publications with scientists from Japan, Canada, Italy, India, UK, Brazil, Iran, Mongolia and Bulgaria. In 2012 the Canadian scientists named a new strontium silicate from the Murun massif as vladykinite. Starting from 2000 he has organized 13 International Conferences “Deep-seated magmatism, its sources and plumes” and published the Proceedings of those conferences in Russian and English, which are reviewed in Canada.

The given book presents the articles of leading scientists studying the problems of the deep-seated magmatism. The geodynamics of Pz-Mz magmatism of the Central Asia, geochemical features of radioactive elements of the Guli complex (Arctic Siberia), deep-seated structure of magmatic systems of Kola alkaline province are considered in the reports. The present issue also discusses the composition of kimberlites and deep-seated xenoliths from them, composition of the low-mantle sources of diamonds, isotope trace-element composition of the primitive mantle, nature of D” layer, Os isotope systematics of platinum deposits. The articles on melt inclusions of salt (carbonatite) melts and sulfide-silicate immiscibility in the upper mantle are of particular interest.

VLADYKINITE, $\text{Na}_3\text{Sr}_4(\text{Fe}^{2+}\text{Fe}^{3+})\text{Si}_8\text{O}_{24}$: A NEW COMPLEX SHEET SILICATE FROM PERALKALINE ROCKS OF THE MURUN COMPLEX, EASTERN SIBERIA, RUSSIA

Chakhmouradian A.R.^{1*}, Cooper M.A.¹, Ball N.¹, Reguir E.P.¹, Medici L.²,
Abdu Y.¹ and Antonov A.A.³

¹ Department of Geological Sciences, University of Manitoba, Winnipeg, MB, R3T 2N2, Canada

² Istituto di Metodologie per l'Analisi Ambientale, Tito Scalo, 85050 Potenza, Italy

³ Centre for Isotopic Research, VSEGEI, 74 Sredniy Prospect, St. Petersburg, 199106, Russia

* Corresponding author; e-mail: chakhmou@cc.umanitoba.ca

Vladykinite, ideally $\text{Na}_3\text{Sr}_4(\text{Fe}^{2+}\text{Fe}^{3+})\text{Si}_8\text{O}_{24}$, is a new complex sheet silicate occurring as abundant prismatic crystals in a dike of coarse-grained peralkaline feldspathoid syenite in the north-central part of the Murun complex in eastern Siberia, Russia (Lat. $58^\circ 22' 48''$ N; Long. $119^\circ 03' 44''$ E). The new mineral is an early magmatic phase associated with aegirine, potassium feldspar, eudialyte, lamprophyllite and nepheline; strontianite (as pseudomorphs after vladykinite) and K-rich vishnevite are found in the same assemblage, but represent products of late hydrothermal reworking. Vladykinite is brittle, has a Mohs hardness of 5 and distinct cleavage on {100}. In thin section, it is colorless, biaxial negative [$\alpha = 1.624(2)$, $\beta = 1.652(2)$, $\gamma = 1.657(2)$, $2V_{\text{meas}} = 44(1)^\circ$, $2V_{\text{calc}} = 45(1)^\circ$] and shows an optic orientation consistent with its structural characteristics ($\mathbf{X}^{\wedge}\mathbf{a} = 5.1^\circ$ in β obtuse, $\mathbf{Z}^{\wedge}\mathbf{c} = 4.7^\circ$ in β acute, $\mathbf{Y} = \mathbf{b}$). The Raman spectrum of vladykinite consists of the following vibration modes (listed in order of decreasing intensity): 401, 203, 465, 991, 968, 915, 348, 167, 129, 264, 1039 and 681 cm^{-1} ; O-H signals were not detected. The Mössbauer spectrum indicates that both Fe^{2+} and Fe^{3+} are present in the mineral ($\text{Fe}^{3+}/\text{Fe}_{\Sigma} = 0.47$), and that both cations occur in a tetrahedral coordination. The mean chemical composition of vladykinite (acquired by wavelength-dispersive X-ray spectrometry and laser-ablation inductively-coupled-plasma mass-spectrometry), with Fe_{Σ} recast into Fe^{2+} and Fe^{3+} in accord with the Mössbauer data, gives the following empirical formula calculated to 24 oxygen atoms: $(\text{Na}_{2.45}\text{Ca}_{0.56})_{\Sigma 3.01}(\text{Sr}_{3.81}\text{K}_{0.04}\text{Ba}_{0.02}\text{La}_{0.02}\text{Ce}_{0.01})_{\Sigma 3.90}(\text{Fe}^{2+}_{0.75}\text{Fe}^{3+}_{0.66}\text{Mn}_{0.26}\text{Zn}_{0.16}\text{Al}_{0.12}\text{Mg}_{0.05}\text{Ti}_{0.01})_{\Sigma 2.01}(\text{Si}_{7.81}\text{Al}_{0.19})_{\Sigma 8.00}\text{O}_{24}$. The mineral is monoclinic, space group $P2_1/c$, $a = 5.21381(13)$, $b = 7.9143(2)$, $c = 26.0888(7)\text{ \AA}$, $\beta = 90.3556(7)^\circ$, $V = 1076.50(5)\text{ \AA}^3$, $Z = 2$. The ten strongest lines in the powder X-ray diffraction pattern are [d_{obs} in \AA (hkl)]: 2.957 (100) ($\bar{1}23$, 123); 2.826 (100) ($\bar{1}17$, 117); 3.612 (58) ($\bar{1}14$, 114); 3.146 (37) (120); 2.470 (32) (210, 01.10); 4.290 (30) ($\bar{1}11$, 111); 3.339 (30) ($\bar{1}06$, 115, 106); 2.604 (28) (200); 2.437 (25) (034); 1.785 (25) (21.10, $\bar{2}34$). The structure of vladykinite, refined by single-crystal techniques on the basis of 3032 reflections with $F_o > 4\sigma F_o$ to $R_1 = 1.6\%$, consists of tetrahedral sheets parallel to (100) and consisting of $(\text{Si}_8\text{O}_{24})^{16-}$ units incorporating four-membered silicate rings and joined into five- and eight-membered rings by sharing vertices with larger tetrahedra hosting Fe^{2+} , Fe^{3+} , Mn, Zn, Al, Mg and Ti. Larger cations (predominantly Na, Sr and Ca) are

accommodated in octahedral and square-antiprismatic interlayer sites sandwiched between the tetrahedral sheets. Structural relations between vladkyinite and other sheet silicates incorporating four-, five- and eight-membered rings are discussed. The name vladkyinite is in honor of Nikolay V. Vladykin (Vinogradov Institute of Geochemistry, Russia), in recognition of his contribution to the study of alkaline rocks. Holotype and cotype specimens of the mineral were deposited in the Robert B. Ferguson Museum of Mineralogy in Winnipeg, Canada.

Keywords: *Vladkyinite, new mineral, sheet silicate, peralkaline rocks, Murun complex, Yakutia, Russia*

INTRODUCTION

Potassic peralkaline syenites (wt.% $K_2O > wt.\% Na_2O$; mol.% $Na_2O+K_2O > mol.\% Al_2O_3$) are an uncommon type of igneous rocks that, in extreme cases, contain an appreciable proportion of kalsilite ($KAlSiO_4$) or leucite (typically replaced by kalsilite-orthoclase intergrowths). Notable examples of these rocks occur in the Murun, Synnyr, Yaksha and Yuzhnosakunsky alkaline complexes in eastern Siberia, and at Khibiny in Kola Peninsula, Russia [10; 1; 14]. These syenites, their associated metasomatites and pegmatites host a plethora of exotic accessory minerals enriched in K, Sr or Ba, which are exceedingly rare or unknown in other rock types. For example, out of some 160 minerals reported from the Murun complex, fifty-seven contain essential K, Ba or Sr, including several species so far endemic to this locality (for details and bibliography, see Appendix 1, online). It is important to note here that most of these exotic minerals are not at all rare at Murun and locally gain the status of rock-forming constituents; a good understanding of their crystal chemistry and paragenetic relations is thus essential to the understanding of the petrogenesis of their host rocks.

In her study of peralkaline syenitic dikes from the Murun complex, Reguir [17] briefly described a previously unknown Na-Fe-Sr silicate (pp. 162-163), but the dearth of available material precluded its detailed examination. Complete characterization of this mineral became possible only when additional samples were provided to us by Professor Nikolay V. Vladykin (Vinogradov Institute of Geochemistry in Irkutsk, Russia), who had also recognized this silicate as a potential new species. The new mineral and its name have been approved by the Commission on New Minerals, Nomenclature and Classification of the International Mineralogical Association (IMA 2011-052). The name vladkyinite (владыкинит) was chosen in honor of Nikolay V. Vladykin, in recognition of his contribution to the geochemistry, petrology and mineralogy of alkaline rocks, including the Murun complex [19.20.21.12.13.22]. Holotype and cotype specimens (unmounted and epoxy-mounted grains, polished thin sections and the crystal used for structure refinement) were deposited in the Robert B. Ferguson Museum of Mineralogy at the University of Manitoba (Winnipeg, Canada) under catalogue number M7853.

GEOLOGICAL PROVENANCE AND PARAGENESIS

The Murun alkaline complex is a large (~60 km²) composite pluton of Cretaceous age emplaced in Archean high-grade metamorphic rocks and Neoproterozoic clastic and carbonate sedimentary rocks [10, 9]. The complex comprises a wide variety of igneous, metasomatic and hydrothermal rocks, but the most volumetrically significant are alkali-rich ultramafites, feldspathoid and quartz syenites, and their extrusive analogues (phonolites, trachytes, leucitites). Murun is known widely as the type locality of the purple gemstone charoite (Evdokimov 1995) and several other compositionally and structurally unusual minerals (Appendix 1, online).

Vladykinite was identified in a dike of coarse-grained mesocratic feldspathoid syenite (lujavrite) at Mt. Maly Murun in the north-central part of the complex. Geographically, Maly Murun is situated in southwestern Yakutia near its administrative border with the Irkutsk Region (Lat. 58° 22' 48" N; Long. 119° 03' 44" E). The host dike, measuring ~2-3 m in width and 20 m in length, comprises aegirine, potassium feldspar, K-Sr-bearing eudialyte, vladykinite, lamprophyllite, nepheline, strontianite and K-rich vishnevite, listed approximately in order of decreasing modal abundance (for formulae, see Appendix 1, online). Note that the cancrinite-group phase tentatively identified here as vishnevite is stoichiometrically close to pitiglianoite, Na₆K₂Si₆Al₆O₂₄(SO₄)·2H₂O; the two minerals can be distinguished only on the basis of structural data [15], which are currently unavailable. In the Maly Murun lujavrite, vladykinite is relatively abundant, locally composing up to 5 % of its volume. The mineral occurs as pointed prismatic crystals of brown color with a rhombic to pseudo-hexagonal cross-section perpendicular to the length, as well as parallel and radiating clusters of such crystals (fig. 1a). The size of individual grains does not exceed a few mm in length and 0.5 mm in width. In hand-specimen, vladykinite resembles acicular titanite common in feldspathoid syenites (but uncommon in their peralkaline varieties); the two minerals, however, differ in their optical properties (see below). The majority of crystals are partially or completely pseudomorphed by strontianite (fig. 1b).

PHYSICAL AND OPTICAL PROPERTIES

The new mineral is macroscopically pinkish to grayish brown, with a vitreous luster and a white streak. It is brittle, has a Mohs hardness of 5 and a distinct cleavage on {100}. The specific gravity of vladykinite could not be measured, but

¹ Deposit item AM-14-109, Appendix, CIF, and Data. Deposit items are stored on the MSA web site and available via the *American Mineralogist* Table of Contents. Find the article in the table of contents at GSW (ammin.geoscienceworld.org) or MSA (www.minsocam.org), and then click on the deposit link.

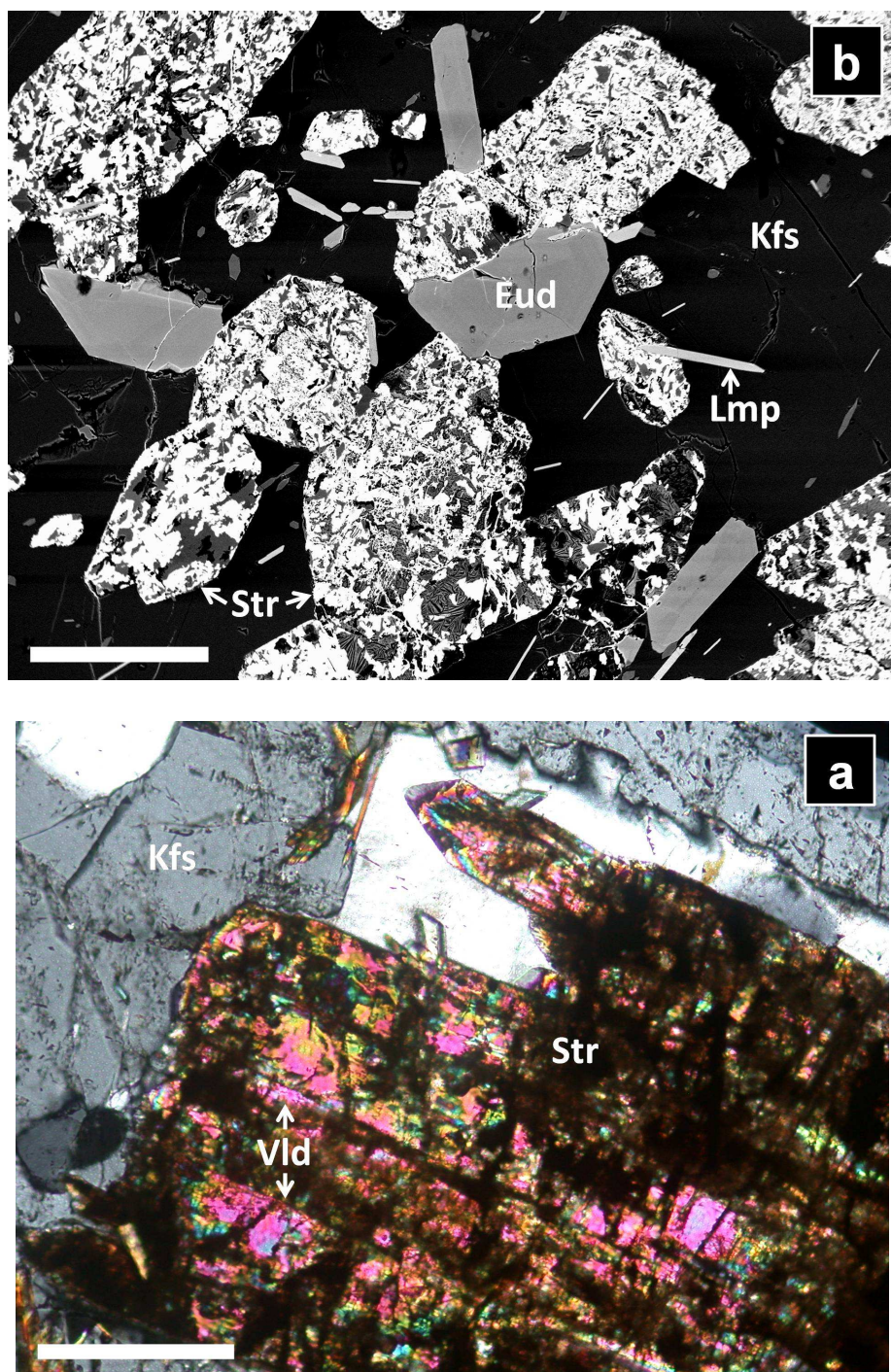


Fig. 1. (a) Prismatic crystals of vladynite (Vld) showing turbid areas of partial replacement by strontianite (Str); the matrix is predominantly potassium feldspar (Kfs); cross-polarized light. (b) Pseudomorphs of strontianite (Str) after vladynite associated with eudalyte (Eud) and lamprophyllite (Lmp); back-scattered-electron image.

Scale bar is 0.2 mm for both images.

is greater than that of di-iodomethane (3.22). The density, calculated on the basis of the chemical and crystallographic data (see below), is 3.51 g/cm^3 . In thin

section, the mineral is colorless, non-pleochroic, and shows a moderate positive relief. The optical properties, determined with a spindle stage, are as follows: $\alpha = 1.624(2)$, $\beta = 1.652(2)$, $\gamma = 1.657(2)$, $2V_{\text{meas}} = 44(1)^\circ$, $2V_{\text{calc}} = 45(1)^\circ$. Vladykinite

is biaxial negative and shows the following optic orientation: $X^a = 5.1^\circ$ (β obtuse), $Z^c = 4.7^\circ$ (β acute), $Y = b$. Based on these properties, vladykinite can be readily distinguished from titanite, which has a much higher relief and birefringence, larger extinction angle ($Z^c \approx 50^\circ$), is pleochroic and biaxial positive [4]. The calculated Gladstone-Dale compatibility index is 0.023 (excellent).

The micro-Raman spectrum, measured on the grain subsequently used for single-crystal analysis (fig. 2), is complex and consists of lattice vibrations in the 100-350 cm^{-1} range and a series of Si-O and Fe-O modes between 400 and 1100 cm^{-1} . Because O-H stretching vibrations (3300-3600 cm^{-1}) were not observed, the presence of structural water or hydroxyl groups in this mineral can be conclusively ruled out.

MÖSSBAUER SPECTROSCOPY

Because Fe was identified as one of the major components in energy-dispersive X-ray spectra of vladykinite, the structural state of Fe was investigated using Mössbauer spectroscopy. The measurements were done at room temperature with a $^{57}\text{Co}(\text{Rh})$ point source, using an Fe foil for the spectrometer calibration. The ^{57}Fe Mössbauer spectrum, collected from several grains extracted from the holotype sample, indicates the presence of two active species, Fe^{2+} (solid line subspectrum in fig. 3) and Fe^{3+} (dashed line). Consequently, the spectrum was fitted using a Voigt-based quadrupole-splitting distribution method to a model based on two species, each represented by a single Gaussian component. The refined parameters for the center shift (CS) relative to $\alpha\text{-Fe}$ at room temperature, and the quadrupole splitting (QS) are as follows: CS = 1.01(1) mm/s, QS = 2.77(3) mm/s for Fe^{2+} ; and CS = 0.23(7) mm/s, QS = 0.87(9) mm/s for Fe^{3+} . The CS values indicate that both Fe^{2+} and Fe^{3+} occur in a tetrahedral coordination. Assuming equal recoil-free fractions for both species, the calculated $\text{Fe}^{3+}/\text{Fe}_\Sigma$ ratio is 0.47(5).

CHEMICAL COMPOSITION

The chemical composition of vladykinite was initially determined by wavelength-dispersive X-ray spectrometry (WDS) using a CAMECA SX 100 fully automated electron-microprobe operated at an accelerating voltage of 15 kV and a beam current of 10 nA. Several crystals were analyzed with a 10- μm beam and found to show little compositional variation (table 1). The following standards were employed for the analysis: albite (Na), andalusite (Al), diopside (Ca, Si), fayalite (Fe), forsterite (Mg), gahnite (Zn), orthoclase (K), spessartine (Mn), titanite (Ti), synthetic SrTiO_3 (Sr), LaPO_4 (La) and CePO_4 (Ce). In addition, F, Cl,

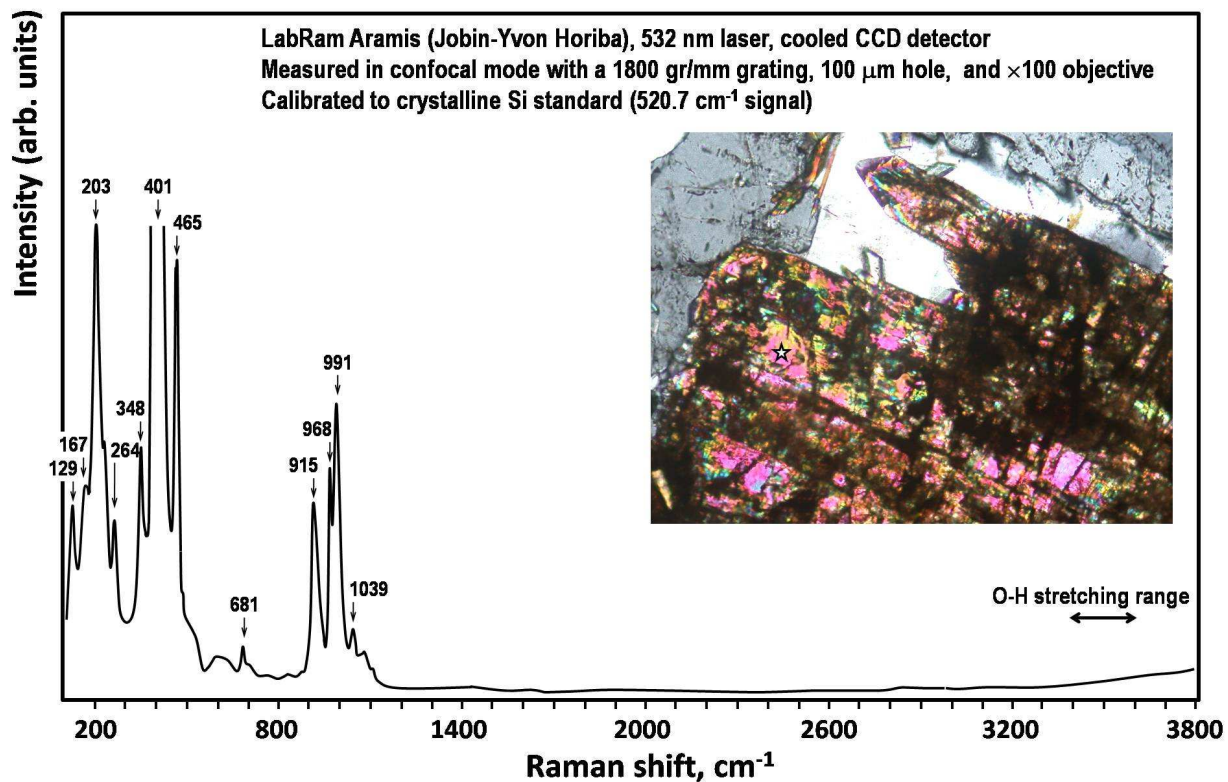


Fig. 2. Raman spectrum of vladykinite (analysis spot indicated by a star in the inset).

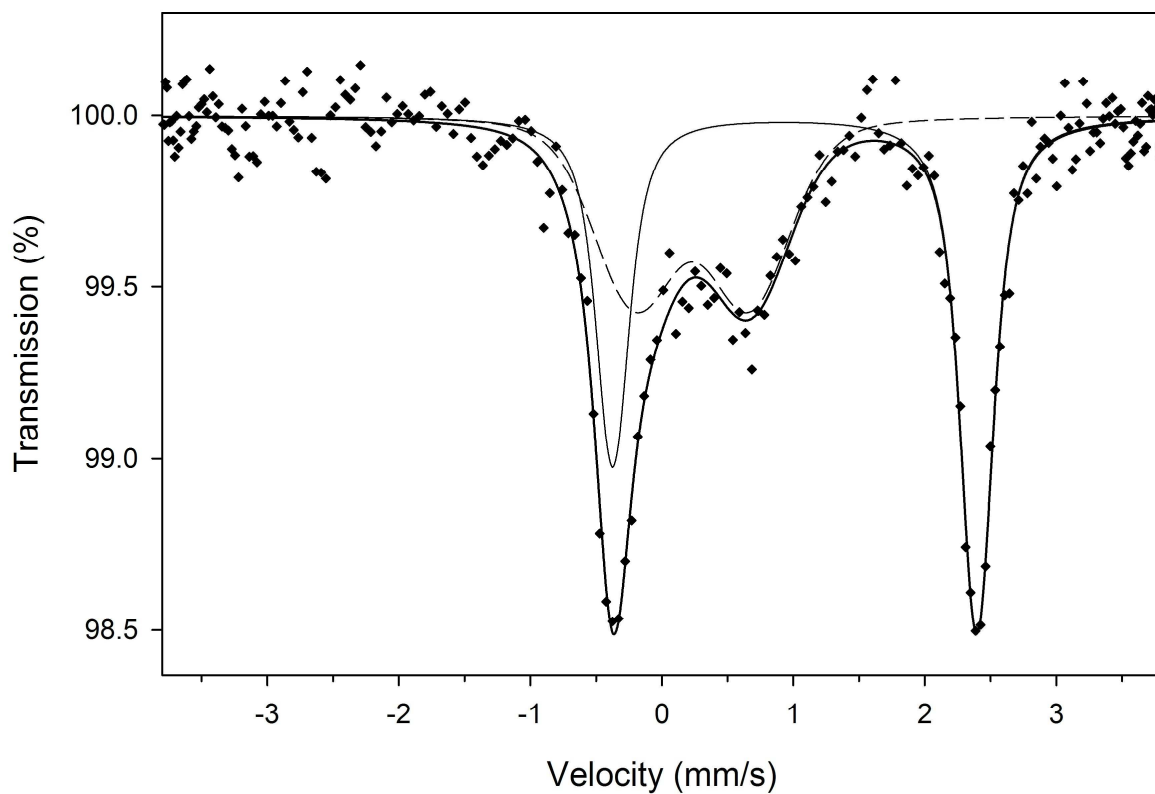


Fig.3. ^{57}Fe Mössbauer spectrum of vladykinite.

Table 1.

Mean chemical composition of vladkyinite.

Oxide*	wt.%	range	ESD
Na ₂ O	6.74	6.41-7.18	0.21
MgO	0.14	0.13-0.15	0.01
Al ₂ O ₃	1.38	1.21-1.70	0.15
SiO ₂	41.66	41.03-42.32	0.39
K ₂ O	0.16	0.15-0.17	0.01
CaO	2.77	2.58-2.96	0.09
TiO ₂	0.10	0.07-0.14	0.02
MnO	1.60	1.41-1.72	0.10
FeO _T [#]	8.98	8.64-9.29	0.19
ZnO	1.33	1.06-1.75	0.25
SrO	34.99	34.28-35.92	0.47
La ₂ O ₃	0.22	0.11-0.33	0.08
Ce ₂ O ₃	0.16	0-0.34	0.09
Total	98.90		
Element‡	ppm	range	ESD
Mg	1010	903-1220	122
Sc	0.52		0.08
Mn	12683	11217-14005	1143
Co	29	28-32	2
Zn	9515	7899-11818	1581
Y	1.02	0.93-1.11	0.07
Ba	1838	1402-2194	312
La	2776	1949-3553	761
Ce	1709	1138-2361	575
Pr	74	44-108	28
Nd	101	58-148	41
Sm	2.4	1.4-3.9	0.9
Eu	0.37	0.17-0.60	0.14
Gd	48	32-65	14
Pb	12.9	11.8-14.2	0.9
Th	22	6-37	12
U	0.27	0.04-0.90	0.32

*Based on 16 WDS analyses.

[#]Based on the Mössbauer data, FeO_T should be recast into FeO (4.76 wt. %) and Fe₂O₃ (4.69 wt. %).

[‡]Based on six LA-ICP-MS analyses.

Cr, Y, Zr, Nb, Ba, Pr, Nd, Sm, Ta and Th were sought, but found not to be present at levels detectable by WDS.

Vladykinite was also analyzed by laser-ablation inductively-coupled-plasma mass-spectrometry (LA-ICP-MS) using a 213-nm Nd-YAG Merchantek laser connected to a Thermo Finnigan Element 2 sector-field mass-spectrometer. All measurements were performed using a beam size of 30 μm , laser-energy density of ca. 5.45 J/cm^2 and repetition rate of 10 Hz. Ablation was done in Ar and He atmospheres, and the rate of oxide production was monitored during instrument tuning by measuring the ThO/Th ratio and kept below 0.2 %. Synthetic glass standard NIST SRM 610 was employed for calibration and quality control. After taking into account potential spectral overlaps and molecular interferences, the following isotopes were chosen for analysis: ^{25}Mg , ^{29}Si , ^{45}Sc , ^{51}V , ^{55}Mn , ^{59}Co , ^{60}Ni , ^{66}Zn , ^{85}Rb , ^{89}Y , ^{90}Zr , ^{93}Nb , ^{137}Ba , ^{139}La , ^{140}Ce , ^{141}Pr , ^{146}Nd , ^{147}Sm , ^{151}Eu , ^{155}Gd , ^{159}Tb , ^{163}Dy , ^{165}Ho , ^{166}Er , ^{169}Tm , ^{172}Yb , ^{175}Lu , ^{178}Hf , ^{181}Ta , ^{208}Pb , ^{232}Th , ^{238}U . All analyses were performed in a low-resolution mode (~ 300) using Pt skimmer and sample cones. Data reduction was carried out online using the GLITTER software [8]. The Si concentrations determined by WDS show the least variation around the mean value (table 1) and were chosen as an internal standard for all analyses. The quality control was achieved by keeping the fractionation at less than 10% and fractionation/error ratio at < 3 . The following elements were not detectable by LA-ICP-MS (their approximate lower detection limits in ppm are given in parentheses): Ni (2), Rb (0.6), Zr (0.5), Nb (0.5), Tb (0.1), Dy (0.2), Ho (0.05), Er (0.2), Tm (0.05), Yb (0.2), Lu (0.05), Hf (0.1), Ta (0.05). For those elements that were quantified by both WDS and LA-ICP-MS, their measured values are within the estimated standard deviation of each other (see Mg, Mn, Zn, La and Ce in table 1).

The mean chemical analysis of vladykinite, based on WDS (Na, Al, Si, Ca, Ti, Fe and Sr) and LA-ICP-MS (Mg, Mn, Zn, La, Ce, Pr, Nd, Ba) data, with Fe_Σ recast into Fe^{2+} and Fe^{3+} in accord with the Mössbauer data (4.76 wt. % FeO and 4.69 wt. % Fe_2O_3), gives the following empirical formula calculated to 24 oxygen atoms: $(\text{Na}_{2.451}\text{Ca}_{0.557})_{\Sigma 3.008}(\text{Sr}_{3.805}\text{K}_{0.038}\text{Ba}_{0.015}\text{La}_{0.023}\text{Ce}_{0.014}\text{Pr}_{0.001}\text{Nd}_{0.001})_{\Sigma 3.897}(\text{Fe}^{2+}_{0.746}\text{Fe}^{3+}_{0.662}\text{Mn}_{0.260}\text{Zn}_{0.164}\text{Al}_{0.118}\text{Mg}_{0.047}\text{Ti}_{0.014})_{\Sigma 2.011}(\text{Si}_{7.813}\text{Al}_{0.187})_{\Sigma 8.000}\text{O}_{24}$. From crystal-chemical considerations (see **CRYSTAL STRUCTURE**), two alternative end-member formulae can be proposed for vladykinite: $\text{Na}_3\text{Sr}_4(\text{Fe}^{2+}\text{Fe}^{3+})\text{Si}_8\text{O}_{24}$ or $(\text{Na}_2\text{Ca})\text{Sr}_4\text{Fe}^{2+}_2\text{Si}_8\text{O}_{24}$. These two expressions differ in the content of the Na and Fe sites and are related to each other via the coupled substitution $\text{Na}^+ + \text{Fe}^{3+} \Leftrightarrow \text{Ca}^{2+} + \text{Fe}^{2+}$. Because the trivalent-cation content in the Fe site (0.78 atoms per formula unit, apfu) is significantly in excess of the Ca content in the Na sites (0.56 apfu), we give preference to the idealized formula $\text{Na}_3\text{Sr}_4(\text{Fe}^{2+}\text{Fe}^{3+})\text{Si}_8\text{O}_{24}$.

CRYSTAL STRUCTURE

Single-crystal data were acquired with a Bruker D8 three-circle diffractometer equipped with a rotating anode generator ($\text{MoK}\alpha$ radiation), multi-layer optics incident beam path and an APEX-II charge-coupled-device (CCD) detector. A

sphere of X-ray diffraction data was collected to $2\theta = 60^\circ$ at 5 s per 0.2° frame and a crystal-to-detector distance of 5 cm. The unit-cell parameters were obtained by least-squares refinement of 9873 reflections with $I > 10\sigma I$. Of 25682 total reflections, there are 11807 individual reflections within the Ewald sphere, including 3159 unique data; the Laue-merging R value is 1.5% in $2/m$. Systematically absent reflections are consistent with the space group $P2_1/c$. The structure of vladyskinite was refined on the basis of 3032 reflections with $F_o > 4\sigma F_o$ to $R_1 = 1.6\%$ (for a fully anisotropic model). The refined unit-cell parameters are: $a = 5.21381(13)$, $b = 7.9143(2)$, $c = 26.0888(7)$ Å, $\beta = 90.3556(7)^\circ$, $V = 1076.50(5)$ Å³, $Z = 2$. Although the departure in β from 90° is small, the Laue-merging R value of 24% for mmm shows that the X-ray intensity data are inconsistent with orthorhombic symmetry (see DISCUSSION).

The crystal structure of vladyskinite consists of complex tetrahedral sheets parallel to (100) and consisting of $(\text{Si}_8\text{O}_{24})^{16-}$ units incorporating four-membered silicate rings joined into five- and eight-membered rings by sharing vertices with larger tetrahedra hosting Fe, Mn, Zn, Al and Mg. The overall topology of the sheet can be formulated as $4^15^48^1$. Larger cations (predominantly Na, Sr and Ca) are accommodated in a variety of interlayer sites sandwiched between the tetrahedral

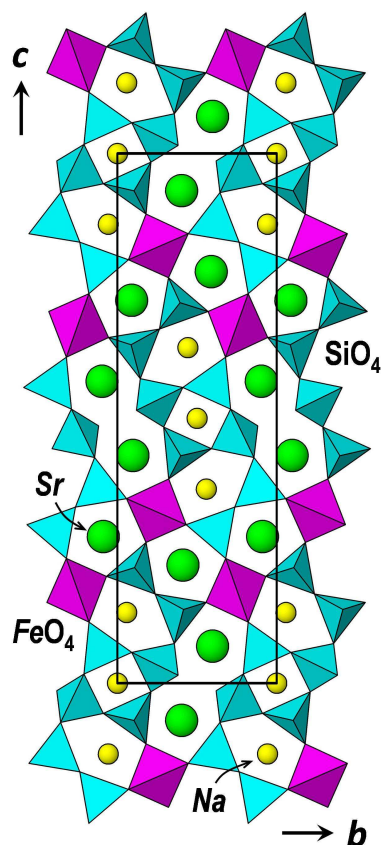


Fig. 4. The crystal structure of vladyskinite viewed perpendicular to (100), showing complex sheets of SiO_4 and $(\text{Fe,Mn,Zn,Al})\text{O}_4$ tetrahedra (FeO_4) and locations of Na and Sr sites. The unit cell is outlined. (Color online.)

sheets (fig. 4; table 2). The two Na sites are both dominated by Na atoms in a distorted octahedral coordination, with $\langle \text{Na} - \text{O} \rangle$ distances of 2.453 and 2.535 Å, respectively (table 3). A site-occupancy refinement revealed that all Ca (0.56 apfu) is ordered in the Na2 site (table 4). There are also two Sr sites that are both dominated by Sr atoms and coordinated by eight O atoms in a square-antiprismatic arrangement with $\langle \text{Sr} - \text{O} \rangle$ distances of 2.634 and 2.624 Å, respectively (table 3). There is a slight deficit in scattering at the Sr_2 site relative to 100% Sr occupancy, which most likely stems from the presence of K and vacancies in this site (table 4). There are four unique Si tetrahedra with $\langle \text{Si} - \text{O} \rangle$ distances ranging from 1.625 to 1.634 Å; both site scattering and $\langle \text{Si} - \text{O} \rangle$ distances suggest that the Si sites are occupied primarily by Si. A single larger tetrahedron ($\langle \text{Fe} - \text{O} \rangle = 1.941$ Å) has a refined site scattering of

Table 2.

The crystal structure of vladyskinite: atomic coordinates and displacement parameters

Site	<i>x</i>	<i>y</i>	<i>z</i>	U_{eq} , Å ²
Na ₁	1/2	1/2	1/2	0.0278(3)
Na ₂	0.48483(11)	0.44221(9)	0.63351(2)	0.0210(2)
Sr ₁	0.49578(3)	0.90294(2)	0.57005(1)	0.01107(5)
Sr ₂	0.50609(3)	0.58890(2)	0.77700(1)	0.01184(6)
Fe	0.00453(5)	0.75589(3)	0.67545(1)	0.01134(9)
Si ₁	0.94527(9)	0.39083(6)	0.71424(2)	0.01073(9)
Si ₂	0.95867(8)	0.10612(6)	0.63401(2)	0.01018(9)
Si ₃	0.05166(8)	0.23197(6)	0.53139(2)	0.00944(9)
Si ₄	0.02973(8)	0.60042(5)	0.56752(2)	0.00895(8)
O ₁	0.2495(2)	0.39304(17)	0.71818(5)	0.0175(3)
O ₂	0.8052(2)	0.56879(16)	0.70091(5)	0.0180(2)
O ₃	0.7963(2)	0.32075(17)	0.76480(5)	0.0170(2)
O ₄	0.8411(2)	0.26336(17)	0.66773(5)	0.0169(2)
O ₅	0.7412(2)	0.58495(19)	0.86101(5)	0.0209(2)
O ₆	0.7921(2)	-0.05618(16)	0.65173(5)	0.0161(2)
O ₇	0.8648(2)	0.14346(16)	0.57432(4)	0.0138(2)
O ₈	0.2852(2)	0.11891(16)	0.51492(5)	0.0155(2)
O ₉	0.1552(2)	0.41060(14)	0.55787(5)	0.0131(2)
O ₁₀	0.1358(2)	0.71048(16)	0.51702(4)	0.0131(2)
O ₁₁	0.7275(2)	0.60334(15)	0.57060(5)	0.0140(2)
O ₁₂	0.1881(2)	0.67881(16)	0.61515(5)	0.0145(2)

Table 3.

Selected bond distances (Å) in the crystal structure of vladyskinite; mean distances for ferraonordite-(Ce) are provided for comparison

2 × Na1 – O9	2.4589(12)	Na2 – O1	2.5634(14)
2 × Na1 – O10	2.5666(12)	Na2 – O2	2.6172(15)
2 × Na1 – O11	2.3326(12)	Na2 – O4	2.4962(14)
		Na2 – O9	2.6208(13)
		Na2 – O11	2.4384(14)
		Na2 – O12	2.4738(14)
<Na1 – O>	2.453	<Na2 – O>	2.535
Sr1 – O5	2.6200(13)	Sr2 – O1	2.5540(13)
Sr1 – O6	2.6443(13)	Sr2 – O1	2.7262(13)
Sr1 – O7	2.7082(12)	Sr2 – O2	2.5371(13)
Sr1 – O8	2.4852(12)	Sr2 – O3	2.6271(13)
Sr1 – O8	2.5060(12)	Sr2 – O3	2.6497(13)
Sr1 – O10	2.7792(12)	Sr2 – O4	2.7010(13)
Sr1 – O11	2.6611(12)	Sr2 – O5	2.5049(13)
Sr1 – O12	2.6697(13)	Sr2 – O6	2.6887(13)

Table 3. (contd)

<Sr1 – O>	2.634	<Sr2 – O>	2.624
Si1 – O1	1.5887(13)	Si2 – O4	1.6447(13)
Si1 – O2	1.6231(14)	Si2 – O5	1.5781(13)
Si1 – O3	1.6320(13)	Si2 – O6	1.6194(14)
Si1 – O4	1.6662(13)	Si2 – O7	1.6563(12)
<Si1 – O>	1.628	<Si2 – O>	1.625
Si3 – O7	1.6455(12)	Si4 – O9	1.6583(12)
Si3 – O8	1.5729(13)	Si4 – O10	1.6763(12)
Si3 – O9	1.6620(13)	Si4 – O11	1.5786(13)
Si3 – O10	1.6562(12)	Si4 – O12	1.6118(12)
<Si3 – O>	1.634	<Si4 – O>	1.631
Fe – O2	1.9293(14)		
Fe – O3	1.9368(13)		
Fe – O6	1.9527(13)		
Fe – O12	1.9447(12)		
<Fe – O>	1.941		
Ferronordite-(Ce), Pushcharovsky et al. (1999):			
<Na1 – O>	2.419	<Na2 – O>	2.527
<Sr – O>	2.629	<REE – O>	2.546
<Si1 – O>	1.634	<Si1 – O>	1.629
<Si3 – O>	1.639	<Fe – O>	1.981

Table 4.

Calculated cation-site occupancies in the crystal structure of vladyskinite

Site	Occupancy (from WDS and LA-ICP-MS)	Scattering, epfu calculated	Scattering, epfu observed, SCSR*
Na1	Na	11	11
Na2	Na _{1.45} Ca _{0.56}	27.2	27.90(9)
Sr1	Sr ₂	76	76
Sr2	Sr _{1.84} K _{0.04} La _{0.02} Ce _{0.01} [] _{0.10}	72.4	70.46(8)
Fe	Fe ²⁺ _{0.75} Fe ³⁺ _{0.66} Mn _{0.26} Zn _{0.16} Al _{0.12} Mg _{0.05} Ti _{0.01}	50.3	47.59(8)

47.59(8) electrons per formula unit (epfu), in reasonable agreement with the assignment of all Fe + Mn + Zn + Mg + Ti, and some of the Al from the chemical analysis to this site (table 4). The <Fe – O> distance calculated assuming the Fe²⁺/Fe³⁺ ratio obtained from the Mössbauer analysis is 1.952 Å SCSR = single-crystal structure refinement.(i.e., 0.572 + 1.38 Å), which is also in agreement with the observed <Fe – O> distance of 1.941 Å. The Fe tetrahedron

is thus occupied by ~60% divalent cations (predominantly Fe²⁺) and 40% trivalent cations (mostly Fe³⁺), providing further support for the proposed end-member formula (see above).

The crystal structure of vladyskinite consists of complex tetrahedral sheets parallel to (100) and consisting of (Si₈O₂₄)¹⁶⁻ units incorporating four-membered silicate rings joined into five- and eight-membered rings by sharing vertices with larger tetrahedra hosting Fe, Mn, Zn, Al and Mg. The overall topology of the sheet can be formulated as 4¹5⁴8¹. Larger cations (predominantly Na, Sr and Ca) are accommodated in a variety of interlayer sites sandwiched between the tetrahedral sheets (Fig. 4; Table 2). The two Na sites are both dominated by Na atoms in a distorted octahedral coordination, with <Na – O> distances of 2.453 and 2.535 Å, respectively (Table 3). A site-occupancy refinement revealed that all Ca (0.56 apfu) is ordered in the Na2 site (Table 4). There are also two Sr sites that are both dominated by Sr atoms and coordinated by eight O atoms in a square-antiprismatic arrangement with <Sr – O> distances of 2.634 and 2.624 Å, respectively (Table 3). There is a slight deficit in scattering at the Sr2 site relative to 100% Sr occupancy, which most likely stems from the presence of K and vacancies in this site (Table 4). There are four unique Si tetrahedra with <Si – O> distances ranging from 1.625 to 1.634 Å; both site scattering and <Si – O> distances suggest that the Si sites are occupied primarily by Si. A single larger tetrahedron (<Fe – O> = 1.941 Å) has a refined site scattering of 47.59(8) electrons per formula unit (epfu), in reasonable agreement with the assignment of all Fe + Mn + Zn + Mg + Ti, and some of the Al from the chemical analysis to this site (Table 4). The <Fe – O> distance calculated assuming the Fe²⁺/Fe³⁺ ratio obtained from the Mössbauer analysis is 1.952 Å (i.e., 0.572 + 1.38 Å), which is also in agreement with the observed <Fe – O> distance of 1.941 Å. The Fe tetrahedron is thus occupied by ~60% divalent cations (predominantly Fe²⁺) and 40% trivalent cations (mostly Fe³⁺), providing further support for the proposed end-member formula (see above).

X-RAY POWDER DIFFRACTION

An X-ray diffraction (XRD) pattern was measured with a Bruker D8 Discover SuperSpeed micro-powder diffractometer equipped with a CuK α source, multi-wire 2D detector and modified Gandolfi attachment. In addition, a pseudo-powder XRD pattern was collected in situ from a polished section using a Rigaku D-max Rapid micro-diffractometer equipped with a curved-image-plate detector variety of beam collimators and motorized stage allowing two angular movements. The data were collected in reflection mode using various sample-to-beam geometries and operating conditions. The patterns obtained by the two techniques are very similar, but the in situ measurements did not detect, or underestimated the intensity of, low-angle reflections ($d > 4$ Å), and showed strong preferred-orientation effects owing to the subparallel alignment of vladyskinite crystals in the sample.

Table 5.

Powder XRD pattern of vladyskinite

NN	I _{meas}	d _{meas} Å	D _{calc} Å	hkl	NN	I _{meas}	d _{meas} Å	D _{calc} Å	hkl
	19	7.523	7.557	0 1 1	29			2.383	2 1 3
2	9	6.692a	6.752	0 1 2	30	10b	2.334a	2.350	1 3 0
3	6	5.839	5.842	0 1 3	31			2.334	1 0 10
4	5	5.167a	5.215	1 0 0	32			2.327	1 0 10
5	14	5.011	5.024	0 1 4	33			2.313	1 3 2
6	30	4.290	4.295	1 1 1	34	16	2.109	2.112	2 2 3
7			4.290	1 1 1	35			2.109	2 2 3
8	8	4.059	4.063	1 0 4	36	18	2.063	2.065	2 1 7
9	9	3.894	3.904	0 2 1	37			2.058	2 1 7
10			3.895	1 1 3	38	10b	1.944a	1.948	2 2 6
11	58	3.612	3.623	1 1 4	39			1.942	0 1 13
12			3.613	1 1 4	40			1.925	0 4 3
13	30	3.339	3.342	1 0 6	41	8	1.893	1.894	1 2 11
14			3.335	1 1 5	42			1.890	1 2 11
15			3.330	1 0 6	43	17	1.852	1.851	0 3 10
16	7	3.258	3.256	0 0 8	44	24	1.800	1.798	2 1 10
17	37	3.146	3.148	1 2 0	45			1.797	0 4 6
18	100	2.957	2.962	1 2 3	46	25	1.785	1.791	2 1 10
19			2.957	1 2 3	47			1.783	2 3 4
20	100	2.826	2.832	1 1 7	48		1.781		2 3 4
21			2.824	1 1 7	49	15	1.743	1.746	1 3 10
22	28	2.604	2.608	2 0 0	50		1.743		1 3 10
23	5	2.553	2.551	1 2 6	51	11	1.684	1.683	0 2 14
24	32	2.470	2.476	2 1 0	52	4	1.639	1.641	3 1 4
25			2.473	0 1 10	53	5	1.616	1.616	3 0 6
26	25	2.437	2.440	0 3 4	54	4	1.593	1.591	3 2 0
27	14b	2.391a	2.406	1 2 7	55	8	1.565	1.566	3 2 3
28			2.401	1 2 7	56		1.564		3 2 3
					57	5	1.548	1.547	3 1 7

Notes: B =broad reflection

^a Reflection not used in the cell refinement

The measured XRD micro-powder pattern and interplanar spacings calculated on the basis of structural data are given in table 5. The unit-cell parameters, refined from the powder XRD data by least-squares techniques, are in good agreement with those determined by single-crystal techniques: $a = 5.215(2)$, $b = 7.897(6)$, $c = 26.05(2)$ Å, $\beta = 90.21(5)^\circ$, $V = 1072.6(7)$ Å³.

DISCUSSION

Relation to other mineral species

Only a small number of phyllosilicate minerals contain complex tetrahedral sheets comprising four-, five- and eight-membered rings, as in vladyskinite (Fig. 4).

The simplest arrangement, consisting of zigzag silicate chains $(\text{Si}_6\text{O}_{17})^{10-}$ running parallel to [001] and connected into a sheet by larger $(\text{Zn, Fe, Mn, Mg})\text{O}_4$ tetrahedra, was reported in the crystal structure of nordite-(Ce) and related minerals [2, 16]. Their general formula can be written as $\text{Na}_3\text{SrLREE}(\text{Zn, Fe}^{2+}, \text{Mn, Mg})\text{Si}_6\text{O}_{17}$, where LREE is a light rare-earth element. A topologically similar sheet (ring symbol $4^15^28^1$) was recently identified in the structure of bussyite-(Ce) $\text{REE}_2\text{CaNa}_6\text{MnBe}_5\text{Si}_9(\text{O, OH})_{30}(\text{F, OH})_4$, where all tetrahedra are similar in size and populated by Si, Be or both [6]. The pattern of Be distribution within the sheet in bussyite-(Ce) is also different from the distribution of tetrahedrally coordinated divalent cations in the nordites (figs. 5a and 5b), but the stoichiometry of the sheet is preserved. A completely different arrangement of silicate rings and stoichiometry are found in the beryllsilicates semenovite-(Ce), $\text{Na}_{0.2}(\text{Ca, Na})_8\text{REE}_2(\text{Fe}^{2+}, \text{Mn, Zn})(\text{Be, Si})_{20}(\text{O, OH, F})_{48}$ (Mazzi et al. 1979) and harstigitite, $\text{Ca}_6\text{MnBe}_4\text{Si}_6\text{O}_{22}(\text{OH})_2$ (Hesse and Stümpel 1986). In contrast to the nordites, Mn and other divalent cations larger than Be, but smaller than Ca occupy octahedral sites in bussyite-(Ce), semenovite-(Ce) and harstigitite. Although tetrahedral sheets in the structure of vladyskinite show the same 1:4:1 proportion among four-, five- and eight-membered rings and, hence, the same stoichiometry as in semenovite-(Ce) or harstigitite (i.e. 10 tetrahedrally coordinated cations per 24 anions), they are topologically unique (cf. figs. 5c and 5d). The structure of vladyskinite does not appear to have any known natural or synthetic analogues at present, but shows a clear structural affinity to the nordites.

The $4^15^48^1$ sheet in vladyskinite can be visualized as consisting of eight-tetrahedra-long segments of nordite-like chains, $(\text{Si}_8\text{O}_{24})^{16-}$ interconnected by sharing all of their available vertices with FeO_4 tetrahedra (figs. 4, 5a and 5d). In both structure types, tetrahedral sheets are sandwiched between layers of NaO_6 octahedra and SrO_8 ($\pm \text{LREEO}_8$) square antiprisms. The NaO_6 , Na_2O_6 and SrO_8 polyhedra are very similar in vladyskinite and ferronordite-(Ce), whereas the FeO_4 tetrahedron is somewhat larger in the latter mineral because it accommodates only Fe^{2+} and other divalent cations [16; table 3].

Paragenesis

In the host lujavrite, vladyskinite is a relatively early liquidus phase precipitated after lamprophyllite, but prior to potassium feldspar, Sr-bearing eudialyte and aegirine. The high modal content of lamprophyllite, eudialyte and vladyskinite, along with the presence of K-rich vishnevite and strontianite, in this rock are undoubtedly due to the extremely evolved, volatile-rich nature of its parental peralkaline melt. The lack of Ba silicates in the lujavrite, and low Ba contents in its constituent minerals (0.9-1.8 wt.% BaO in lamprophyllite, 0.2 wt.% in vladyskinite, and below detection in the feldspar) suggest that this melt was derived from a more primitive magma by fractional crystallization of potassium feldspar, in which Ba is much more compatible than Sr [7]; BaO values up to 3

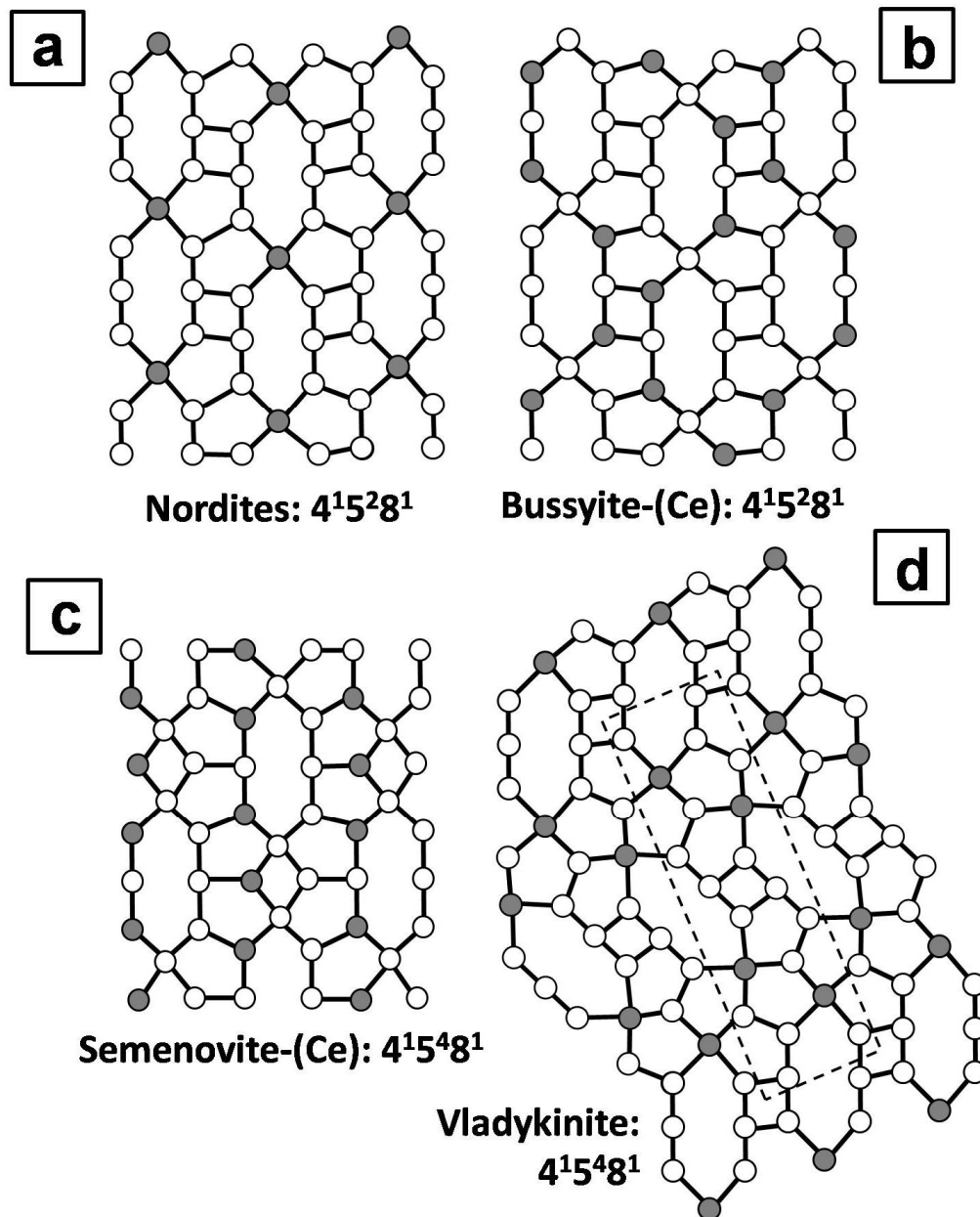


Fig.5. Comparison of the tetrahedral sheet topology in the structures of:

(a) ferrorordite-(Ce) and related minerals [16]; (b) bussyite-(Ce) [6]; (c) semenovite-(Ce) [11]; and (d) vladykinite (this work). Silicon atoms are indicated by empty circles, and other tetrahedrally coordinated cations (i.e. mostly Be in bussyite-(Ce) and semenovite-(Ce); Fe^{2+} , Mn and Zn in the nordites; Fe^{2+} and Fe^{3+} in vladykinite) by filled circles.

wt.% were reported in syenitic feldspars from Murun by Konev et al. [9] and Reguir [17]. The evolution of the lujavrite culminated with the release of a sulfate-carbonate-rich fluid, which reacted with the early magmatic mineral assemblage to produce vishnevite and strontianite. At this stage, vladykinite became chemically unstable and underwent pseudomorphization by strontianite (fig. 1). Precipitation of SrCO_3 and removal of silica during the replacement imply alkaline conditions, but a quantitative assessment of these conditions cannot be made at present

because thermodynamic data for vladyskinite are not available. Similar late-stage processes have been documented elsewhere at Maly Murun, where strontianite developed at the expense of fluorapatite and fluorstrophite [3].

This work was supported by the Natural Sciences and Engineering Research Council of Canada and Canada Foundation for Innovation. The authors are grateful to Frank C. Hawthorne, for access to the X-ray facilities at the University of Manitoba. Panseok Yang is thanked for his help with LA-ICP-MS. We also acknowledge Sergey Krivovichev and two anonymous referees for their constructive comments on the earlier version of this manuscript, and Associate Editor Hongwu Xu for speedy handling.

REFERENCES CITED

1. **Ageeva O.A. and Borutzky B.Ye.** (2004) Kalsilite in the rocks of Khibiny massif: morphology, paragenesis, genetic conditions. *New Data on Minerals*, 39, 40-49.
2. **Bakakin V.V., Belov N.V., Borisov S.V., and Solovyeva L.P.** (1970) The crystal structure of nordite and its relationship to melilite and datolite-gadolinite. *American Mineralogist*, 55, 1167-1181.
3. **Chakhmouradian A.R., Reguir E.P., and Mitchell R.H.** (2002) Strontium-apatite: New occurrences, and the extent of Sr-for-Ca substitution in apatite-group minerals. *Canadian Mineralogist*, 40, 121-136.
4. **Deer W.A., Howie R.A., and Zussman J.** (1997) *Rock-forming Minerals. Volume 1A: Orthosilicates.* The Geological Society, Bath, UK, 932 pp.
5. **Evdokimov M.D.** (1995) Charoite: a unique mineral from a unique occurrence. *World of Stones*, 1995 (7), 3-11.
6. **Grice J.D., Rowe R., Poirier G., Pratt A., and Francis J.** (2009) Bussyite-(Ce), a new beryllium silicate mineral species from Mont Saint-Hilaire, Quebec. *Canadian Mineralogist*, 47, 193-204.
7. **Henderson C.M.B. and Pierozynski W.J.** (2012) An experimental study of Sr, Ba and Rb partitioning between alkali feldspar and silicate liquid in the system nepheline – kalsilite – quartz at 0.1 GPa $P(\text{H}_2\text{O})$: a revisitation and reassessment. *Mineralogical Magazine*, 76, 157-190.
8. **Hesse K.-F. and Stümpel G.** (1986) Crystal structure of harstigitite, $\text{MnCa}_6\text{Be}_4[\text{SiO}_4]_2[\text{Si}_2\text{O}_7]_2(\text{OH})_2$. *Zeitschrift für Kristallographie*, 177, 143-148.
9. **Konev A.A., Vorob'ev E.I., and Lazebnik K.A.** (1996) *Mineralogy of the Murun Alkaline Massif. Siberian Branch RAS press, Novosibirsk, Russia, 221 pp.* (in Russian).
10. **Kostyuk V.P., Panina L.I., Zhidkov A.Ya., Orlova M.P., and Bazarova T.Yu.** (1990) *Potassic Alkaline Magmatism of the Baikal-Stanovoy Rift System. Nauka, Novosibirsk, Russia, 237 pp.* (in Russian).
11. **Mazzi F., Ungaretti L., and Dal Negro A.** (1979) The crystal structure of semenovite. *American Mineralogist*, 64, 202-210.
12. **Mitchell R.H. and Vladykin N.V.** (1993) Rare-earth element-bearing tausonite and potassium barium titanates from the Little Murun potassic alkaline complex. *Mineralogical Magazine*, 57, 651-668.
13. **Mitchell R.H. and Vladykin N.V.** (1996) Compositional variation of pyroxene and mica from the Little Murun ultrapotassic complex, Aldan Shield, Russia. *Mineralogical Magazine*, 60, 907-925.
14. **Pakhomovsky Ya.A., Yakovenchuk V.N., and Ivanyuk G.Yu.** (2009) Kalsilite of the Khibiny and Lovozero alkaline plutons, Kola Peninsula. *Geology of Ore Deposits*, 51, 822-826.

15. **Pekov I.V., Olysyh L.V., and Chukanov N.V.** (2011) Crystal chemistry of cancrinite-group minerals with an *AB*-type framework: a review and new data. I. Chemical and structural variations. *Canadian Mineralogist*, 49, 1129-1150.
16. **Pushcharovsky D.Yu., Pekov I.V., Pluth J.J., Smith J.V., Ferraris G., Vinogradova S.A., Arakcheeva, A.V., Soboleva, S.V., and Semenov, E.I.** (1999) Raite, manganonordite-(Ce) and ferronordite-(Ce) from the Lovozero massif: crystal structures and mineralogical geochemistry. *Crystallography Reports*, 44, 565-574.
17. **Reguir E.P.** (2001) Aspects of the Mineralogy of the Murun Alkaline Complex, Yakutia, Russia. Unpublished MSc Thesis, Lakehead University, Thunder Bay, Canada, 193 pp.
18. **van Achterbergh E., Ryan C.G., and Griffin W.L.** (2001) GLITTER on-line interactive data reduction for the LA-ICPMS microprobe. Macquarie Research Ltd., Sydney.
19. **Vladykin N.V.** (1981) Geology of the Murun massif, the place of pseudoleucite (synnyrite-like) syenites in the massif, and their chemical composition. In *Problemy Osvoeniya Zony BAM*. Novosibirsk, Russia, 106-113 (in Russ.).
20. **Vladykin N.V.** (1997) Geochemistry and genesis of lamproites of the Aldan Shield. *Russian Geology and Geophysics*, 38, 128-141.
21. **Vladykin N.V.** (2009) Potassium alkaline lamproite-carbonatite complexes: petrology, genesis, and ore reserves. *Russian Geology and Geophysics*, 50, 1119-1128.
22. **Vladykin N.V. and Tsaruk I.I.** (2003) Geology, chemistry and genesis of Ba-Sr-bearing ("benstonite") carbonatites of the Murun Massif. *Russian Geology and Geophysics*, 44, 315-330.

APPENDIX 1 (ONLINE)

Mineralogy of alkaline igneous and associated hydrothermal and metasomatic rocks, Murun complex, eastern Siberia, Russia.

GEOCHEMICAL FEATURES OF RADIOACTIVE ELEMENTS IN ULTRAMAFIC-ALKALINE ROCKS (EXAMPLE –LARGEST IN THE GLOBE GULI COMPLEX)

Kogarko L. N.

*Vernadsky Institute of Geochemistry and Analytical Chemistry,
Russian Academy of Sciences, Moscow*

The study of radioactive element distribution in the rocks of the Guli Complex revealed an increase of uranium and thorium contents in the final products of magmatic differentiation. In the carbonatite complex, the radioactive elements are mainly accumulated in the early rocks – phoscorites, while their contents in the late phases, dolomitic carbonatites, decrease. The Th/U ratio increases from near-chondritic values in the weakly differentiated highly-magnesian primary magmas to the late rocks – phoscorites, calcitic carbonatites, and dolomitic carbonatites. The majority of radioactive elements are hosted in rare-metal accessory minerals: perovskite, pyrochlore, calzirtite, and apatite. Rock-forming minerals are characterized by extremely low contents of radioactive elements.

INTRODUCTION

After the break up of the Soviet Union, Russia lost the control over most important sources of radioactive raw material. This determined the elevated interest to the study of uranium and thorium geochemistry in rocks. Among all magmatic formations, alkaline and carbonatite magmatism is characterized by the highest potential with respect to radioactive elements. The great number of endogenous uranium and thorium deposits is related to the rocks of elevated alkalinity. This work is aimed study the geochemistry of radioactive elements in the rocks of the world's largest Guli ultrabasic alkaline massif located in the Meymecha-Kotuy province (Polar Siberia).

The Guli Massif occupies the territory between the Kotui and Meymecha rivers, at the boundary of the Siberian Platform and Khatanga trough. The massif has an oval shape 35×45 km in size and spans an area of 1500-1600 km², including portion overlain by Quaternary sediments [1]. According to geophysical data, the massif has almost vertical contacts and presumably a pipe-like morphology [1]. The host rocks are represented by alkaline volcanics including meymecheite flows. The Guli Massif, as other ultrabasic-alkaline massifs of the province, was formed in several phases (table 1).

The predominant rocks of the massif are dunites, which occupy around 60 % of the total area, and ultra-basic rocks spanning 30 %. All other varieties, including

melilitolites, ijolites, alkaline syenites, and carbonatites occupy only 10 % of the area.

Table 1

Intrusive phases of the Guli Complex

Intrusive phases	Subphase	Rock
7	4	Dolomitic carbonatites
	3	Fine-grained calcitic carbonatites
	2	Coarse-grained calcitic carbonatites
	1	Phoscorites and ore phoscorites
6		Granites
5	2	Microshonkinite
	1	Agpaitic syenites, quartz syenites
4		Ijolites and ijolite-pegmatites
3	3	Jacupirangites and melteigites
	2	Nephelinites and olivine nephelinites, nepheline picrites, micaceous pyroxene picrites
	1	Melteigites, malignites, and shonkinites
2		Melilitic rocks
1	2	Ore pyroxenites (koswites), olivine pyroxenites, peridotites
	1	Dunites

The uranium and thorium contents were analyzed by ICP-MS on a Finnigan Element mass spectrometer using BE-N and IF-G international standards. The distribution of radioactive elements in the minerals was studied using CAMECA 100 microprobe and in situ laser ablation. Around 90 rock samples of the Guli massif and 120 minerals from these samples were analyzed and obtained results are presented in tables 2 and 3.

DISTRIBUION OF RADIOACTIVE ELEMENTS IN THE ROCKS

Since uranium and thorium are incompatible lithophile elements with extremely low partition coefficients in major rock-forming minerals, they are accumulated in the residual products of crystallization differentiation. Owing to the strong lithophile properties, the radioactive elements (U, Th) form oxygen compounds with predominant ionic binding. The ionic radius of thorium, which occurs in tetravalent ($\text{Th}^{4+} - 0.95 \text{ \AA}$) state in the endogenous processes, is close to those of rare-earth elements ($0.8-0.97 \text{ \AA}$), uranium ($\text{U}^{4+} - 0.89 \text{ \AA}$), zirconium ($\text{Zr}^{4+} - 0.82 \text{ \AA}$), and calcium ($\text{Ca}^{2+} - 1.04 \text{ \AA}$). Uranium under endogenous conditions exists in the tetravalent and hexavalent states depending on the redox potential of the mineral-forming environment and readily forms oxygen complex of uranyl-ion (UO_2)²⁺ type.

The study of uranium and thorium geochemistry in rocks from different regions showed intense accumulation of these elements during magmatic differentiation [2]. The high contents of radioactive elements in the alkaline rocks

were noted by Fersman [3], Wedepohl [4] and many other works. Similar tendency was established by us for the highly differentiated rocks of the Guli Massif. The analysis results are listed in table 2. The average contents of radioactive elements for different rock types were taken as the arithmetic mean values. The characteristic feature of the distribution of radioactive elements in the rocks of the Guli Massif is their extremely wide variations. This especially true for uranium, the contents of which in dunites and koswites vary sometimes within over two orders of magnitude. It should be noted that the highly magnesian magmas approximating primary compositions (meymechites, picrites, and olivine melanephelinites) have more stable contents of radioactive elements. From the oldest rocks (dunites and koswites) to the youngest carbonatites, the uranium and thorium contents significantly increase (from $0.04 \times 10^{-4} \% \text{ U}$ and $0.12 \times 10^{-4} \% \text{ Th}$ in the dunites to $39 \times 10^{-4} \% \text{ U}$ and $209 \times 10^{-4} \% \text{ Th}$ in the phoscorites). It is noteworthy that the uranium and thorium contents in the youngest rocks of the massif, dolomitic carbonatites, decrease to $0.84 \times 10^{-4} \% \text{ U}$ and $10.39 \times 10^{-4} \% \text{ Th}$. The relatively low contents of radioactive elements in the dolomitic carbonatites are related to the intense fractionation of these elements in perovskites, pyrochlores, and calzirtites.

Table 2 a

Distribution of radioactive elements in the rocks of the Guli Massif, $n \times 10^{-4} \%$

Dunites				Peridotites				Koswites			
N	U	Th	Th/U	N	U	Th	Th/U	N	U	Th	Th/U
8513	0.05	0.13	2.79	85-60	0.52	1.98	3.81	863	0.20	0.30	1.50
85-153	0	0.02	0	85-63	0.15	0.94	6.27	868	0.20	0.70	3.50
85-82	0.02	0.05	2.67	85-77	0	0.04	0	8510/1	1.0	5.50	5.50
85-84	0.01	0.02	2.55	average	0.22	0.99	3.36	8514	0.20	0.30	1.50
85-87	0.02	0.06	3.44	—	—	—	—	85-148	0.20	2.10	10.5
85-58	0.33	0.80	2.42	Olivinites				85-149	0.20	0.30	1.50
Gkh-40	0.01	0.05	3.42	N	U	Th	Th/U	85-151	0.20	0.50	2.50
85-75	0.002	0.03	11.3	Gkh-35	1.57	5.06	3.22	85-76	1.30	6.00	4.62
85-64	0.02	0.11	4.84	85-59	0.10	0.41	4.14	85-80	0.05	0.19	4.23
85-153a	0	0.04	0	average	0.83	2.73	3.68	85-81	0.06	0.21	3.43
85-146	0	0.03	0	—	—	—	—	average	0.36	1.61	3.88
average	0.04	0.12	3.04	—	—	—	—	—	—	—	—

The great amounts of these minerals are formed in the earliest carbonatites of the phoscorite series. According to Sr, Nd, and Pb isotopic data, the syenites, quartz syenites, and granites of the Guli Massif represent remobilized crustal material [12]. Therefore, the concentrations of radioactive elements in these rocks are not determined by the evolution of the Guli magmatic system, but reflect the differentiation of crustal material. Unlike the syenites and quartz syenites, the agpaite nepheline syenites of the Guli Massif, according to our isotopic data, have mantle sources similar to those of the meymechites, picrites, olivine

melanephelinites, their derivatives, and carbonatites. The agpaitic nepheline syenites have extremely high contents of radioactive elements, which are close to economic concentrations (U 36.07×10^{-4} %, Th 134.9×10^{-4} %). These rocks show more than two times higher contents of radioactive elements than those of the agpaitic nepheline syenites of the superlarge Lovozero deposit (Kola Peninsula). Thus, the late derivatives, phoscorites and alkali-over saturated nepheline syenites, have the highest contents of radioactive elements among the rocks of the Guli Complex. The accumulation of radioactive elements during magmatic differentiation of the Guli Complex is well illustrated by the variations of the uranium and thorium contents versus Mg number in rock (fig. 1). The MgO content usually characterizes the degree of differentiation of magmatic system, which is controlled by olivine and pyroxene fractionation.

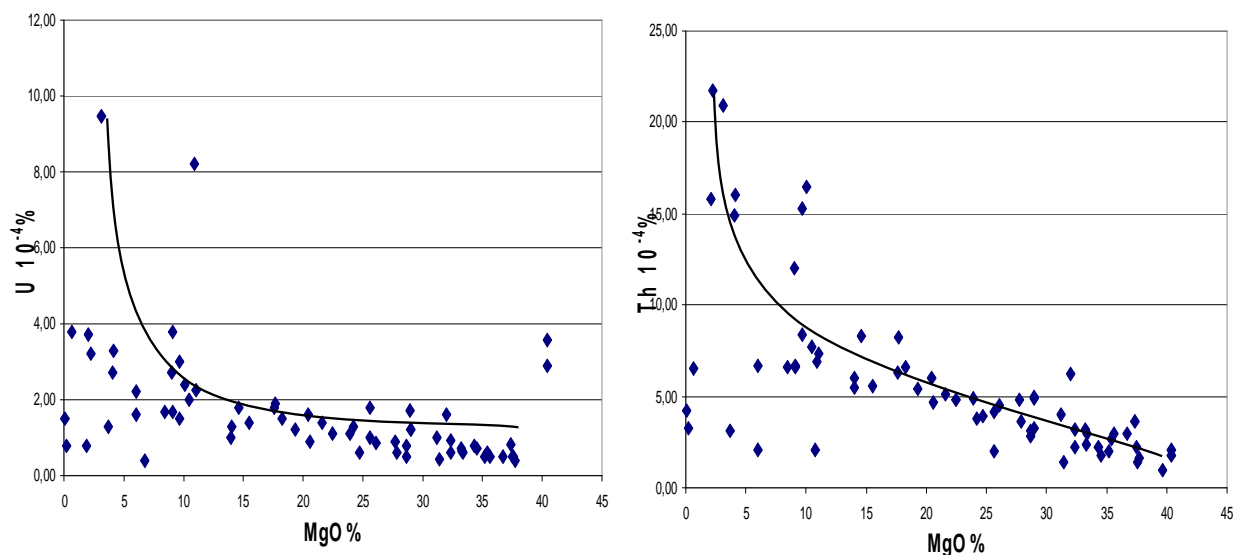


Fig. 1. Variations of uranium (a) and thorium (b) contents versus Mo of silicate rocks of the Guli Massif.

The rocks of the carbonatite complex are omitted, since their genesis differs from genesis of silicate rocks. The concentration of radioactive elements in the agpaitic nepheline syenites is too high to be plotted in the diagram (the MgO content in these rocks is 1,8 %).

In spite of the chemical affinity of uranium and thorium, these elements are separated in the endogenous processes especially when uranium is transformed into hexavalent state. The Th/U ratio is the measure of compatibility of these elements. During mantle partial melting, this ratio is characterized by chondritic values (3,82) both in the generated melts and in residues. Highly magnesian undifferentiated magmas of the Guli complex, including meymechites, picrites, olivine melanephelinites, also have near-chondritic Th/U ratios, in spite of definite variations (table 2). During magmatic differentiation, the Th/U ratio increases, which is most expressed in the melilite rocks (Th/U = 4,95) and especially in the carbonatites-phoscorites and youngest dolomitic carbonatites, where it reaches 14,65 and 12,61, respectively. Undoubtedly, the growth of Th/U ratio records

fractional crystallization of minerals, which are characterized by different partition coefficients for uranium and thorium; significant contents of radioactive elements should be accumulated in these minerals to affect the Th/U ratio. Among these mineral phases are presumably apatite, which concentrates radioactive elements in amounts of hundreds g/t and, according to the large data base [5], some apatites accumulate uranium to a greater extent than thorium. It should be noted that available data on the uranium and thorium partition coefficients in apatite remain still controversial [6].

Table 2 b

Distribution of radioactive elements in the rocks of the Guli Massif, $n \times 10^4\%$

Meymechites					Picrite				
rock	N	U	Th	Th/U	rock	N	U	Th	Th/U
meymechite	E-1	0.20	1.00	5.00	picrite	122	1.30	3.80	2.92
meymechite	117	0.40	1.10	2.75	picrite	119	1.10	4.90	4.45
meymechite	130	0.50	1.40	2.80	picrite	125	1.10	4.80	4.36
meymechite	50C	0.50	3.00	6.00	picrite	147	1.60	6.00	3.75
meymechite	131	0.60	2.70	4.50	picrite	143	1.80	6.30	3.50
meymechite	116	0.50	2.00	4.00	picrite	129	1.40	5.60	4.00
meymechite	133	0.70	1.80	2.57	picrite	229	1.90	8.20	4.32
meymechite	1139	0.80	2.20	2.75	picrite	230	0.60	3.60	6.00
meymechite	121	0.70	3.20	4.57	picrite	232	1.20	5.40	4.50
meymechite	134	0.60	2.20	3.67	picrite	238	1.50	6.60	4.40
meymechite	144	0.92	3.20	3.48	picrite	169A	1.80	6.40	3.56
meymechite	118	0.44	1.40	3.18	Ne-picrite	861	1.40	5.10	3.64
meymechite	132	0.50	2.80	5.60	Ne-picrite	166	0.87	4.50	5.15
meymechite	8313	0.80	3.10	3.88	Ne-picrite	168	1.80	8.30	4.61
meymechite	231	0.50	2.20	4.40	Ol-melanephelinite	858	2.70	12.00	4.44
meymechite	233	0.40	1.60	4.00	Ol-melanephelinite	8510	1.60	6.20	3.88
meymechite	146	0.83	3.65	4.37	Ol-melanephelinite	1136	1.20	4.90	4.08
average		0.58	2.27	3.97	Ol-melanephelinite	1137	1.20	5.00	4.17
Agpaitic nepheline syenites					Ol-melanephelinite	1137a	1.20	5.00	-
rock	N	U	Th	Th/U	Ol-melanephelinite	1143	0.90	4.80	5.33
Agpait. nephelin- ite syenite	1	36.07	134.9	3.74	Ol-melanephelinite	165	0.90	4.70	5.22
average		36.07	134.9	3.74	Ol-melanephelinite	167	2.00	7.70	3.85
Granites					Ol-melanephelinite	167a	2.00	7.70	-
rock	N	U	Th	Th/U	melteigite	192	2.26	7.34	3.25
granite	97	3.8	6.5	1.71	melteigite	195	1.66	6.63	3.99
orthoclasite	89	0.20	0.30	1.50	melteigite	193	2.20	2.10	0.95
average	-	2	3.40	1.61	melteigite	169B	1.60	6.70	4.19
					Ol-melanephelinite	123	1.00	4.01	4.02
					Ol-melanephelinite	1132	0.40	0.50	1.25
					Ol-melanephelinite	118	0.66	2.41	3.66
					Ol-melanephelinite	9B	3.80	6.70	1.76
					average	-	1.50	5.58	3.90

The Th/U ratio in the crustal-derived syenites and granites are significantly lower than chondritic values and values typical of the rocks of the Guli Massif (Th/U = 2,48 in the syenites and 1,61 in the granites). The Th contents in the crustal rocks of the Guli Complex are close to those derived by Rudnik et al. [7] for the Earth's crust (Th = $5,6 \times 10^{-4}$ %), however uranium concentrations in the granites are significantly higher. According to Rudnick et al. [7], the uranium

Table 2 c

Melilite rocks					Malignite				
rock	N	U	Th	Th/U	rock	N	U	Th	Th/U
kugdite	48	0.40	5.08	12.81	malignite	859	2.70	14.90	5.52
kugdite	18	1.90	4.22	2.22	malignite	1985-70	3.30	16.00	4.85
kugdite	14	2.03	12.34	6.08	malignite	1985-71	3.20	21.70	6.78
kugdite	2	1.27	1.05	0.83	malignite	1985-74	3.70	15.80	4.27
kugdite	38	1.04	5.30	5.11	malignite	1985-13	9.48	20.90	2.20
kugdite	42	1.44	3.83	2.66	average	—	4.48	17.86	4.72
average	—	1.35	5.30	4.95					
Ijolites					Syenites				
ijolite	116	0.11	0.80	5.72	syenite	140	1.50	4.20	2.80
ijolite	47	1.83	0.80	3.86	syenite	141	0.80	3.30	4.13
ijolite	131	12.90	1.30	0.64	syenite	90	0.80	0.50	0.63
average	—	4.95	1.10	3.41	syenite	91	1.3	3.10	2.38
					average	—	1.1	2.78	2.48
Phoscorites					Phase II carbonatites				
phoscorite	106	42.39	446.64	10.54	sovite	124a	0.5	16	32.00
phoscorite	102	4.86	325.13	66.90	sovite	100	0.2	1.9	9.50
phoscorite	157	2.72	2.02	0.74	sovite	104	1.4	2.9	2.07
phoscorite	158	123.53	477.72	3.87	sovite	125	294	916	3.12
Phase I carbonatites	107	0.7	2.7	3.86	sovite	124b	0.5	13.7	27.40
Phase I carbonatites	161	0.3	0.6	2.00	sovite	112	0.4	0.7	1.75
average	—	29.08	209.1	14.6	sovite	105	1.2	16.9	14.08
					sovite	109	0.7	0.6	0.86
Dolomitic carbonatites					sovite	162	0.2	0.3	1.50
Dolomitic carbonatite	1985-117	0.6	14.10	23.50	sovite	160	0.2	0.3	1.50
Dolomitic carbonatite	1985-123	0.6	9.2	15.33	sovite	71a	2.94	0.42	0.14
Dolomitic carbonatite	1985-126	1.6	34.1	21.31	average	—	25.98	82.55	8.01
Dolomitic carbonatite	1985-113	1.5	1.1	0.73					
Dolomitic carbonatite	1985-103	0.5	3.8	7.60					
Dolomitic carbonatite	1985-119	0.5	7.3	14.60					
rock	N	U	Th	Th/U					
Dolomitic carbonatite	121	0.6	3.1	5.17					
average	—	0.84	10.39	12.61					

content in the average Earth's crust is $1,3 \times 10^{-4}$ %. One can suggest that somewhat elevated uranium contents in the syenites and granites of the Guli Massif are related to the influx of easily mobile uranium from the Guli magmatic system.

The established tendency in the growth of Th/U ratio during magmatic differentiation of the Guli Massif is possibly related to the uranium loss during degassing of volatiles, primarily CO₂ and water, because uranium forms mobile complexes of UO₂CO₃·nH₂O type, which are well transferred into host crustal rocks.

DISTRIBUTION OF RADIOACTIVE ELEMENTS IN THE MINERALS OF THE GULI MASSIF

The use of in situ laser ablation offered an opportunity to estimate the concentrations of radioactive elements in major rock-forming and some accessory minerals. The contents of radioactive elements in the rock-forming olivines, pyroxenes, micas, melilites, spinels, Ti-magnetite, and carbonates are very low: tenths and hundredths grams per ton. Significantly higher contents of thorium and uranium ($1,7-1,23 \times 10^{-4}$ % and $1,5-0,73 \times 10^{-4}$ %, respectively) were found in a egrines from agpaitic nepheline syenites. It is conceivable that radioactive elements substitute calcium and titanium in rock-forming minerals. The necessity for charge balance significantly constrains such isomorphic substitutions. Notably higher concentrations of radioactive elements were established in apatites from carbonatites. In apatites from alkaline rocks, radioactive elements presumably substitute rare-earth elements with simultaneous substitution of calcium for sodium. For instance, one apatite from phoscorite contains 377×10^{-4} % U and 537×10^{-4} % Th. It should be noted that the contents of radioactive elements in the apatites significantly vary even within the same rock. In some apatite grains from phoscorite, the concentrations of radioactive elements sharply decrease to $0,88 \times 10^{-4}$ % Th and $1,01 \times 10^{-4}$ %. All studied apatites from the carbonatite complex of the Guli Massif are characterized by extremely low Th/U ratios varying from 0,08 to 1,42. The predominant uranium fractionation with apatite presumably also facilitated an increase of Th/U ratio in the final products of magmatic differentiation of the Guli Complex. The oldest carbonatites of the Guli Complex contain calzirtite accumulating radioactive elements to a greater extent as compared to the rock-forming minerals and apatite. In calzirtite, radioactive elements are accommodated in sites of titanium and zirconium. According to our data, the thorium and uranium contents in calzirtite from the phoscorite of the Guli Massif accounts for 0,11 % and 0,28 %, respectively. According to [8], calzirtite from carbonatite contains 389 g/t U and 0,26 g/t Th. Sufficiently high contents of radioactive elements were noted in the baddeleyite from carbonatites: hundreds g/t Th and thousands g/t U. In baddeleyite, uranium and thorium are substituted for zirconium. One of major mineral-carrier of radioactive elements in the rocks of the Guli Massif is perovskite, which is formed at the early stages of evolution in highly

magnesian primary magmas of the Guli complex (olivine melanephelinites) and

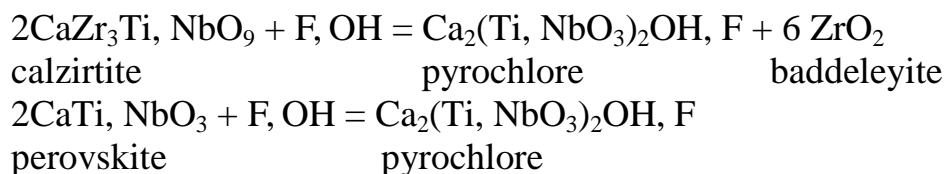
Table 3

Contents of radioactive elements in the minerals of the Guli Massif, $n \times 10^{-4} \%$

Olivine		min	max	Apatite		min	max
dunite	Th	0.19	0.25	phoscorite	Th	0.966	537
	U	0.17	0.17		U	1.010	377
koswite	Th	0.002	0.005	carbonatite	Th	0.015	1.56
	U	0.002	0.004		U	0.003	13.4
melteigite	Th	0.004	0.005	Melilite		min	max
	U	0.003	0.004	melilitolite	Th	0.003	0.004
carbonatite	Th	0.002	0.006		carbonatite	U	0.001
	U	0.003	0.23	Th		0.001	0.005
Pyroxene		min	max			min	max
dunite	Th	0.078	0.13	Mica		min	max
	U	0.013	0.034	dunite	Th	0.006	
koswite	Th	0.028	0.071		melteigite	U	0.004
	U	0.005	0.017	Th		0.005	76.7
melteigite	Th	0.024	0.34		U	0.003	33.1
	U	0.002	0.075		Calcite		min
carbonatite	Th	0.076	0.179	carbonatite	Th	2.640	15.9
	U	0.017	0.609		U	0.031	0.198
melilitolite	Th	0.002	0.005	Monticellite		min	max
	U	0.002	0.003	carbonatite	Th	0.001	0.005
malignite	Th	0.010	1.14			U	0.001
	U	0.010	0.12	Perovskite		min	max
ijolite	Th	1.35	1.65	nephelinites and carbonatites	Th	557	13600
	U	0.35	0.59		U	118	300
syenite	Th	0.005	0.23	Pyrochlore		min	max
	U	0.003	0.509	carbonatite	Th	119300	164200
agpait. nephelin. syen.	Th	0.016	1.70			U	3200
	U	0.019	1.55				

continues to crystallize up to the latest stages of magmatic differentiation in the carbonatites. In perovskites, the radioactive elements substitute titanium; this site is also occupied by rare-earth elements, niobium, tantalum, and zirconium. The thorium and uranium contents in perovskites of some nephelinites reach 1,36 and 0,03 %, respectively. According to our data, the uranium and thorium contents in the perovskites from carbonatites account for few hundreds and several hundreds g/t, respectively. Extremely high concentrations of radioactive elements are noted in the pyrochlores of the Guli Massif. These elements are incorporated in pyrochlore in the titanium site. Niobium, tantalum, and zirconium accommodate the same position. According to our data [9], pyrochlore contains 11,93 % ThO₂ and 0,32 % UO₂, while other grain of the same carbonatite contains up to 16,42 %

ThO₂ and 2,59 % UO₂. The high contents of radioactive elements and elevated Th/U ratios in pyrochlore indicate that precisely this mineral was responsible for the significant increase in the Th/U ratio in the carbonatite complex of the Guli Massif. The Th/U ratio significantly decreases from early to late pyrochlores (from 37,3 to 6,3). Similar variations in the Th/U ratio were noted in the carbonatites of other regions [10]. The magmatic differentiation of the carbonatite complex of the Guli Massif is accompanied by definite evolution of rare-metal mineralization: with increasing fluorine activity at the late evolution stages the earlier calzirtite is replaced by pyrochlore and baddeleyite, while early perovskite is also replaced by pyrochlore.



In course of these reactions, the radioactive elements are accumulated in pyrochlores owing to extremely high uranium and thorium partition coefficients. The described type of reactions of rare-metal minerals in the Guli carbonatites is widely spread in the similar rocks from other regions, for instance, in the large Kovdor carbonatite complex at the Kola peninsula [10]. According to experimental data [11], perovskite is replaced by pyrochlore at approximately 800°C and fluorine concentration in the mineral-forming environment around 1,5 %. The main mineral-carrier of thorium and uranium in the agpaitic nepheline syenites is thorite. Somewhat higher contents of radioactive elements were noted in the minerals of eudialyte-aqualite group: $31\text{-}77 \times 10^{-4} \%$ Th and $74\text{-}177 \times 10^{-4} \%$ U.

CONCLUSIONS

The study of the distribution of radioactive elements in the rocks of the Guli Complex showed an increase of uranium and thorium concentrations in the final products of magmatic differentiation: carbonatite complex and agpaitic nepheline syenites.

In the rocks of the carbonatite complex, the radioactive elements are mainly accumulated in the oldest rocks-phoscorites, while their contents in the youngest rocks-dolomitic carbonatites-significantly decrease.

The Th/U ratio increases from near-chondritic value in the weakly differentiated highly magnesian primary magmas to the later phoscorites, calcite carbonatites, and dolomitic carbonatites. The majority of radioactive elements are contained in the rare-metal accessory minerals: perovskite, pyrochlore, calzirtite, and apatite. The rock-forming minerals have extremely low contents of radioactive elements.

The work was supported by the Russian Foundation for Basic Research (project no. 11-05-12004-OFI-M)

Работа выполнена при финансовой поддержке Программы ОНЗ 9 и РФФИ-ОФИ-13-05-12021

REFERENCES

1. **Egorov, L.S.**, Ijolite-Carbonatite Plutonism, Illustrated by the Example of the Meymecha-Kotuy Complex in Arctic Siberia (Nedra, Leningrad, 1991) [in Russian].
2. **V I. Gerasimovsky et al.**, The Geochemistry of the Lovozero Alkaline Massif, Nauka, Moscow, 1966.
3. **A. E. Fersman**, Geochemistry (Goskhimizdat, Leningrad, 1939), Vol. 4 [in Russian].
4. **K. H. Wedepohl**, Handbook of Geochemistry, Springer, Berlin, 1969-1978.
5. **M. Chu, K. Wang, W. Griffin, S. Chung, S. O'Reilly, N. Pearson, and Y Iizuka**, Apatite Composition: Tracing Petrogenetic Processes in Transhimalayan Granitoids, *J. Petrol.* 50 (10), 1829—1855 (2009).
6. **S. Klemme and C. Dalpu**, Element Partitioning between Apatite and Carbonatite Melt, *Am. Mineral.* 88, 639-646 (2003).
7. **R. Rudnik and S. Gao**, Composition of the Continental Crust, *Treat. Geochem.* 3, 1-56 (2003).
8. **F. Y. Wu, Y. H. Yang, R. Mitchell, F. Bellatreccia, Q. L. Li and Z. H. Zhao**, In Situ U-Pb and Nd-Hf-(Sr) Isotopic Investigation of Zirconolite and Calzirtite, *Chem. Geol.* 277, 178-195 (2010).
9. **T. Williams and L. Kogarko**, New Data on Rare-Metal Mineralization in the Guli Massif Carbonatites, Arctic Siberia, *Geochem. Int.* 34, 433-440 (1996).
10. **Yu. L. Kapustin**, Mineralogy of Carbonatites, Nauka, Moscow, 1971 [in Russian].
11. **B. C. Jago and J. Gittins**, Pyrochlore Crystallization in Carbonatites: the Role of Fluorine, *S. Afr. J. Geol.* 96 (3), 149-159 (1993).
12. **L. N. Kogarko and R. E. Zartman**, New Data on the Age of the Guli Intrusion and Implications for the Relationships between Alkaline Magmatism in the Maymecha-Kotuy Province and the Siberian Super-plume: U-Th-Pb Isotopic Systematics, *Geochem.*

THE COMPOSITION OF THE LOWER MANTLE: SOURCE OF DIAMONDS WITH HIGH-PRESSURE MINERAL INCLUSIONS

Ryabchikov I. D.¹ and Kaminsky F. V.²

*Institute of Geology of Ore Deposits, Petrography, Mineralogy, and Geochemistry, Russian
Academy of Sciences, Staromonetnyi per. 35, Moscow, 119017 Russia¹;
KM Diamond Exploration Ltd, West Vancouver, Canada².*

The presence of diamonds with mineral inclusions, which, according to the data of experimental petrology, may be stable only at pressures of the lower mantle, provides unambiguous evidence for vertical movements resulting in transport of the material from deep geospheres (probably from the mantle/core boundary) to the Earth's surface or upper horizons of the crust. Numerous data demonstrate that peridotites dominate in the upper mantle, although eclogites are widely abundant and some other rock types are observed. The composition of the lower mantle zones may be studied from the composition of minerals included in sub-lithospheric diamonds. Multiphase mineral inclusions are rarely observed in such diamonds, and therefore, we may judge on the rock types hosting these diamonds on the basis of the chemistry of individual minerals.

Mineral inclusions in lower mantle diamonds are represented by the mineral association of MgSi-perovskite (*MPv*) + CaSi-perovskite (*CPv*) + ferropericlasite (*FP*). These phases have structures of typical oxides (perovskite CaTiO_3 and periclasite MgO). Therefore, we may conclude that the oxide, but not silicate set of mineral phases, is the fundamental difference of the lower mantle from the upper mantle. The upper horizons of the lower mantle should also contain a high aluminum mineral represented by garnet in products of experiments and the tetragonal phase of pyrope-almandine composition (TAPP) in inclusions in diamonds. With increasing depth and pressure, aluminum solubility in *MPv* increases and garnet disappears. In addition, disproportionating of Fe^{2+} into Fe^{3+} strongly incorporated in *MPv* and Fe^0 results in the appearance of a metal phase (indicated as Met below). *FP* is the most abundant lower mantle mineral, which is observed as an inclusion in sublithospheric diamonds. There is an extensive database on the compositions of ferropericlasite inclusions in diamonds [1].

Assuming that the bulk composition of lower mantle rocks is identical to pyrolite [2], we calculated Mg# of *FP* (atomic values of the $\text{Mg}/(\text{Mg} + \text{Fe})$ ratio) using the method suggested in [3, 4].

We applied equations of partition coefficients Ni/Fe and Mg/Fe between Met, *FP*, and *MPv* for these calculations:

$$K_d^{FP/MPv} (\text{Ni/Fe}) = (\text{Ni/Fe})^{FP}/(\text{Ni/Fe})^{MPv}, (1)$$

$$K_d^{FP/MPv} (\text{Mg/Fe}) = (\text{Mg/Fe})^{FP}/(\text{Mg/Fe})^{MPv}, (2)$$

$$K_d^{\text{Met}/FP} (\text{Ni/Fe}) = (\text{Ni/Fe})^{\text{Met}}/(\text{Ni/Fe})^{FP}. (3)$$

$K_d^{F P/MPv} (\text{Ni/Fe}) = 5$, the average value of the experimental data [5], was accepted. The $K_d^{\text{Met}/FP} (\text{Ni/Fe})$ values were previously calculated for various temperatures and pressures [3, 4].

In addition, we applied the mass balance equations like

$$\sum_i C_i \cdot F_i = C_i^0 (4)$$

where C_i is the concentration of this component in the i th phase; C_i^0 is the concentration of the component in the whole system; F_i is the portion of the i th phase in the system. The assumption that aluminum is entirely incorporated in MPv and calcium in CPv allows us to reduce the number of equations (4) to two. The simultaneous equations were solved using the algorithms available in the MATLAB software.

At a fixed bulk composition of the system, Mg# of FP and MPv has been controlled by the $K_d^{F P/MPv} (\text{Mg/Fe})$ values. This parameter was measured experimentally in many studies ([6] and references therein). It was demonstrated that this value for pyrolite ranged within 0.4-0.85 depending on the pressure and, consequently, on depth in the lower mantle, which is partly explained by variation of the aluminum concentration in MPv [6]. At such values of $K_d^{F P/MPv} (\text{Mg/Fe})$, the calculated variation of Mg# for the bulk pyrolite composition provides a range of 0.82-0.88 (fig. 1). The results presented in fig. 2 demonstrate that, except for the data on Brazilian diamonds containing an unusually high proportion of iron-rich ferropericlasses or magnesiowustites, 92 % of the values for Mg# of FP inclusions plot in this range. As a whole, this is consistent with the assumption that the composition of the lower mantle is close to pyrolite in relation to major components.

However, it is necessary to discuss the probable influence of other factors on compositional variations of lower mantle phases. The formation of the metal phase as a result of FeO disproportionation should result in an increase of Mg# of both FP and MPv . The content of the iron-nickel alloy is close to 1 % under the lower mantle conditions [8]. As is evident from fig. 1, the value of Mg/(Mg + Fe) increases in comparison with the system free of the metal phase by ~0.02 ranging from 0.87 to 0.9. However, the concentration of nickel in ferropericlasse should decrease remarkably due to its transition into the metal phase, as was demonstrated in [3, 4] (fig. 3). In fact, the concentration of Ni in FP with a Mg# > 0.8 is close to 1% (fig. 2), which is significantly higher than that estimated for lherzolite with 1 % of the metal alloy. Hence, FeO disproportionation does not have a significant influence on the composition of ferropericlasses captured by lower mantle diamonds.

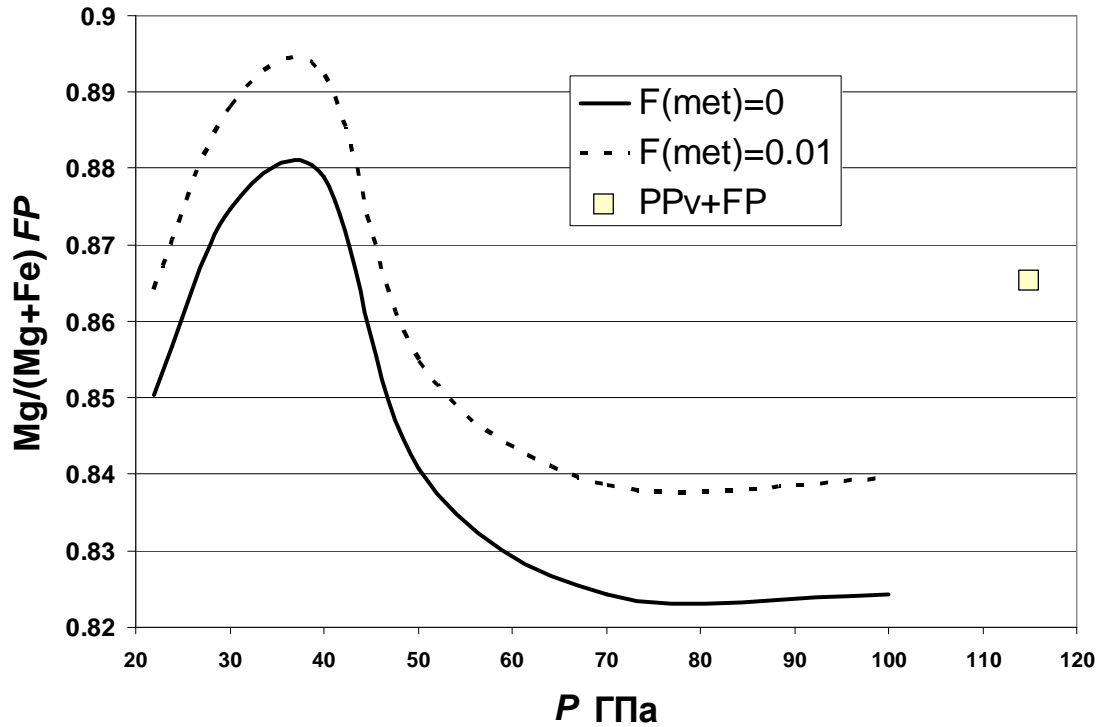


Fig. 1. Calculated Mg# of ferropericlasite for the bulk composition of pyrolite depending on pressure in the lower mantle.

The coefficients of Mg/Fe exchange between *FP* and *MPv* are taken from [6]. *F(Met)* is the weight fraction of the metal phase in the system. *PPv* is the post-perovskite phase with CaIrO_3 -type structure, for which the coefficient of exchange with *FP* is taken from [5].

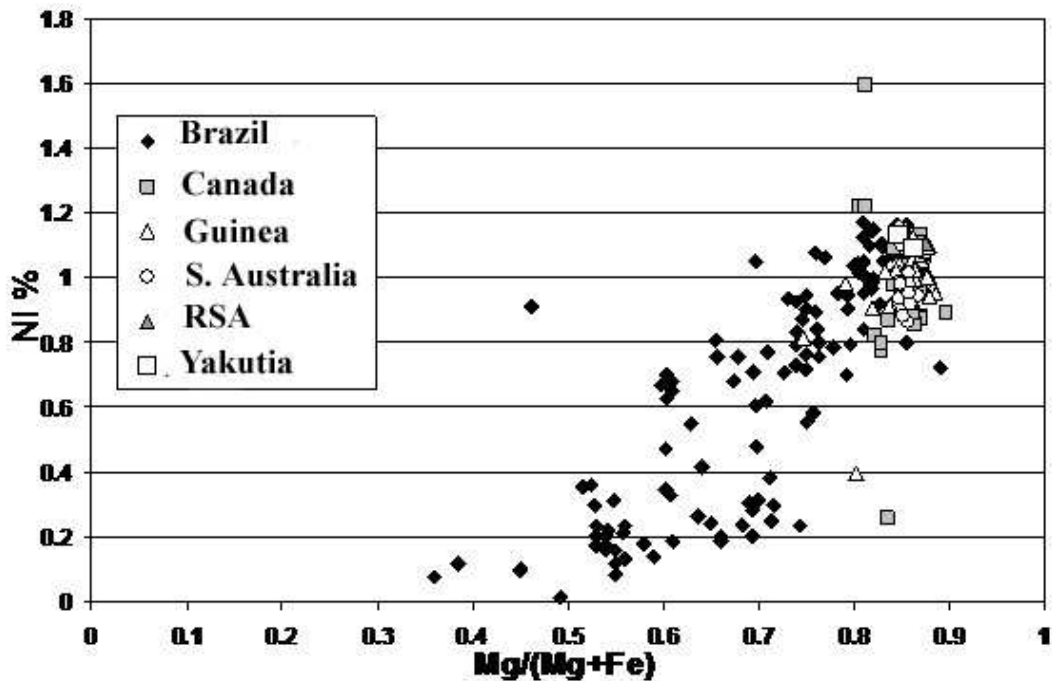


Fig. 2. Dependence of the nickel concentration on Mg# for ferropericlasite in diamond inclusions from various regions worldwide.

References are given in [1]; the data for Yakutia are taken from [7].

Different bulk compositions of rocks are another factor that may control the compositional variations of sublithospheric *FP*. The abundance of the lower mantle minerals included in diamonds (ferropericlase, 56 %; MgSi-perovskite, 8 %; CaSi-perovskite, 12 %; other minerals, 24 %) differs significantly from the calculated values for pyrolite (ferropericlase, 18 %; MgSi-perovskite, 77 %; CaSi-perovskite, 5 %), which was considered [1] as proof of the difference between the compositions of the lower mantle and the upper mantle. In particular, the presence of more high-temperature rocks, such as harzburgite, in addition to primitive lherzolite in the lower mantle may result in the appearance of ferropericlases with slightly different compositions in comparison with the minerals of lower mantle rocks of the pyrolite composition. On the one hand, Mg# of the bulk composition of mantle substrate increases, and, on the other hand, the constants of exchange reactions between components of *FP* and *MPv* change.

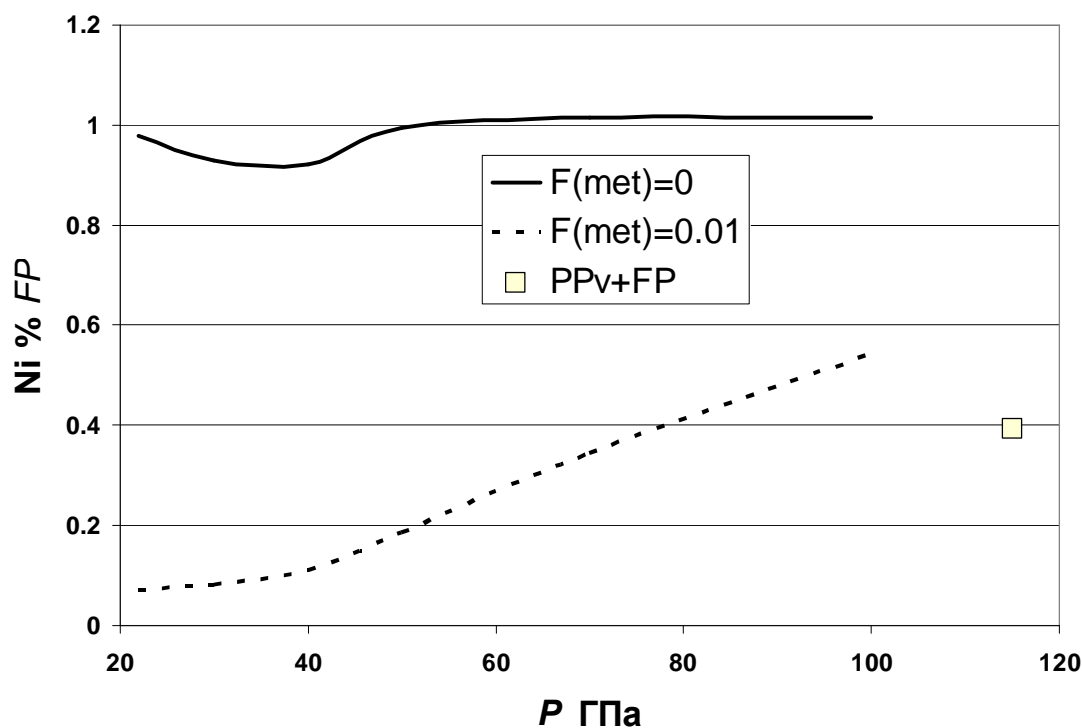


Fig. 3. Calculated values of nickel concentrations in ferro-periclase in dependence on pressure for the pyrolitic bulk composition.

Constants of Ni/Fe and Mg/Fe exchange are taken from [4, 6].

Comparison of the data from [5, 6] demonstrates that at low Al_2O_3 concentrations typical of rocks of the harzburgite composition, $K_d^{F P/MPv}$ (Mg/Fe) values should decrease remarkably at pressures >70 GPa due to the transition of iron to the low-spin state in ferro-periclase. The calculations performed for the typical composition of mantle harzburgite (Sample 125-780C-6R-1,61-62 [9]) using the $K_d^{F P/MPv}$ (Mg/Fe) values given in [5] demonstrated that at pressures up to 100 GPa Mg# of ferropericlases from rocks of the harzburgite composition were consistent with the values estimated for the pyrolitic lower mantle (fig. 4). At

higher pressures corresponding to the D'' zone at the boundary between the mantle and the metallic core, when magnesium metasilicate is represented by the post-perovskite phase with the CaIrO_3 -type structure, the affinity of siderophile elements (Fe and Ni) to this phase is higher than that to MPv [5]. Consequently, $Mg\#$ of ferropericlase increases up to 0.9, which is remarkably higher than for the pyrolitic bulk composition and becomes close to the maximal values observed in FP captured by diamonds.

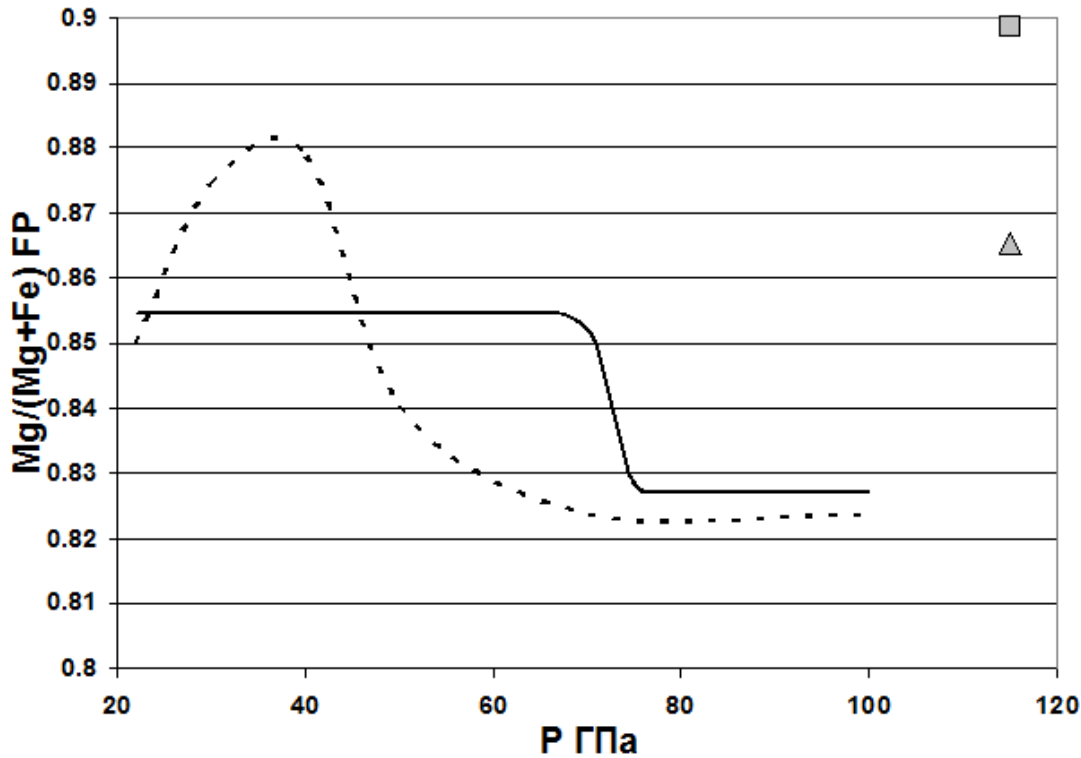


Fig. 4. Calculated $Mg\#$ of ferropericlase for the bulk composition of pyrolite (dashed line) and harzburgite (solid line) in dependence on pressure in the lower mantle.

The coefficients of Mg/Fe exchange between FP and MPv for lherzolite are taken from [6]; for harzburgite, from [5]. The triangle (for lherzolite) and square (for harzburgite) are the results of calculations for the equilibrium of FP with post-perovskite phase (CaIrO_3 -type structure), for which the exchange coefficient is taken from [5].

Diamonds from Brazilian deposits contains a significant number of ferropericlase and magnesiowustite inclusions with much higher $Mg\#$ than that of the minerals of the lower mantle parageneses of peridotite composition (fig. 2) [10-12]. It is natural to assume that the presence of such material with a low $Mg\#$ may be related to subduction of the oceanic crust to the lower mantle. However, we should take into account that the average composition of MORB has significantly higher $Mg\#$ ($Mg/(Mg + Fe) = 0.61$ for N-MORB) in comparison with the least magnesium ferropericlases from inclusions in Brazilian diamonds ($Mg/(Mg + Fe) < 0.5$, fig. 2). In addition, FP is absent in mineral associations of the bulk N-MORB composition under the lower mantle temperatures and pressures. Instead of this phase, high-

pressure silica polymorphs (stishovite, and phases with CaCl₂-type and then α -PbO₂-type structures at higher pressures [13]) coexist with “perovskites” (*MPv* and *CPv*).

We may assume that the formation of iron-rich fer-ropericlases occurred in rocks that are a mixture of peridotitic and basaltic compositions. Our calculations demonstrate that the mixture of 50 % pyrolite + 50 % N-MORB provides ferropericlasite with $Mg/(Mg + Fe) = 0.66$ under the lower mantle conditions at 70 GPa, which is still much higher than the values for the most iron-rich magnesiowustites in diamonds from Brazilian deposits. In addition, we should mention that a mixture of such composition will contain only ≈ 1 % of *FP*; further increase of the N-MORB content will result in disappearance of ferropericlasite and the formation of silica phases.

In principle, the source of lower mantle rocks with iron-rich magnesiowustite may be represented by layered intrusions of ultrabasic-basic composition (like Skaergaard), including iron-rich late differentiates, and subducted to the lower mantle. However, this scenario seems unlikely.

More likely we may assume that iron-rich *FP* may be formed as a result of magma fractional crystallization directly in the lower mantle. Such a likelihood is supported by the experimental data [14, 15] demonstrating that constants of Mg/Fe exchange between the melt and lower mantle phases ($K_d = (Mg/Fe)_{melt}/(Mg/Fe)_{crystals}$) are always < 1 , similarly to those for olivine and pyroxenes under crustal conditions; consequently, the Fe/Mg ratio increases during fractional crystallization.

We may note that some researchers assume the presence of cumulates of iron-rich magnesiowustite near the core/lower mantle boundary, the origin of which results from solidification of the basal magmatic ocean at the early stages of the Earth's history [14].

As a whole, comparison of the results of model calculations with the database on the composition of fer-ropericlasite inclusions in diamonds demonstrates that the lower mantle is mostly composed of rocks of peridotitic composition most likely including fertile varieties close to pyrolite, as well as more refractory rocks of harzburgitic composition. Study of the composition and conditions of the formation of the lower mantle minerals transported as inclusion in diamonds to the surface zones of the Earth is very important, because it provides information necessary for understanding of the mechanism of the origin of mantle plumes and the nature of the material participating in uprising flows of matter in deep geospheres. It is also important that this material is one of the components of kimberlite magmas.

This study was supported by the Russian Foundation for Basic Research (project nos. 11-05-00247-a and 11-05-12004-ofi-m), the Earth Science Section (program no. 2), and the Presidium of the Russian Academy of Sciences (program no. 2).

REFERENCES

1. **F. V. Kaminsky**, *Earth-Sci. Rev.* 110, 127 (2012).
2. **H. Palme and H. S. C. O' Neill**, in *Treatise on Geochemistry*, vol. 2: The Mantle and Core (Elsevier, Amsterdam, 2003), pp. 1–38.
3. **D. Ryabchikov**, *Dokl. Earth Sci.* 438 (2), 788 (2011).
4. **D. Ryabchikov and F. V. Kaminsky**, *Geol. Ore Deposits* 55, 1 (2013).
5. **L. Auzende, J. Badro, F. J. Ryerson, et al.**, *Earth Planet. Sci. Lett.* 269, 164 (2008).
6. **T. Irifune, T. Shinmei, C. A. McCammon, et al.**, *Science* 327, 193 (2010).
7. **D. A. Zedgenizov, E. S. Efimova, A. M. Logvinova, et al.**, *Dokl. Earth Sci.* 377A, 319 (2001).
8. **D. J. Frost and C. A. McCammon**, *Annu. Rev. Earth. and Planet. Sci* 36, 389 (2008).
9. **J. A. Pearce, S. R. Van der Laan, R. J. Arculus, et al.**, *Proc. Ocean Drill. Program. Sci. Results* 125, 623 (1992).
10. **F. V. Kaminsky, O. D. Zakharchenko, R. Davies, W. L. Griffin, G. K. Khachatryan-Blinova, A. A. Shiryaev**, *Contrib. Mineral. Petrol.* 140, 734 (2001).
11. **F. V. Kaminsky, G. K. Khachatryan, P. Andreazza, et al.**, *Lithos* 112, 833 (2009).
12. **P. C. Hayman, M. G. Kopylova, and F. V. Kaminsky**, *Contrib. Mineral. Petrol.* 149, 430 (2005).
13. **K. Hirose, N. Takafuji, N. Sata, and Y. Ohishi**, *Earth Planet. Sci. Lett.* 237, 239 (2005).
14. **R. Nomura, H. Ozawa, S. Tateno, et al.**, *Nature* 473, 199 (2011).
15. **D. Andrault, S. Petitgirard, G. Lo Nigro, et al.**, *Nature* 487, 354 (2012).

TRACE ELEMENT COMPOSITION OF PRIMITIVE MANTLE – NON-CHONDRITE MODEL

Koctizin YR. A.

*Vernadsky Institute of Geochemistry and Analytical Chemistry,
Russian Academy of Sciences; e-mail @geokhi.ru*

ABSTRACT

The analysis of the isotope data obtained by now for the rocks of various genesis gives estimation of $^{143}\text{Nd}/^{144}\text{Nd}$, $^{176}\text{Hf}/^{177}\text{Hf}$, $^{87}\text{Sr}/^{86}\text{Sr}$, $^{206}\text{Pb}/^{204}\text{Pb}$, $^{207}\text{Pb}/^{204}\text{Pb}$, $^{208}\text{Pb}/^{204}\text{Pb}$ and Sm/Nd, Lu/Hf, Rb/Sr, U/Th/Pb values in the primitive mantle of the Earth. The model of chondrite homogeneous reservoir (CHUR) for the composition of the primitive mantle [1], taken at first as a basis, causes a number of doubts: (1) high magmatic productivity of depleted mantle (DM), with the absence a steady isotope signal from the primitive mantle (PM); (2) a great number of geochemically enriched rocks, in particular alkaline basalts, showing the isotope characteristics similar to those of DM; (3) depletion of the source of HIMU basalts in Nd-Sr-Hf isotope system and its enrichment in U-Pb system; (4) mass balance calculations for Sm-Nd isotope system of the crust and mantle force to limit the mass of DM which was a source for the crust to 1/4 - 1/5 of the total mantle mass. However, in this case the balance is broken down for a number of other elements in Rb-Sr and U-Pb systems; (5) melts from PM at high melting degrees should have Nd isotope composition and Sm/Nd values similar to those of the source; however the rocks being similar to CHUR by both parameters have not been found yet.

The above conflicting issues can be solved only if we assume that Sm/Nd value in the primitive mantle differs from CHUR composition by 8 %. Correlation of isotope ratios in mantle rocks allows other parameters of the primitive mantle source to be sought. It also allows using element ratios instead of isotope ratios:

$$\begin{aligned} \epsilon_{\text{Nd}} &= +9; \quad ^{143}\text{Nd}/^{144}\text{Nd} = 0,51309; \quad \text{Sm}/\text{Nd} = 0,350; \\ \epsilon_{\text{Hf}} &= +14; \quad ^{176}\text{Hf}/^{177}\text{Hf} = 0,28318; \quad \text{Lu}/\text{Hf} = 0,268; \\ \epsilon_{\text{Sr}} &= -22; \quad ^{87}\text{Sr}/^{86}\text{Sr} = 0,7029; \quad \text{Rb}/\text{Sr} = 0,0206; \\ ^{206}\text{Pb}/^{204}\text{Pb} &= 18,37; \quad ^{207}\text{Pb}/^{204}\text{Pb} = 15,49; \quad ^{208}\text{Pb}/^{204}\text{Pb} = 37,97; \\ ^{238}\text{U}/^{204}\text{Pb} &= 8,82; \quad \text{r.e. U}/\text{Pb} = 0,1405; \quad ^{232}\text{Th}/^{238}\text{U} = 3,81, \quad \text{r.e. Th}/\text{U} = 3,68. \end{aligned}$$

A possible analytical uncertainty of Nd isotope composition analysis does not exceed $\pm 1 \epsilon_{\text{Nd}}$.

Following the model by DePaolo and Vasserburg [1, 5] the most popular, standard isotope-geochemical models of the mantle structure and evolution [2-4] assume that Sm-Nd system of the primitive mantle corresponds to the chondritic homogeneous reservoir (CHUR). It was called homogeneous because chondrites of

different groups turned out to be homogeneous as regard to Sm/Nd value [6, 7]. Lu-Hf isotope system uses the data by Tatsumoto et al., [8] specified later by Bouvier et al., [9] obtained by them for the collection of chondrites.

The correlation between mantle composition and chondrites is not observed in Rb-Sr and U-Pb isotope systems: Rb/Sr value is one order higher in chondrites as compared with the Earth's mantle while U/Pb value is one order lower [10] that results from high volatility of lead and rubidium and their loss during the Earth's accretion. Thus, it had been considered for a long time that Sm/Nd and Lu/Hf values of the Earth's mantle are similar to chondrite.

It is impossible to check this assumption via a direct comparison of chondrite composition and that of rocks. Rare lherzolite nodules which could characterize the primitive mantle of the Earth [11-14], demonstrate a wide scatter in Sm, Nd, Lu, Hf contents and their ratios so they can provide reliable estimates.

However, a great scope of data on Nd and Hg isotope composition has been accumulated for various rocks of the mantle origin which can be used to estimate Sm/Nd and Lu/Hf values both for the source and for the whole mantle that participated in the petrogenesis during the whole Earth's history. The present article is devoted to this problem.

The data on real composition of the primitive, not differentiated mantle has fundamental value not only for geochemistry, but for other branches of Earth sciences as well; for correct understanding of the processes occurring in its bowels. Only knowing the composition of the primitive mantle we can discuss the composition and ways of generation of enriched and depleted mantle, the nature of isotope and chemical inhomoginities in the mantle, the interaction between the crust and the mantle.

CHONDRITE MODEL OF EARTH MANTLE IN ND-SR ISOTOPE SYSTEM

The negative correlation between Nd and Sr isotopes found by DePaolo and Vasserburg [1, 5] for the mantle rocks (fig. 1) provided a new model of mantle evolution. According to that model the initial, primitive mantle in Sm-Nd system corresponded to CHUR with modern values¹.

$$\varepsilon_{Nd}^T = \left[\frac{\left(\frac{^{143}Nd}{^{144}Nd} \right)_{Sample}^T}{\left(\frac{^{143}Nd}{^{144}Nd} \right)_{CHUR}^T} - 1 \right] \cdot 10^4 \quad (1)$$

$$\left(\frac{^{143}Nd}{^{144}Nd} \right)_{Sample}^T = \left(\frac{^{143}Nd}{^{144}Nd} \right)_{Sample}^0 - \left(\frac{^{147}Sm}{^{144}Nd} \right)_{Sample} \cdot [exp(\lambda \cdot T) - 1]$$

$$\left(\frac{^{143}Nd}{^{144}Nd} \right)_{CHUR}^T = 0.512638 - 0.1967 \cdot [exp(\lambda \cdot T) - 1]$$

¹ All Nd isotope ratios given in this paper are normalized from $^{146}Nd/^{144}Nd = 0.7219$

In due time the depleted mantle (DM) with higher Sm/Nd values generated as a result of the extraction of the crust with lower Sm/Nd value. As radiogenic ^{143}Nd is formed from ^{147}Sm decay $^{143}\text{Nd}/^{144}\text{Nd}$ value becomes higher if Sm/Nd value is higher, that is typical of the depleted mantle.

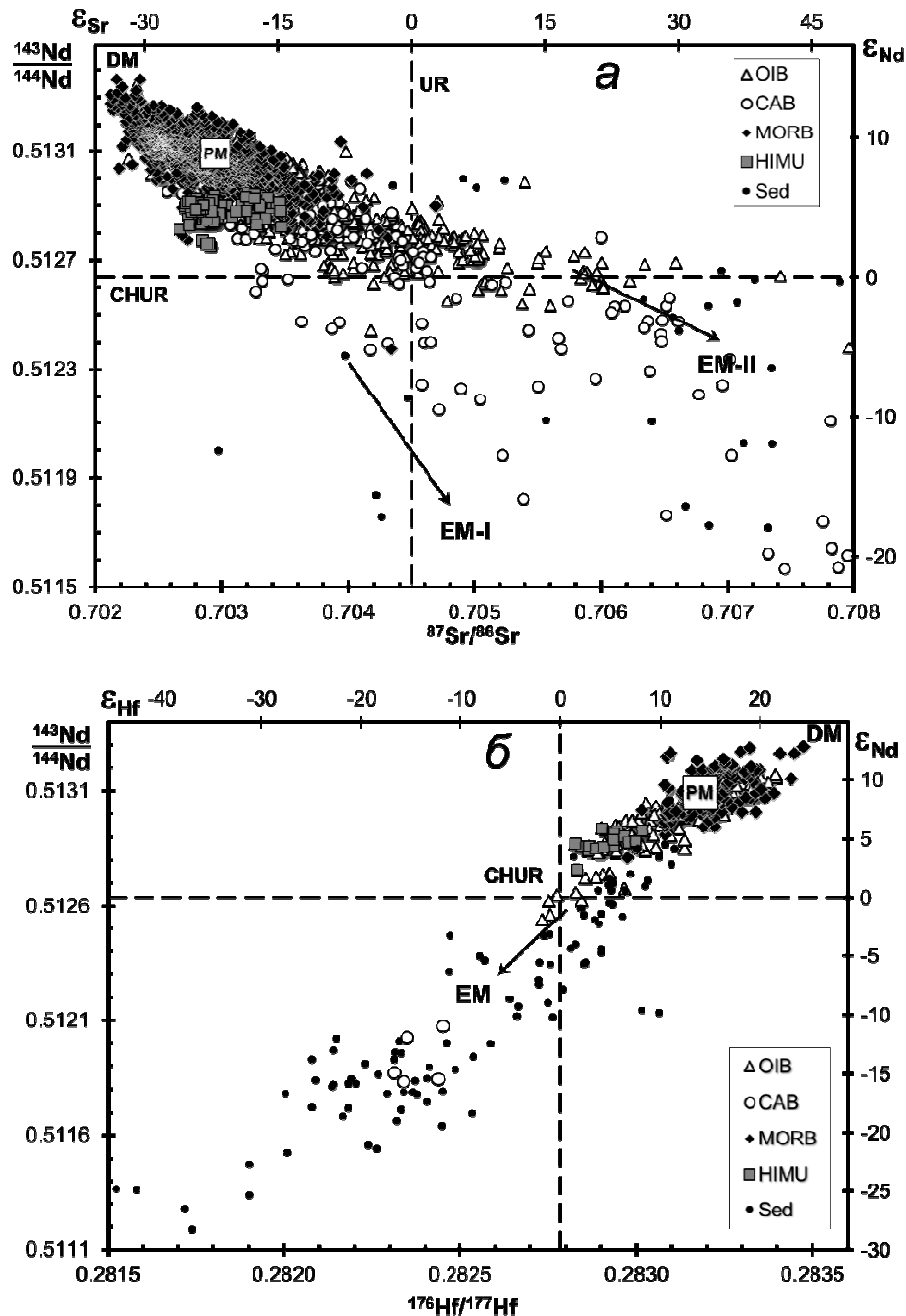


Fig. 1. Nd, Sr, Hf isotope ratios in mid-ocean ridge (MORB), oceanic (OAB) and continental (CAB) alkaline basalts, in basalts with increased U/Pb values in the source (HIMU), as well as in various sedimentary rocks (Sed).

The composition of the primitive mantle (PM) is shown from present studies (see below) and does not correlate with the chondrite model by DePaolo and Vasserburg [1, 5]. $(^{143}\text{Nd}/^{144}\text{Nd})_{\text{CHUR}} = 0,512638$ and $(^{147}\text{Sm}/^{144}\text{Nd})_{\text{CHUR}} = 0,1967$; i.e. $\text{Sm}/\text{Nd} = 0,325$ [15]. A scatter of this value is widely used as one more way to represent the isotope data.

Negative correlation between $^{143}\text{Nd}/^{144}\text{Nd}$ and $^{87}\text{Sr}/^{86}\text{Sr}$ in various mantle rocks suggested that their source (sources) demonstrate global negative correlation between Sm/Nd and Rb/Sr values. This conclusion correlates with geochemical data: geochemically depleted rocks show increased Sm/Nd and decreased Rb/Sr values while enriched rocks show decreased Sm/Nd and increased Rb/Sr values.

Because the primitive mantle is different from chondrite in Rb-Sr system it was simply called as homogeneous reservoir (UR), and strontium isotope composition in it was defined as a crossing point of trend of indirect correlation of Sr and Nd isotope ratios with ϵCHUR line or $\epsilon_{\text{Nd}} = 0$ on fig. 1a. From the value $(^{87}\text{Sr}/^{86}\text{Sr})_{\text{UR}} = 0,7045$ it is easy to calculate $(\text{Rb}/\text{Sr})_{\text{UR}}$ value if we accept the age of the Earth T as 4,56 Ga, and the primary Sr isotope ratio as $(^{87}\text{Sr}/^{86}\text{Sr})_{\text{BABI}} = 0,69897$ [16]:

$$\left(\frac{^{87}\text{Rb}}{^{87}\text{Sr}}\right)_{\text{UR}} = \frac{\left(\frac{^{87}\text{Sr}}{^{86}\text{Sr}}\right)_{\text{UR}} - \left(\frac{^{87}\text{Sr}}{^{86}\text{Sr}}\right)_{\text{BABI}}}{\exp(\lambda_{87}T) - 1} \quad (2)$$

Hence it follows that $(\text{Rb}/\text{Sr})_{\text{UR}} = 0,0286$.

Similarly to ϵ_{Nd} (formula 1), ϵ_{Sr} value for any time T is calculated relative to UR composition.

As seen from fig. 1 with a greater scope of data for mid ocean ridge basalts (MORB) [17-45], intra-plate ocean island basalts (OIB) [46-73], continental basalts [12, 74-82] and silicate-fragmentary sediments and sedimentary rocks [83-97] the mantle trend became slightly fuzzy than it looked originally [1], but as a whole the pattern has not changed. Left top quadrant on fig.1a with low Sr isotope and high Nd isotope ratios corresponds to the depleted mantle. Right bottom quadrant corresponds to the enriched sources; moreover, the origin of the enriched mantle is usually related to subduction and partial contribution of the crust's substance into a deep-seated mantle [2-4].

In Lu-Hf system the composition of the primitive mantle is also regarded as the chondritic [8, 9], with following recent values $\text{Lu}/\text{Hf} = 0,235$ and $^{176}\text{Hf}/^{177}\text{Hf} = 0,282785$. ϵ_{Hf} value is calculated relative to this isotope ratio. Though the published Hf isotope data are much less, as compared to those for Sr and Nd figure 1 shows a clear direct correlation between Nd isotope and Hf isotope data in various rocks [35, 38, 39, 43, 44, 98-102] that suggests a direct correlation between Sm/Nd and Lu/Hf values in sources of these rocks.

Both plots (fig. 1a and fig. 1b) show that the isotope composition of a prospective primitive mantle ($\epsilon_{\text{Nd}} = 0$, $\epsilon_{\text{Hf}} = 0$, $\epsilon_{\text{Sr}} = 0$) [6-8] lies within trends for mantle rocks that confirms a correct use of those values as the beginning of isotope co-ordinates. However, as it is discussed below, there are reasons using the more available data to analyze again the model proposed by DePaolo and Vasserburg [1, 5] and developed by other researchers.

CONTRADICTIONS TO CHONDRITE MODEL

The assumption that in the Sm-Nd isotope system the primitive mantle is similar to chondrites [1, 5] has been never strictly proved. A greater scope of isotope data for the rocks of mantle origin also induces debates concerning the chondrite model. We will consider the most significant discrepancies [103].

PRODUCTIVITY OF DEPLETED AND NON-DEPLETED MANTLE

If we follow the model by DePaolo and Vasserburg, the most productive source for melts was the depleted mantle ($\epsilon_{Nd} > 0$, $\epsilon_{Hf} > 0$, $\epsilon_{Sr} < 0$). This situation is strange enough, as it would be logical to expect that preceding melting of mantle sources would lead to removal of the most easily melted, mobile component, and with other things being equal the depleted sources should be less productive than non-depleted.

The primitive not depleted mantle with $\epsilon_{Nd} = 0$, $\epsilon_{Hf} = 0$, $\epsilon_{Sr} = 0$, on the contrary, does not show any rocks of homogeneous isotope composition. If the primitive mantle exists and its share by different estimations ranges from $\frac{1}{2}$ to $\frac{3}{4}$ of the mantle's mass [2-4] it would be logical to expect frequent occurrence of rocks with its isotope labeling. We would observe a steady cluster of the rocks whose source was a non-depleted mantle. However, it is not true. The geological community has already recognized this circumstance using T_{DM}^{Nd} [104] instead of T_{CHUR}^{Nd} for estimations of modeled age of the rocks substratum as was initially proposed by DePaolo and Vasserburg [1, 5].

SOURCES OF ALKALINE BASALTS

Alkaline basalts of continents and oceans, enriched by incoherent elements are mainly the products of the depleted mantle (fig. 1). This contradiction is traditionally explained by the mantle metasomatism of the source prior to its melting [105]. Probably, the metasomatism contributes to the origin of alkaline basalts, however the reason of transfer of lithophile elements from the depleted mantle is not still clear. At that the primitive mantle remains unchanged.

ISOTOPE SYSTEMATICS OF HIMU BASALTS

The origin of HIMU basalts is still a subject of intense debate in the geochemical models which use the chondrite Earth's composition. These basalts occur both in oceanic and in continental setting: on several islands in the French Polynesia chain in the Pacific ocean [39, 50, 64, 65, 106-109], in a chain of islands in the Atlantic ocean stretching from Saint Helena island to coast of Cameroon towards far inland [39, 110-112], on Komorsky archipelago [63, 111], within the East African rift system [113], as well as on the Antarctic Pacific coast, Hobbs Coast [81]. In continental setting they include rift alkaline basalts, in oceanic they comprise mainly alkaline basalts of island chains interpreted as traces of "hot

spots".

Like any alkaline basalts, HIMU basalts are enriched by many lithophile elements, including U, Pb, Rib, Sr, LREE. They are united into a specific group judging from the increased values of lead, first of all $^{206}\text{Pb}/^{204}\text{Pb}$ ratio that suggests high U/Pb values in their source, i.e. high $^{238}\text{U}/^{204}\text{Pb}$ values. Thus, their sources are enriched in U-Pb isotope system: figure 2 shows that μ value can be high as 22, whereas in the mantle it is significantly lower, about 8-9 [114, 115].

This phenomenon can be explained by lead removal with island-arc magmas from subsiding oceanic plates in subduction zones [4, 37]. As a result, the rocks demonstrating increased U/Pb values due to the loss of lead could be generated. As the main argument in favor of this assumption Hofmann et al. [37, 116] and their followers [117] pointed out lower U/Pb values in island-arc basalts as compared with other oceanic rocks. figure 3a shows that Coe/Pb value is lower [118-125] in island arc basalts as compared with MORB, alkaline basalts of oceans and continents including HIMU basalts. Nevertheless, fig. 3 demonstrates that formation of island arc basalts cannot lead to increase of U/Pb value in the mantle because μ amounts to 8,8 as an average, i.e. similar to mantle bulk composition (see fig. 8). It is obvious that removal of any quantity of island arc melts from the rocks that have the same initial U/Pb value cannot lead to its change.

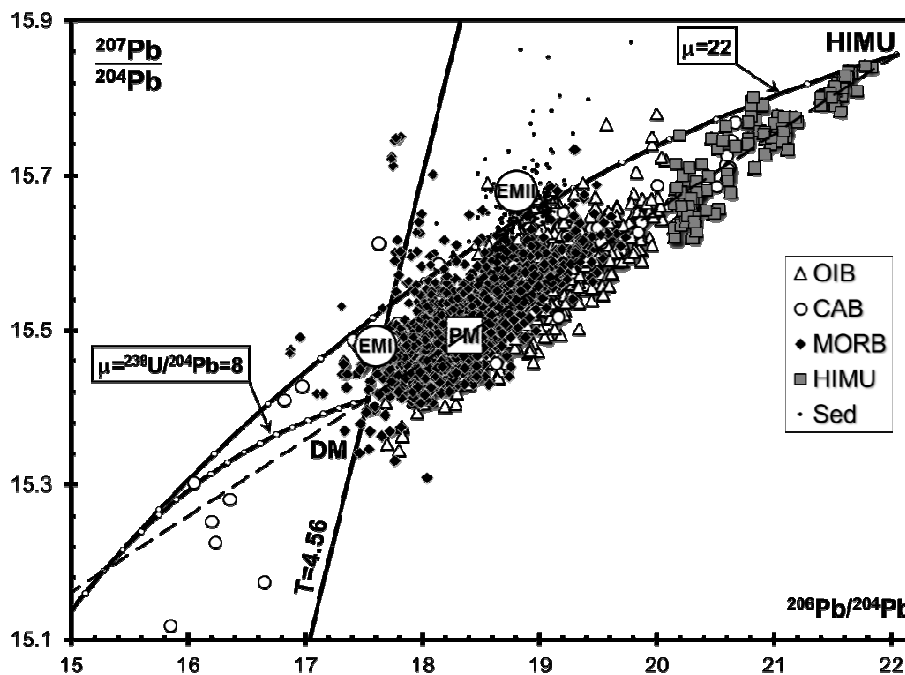


Fig. 2. Isotope lead ratios in the same rocks shown in fig. 1. HIMU basalts are arbitrarily distinguished on border $^{206}\text{Pb}/^{204}\text{Pb} > 20$.

Figure 3 b exhibits that U/Pb value in MORB dolerites and alkaline basalts from oceans and continents increases with the increase of uranium and lead concentrations i.e. with the enrichment by lithophile elements.

Fig. 3 b shows that $^{238}\text{U}/^{204}\text{Pb}$ value in HIMU basalts makes up 34 (n = 69) as an average that well agrees with the increased μ value in their source (fig. 2).

However, the enrichment of sources of HIMU basalts in U-Pb system does not agree with Sr-Nd isotope systematics by De Paolo and Vasserburg (fig. 1a) according to which they are generated from the depleted source ($\epsilon_{Nd} = +5, 1 \pm 0, 9$; $\epsilon_{Sr} = -22 \pm 6$).

This is one more essential contradiction of modern isotope geodynamics.

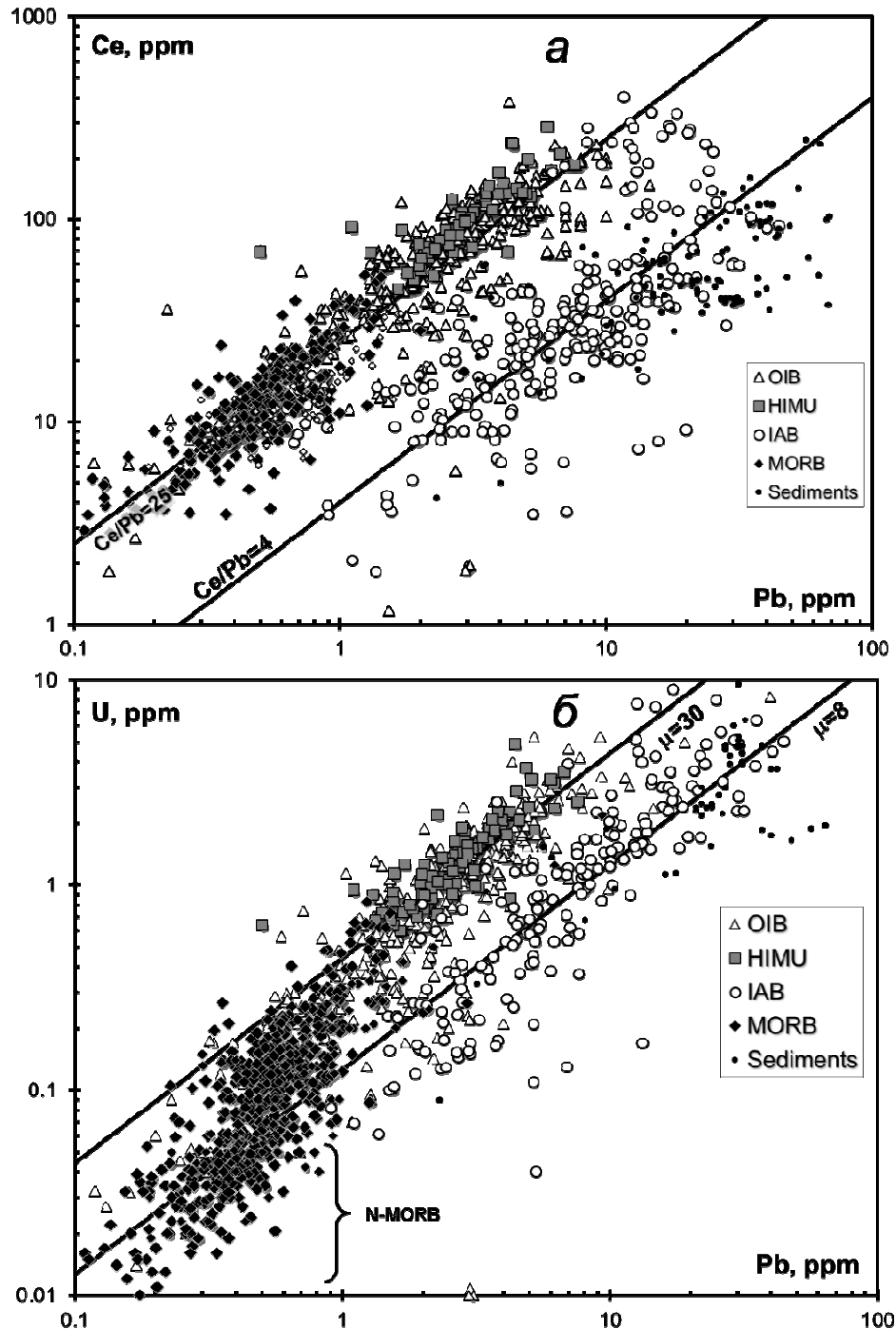


Fig. 3. Ratios between cerium, lead and uranium in the same rocks shown in fig. 1, as well as in island arc basalts (IAB).

DISBALANCE OF SYSTEM CRUST – UPPER MANTLE

Mass balance modeled calculations for Sm-Nd isotope system of the crust and the mantle force to limit a share of the depleted mantle to 1/4 -1/5 of its total mass [2-4]. Only in this case Sm/Nd value in the depleted mantle could be change due to the extraction of the crust to the value so it could guarantee the difference in Nd isotope composition observed today between DM and CHUR as $\epsilon_{Nd} = 8-12$.

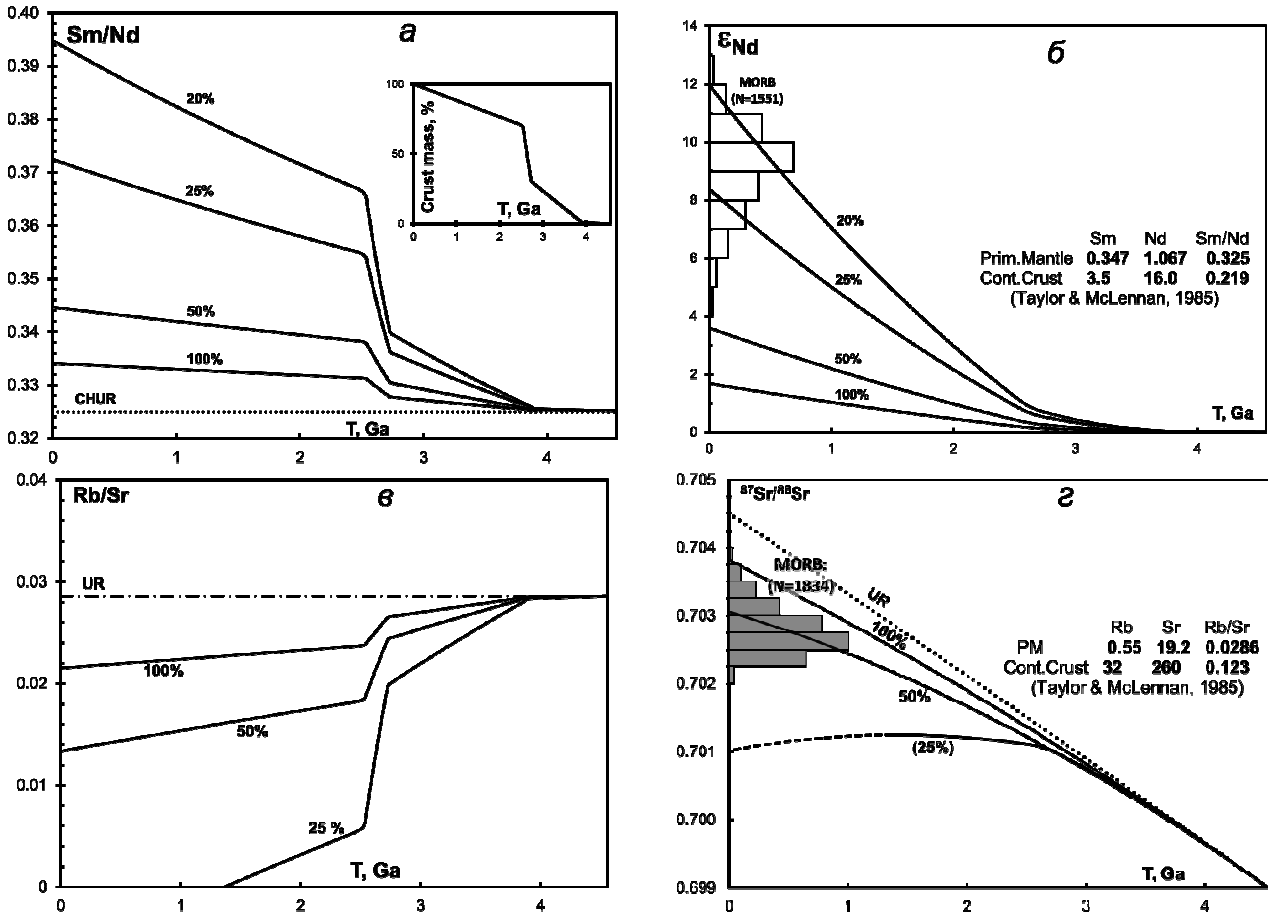


Fig. 4. Examples of numerical modeling of Sm/Nd (a) and Rb/Sr (c) values of isotope composition of neodymium (b) and strontium (d) in the depleted mantle as a result of the continental crust extraction.

The trajectory of growth of relative crust's mass is shown on the inset of diagram according to [126]. The plots a and b show four options of calculations: with the extraction of the crust from the whole ("100 %" plot), from half ("50 %"), from a quarter ("25 %") and 1/5 ("20 %") of total mantle's volume. Three options are shown for Rb-Sr system - 100 %, 50 % and 25 %. In the latter case rubidium is not sufficient for the crust generation, and the modeled "25 %" plot on the diagram stops at 1,3 Ga. For comparison with modeled plots diagrams b and d give the data for MORB as histograms.

To illustrate this situation fig. 4 demonstrates the results of numerical modeling of continental crust extraction out of the mantle. The data for calculations are given on fig. 4 b and fig. 4 d. The rate of crust generation was

taken as variable, as shown in inset on fig. 4a and, according to the conclusions by Taylor and McLennan [126]. However, the crust's growth doesn't influence much Nd and Sr isotope composition in the depleted mantle. In particular, at linear growth of the crust the plots of isotope compositions given on fig. 4 b and fig. 4 d practically coincide. When the crust substance having lower Sm/Nd value = 0,219 is extracted from the mantle substance with initial Sm/Nd = 0,325 (fig. 4 a) the residual, depleted substance have higher Sm/Nd value and this values depends on the amount of the removed crustal component. Therefore, the recent $^{143}\text{Nd}/^{144}\text{Nd}$ value in DM depends on its volume, whether the crust is extracted from the whole mantle or from its small part.

Figure 4b shows that if the source for crust was all mantle the resulting shift in Nd isotope ratio makes $\sim 1,7 \epsilon_{\text{Nd}}$. For half of the mantle the effect would make about $\sim 3,6 \epsilon_{\text{Nd}}$. If 25 % of the CHUR mantle was a source for the earth crust the depleted mantle should differ today from primitive mantle by $\sim 8,4 \epsilon_{\text{Nd}}$ as an average. This value is similar to usual isotope values in MORB though they are slightly lower (fig. 4) and, according to calculations, the observable Nd isotope composition in the MORB source suggests that the depleted mantle makes up 20 - 25 % from all volume of the mantle of the chondrite composition. As the share of the upper mantle (to seismic border of 660 km) makes up 27 % from all mantle, this agreement suggested the identification of the upper mantle with the depleted mantle, that is widely accepted at present.

Strictly speaking, the share of the mantle should be limited by 22-23 % so that Nd isotope composition in the modeled DM corresponds to observable 9-10 ϵ_{Nd} . However, the balance between the crust, primitive and depleted mantle in Sm-Nd system doesn't agree with other isotope systems, in particular with Rb-Sr. Figure 4 demonstrates that if the crust is formed out of 25 % of the mantle, rubidium is not sufficient, and Sr isotope composition (fig. 4) in such depleted mantle is much lower than that observed in MORB. This disbalance is long known [126] and is true not only for rubidium: lead and uranium are also not sufficient to generate the continental crust.

In order to correlate Rb, Pb, U concentrations with the contents of other elements, as well as to correlate Sr isotope composition (fig. 4d) between the crust, primitive and depleted mantle, we should assume that the substance for crust generation was brought from not less than half of the mantle's volume.

Sm-Nd isotope system in oceanic basalts and peridotites

Chemical features of samarium and neodymium are similar. The coefficients of total Sm and Nd distribution during the partial melting of peridotites are not significantly different, not more than by 10-20 % [127]. So, that at small shares of partial melting Sm/Nd value in the melt can differ as much as by 10-20 % from that of the source [128]. At greater melting degrees, about several dozens of percentage, that correspond to the melting of tholeiitic or ultramafic melts the

melts should be only slightly different in Sm/Nd value from the rocks of the source. Thus, at initial chondrite Earth's composition the recent derivatives of the primitive mantle at high melting degrees should have a composition similar to CHUR:

$$\begin{cases} Sm / Nd \approx 0.325 \\ {}^{143}Nd / {}^{144}Nd = 0.512638 \rightarrow (\epsilon_{Nd} \approx 0) \end{cases}$$

The differentiation of substance slightly complicates this pattern, but doesn't deliver from contradictions.

Line 1 shows the model of formation of enriched rocks E from PM source of (with lower Sm/Nd values) and complementary depleted rocks D at various melting degrees in the past. All isotope values change with time as a result of ${}^{147}\text{Sm}$ decay, and present rocks lie on line 2. For better reliability ${}^{147}\text{Sm}/{}^{144}\text{Nd}$ value is to be given on abscissa axis, but this ratio differs from Sm/Nd by almost a constant value 0,6046. Any mixtures of E and D also form the lines passing through PM. The line 3 models modern differentiation of PM source. Note that both line 2 and line 3, as well as any others showing the differentiation of PM source at different time, are the straight lines passing through PM, and, the higher is the melting degree, the closer are the points E and D to PM.

The behavior of Sm-Nd isotope system during partial melting is schematically given on fig. 5. Points along a line 1 schematically show result of differentiation of primary PM source into enriched (E) and depleted (D) compositions in the past. As a result of ${}^{147}\text{Sm}$ decay these rocks have become similar to state shown by line 2. All points corresponding to enriched and depleted rocks (E and D), lie on one straight line (isochron) including initial, primitive PM source. Recent differentiation of PM source is given by straight line 3. Any mixtures of the depleted and enriched rocks in these co-ordinates should lie within a bunch of the straight lines passing through PM point [129].

The higher is the melting degree of the primitive source, the closer are the points E and D to PM. Following the model of chondrite composition of the primitive mantle we can expect that many tholeiitic basalts of oceanic islands (plume-basalts, basalts of "hot spots"), containing a considerable component of the bottom, non-depleted mantle [2-4], on the diagram on fig. 5 should lie close to point PM.

This is true for Lu-Hf systems.

Now we will compare the considered scheme (fig. 5) with real distribution of the data for the rocks of the mantle origin. Figure 6 shows the isotope data for oceanic basalts and sediments in the same co-ordinates, like on the above scheme. The data for oceanic basalts forms a clear trend, but that is amazing, this trend passes away from a point corresponding to modeled composition of the primitive mantle following DePaolo and Vasserburg.

None of more than 2700 points which are available today in our database for oceanic and continental basalts lies close CHUR.

It is true for lherzolites as well, on fig. 6a they lie within a field of basalts and are not crossed with a small area of chondrites.

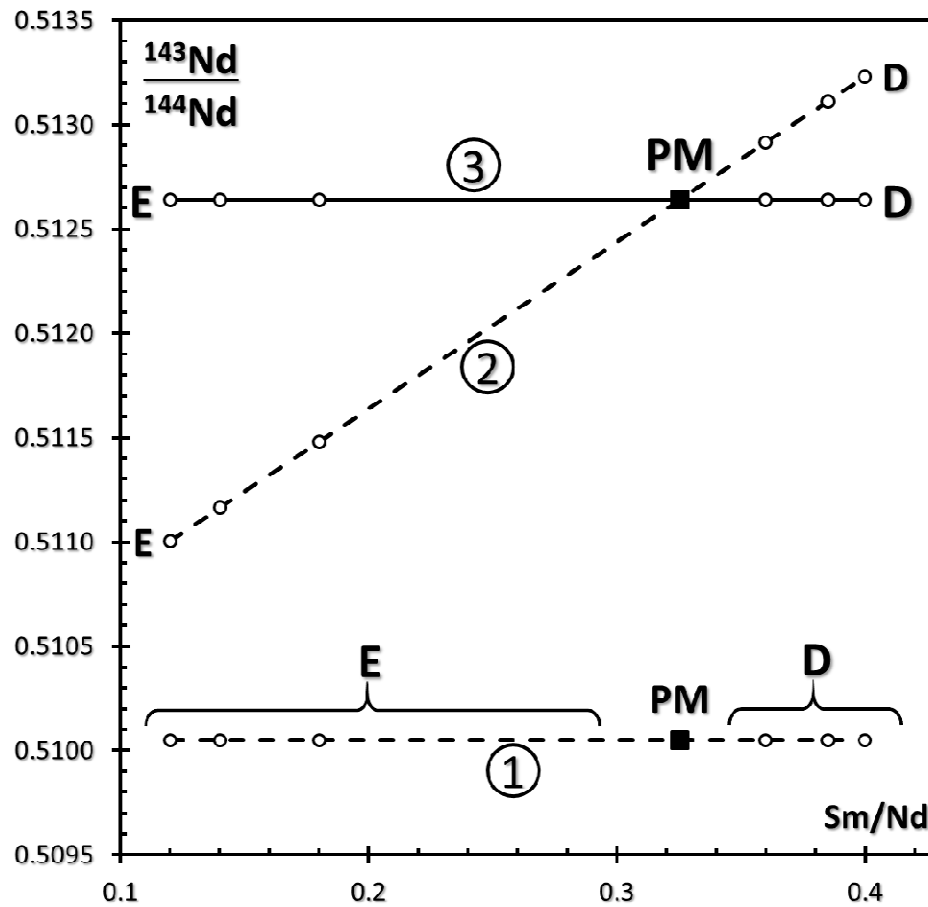


Fig. 5. Ratio between primitive (PM) source and enriched (E) and depleted (D) derivatives.

The same picture is observed in Lu-Hf system, the data for this system is given on figure 6. The main difference between fig.6 a and fig.6 b is the number of points: data for volcanic rocks in Lu-Hf isotope system are much scarce as compared with Sm-Nd system. Nevertheless, fig.6 shows a clear trend for oceanic basalts, and this trend lies apart from chondritic data [9].

The data given on figure 6 can indicate that (1) all known mantle magmatic rocks generated from the depleted mantle only, and the primitive mantle is absolutely “dead” as a magmatic source or (2) Sm/Nd and Lu/Hf values of the primitive mantle do not correlate with CHUR.

Though according to the models of the mantle composition available by now [2 - 4] the major part of magmatic rocks were generated from the depleted source; none of these models suggests absolute isolation of the lower mantle from the upper one. This conclusion can be obtained from fig. 6 if we use the chondrite composition of the primitive mantle. The seismic tomography [130, 131] shows an active contribution of the lower mantle into the geodynamic processes taking place on the surface. In addition, the mass balance contradictions in the system primitive

mantle - crust - the depleted mantle discussed above (fig. 4) do not allow to limit the volume of the depleted mantle by only its small part.

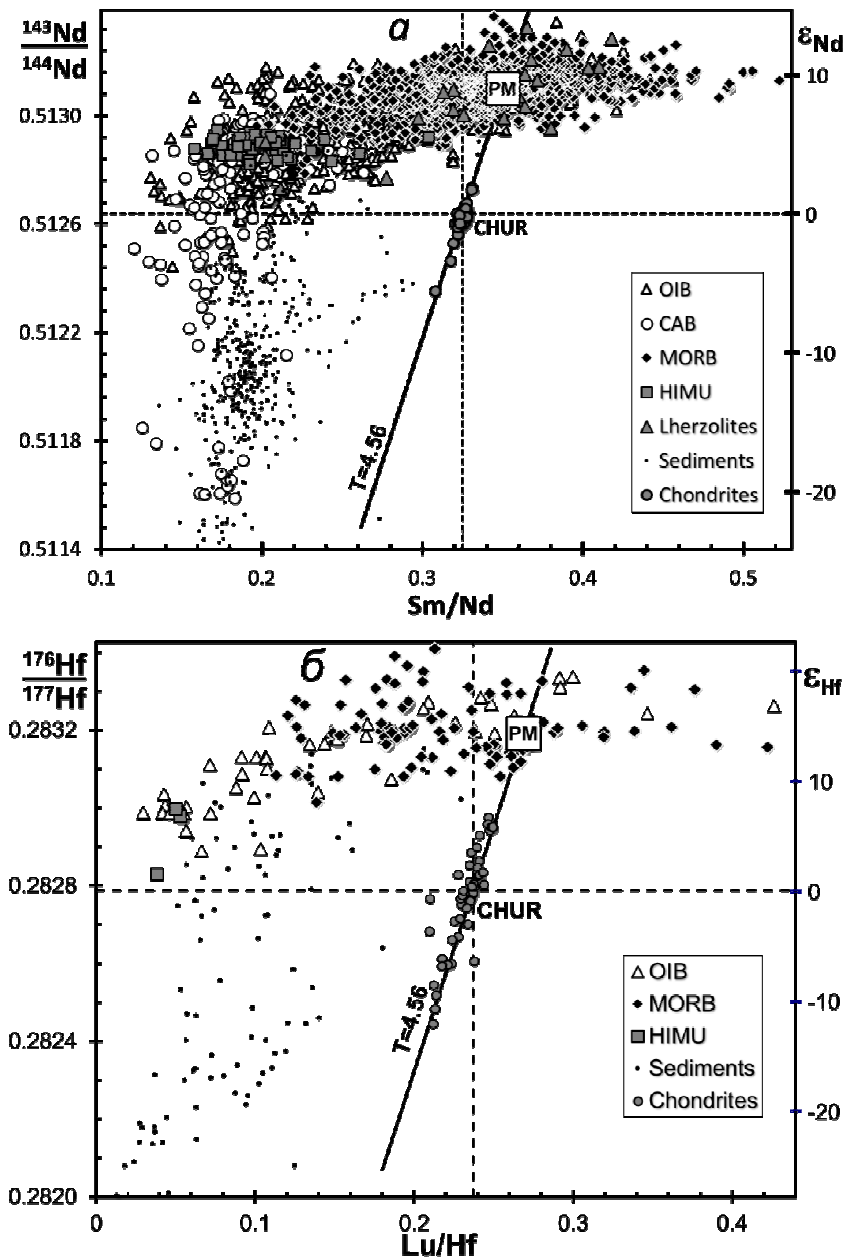


Fig. 6. Dependences between Nd isotope composition and Sm/Nd values (a) and Hf isotope composition and Lu/Hf values (b) in basalts.

Mid-ocean ridges basalts (MORB), intra-plate oceanic basalts (OIB), continental alkaline basalts (CAB), basalts HIMU, silicate-fragmentary sediments (Sed), lherzolites and chondrites. The continuous bold line means geochron (4,56 Ga), passing through CHUR. Other legends see in the text.

Thus, the data given on figure 6 show that the mantle most likely doesn't have the sources with CHUR composition, i.e. the primitive mantle demonstrates the non-chondritic distribution of elements.

ELEMENT RATIOS IN THE PRIMITIVE MANTLE Sm/Nd, Lu/Hf AND Rb/Sr

The contradictions listed in the previous section caused by supposition that Sm/Nd and Lu/Hf values in the primitive Earth's mantle are chondritic force us searching for more adequate estimations of these ratios and associated Nd, Hf and other elements isotope compositions. It can be easily done using the data given on fig. 6.

Supposing that the primary Nd and Hf isotope composition in the Solar system was homogeneous, a point corresponding to the primitive mantle, should lie on the geochron in both isotope systems (on fig. 6 line T = 4,56 Ga). On the other hand, when discussing fig. 5 we found out that the composition of the primitive mantle on fig. 6, most likely, is somewhere within the trend of oceanic basalts. Thus, the required point should lie on crossing of geochron with the trend of mantle rocks on fig. 6, and its most probable location is noted by point PM with the following parameters:

$$\epsilon_{Nd} = +9; {}^{143}\text{Nd}/{}^{144}\text{Nd} = 0,51309; \text{Sm}/\text{Nd} = 0,350;$$

$$\epsilon_{Hf} = +14; {}^{176}\text{Hf}/{}^{177}\text{Hf} = 0,28319; \text{Lu}/\text{Hf} = 0,268.$$

The uncertainty as ± 1 of ϵ_{Nd} or ϵ_{Hf} which is quite possible, leads to uncertainty as $\pm 0,8$ % of Sm/Nd and Lu/Hf values.

Negative correlation between Nd and Sr isotope ratios allows finding the parameters of the primitive mantle in Rb-Sr system (point PM on fig. 1): $\epsilon_{Sr} = -22$; ${}^{87}\text{Sr}/{}^{86}\text{Sr} = 0,7029$, using the formula given above (2) we can obtain for the primitive mantle $({}^{87}\text{Rb}/{}^{86}\text{Sr})_{PM} = 0,0595$ and $(\text{Rb}/\text{Sr})_{PM} = 0,0206$.

Figure 7 demonstrates the change of Sm/Nd and Rb/Sr values (fig. 7 a, 7 c) in the depleted mantle due to the crust extraction as well as variations in Nd and Sr isotope compositions (fig. 7 b, d) of the primitive (PM) and depleted (DM) mantle. It is remarkable that modeled compositions of both primitive and depleted substance lie in the field of MORB, i.e. basalts of mid-ocean ridges basalts were generated both from the depleted and the primitive enriched sources that correlates with variations of their element composition.

The obtained composition of the primitive mantle in Sm-Nd, Lu-Hf and Rb-Sr isotope systems remove all contradictions of modern isotope geodynamics outlined in the previous section. Now there is no necessity to find an answer to the question why the primitive mantle is dead - we can define what rocks are closer to the primitive mantle as regard to Nd, Hf, Sr isotope compositions analyzing fig. 1, fig. 6 and fig. 7.

A logical conclusion can be reached: the sources of both alkaline, and HIMU basalts are enriched by incoherent elements to various extent. They have the increased La/Lu (lower Sm/Nd) values in comparison with the primitive mantle. It does not exclude the possibility of metasomatic change of sources of these rocks. However, the metasomatic transformation is not obligatory for sources of all

alkaline basalts with $\epsilon_{Nd} > 0$.

If the proposed scheme is true, changes in Sm/Nd, Lu/Hf and Rb/Sr values in the depleted mantle due to the extraction of the crust throughout the whole history of the Earth rendered only moderate effect on variations of Nd, Hf, Sr isotope composition in modern mantle rocks in comparison with their observable isotope heterogeneity. The reasons of isotope variations in rocks of the mantle origin are considered in details in a separate publication [132]. Here, we can note only the common features.

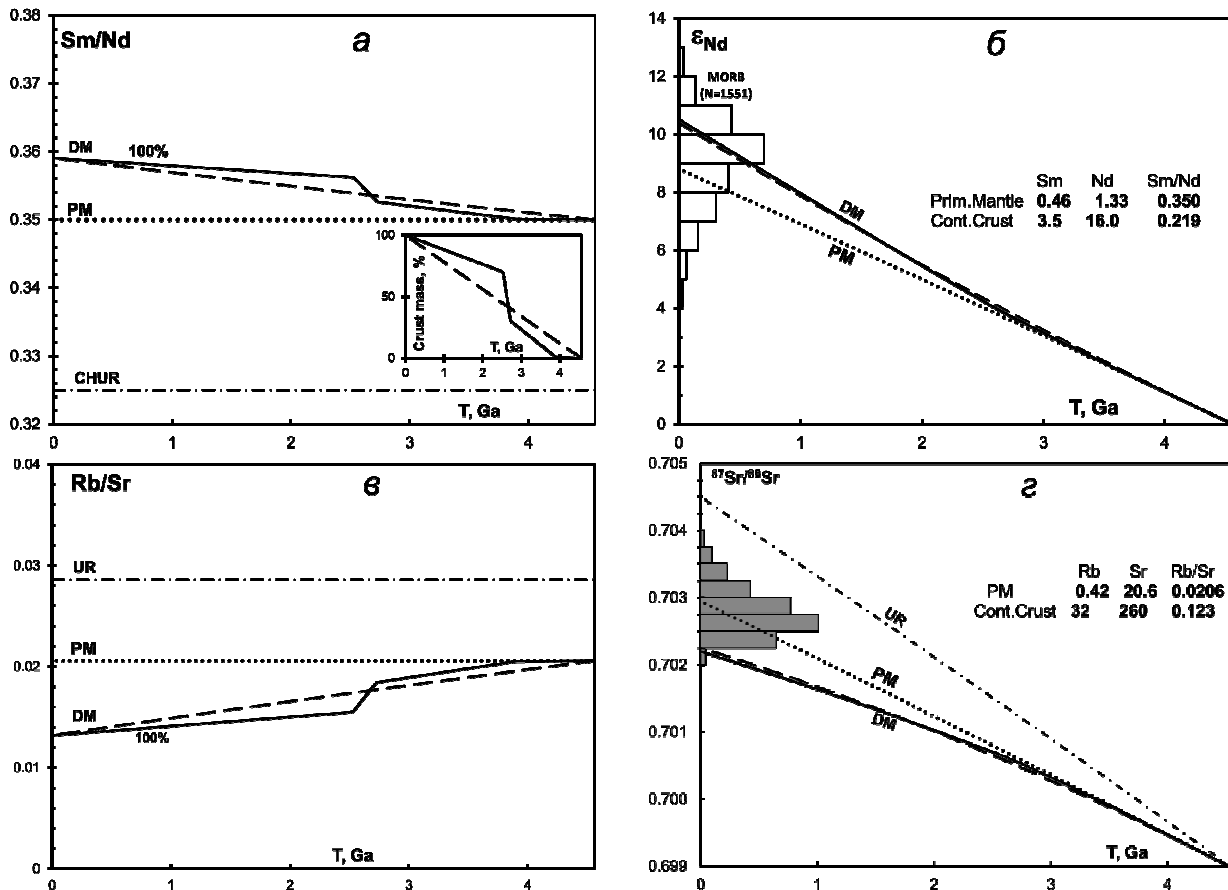


Fig. 7. Balance calculations of influence of continental crust growth on the composition of the depleted mantle in Sm-Nd and Rb-Sr isotope systems in case of non-chondritic composition of the primitive mantle.

Accepted differences in Rb/Sr and Sm/Nd ratios from model by DePaolo and Vasserburg [1, 5] can be seen on plots a and c. Calculations are done for two trajectories of dynamics of crust growth, as shown in inset of the plot a: non-uniform growth (a continuous line) according to Taylor's and McLennan's hypothesis [126] and linear growth (dotted line). It is supposed that the crustal material was taken from all volume of the mantle, or just the same, convecting mantle had possibility to mix. The plots b and d show that the difference in character of growth of the continental crust insignificantly influences the isotope ratios.

As it was supposed earlier [1-5], the depleted mantle sources demonstrate higher Nd and Hf isotope ratios and lower Sr ratios than the composition of the

primitive mantle. On fig. 1 a they lie above and to the left of point PM, while on fig. 1b they lie above and to the right of it. However, unlike CHUR-model, the range of isotope variations of the depleted mantle in the proposed model is significantly narrower, it can be evaluated from figures 7 b and 7 d.

A real scatter in Nd, Hf, Sr isotope ratios is wider than the difference between modeled composition of the primitive and depleted mantle that on one hand can specify an irregular depletion of mantle sources while on another hand it means the redistribution of elements and local formation of the enriched compositions in the mantle [132].

Th/U/Pb Ratios

Correlation of lead and neodymium isotope composition in mantle rocks provide $^{206}\text{Pb}/^{204}\text{Pb}$, $^{207}\text{Pb}/^{204}\text{Pb}$, $^{208}\text{Pb}/^{204}\text{Pb}$ values, correlating with the primitive mantle source. These values lie on crossing of each trend on fig. 8 with $\epsilon_{\text{Nd}} = 9,0$ and amount to 18,368; 15,494 and 37,967, accordingly. This composition is shown on fig. 2 as well. The obtained estimation, as well as former ones [3] lie to the right of the geochron that most likely is a result of gradual increase U/Pb value in the mantle [133].

Plots on fig. 8 point out that none of stable cluster corresponding to the real mantle source lies in the field $\epsilon_{\text{Nd}} = 0$. The available isotope data for lead can be used for calculating U/Pb and Th/U values in the source rocks. Correlations of these values with ϵ_{Nd} also allow finding the values typical of the primitive mantle. Figure 8 shows that $\mu_{\text{Pb}} = 8,82$, $\kappa_{\text{Pb}} = 3,808$ that correlates with weight ratios U/Pb = 0,1405 and Th/U = 3,68.

THE ELEMENTS WHICH ARE NOT RELATED TO RADIOACTIVE DECAY

The correlation between other elements which do not influence any isotope ratios is a problem with a less certain solution. The approach used here is shown on fig. 9: the point of crossing of correlation trends for MORB between tested element ratios and Sm/Nd with the value Sm/Nd=0,350 is regarded to be the most similar to the composition of the primitive mantle. This approach yields quite reasonable results if elements are close to each other as regard of incompatibility, i.e. they lie close to each other on fig. 10. For example, the estimated U/Pb value gives 0,143 that well agrees with the above value 0,1405 calculated from the isotope data: the difference is less than 2 %. However, we have to apply such approach carefully to pairs of elements with significantly different geochemical features. So, for example, Lu/Hf value calculated using this approach is equal 0,207 that is by 23 % lower than the more reliable estimation from the isotope data.

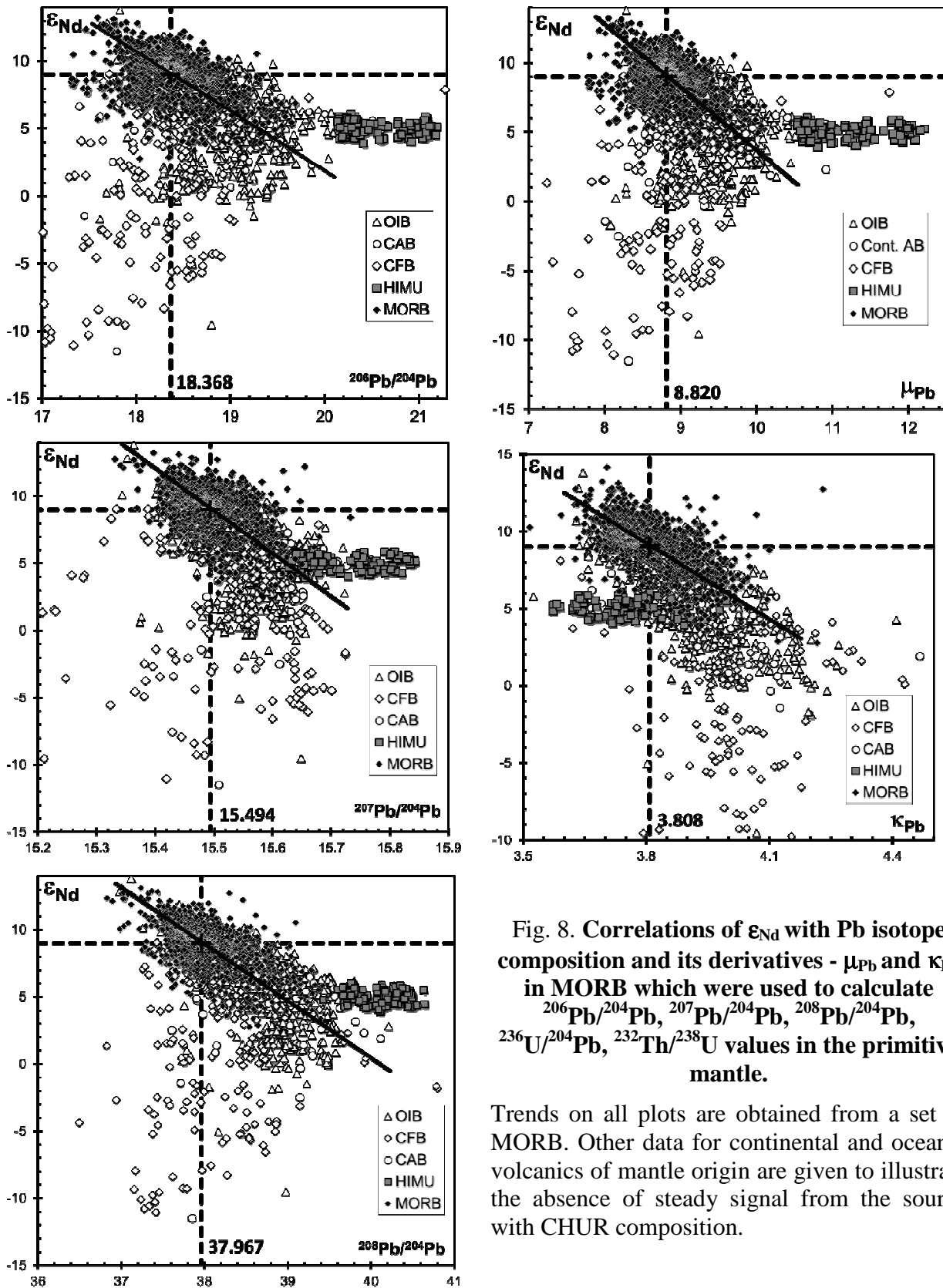


Fig. 8. Correlations of ϵ_{Nd} with Pb isotope composition and its derivatives - μ_{Pb} and κ_{Pb} in MORB which were used to calculate $^{206}Pb/^{204}Pb$, $^{207}Pb/^{204}Pb$, $^{208}Pb/^{204}Pb$, $^{236}U/^{204}Pb$, $^{232}Th/^{238}U$ values in the primitive mantle.

Trends on all plots are obtained from a set of MORB. Other data for continental and oceanic volcanics of mantle origin are given to illustrate the absence of steady signal from the source with CHUR composition.

Values given on fig. 9 $Hf/Nd = 0,258$, $Sr/Nd = 14,3$ and $Th/Rb = 0,145$ allow connecting of all above elements in a uniform system. As the developed approach

is applicable only for elements-impurities and allows calculating only ratios of elements, instead of their absolute concentrations the content of at least one element has to be calculated by an independent way. At this stage we accept the Nd content in the primitive mantle according to Palme, O'Neill [134] to be equal 1,327 mkg/g. The concentrations of other elements are given in table 1.

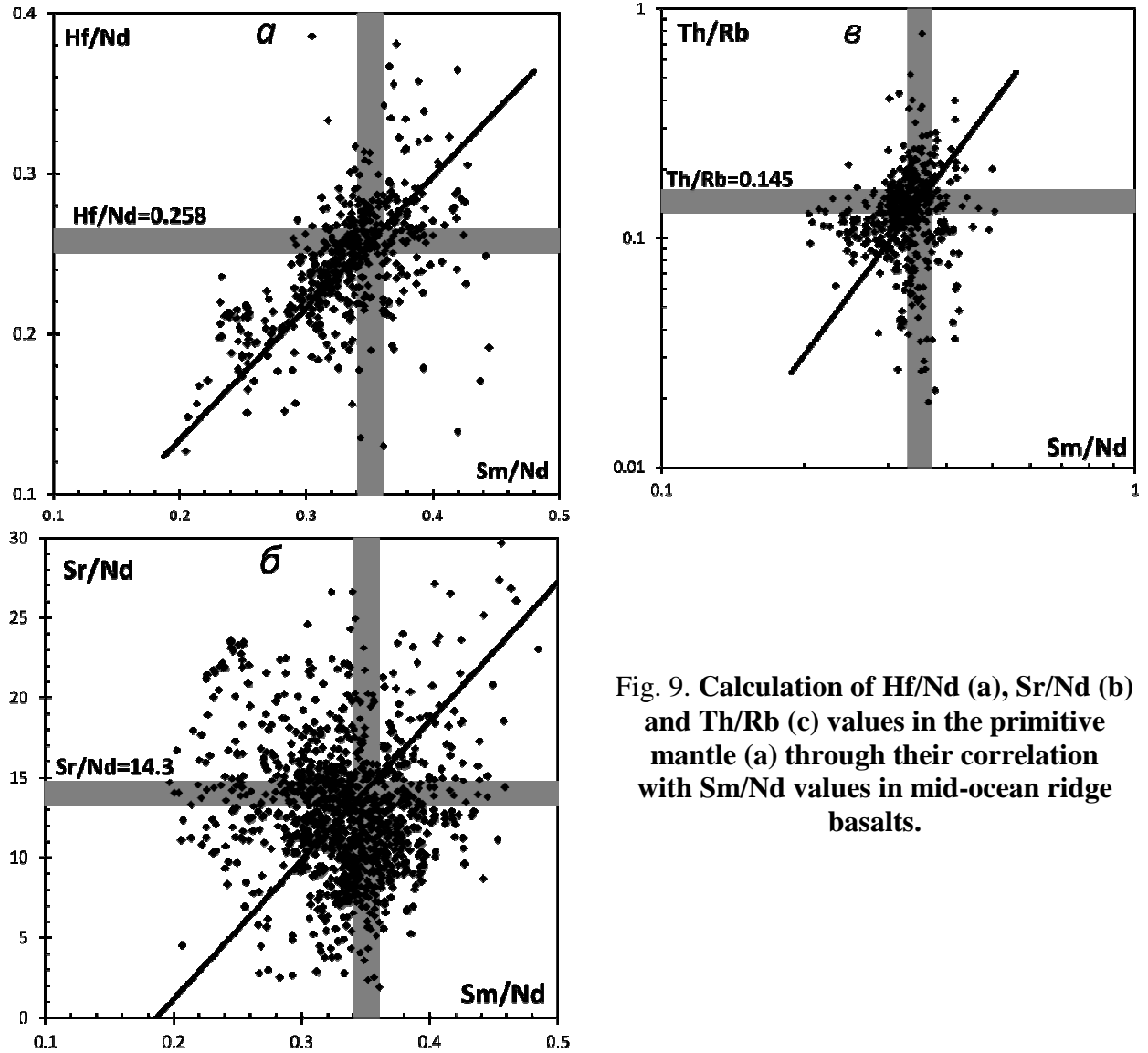


Fig. 9. Calculation of Hf/Nd (a), Sr/Nd (b) and Th/Rb (c) values in the primitive mantle (a) through their correlation with Sm/Nd values in mid-ocean ridge basalts.

Figure 10 shows the comparison of element concentrations obtained from the present study with earlier published models by different scientists [134-136]. For evident comparison all data are normalized from PM composition by Palme, O'Neill [134]. All elements from Lu to Rb are plotted on abscissa axis according to the increase of their incompatibility with mantle melts, i.e. according to the enrichment of the continental crust as compared with the primitive mantle. However, the diagram gives only those elements which were discussed in the present study.

Table 1.

**Recommended estimations of concentrations of elements-impurities
in the primitive mantle (PM)**

Element	Concentration in the primitive mantle, ppm	Source
Rb	0.391	Rb/Sr = 0.0206; $\epsilon_{Sr} = -22$ ($\epsilon_{Sr} \approx -2.5 \epsilon_{Nd}$), fig. 1 a
Pb	0.1096	U/Pb = 0.1405; correlation μ_{Pb} and ϵ_{Nd} (fig. 8)
Th	0.0567	Th/Rb = 0.145; correlation Th/Rb и Sm/Nd (fig. 9)
U	0.0154	Th/U = 3.68; correlation κ_{Pb} and ϵ_{Nd} (fig. 8)
Sr	19.0	Sr/Nd = 14.3; correlation Sr/Nd and Sm/Nd (fig. 9)
Nd	1.327	[134]
Hf	0.336	Hf/Nd = 0.252; correlation Hf/Nd and Sm/Nd (fig. 9)
Sm	0.464	Sm/Nd = 0.350; $\epsilon_{Nd} = 9$, fig.6 a
Lu	0.090	Lu/Hf = 0.268; $\epsilon_{Hf} = 14$ ($\epsilon_{Hf} \approx +1.6 \epsilon_{Nd}$), fig. 1 b

Figure 10 shows that the composition of the primitive mantle is different from the proposed earlier in more depletion by the most incompatible elements and small enrichment by compatible elements that results from the increased Sm/Nd and Lu/Hf and lower Rb/Sr values. Nevertheless, the depletion by the most incompatible elements is significantly less, than it is supposed for the depleted mantle source [137, 138].

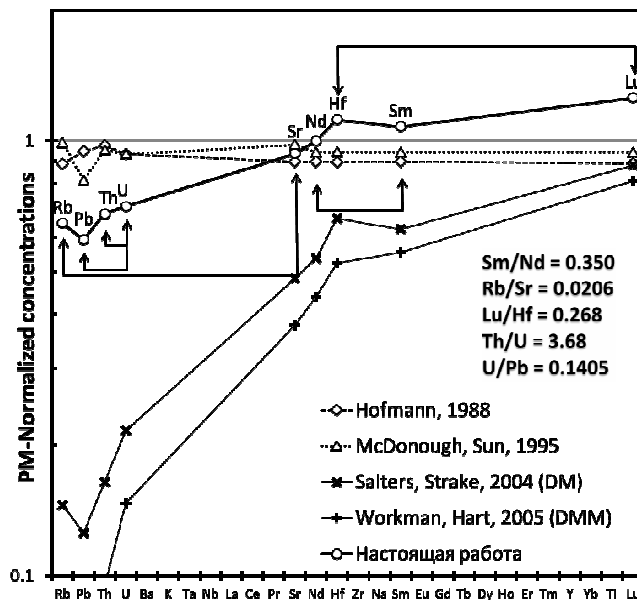


Fig. 10. Estimations of primitive mantle composition from different authors [135, 136] and those obtained in the present study, normalized by Palme, O'Neill [134].

Arrows connect pairs of elements whose ratios are obtained from the isotope data. The order of elements from right to left corresponds to growth of degree of their incompatibility in the mantle from [134], i.e. to degree of enrichment of the continental crust by these elements relative to the primitive mantle. For comparison we give two models of the depleted source from [137, 138].

CONCLUSIONS

The rocks of the mantle origin do not show any varieties which could be similar to CHUR both by Sm/Nd, and by $^{143}\text{Nd}/^{144}\text{Nd}$ values, that most likely indicates the absence of such substance on the Earth.

The assumption that Sm/Nd and Lu/Hf values of the primitive mantle of the Earth [1, 5-8] are similar to chondrite leads to a chain of contradictions which were not solved for the last three decades of intensive isotope studies. These contradictions can be removed if we assume slight difference in the composition of the primitive mantle and chondrites: by 8 % as regard to Sm/Nd value and by 12 % as regard to Lu/Hf value. The supposed recent composition of the of primitive mantle in Sm-Nd, Lu-Hf, Rb-Sr and U-Th-Pb isotope systems is the following:

$\epsilon_{\text{Nd}} = +9$	$^{143}\text{Nd}/^{144}\text{Nd} = 0.51309$	$^{147}\text{Sm}/^{144}\text{Nd} = 0.2119$	$\text{Sm}/\text{Nd} = 0.350$
$\epsilon_{\text{Hf}} = +14$	$^{176}\text{Hf}/^{177}\text{Hf} = 0.28318$	$^{176}\text{Lu}/^{177}\text{Hf} = 0.0381$	$\text{Lu}/\text{Hf} = 0.268$
$\epsilon_{\text{Sr}} = -22$	$^{87}\text{Sr}/^{86}\text{Sr} = 0.7029$	$^{87}\text{Rb}/^{86}\text{Sr} = 0.0595$	$\text{Rb}/\text{Sr} = 0.0206$
	$^{206}\text{Pb}/^{204}\text{Pb} = 18.368$	$^{238}\text{U}/^{204}\text{Pb} = 8.82$	$\text{U}/\text{Pb} = 0.1405$
	$^{207}\text{Pb}/^{204}\text{Pb} = 15.494$		
	$^{208}\text{Pb}/^{204}\text{Pb} = 37.967$	$^{232}\text{Th}/^{238}\text{U} = 3.81$	$\text{Th}/\text{U} = 3.68$

The uncertainty of Nd isotope composition can reach $\pm 1 \epsilon_{\text{Nd}}$. The isotope effect in Sm-Nd, Lu-Hf and Rb-Sr systems from the extraction of the earth crust from the mantle substance substances is much less than the observable isotope variations in mantle rocks.

Работа выполнена при финансовой поддержке РФФИ, грант 11-05-00062

REFERENCES

1. **DePaolo D.J., Wasserburg G.J.** Nd isotopic variations and petrogenetic models. // Geophysical Research Letters. 1976. V. 3. P. 249-252.
2. **Zindler A., Hart S.** Chemical Geodynamics. // Annual Review of Earth and Planetary Sciences. 1986. V. 14. P. 493-571.
3. **Allegre C.J., Lewin E.** Chemical Structure and History of the Earth: Evidence from Global Non-Linear Inversion of Isotopic Data in a Three Box Model. // Earth and Planetary Science Letters. 1989. V. 96. P. 61-88.
4. **Hofmann A.W.** Mantle Geochemistry - The Message from Oceanic Volcanism. // Nature. 1997. V. 385. P. 219-229.
5. **DePaolo D.J., Wasserburg G.J.** Inferences about magma sources and mantle structure from variations of $^{143}\text{Nd}/^{144}\text{Nd}$. // Geophysical Research Letters. 1976. V. 3. P. 743-746.
6. **Jacobsen S.B., Wasserburg G.J.** Sm-Nd isotopic evolution of chondrites. // Earth and Planetary Science Letters. 1980. V. 50. P. 139-155.
7. **Jacobsen S.B., Wasserburg G.J.** Sm-Nd isotopic evolution of chondrites and achondrites, II. // Earth and Planetary Science Letters. 1983. V. 67. P. 137-150.

8. **Tatsumoto M., Unruh D.M., Patchett P.J.** U-Pb and Lu-Hf systematics of Antarctic meteorites. // 6th Symp. Antarctic Meteorites. Natl. Inst. Polar Res. 1981. Tokyo. 237-249.
9. **Bouvier A., Vervoort J.D., Patchett P.J.** The Lu-Hf and Sm-Nd isotopic composition of CHUR: constraints from unequilibrated chondrites and implications for the bulk composition of terrestrial planets. // Earth and Planetary Science Letters. 2008. V. 273. P. 48-57.
10. **Wasson J.T., Kallemeyen G.W.** Composition of chondrites. // Philosophical Transactions of the Royal Society of London - A. 1988. V. 325. P. 535-544.
11. **Griffin W.L., O'Reilly S.Y., Stabel A.** Mantle Metasomatism Beneath Western Victoria, Australia. 2. Isotopic Geochemistry of Cr-Diopside Iherzolites and Al-Augite Pyroxenites. // Geochimica et Cosmochimica Acta. 1988. V. 52. P. 449-459.
12. **Kramm U., Wedepohl K.H.** Tertiary basalts and peridotite xenoliths from the Hessian Depression (NW Germany) reflecting mantle compositions low in radiogenic Nd and Sr. // Contributions to Mineralogy and Petrology. 1990. V. 106. P. 1-8.
13. **Alibert C.** Peridotite Xenoliths from Western Grand-Canyon and the Thumb - A Probe into the Subcontinental Mantle of the Colorado Plateau. // Journal of Geophysical Research, B, Solid Earth and Planets. 1994. V. 99. P. 21605-21620.
14. **Ionov D.A., Prikhodko V.S., Oreilly S.Y.** Peridotite Xenoliths in Alkali Basalts from the Sikhote-Alin, Southeastern Siberia, Russia - Trace-Element Signatures of Mantle Beneath a Convergent Continental-Margin. // Chemical Geology. 1995. V. 120. P. 275-294.
15. **Wasserburg G., Jacousen S., DePaolo D., McCulloch M., Wen T.** Precise determination of SmNd ratios, Sm and Nd isotopic abundances in standard solutions. // Geochimica et Cosmochimica Acta. 1981. V. 45. P. 2311-2323.
16. **Papanastassiou D.A., Wasserburg J.G.** Initial strontium isotopic abundances and the resolution of small time differences in the formation of planetary objects. // Contributions to Mineralogy and Petrology. 1969. V. 5. P. 361-375.
17. **Cohen R.S., Evensen N.M., Hamilton P.J., O'Nions R.K.** U-Pb, Sm-Nd and Rb-Sr systematics of mid-ocean ridge basalt glasses. // Nature. 1980. V. 283. P. 149-153.
18. **Cohen R.S., O'Nions R.K.** The lead, neodymium and strontium isotopic structure of ocean ridge basalts. // Journal of Petrology. 1982. V. 23. P. 299-324.
19. **O'Nions R.K., Hamilton P.J., Evensen N.M.** Variations in $^{143}\text{Nd}/^{144}\text{Nd}$ and $^{87}\text{Sr}/^{86}\text{Sr}$ ratios in oceanic basalts. // Earth and Planetary Science Letters. 1977. V. 34. P. 13-22.
20. **Zindler A., Staudigel H., Batiza R.** Isotope and trace element geochemistry of young Pacific seamounts: implications for the scale of upper mantle heterogeneity. // Earth and Planetary Science Letters. 1984. V. 70. P. 175-195.
21. **Macdougall J.D., Lugmair G.W.** Sr and ND Isotopes in Basalts from the East Pacific Rise - Significance for Mantle Heterogeneity. // Earth and Planetary Science Letters. 1986. V. 77. P. 273-284.
22. **Graham D.W., Zindler A., Kurz M.D., Jenkins W.J., Batiza R., Staudigel H.** He, Pb, Sr and Nd Isotope Constraints on Magma Genesis and Mantle Heterogeneity Beneath Young Pacific Seamounts. // Contributions to Mineralogy and Petrology. 1988. V. 99. P. 446-463.
23. **Klein E.M., Langmuir C.H., Zindler A., Staudigel H., Hamelin B.** Isotope Evidence of a Mantle Convection Boundary at the Australian-Antarctic Discordance. // Nature. 1988. V. 333. P. 623-629.
24. **Hegner E., Tatsumoto M.** Pb, Sr, and Nd Isotopes in Basalts and Sulfides from the Juan-de-Fuca Ridge. // Journal of Geophysical Research, B, Solid Earth and Planets. 1987. V. 92. P. 1380-1386.
25. **Dosso L., Hanan B.B., Bougault H., Schilling J.G., Joron J.L.** Sr-Nd-Pb Geochemical Morphology Between 10°N and 17°N on the Mid-Atlantic Ridge - A New MORB Isotope

- Signature. // *Earth and Planetary Science Letters*. 1991. V. 106. P. 29-43.
26. **Hickeyvargas R.** Isotope Characteristics of Submarine Lavas from the Philippine Sea - Implications for the Origin of Arc and Basin Magmas of the Philippine Tectonic Plate. // *Earth and Planetary Science Letters*. 1991. V. 107. P. 290-304.
 27. **Mertz D.F., Devey C.W., Todt W., Stoffers P., Hofmann A.W.** Sr-Nd-Pb Isotope Evidence Against Plume Asthenosphere Mixing North of Iceland. // *Earth and Planetary Science Letters*. 1991. V. 107. P. 243-255.
 28. **Muhe R., Devey C.W., Bohrmann H.** Isotope and Trace-Element Geochemistry of MORB from the Nansen-Gakkel Ridge at 86-Degrees North. // *Earth and Planetary Science Letters*. 1993. V. 120. P. 103-109.
 29. **Bach W., Hegner E., Erzinger J., Satir M.** Chemical and Isotopic Variations Along the Superfast Spreading East Pacific Rise from 6-Degrees-S to 30- Degrees-S. // *Contributions to Mineralogy and Petrology*. 1994. V. 116. P. 365-380.
 30. **Cousens B.L., Allan J.F., Leybourne M.I., Chase R.L., Vanwagoner N.** Mixing of Magmas from Enriched and Depleted Mantle Sources the Northeast Pacific - West-Valley Segment, Juan-de-Fuca Ridge. // *Contributions to Mineralogy and Petrology*. 1995. V. 120. P. 337-357.
 31. **Mahoney J.J., Jones W.B., Frey F.A., Salters V.J.M., Pyle D.G., Davies H.L.** Geochemical Characteristics of Lavas from Broken Ridge, the Naturaliste Plateau and Southernmost Kerguelen Plateau - Cretaceous Plateau Volcanism in the Southeast Indian-Ocean. // *Chemical Geology*. 1995. V. 120. P. 315-345.
 32. **Staudigel H., Davies G.R., Hart S.R., Marchant K.M., Smith B.M.** Large-Scale Isotopic Sr, Nd and O Isotopic Anatomy of Altered Oceanic-Crust - DSDP/ODP Sites-417/418. // *Earth and Planetary Science Letters*. 1995. V. 130. P. 169-185.
 33. **Bach W., Erzinger J., Dosso L., Bollinger C., Bougault H., Etoubleau J., Sauerwein J.** Unusually Large Nb-Ta Depletions in North Chile Ridge Basalts at 36-Degrees-50' to 38-Degrees-56's - Major- Element, Trace-Element, and Isotopic Data. // *Earth and Planetary Science Letters*. 1996. V. 142. P. 223-240.
 34. **Niu Y.L., Waggoner D.G., Sinton J.M., Mahoney J.J.** Mantle Source Heterogeneity and Melting Processes Beneath Sea-Floor Spreading Centers - The East Pacific Rise, 18-Degrees-19S. // *Journal of Geophysical Research, B, Solid Earth and Planets*. 1996. V. 101. P. 27711-27733.
 35. **Salters V.J.M.** The Generation of Midocean Ridge Basalts from the Hf and Nd Isotope Perspective. // *Earth and Planetary Science Letters*. 1996. V. 141. P. 109-123.
 36. **Muhe R., Bohrmann H., Garbeschönberg D., Kassens H.** E-MORB Glasses from the Gakkel Ridge (Arctic Ocean) at 87-Degrees-N - Evidence for the Earth Most Northerly Volcanic Activity. // *Earth and Planetary Science Letters*. 1997. V. 152. P. 1-9.
 37. **Rehkamper M., Hofmann A.W.** Recycled Ocean Crust and Sediment in Indian-Ocean MORB. // *Earth and Planetary Science Letters*. 1997. V. 147. P. 93-106.
 38. **Schiano P., Birck J.L., Allegré C.J.** Osmium-Strontium-Neodymium-Lead Isotopic Covariations in Midocean Ridge Basalt Glasses and the Heterogeneity of the Upper-Mantle. // *Earth and Planetary Science Letters*. 1997. V. 150. P. 363-379.
 39. **Salters V.J.M., White W.M.** Hf Isotope Constraints on Mantle Evolution. // *Chemical Geology*. 1998. V. 145. P. 447-460.
 40. **Smith S.E., Casey J.F., Bryan W.B., Dmitriev L., Silantyev S., Magakyan R.** Geochemistry of Basalts from the Hayes Transform Region of the Mid-Atlantic Ridge. // *Journal of Geophysical Research, B, Solid Earth and Planets*. 1998. V. 103. P. 5305-5329.
 41. **Schilling J.G., Kingsley R., Fontignie D., Poreda R., Xue S.** Dispersion of the Jan-Mayen and Iceland Mantle Plumes in the Arctic - A He-Pb-Nd-Sr Isotope Tracer Study of Basalts from the Kolbeinsey, Mohns, and Knipovich Ridges. // *Journal of Geophysical*

- Research, B, Solid Earth and Planets. 1999. V. 104. P. 10543-10569.
42. **Bourdon E., Hemond C.** Looking for "missing endmember" in South Atlantic Ocean mantle around Ascension Island". // *Mineralogy and Petrology*. 2001. V. 71. P. 127-138.
 43. **Chauvel C., Blichert-Toft J.** A hafnium isotope and trace element perspective on melting of the depleted mantle. // *Earth and Planetary Science Letters*. 2001. V. 190. P. 137-151.
 44. **Woodhead J.D., Hergt J.M., Davidson J.P., Eggins S.M.** Hafnium isotope evidence for 'conservative' element mobility during subduction zone processes. // *Earth and Planetary Science Letters*. 2001. V. 192. P. 331-346.
 45. **Haase K.M.** Geochemical constraints on magma sources and mixing processes in Easter Microplate MORB (SE Pacific): a case study of plum-ridge interaction. // *Chemical Geology*. 2002. V. 182. P. 335-355.
 46. **Hofmann A.W., Feigenson M.D., Raczek I.** Case studies on the origin of basalt: III. Petrogenesis of the Mauna Ulu eruption, Kilauea, 1969-1971. // *Contributions to Mineralogy and Petrology*. 1984. V. 88. P. 24-35.
 47. **Roden M.F., Frey F.A., Clague D.A.** Geochemistry of tholeiitic and alkalic lavas from the Koolau Range, Oahu, Hawaii: implications for Hawaiian volcanism. // *Earth and Planetary Science Letters*. 1984. V. 69. P. 141-158.
 48. **Wright E., White W.M.** The Origin of Samoa - New Evidence from Sr, Nd, and Pb Isotopes. // *Earth and Planetary Science Letters*. 1987. V. 81. P. 151-162.
 49. **Roden M.F., Irving A.J., Murthy V.R.** Isotopic and Trace-Element Composition of the Upper Mantle Beneath a Young Continental Rift - Results from Kilbourne-Hole, New-Mexico. // *Geochimica et Cosmochimica Acta*. 1988. V. 52. P. 461-473.
 50. **Nakamura Y., Tatsumoto M.** Pb, Nd, and Sr Isotopic Evidence for a Multicomponent Source for Rocks of Cook-Austral Islands and Heterogeneities of Mantle Plumes. // *Geochimica et Cosmochimica Acta*. 1988. V. 52. P. 2909-2924.
 51. **Gautier I., Weis D., Mennessier J.P., Vidal P., Giret A., Loubet M.** Petrology and Geochemistry of the Kerguelen Archipelago Basalts (South Indian-Ocean) - Evolution of the Mantle Sources from Ridge to Intraplate Position. // *Earth and Planetary Science Letters*. 1990. V. 100. P. 59-76.
 52. **Chen C.Y., Frey F.A., Garcia M.O., Dalrymple G.B., Hart S.R.** The Tholeiite to Alkalic Basalt Transition at Haleakala Volcano, Maui, Hawaii. // *Contributions to Mineralogy and Petrology*. 1991. V. 106. P. 183-200.
 53. **Tatsumoto M., Nakamura Y.** Dupal Anomaly in the Sea of Japan - Pb, Nd, and Sr Isotopic Variations at the Eastern Eurasian Continental- Margin. // *Geochimica et Cosmochimica Acta*. 1991. V. 55. P. 3697-3708.
 54. **Halliday A.N., Davies G.R., Lee D.C., Tommasini S., Paslick C.R., Fitton J.G., James D.E.** Lead Isotope Evidence for Young Trace-Element Enrichment in the Oceanic Upper Mantle. // *Nature*. 1992. V. 359. P. 623-627.
 55. **Desonie D.L., Duncan R.A., Natland J.H.** Temporal and Geochemical Variability of Volcanic Products of the Marquesas Hotspot. // *Journal of Geophysical Research, B, Solid Earth and Planets*. 1993. V. 98. P. 17649-17665.
 56. **Weis D., Frey F.A., Leyrit H., Gautier I.** Kerguelen Archipelago Revisited - Geochemical and Isotopic Study of the Southeast Province Lavas. // *Earth and Planetary Science Letters*. 1993. V. 118. P. 101-119.
 57. **Hemond C., Devey C.W., Chauvel C.** Source Compositions and Melting Processes in the Society and Austral Plumes (South-Pacific Ocean) - Element and Isotope (Sr, Nd, Pb, Th) Geochemistry. // *Chemical Geology*. 1994. V. 115. P. 7-45.
 58. **Nohara M., Hirose K., Eissen J.P., Urabe T., Joshima M.** The North Fiji Basin Basalts and Their Magma Sources .2. Sr-Nd Isotopic and Trace-Element Constraints. // *Marine Geology*. 1994. V. 116. P. 179-195.

59. **Esperanca S., Crisci G.M.** The Island of Pantelleria - A Case for the Development of DMM-HIMU Isotopic Compositions in a Long-Lived Extensional Setting. // *Earth and Planetary Science Letters*. 1995. V. 136. P. 167-182.
60. **Halliday A.N., Lee D.C., Tommasini S., Davies G.R., Paslick C.R., Fitton J.G., James D.E.** Incompatible Trace-Elements in OIB and MORB and Source Enrichment in the Sub-Oceanic Mantle. // *Earth and Planetary Science Letters*. 1995. V. 133. P. 379-395.
61. **Rocholl A., Stein M., Molzahn M., Hart S.R., Worner G.** Geochemical Evolution of Rift Magmas by Progressive Tapping of a Stratified Mantle Source Beneath the Ross Sea Rift, Northern Victoria-Land, Antarctica. // *Earth and Planetary Science Letters*. 1995. V. 131. P. 207-224.
62. **Mahoney J.J., White W.M., Upton B.G.J., Neal C.R., Scrutton R.A.** Beyond EM-1 - Lavas from Afanasy-Nikitin Rise and the Crozet Archipelago, Indian-Ocean. // *Geology*. 1996. V. 24. P. 615-618.
63. **Spath A., Leroex A.P., Duncan R.A.** The Geochemistry of Lavas from the Comores Archipelago, Western Indian-Ocean - Petrogenesis and Mantle Source Region Characteristics. // *Journal of Petrology*. 1996. V. 37. P. 961-991.
64. **Woodhead J.D.** Extreme HIMU in an Oceanic Setting - The Geochemistry of Mangaia Island (Polynesia), and Temporal Evolution of the Cook-Austral Hotspot. // *Journal of Volcanology and Geothermal Research*. 1996. V. 72. P. 1-19.
65. **Chauvel C., Mcdonough W., Guille G., Maury R., Duncan R.** Contrasting Old and Young Volcanism in Rurutu Island, Austral Chain. // *Chemical Geology*. 1997. V. 139. P. 125-143.
66. **Turner S., Hawkesworth C., Rogers N., King P.** U-Th Isotope Disequilibria and Ocean Island Basalt Generation in the Azores. // *Chemical Geology*. 1997. V. 139. P. 145-164.
67. **Volker F., Altherr R., Jochum K.P., Mcculloch M.T.** Quaternary Volcanic Activity of the Southern Red-Sea - New Data and Assessment of Models on Magma Sources and Afar Plume Lithosphere Interaction. // *Tectonophysics*. 1997. V. 278. P. 15-29.
68. **Widom E., Carlson R.W., Gill J.B., Schmincke H.U.** Th-Sr-Nd-Pb Isotope and Trace-Element Evidence for the Origin of the Sao-Miguel, Azores, Enriched Mantle Source. // *Chemical Geology*. 1997. V. 140. P. 49-68.
69. **Dodson A., Depaolo D.J., Kennedy B.M.** Helium-Isotopes in Lithospheric Mantle - Evidence from Tertiary Basalts of the Western USA. // *Geochimica et Cosmochimica Acta*. 1998. V. 62. P. 3775-3787.
70. **Deniel C.** Geochemical and Isotopic (Sr, Nd, Pb) Evidence for Plume- Lithosphere Interactions in the Genesis of Grande-Comore Magmas (Indian-Ocean). // *Chemical Geology*. 1998. V. 144. P. 281-303.
71. **Elburg M., Foden J.** Sources for magmatism in Central Sulawesi: geochemical and Sr-Nd-Pb isotopic constraints. // *Chemical Geology*. 1999. V. 156. P. 67-93.
72. **Kurz M.D., Geist D.** Dynamics of the Galapagos Hotspot from Helium Isotope Geochemistry. // *Geochimica et Cosmochimica Acta*. 1999. V. 63. P. 4139-4156.
73. **Janney P.E., Macdougall J.D., Natland J.H., Lynch M.A.** Geochemical evidence from the Pukapuka volcanic ridge system for a shallow enriched mantle domain beneath the South Pacific Superswell. // *Earth and Planetary Science Letters*. 2000. V. 181. P. 47-60.
74. **Hawkesworth C.J., Norry M.J., Roddick J.C., Baker P.E., Francis P.W., Thorpe R.S.** $^{143}\text{Nd}/^{144}\text{Nd}$, $^{87}\text{Sr}/^{86}\text{Sr}$, and incompatible element variations in calc-alkaline andesites and plateau lavas from South America. // *Earth and Planetary Science Letters*. 1979. V. 42. P. 45-57.
75. **Chauvel C., Jahn B.M.** Nd-Sr isotope and REE geochemistry of alkali basalts from the Massif Central, France. // *Geochimica et Cosmochimica Acta*. 1984. V. 48. P. 93-110.
76. **Worner G., Schmincke H.U., Staudigel H., Zindler A.** Sr, Nd, and Pb Isotope

- Geochemistry of Tertiary and Quaternary Alkaline Volcanics from West Germany. // *Earth and Planetary Science Letters*. 1986. V. 79. P. 107-119.
77. **Musselwhite D.S., Mccurry M., Depaolo D.J.** The Evolution of a Silicic Magma System - Isotopic and Chemical Evidence from the Woods Mountains Volcanic Center, Eastern California. // *Contributions to Mineralogy and Petrology*. 1989. V. 101. P. 19-29.
78. **Chazot G., Bertrand H.** Mantle Sources and Magma-Continental Crust Interactions During Early Red Sea-Gulf of Aden Rifting in Southern Yemen - Elemental and Sr, Nd, Pb Isotope Evidence. // *Journal of Geophysical Research, B, Solid Earth and Planets*. 1993. V. 98. P. 1819-1835.
79. **Ionov D.A., Oreilly S.Y., Ashchepkov I.V.** Feldspar-Bearing Iherzolite Xenoliths in Alkali Basalts from Hamar-Daban, Southern Baikal Region, Russia. // *Contributions to Mineralogy and Petrology*. 1995. V. 122. P. 174-190.
80. **O'Brien H.E., Irving A.J., Mccallum S., Thirlwall M.F.** Strontium, Neodymium, and Lead Isotopic Evidence for the Interaction of Postsubduction Asthenospheric Potassic Mafic Magmas of the Highwood Mountains, Montana, USA, with Ancient Wyoming Craton Lithospheric Mantle. // *Geochimica et Cosmochimica Acta*. 1995. V. 59. P. 4539-4556.
81. **Hart S.R., Blusztajn J., Lemasurier W.E., Rex D.C.** Hobbs Coast Cenozoic Volcanism - Implications for the West Antarctic Rift System. // *Chemical Geology*. 1997. V. 139. P. 223-248.
82. **Marzoli A., Renne P.R., Piccirillo E.M., Francesca C.** Silicic magmas from the continental Cameroon Volcanic Line (Oku, Bambouto and Ngaoundere): Ar-40-Ar-39 dates, petrology, Sr-Nd-O isotopes and their petrogenetic significance. // *Contributions to Mineralogy and Petrology*. 1999. V. 135. P. 133-150.
83. **Taylor S.R., McLennan S.M., McCulloch M.T.** Geochemistry of loess, continental crustal composition and crustal model ages. // *Geochimica et Cosmochimica Acta*. 1983. V. 47. P. 1897-1905.
84. **Briqueu L., Javoy M., Lancelot J.R., Tatsumoto M.** Isotope Geochemistry of Recent Magmatism in the Aegean Arc - Sr, Nd, Hf, and O Isotopic-Ratios in the Lavas of Milos and Santorini - Geodynamic Implications. // *Earth and Planetary Science Letters*. 1986. V. 80. P. 41-54.
85. **Goldstein S.J., Jacobsen S.B.** The Nd and Sr Isotopic Systematics of River-Water Dissolved Material - Implications for the Sources of Nd and Sr in Seawater. // *Chemical Geology*. 1987. V. 66. P. 245-272.
86. **Goldstein S.J., Jacobsen S.B.** Rare-Earth Elements in River Waters. // *Earth and Planetary Science Letters*. 1988. V. 89. P. 35-47.
87. **Nelson B.K., DePaolo D.J.** Comparison of Isotopic and Petrographic Provenance Indicators in Sediments from Tertiary Continental Basins of New-Mexico. // *Journal of Sedimentary Petrology*. 1988. V. 58. P. 348-357.
88. **Asmerom Y., Jacobsen S.B.** The Pb Isotopic Evolution of the Earth - Inferences from River Water Suspended Loads. // *Earth and Planetary Science Letters*. 1993. V. 115. P. 245-256.
89. **Mcdermott F., Defant M.J., Hawkesworth C.J., Maury R.C., Joron J.L.** Isotope and Trace-Element Evidence for Three Component Mixing in the Genesis of the North Luzon Arc Lavas (Philippines). // *Contributions to Mineralogy and Petrology*. 1993. V. 113. P. 9-23.
90. **Bosch D., Lancelot J., Boulegue J.** Sr, Nd and Pb Isotope Constraints on the Formation of the Metalliferous Sediments in the Nereus Deep, Red-Sea. // *Earth and Planetary Science Letters*. 1994. V. 123. P. 299-315.
91. **Cousens B.L., Allan J.F., Gorton M.P.** Subduction Modified Pelagic Sediments as the

- Enriched Component in Back-Arc Basalts from the Japan Sea - Ocean Drilling Program Site-797 and Site-794. // *Contributions to Mineralogy and Petrology*. 1994. V. 117. P. 421-434.
92. **German C.R., Barreiro B.A., Higgs N.C., Nelsen T.A., Ludford E.M., Palmer M.R.** Seawater-Metasomatism in Hydrothermal Sediments (Escanaba Trough, Northeast Pacific). // *Chemical Geology*. 1995. V. 119. P. 175-190.
93. **Allegré C.J., Dupre B., Negrel P., Gaillardet J.** Sr-Nd-Pb Isotope Systematics in Amazon and Congo River Systems - Constraints About Erosion Processes. // *Chemical Geology*. 1996. V. 131. P. 93-112.
94. **Dupre B., Gaillardet J., Rousseau D., Allegré C.J.** Major and Trace-Elements of River-Borne Material - The Congo Basin. // *Geochimica et Cosmochimica Acta*. 1996. V. 60. P. 1301-1321.
95. **Ling H.F., Burton K.W., Onions R.K., Kamber B.S., Vonblanckenburg F., Gibb A.J., Hein J.R.** Evolution of Nd and Pb Isotopes in Central Pacific Seawater from Ferromanganese Crusts. // *Earth and Planetary Science Letters*. 1997. V. 146. P. 1-12.
96. **Gallet S., Jahn B.M., Lanoe B.V., Dia A., Rossello E.** Loess Geochemistry and Its Implications for Particle Origin and Composition of the Upper Continental-Crust. // *Earth and Planetary Science Letters*. 1998. V. 156. P. 157-172.
97. **Pettke T., Halliday A.N., Hall C.M., Rea D.K.** Dust production and deposition in Asia and the north Pacific Ocean over the past 12 Myr. // *Earth and Planetary Science Letters*. 2000. V. 178. P. 397-413.
98. **Salters V.J.M., Hart S.R.** The Mantle Sources of Ocean Ridges, Islands and Arcs - The Hf-Isotope Connection. // *Earth and Planetary Science Letters*. 1991. V. 104. P. 364-380.
99. **Godfrey L.V., Lee D.C., Sangrey W.F., Halliday A.N., Salters V.J.M., Hein J.R., White W.M.** The Hf Isotopic Composition of Ferromanganese Nodules and Crusts and Hydrothermal Manganese Deposits - Implications for Seawater Hf. // *Earth and Planetary Science Letters*. 1997. V. 151. P. 91-105.
100. **Nowell G.M., Kempton P.D., Noble S.R., Fitton J.G., Saunders A.D., Mahoney J.J., Taylor R.N.** High-Precision Hf Isotope Measurements of MORB and OIB by Thermal Ionization Mass-Spectrometry - Insights into the Depleted Mantle. // *Chemical Geology*. 1998. V. 149. P. 211-233.
101. **Vervoort J.D., Patchett P.J., Blicherttoft J., Albarede F.** Relationships Between Lu-Hf and Sm-Nd Isotopic Systems in the Global Sedimentary System. // *Earth and Planetary Science Letters*. 1999. V. 168. P. 79-99.
102. **David K., Frank M., O'Nions R.K., Belshaw N.S., Arden J.W.** The Hf isotope composition of global seawater and the evolution of Hf isotopes in the deep Pacific Ocean from Fe-Mn crusts. // *Chemical Geology*. 2001. V. 178. P. 23-42.
103. **Костицын Ю.А.** Sm-Nd и Lu-Hf изотопные системы Земли: отвечают ли они хондритам? // *Петрология*. 2004. Т. 12. № 5. С. 451-466.
104. **DePaolo D.J.** Neodymium isotopes in the Colorado Front Range and crust-mantle evolution in the Proterozoic. // *Nature*. 1981. V. 291. P. 193-196.
105. **Menzies M., Murthy V.R.** Nd and Sr isotope geochemistry of hydrous mantle nodules and their host alkali basalts: implications for local heterogeneities in metasomatically-veined mantle. // *Earth and Planetary Science Letters*. 1979. V. 46. P. 323-334.
106. **Chauvel C., Hofmann A.W., Vidal P.** HIMU-EM: The French-Polynesian Connection. // *Earth and Planetary Science Letters*. 1992. V. 110. P. 99-119.
107. **Eiler J.M., Farley K.A., Valley J.W., Hauri E., Craig H., Hart S.R., Stolper E.M.** Oxygen-Isotope Variations in Ocean Island Basalt Phenocrysts. // *Geochimica et Cosmochimica Acta*. 1997. V. 61. P. 2281-2293.
108. **Hauri E.H., Hart S.R.** Re-Os Isotope Systematics of HIMU and EMII Oceanic Island

- Basalts from the South-Pacific Ocean. // *Earth and Planetary Science Letters*. 1993. V. 114. P. 353-371.
109. **Schiano P., Burton K.W., Dupre b., Birck J.L., Guille G., Allegré C.J.** Correlated Os-Pb-Nd-Sr isotopies in the Austral-Cook chain basalts: the nature of mantle components in plume sources. // *Earth and Planetary Science Letters*. 2001. V. 186. P. 527-537.
110. **Graham D.W., Humphris S.E., Jenkins W.J., Kurz M.D.** Helium Isotope Geochemistry of Some Volcanic Rocks from Saint-Helena. // *Earth and Planetary Science Letters*. 1992. V. 110. P. 121-131.
111. **Reisberg L., Zindler A., Marcantonio F., White W., Wyman D., Weaver B.** Os Isotope Systematics in Ocean Island Basalts. // *Earth and Planetary Science Letters*. 1993. V. 120. P. 149-167.
112. **Ballentine C.J., Lee D.C., Halliday A.N.** Hafnium Isotopic Studies of the Cameroon Line and New HIMU Paradoxes. // *Chemical Geology*. 1997. V. 139. P. 111-124.
113. **Simonetti A., Bell K.** Nd, Pb and Sr Isotopic Data from the Mount-Elgon Volcano, Eastern Uganda Western Kenya - Implications for the Origin and Evolution of Nephelinite Lavas. // *Lithos*. 1995. V. 36. P. 141-153.
114. **Zartman R.E., Doe B.R.** Plumbotectonics - The model. // *Tectonophysics*. 1981. V. 75. P. 135-162.
115. **Zartman R.E., Haines S.M.** The Plumbotectonic Model for Pb Isotopic Systematics Among Major Terrestrial Reservoirs - A Case for Bi-Directional Transport. // *Geochimica et Cosmochimica Acta*. 1988. V. 52. P. 1327-1339.
116. **Hofmann A.W., Jochum K.P., Seufert M., White W.M.** Nb and Pb in oceanic basalts: new constraints on mantle evolution. // *Earth and Planetary Science Letters*. 1986. V. 79. P. 33-45.
117. **Miller D.M., Goldstein S.L., Langmuir C.H.** Cerium/Lead and Lead-Isotope Ratios in Arc Magmas and the Enrichment of Lead in the Continents. // *Nature*. 1994. V. 368. P. 514-520.
118. **Edwards C., Menzies M., Thirlwall M.** Evidence from Muriah, Indonesia, for the Interplay of Supra-Subduction Zone and Intraplate Processes in the Genesis of Potassic Alkaline Magmas. // *Journal of Petrology*. 1991. V. 32. P. 555-592.
119. **Gribble R.F., Stern R.J., Bloomer S.H., Stuben D., Ohearn T., Newman S.** MORB Mantle and Subduction Components Interact to Generate Basalts in the Southern Mariana Trough Back-Arc Basin. // *Geochimica et Cosmochimica Acta*. 1996. V. 60. P. 2153-2166.
120. **Thirlwall M.F., Graham A.M., Arculus R.J., Harmon R.S., Macpherson C.G.** Resolution of the Effects of Crustal Assimilation, Sediment Subduction, and Fluid Transport in Island-Arc Magmas: Pb-Sr-Nd-O Isotope Geochemistry of Grenada, Lesser Antilles. // *Geochimica et Cosmochimica Acta*. 1996. V. 60. P. 4785-4810.
121. **Hoogewerff J.A., Vanbergen M.J., Vroon P.Z., Hertogen J., Wordel R., Sneyers A., Nasution A., Varekamp J.C., Moens H.L.E., Mouchel D.** U-Series, Sr-Nd-Pb Isotope and Trace-Element Systematics Across an Active Island Arc-Continent Collision Zone - Implications for Element Transfer at the Slab-Wedge Interface. // *Geochimica et Cosmochimica Acta*. 1997. V. 61. P. 1057-1072.
122. **Kepezhinskas P., Mcdermott F., Defant M.J., Hochstaedter A., Drummond M.S., Hawkesworth C.J., Koloskov A., Maury R.C., Bellon H.** Trace-Element and Sr-Nd-Pb Isotopic Constraints on a 3- Component Model of Kamchatka Arc Petrogenesis. // *Geochimica et Cosmochimica Acta*. 1997. V. 61. P. 577-600.
123. **Stracke A., Hegner E.** Rifting-related volcanism in an oceanic post-collisional setting: the Tabar-Lihir-Tanga-Feni (TLTF) island chain, Papua New Guinea. // *Lithos*. 1998. V. 45. P. 545-560.
124. **Shinjo R.** Geochemistry of high Mg andesites and the tectonic evolution of the Okinawa

- Trough-Ryukyu arc system. // *Chemical Geology*. 1999. V. 157. P. 69-88.
125. **Turner S., Foden J.U.** Th and Ra disequilibria, Sr, Nd and Pb isotope and trace element variations in Sunda arc lavas: predominance of a subducted sediment component. // *Contributions to mineralogy and Petrology*. 2001. V. 142. P. 43-57.
126. **Taylor S.R., McLennan S.M.** The continental crust: its composition and evolution. 1985. Oxford: Blackwell. 312.
127. **Shimizu H.** Experimental study on rare-earth element partitioning in minerals formed at 20 and 30 kb for basaltic systems. // *Geochemical Journal*. 1980. V. 14. P. 185-202.
128. **Gast P.W.** Trace element fractionation and the origin of tholeiitic and alkaline magma types. // *Geochimica et Cosmochimica Acta*. 1968. V. 32. P. 1057-1086.
129. **Langmuir C.H., Vocke R.D., Hanson G.N., Hart S.R.** A general mixing equation with applications to icelandic basalts. // *Earth and Planetary Science Letters*. 1978. V. 37. P. 380-392.
130. **Yung J., Nataf H.-C.** Detection of mantle plumes in the lower mantle by diffraction tomography: Hawaii. // *Earth and Planetary Science Letters*. 1988. V. 159. P. 99-115.
131. **Rubie D.C., van der Hilst R.D.** Processes and consequences of deep subduction: introduction. // *Physics of the Earth and Planetary Interiors*. 2001. V. 127. P. 1-7.
132. **Yu. A. Kostitsyn.** Relationships between the Chemical and Isotopic (Sr, Nd, Hf, and Pb) Heterogeneity of the Mantle.// *Geochemistry International*.2007. Vol. 45. N. 12. P. 1173-1196.
133. **Yu. A. Kostitsyn** Isotopic Constraints on the Age of the Earth's Core: Mutual Consistency of the Hf-W and U-Pb Systems// *Geochemistry International*,2012, Vol. 50, No. 6, pp. 481-501
134. **Palme H., O'Neill H.S.C.** Cosmochemical estimates of mantle composition. // *Treatise on geochemistry*. 2003. V. 2. P. 1-38.
135. **Hofmann A.W.** Chemical Differentiation of the Earth - The Relationship Between Mantle, Continental-Crust, and Oceanic-Crust. // *Earth and Planetary Science Letters*. 1988. V. 90. P. 297-314.
136. **Mcdonough W.F., Sun S.S.** The Composition of the Earth. // *Chemical Geology*. 1995. V. 120. P. 223-253.
137. **Workman R.K., Hart S.R.** Major and trace element composition of the depleted MORB mantle (DMM). // *Earth and Planetary Science Letters*. 2005. V. 231. P. 53-72.
138. **Salters V.J., Stracke A.** Composition of the depleted mantle. // *Geochemistry, Geophysics, Geosystems*. 2004. V. 5.

LATE PALEOZOIC-EARLY MESOZOIC WITHIN-PLATE MAGMATISM IN NORTH ASIA: TRAPS, RIFTS, GIANT BATHOLITHS, AND THE GEODYNAMICS OF THEIR ORIGIN

Yarmolyuk V.V.¹, Kuzmin M.I.², and Kozlovsky A. M.¹

¹ *Institute of the Geology of Ore Deposits, Petrography, Mineralogy, and Geochemistry, Russian Academy of Sciences, Moscow,*

² *Vinogradov Institute of Geochemistry, Siberian Branch, Russian Academy of Sciences, Irkutsk*

A number of large areas of igneous provinces produced in North Asia in the Late Paleozoic and Early Mesozoic include Siberian and Tarim traps and giant rift systems. Among them, the Central Asian Rift System (CARS) has the most complicated structure, evolved during the longest time, and is a large (3000 x 600 km) latitudinally oriented belt of rift zones extending from Transbaikalia and Mongolia to Middle Asia and including the Tarim traps in western China. CARS was produced in the Late Carboniferous, and its further evolution was associated with the lateral migration of rifting zones; it ended in the Early Jurassic and lasted for approximately 110 Ma. CARS was produced on an active continental margin of the Siberian continent and is noted for largest batholiths, which were emplaced simultaneously with rifting. The batholiths are surrounded by rift zones and compose, together with them, concentrically zoned magmatic areas, with crustal (granitoid) magmatism focused within their central portions, whereas mantle (rift-related) magmatism is predominant in troughs and grabens in peripheral zones. The batholiths show geological and isotopic geochemical evidence that their granitoids were produced by the anatexis of the host rocks at active involvement of mantle magmas. Zonal magmatic areas of the type are viewed as analogues of large igneous provinces formed in the environments characteristic of active continental margins. Large within-plate magmatic provinces in North Asia are thought to have been generated in relation to the overlap of at least two mantle plumes by the Siberian continent during its movement above the hot mantle field. In the continental lithosphere, mantle plumes initiated within-plate magmatic activity and facilitated rifting and the generation of traps and alkaline basite and alkali-salic magmatic associations. Because of the stressed states during collision of various type in the continental margin, the mantle melts did not ascend higher than the lowest crustal levels. The thermal effect of these melts on the crustal rocks induced anatexis and eventually predetermined the generation of the batholiths.

INTRODUCTION

In the Late Paleozoic, practically all North Asia was affected by magmatic processes, which have produced the Siberian and Tarim traps and large magmatic area in structures surrounding the platform. Simultaneously magmatic areas of concentrically zonal structure were produced in the southern surroundings of the

Siberian craton (in Mongolia and eastern Transbaikalia); such zones were discovered by the Joint Soviet-Mongolian Expedition [39]. It was demonstrated in the western termination of the Mongolia-Okhotsk lineament [76] that the centers of such areas are large batholith "cores" consisting of granodiorite-granite massifs, and their peripheries are traced by zones of alkaline intrusions (zones of so-called diffuse magmatism). In the absence of necessary geological, geochronologic, and isotopic geochemical data, the genesis of this zoning was not then adequately interpreted.

Studies conducted over the past decade have shown that the magmatism of this epoch was induced by the effect of the North Asian [9, 66, 67, 63], as was demonstrated later, African [30, 31] superplume on the Siberian continent (including the Siberian craton itself and its surrounding structures), with the Siberian continent drifting above the plume throughout the whole Phanerozoic. The interaction of discrete hotspots of this superplume with the continent resulted in a number of magmatic areas, whose structural, compositional, and evolutionary differences were predetermined by the tectonic environment of the magmatic processes. While the Tarim and Siberian traps can be fully related to autonomous sub-lithospheric mantle activity, within-plate processes in the southern (in modern coordinates) margin of the paleocontinent (structures of the Central Asian Foldbelt, CAFB) developed in an active continental margin (ACM), as is pronounced in the magmatic associations. The convergence processes were correlated there with a marginal magmatic belt, which extends across Middle Asia, western China, Mongolia, and Transbaikalia for more than 3000 km and has a width of up to 800 km. Structures of this belt are overprinted by the Central Asian Rift System, whose discrete zones evolved throughout the Permian and Triassic.

Discrete evolution stages were responsible for the generation of various groups of magmatic associations. The oldest of them is typical of the environment of convergent boundaries of lithospheric plates. This group comprises volcanic associations of a differentiated complex of calc-alkaline and subalkaline rocks encompassing a broad spectrum of compositions (basalts, andesites, dacites, and rhyolites) and granitoids of corresponding composition (granodiorites, normal and subalkaline granites, and granosyenites). These associations were produced in the Early and Middle Carboniferous in southern Mongolia, and until the Late Carboniferous, in central and northern Mongolia-Transbaikalia [40, 61]. The marginal magmatic belt thus produced has a petrochemical zoning accentuated, first and foremost, by an increase of K_2O concentration in similar basalts and andesites toward intracontinental portions of the belt [61]. This type of zoning is typical of suprasubduction magmatism and, when considered along with geological data, testifies that this group of associations was formed in an environment of convergent lithospheric plates.

The other group of associations was generated within a time span starting in the terminate Late Carboniferous through the Late Jurassic. The rocks of this group exhibit compositional parameters and structural control typical of continental rifts.

These rocks are dominated by a bimodal (basalt-comendite-pantellerite) volcanic complex hosted in arrays of long grabens. Rift zones are traced by lengthway dike belts and numerous massifs of alkaline granites and syenites. Zones of bimodal magmatic rocks of this age are recognized as the Late Paleozoic-Early Mesozoic Central Asian Rift System (CARS) [62], which occurs throughout the whole territory of CAFB. Northwestern China, where the Early Permian Tarim traps were discovered at the western termination of CARS, was most thoroughly studied by Chinese geologists during the past decade [54, 6, 74, 41, 32]. This discovery extended the spectrum of rocks and modes of within-plate magmatic activity in the southern margin of the Siberian paleocontinent and provided further arguments in support of the within-plate nature of the rift system.

At the same time, CARS exhibits certain features generally atypical of classical rifts. It hosts not only traps and alkaline bimodal complexes but also granites of normal alkalinity, including those composing the largest batholiths in Asia: Angara-Vitim, Khangai, and Khentei. Together with rift zones bordering these batholiths, they compose autonomously developing concentrically zoned magmatic areas [30, 31, 66, 65, 60]. We believe that such an unusual combination of magmatic rocks typical, on the one hand, of rift zones and, on the other hand, of convergent zones was predetermined by the unusual geodynamic environment at the ACM of the Siberian continent, with this environment resulting in the interaction of a convergent boundary of the paleocontinent with mantle hotspots superimposed by this continent during its plate-tectonic motions [30, 31, 63].

Our studies were centered on the pervasively occurring spatiotemporal patterns and styles of within-plate activity at the Siberian paleocontinent and on their relations with the interaction of the continent with mantle hotspots (mantle plumes). We focused our attention first of all on magmatism in CARS, which shows, as was mentioned above, certain features atypical of continental rifting areas.

LATE PALEOZOIC-EARLY MESOZOIC WITHIN-PLATE MAGMATIC AREAS IN NORTH ASIA: EVOLUTIONARY STAGES AND DISTINCTIVE STRUCTURAL FEATURES

Table 1 summarizes data on the age of within-plate processes at the Siberian continent (North Asia), according to which the evolutionary history of the system comprises the following three major stages: (1) Late Carboniferous-Early Permian, (2) Permian-Early Triassic, and (3) Late Triassic-Early Jurassic. Figure 1 presents a schematic map of the distribution of the magmatic area produced during each of the stages.

Late Carboniferous-Early Permian Stage

This stage took place within the time span of 320-275 Ma and was responsible for the origin of spatially separated areas of within-plate magmatism in Tarim-southern Mongolia and Barguzin.

The **Tarim-southern Mongolia area** comprises the Tarim *traps* in the west and the *rift zones* in the Gobi-Tien Shan and the Main Mongolian Lineament in the east (Fig. 2).

The **Tarim traps** are lava piles of the alkaline basalt and tholeiite series [54], which occur over an area of approximately 2.5×10^5 km² at the Tarim microcontinent. The eruptions are thought to occur within the time span of 275-290 Ma [54, 74, 42, 32]. The northeastern part of the Tarim microcontinent hosts, along with traps, widespread Early Cretaceous bimodal associations (trachybasalts and acid tuffs) [42, 32]. Farther eastward, such associations are widespread in the Gobi-Tien Shan rift zone [62, 29, 28].

In the east, the trap area is bounded by zones of picrodolerite and picrite intrusions accompanied by Cu-Ni ore mineralization. The rocks of these intrusions are highly magnesian, have elevated alkalinity (particularly potassic), and are rich in titanium [43]. The rocks have been dated by various methods (SHRIMP, Re-Os, Sm-Nd, Rb-Sr, and K-Ar) at a narrow time interval of 288-282 Ma [37, 41]. The intrusions compose belts within fault zones that separate and bound the Tarim and Junggar microcontinents and grade into chains of grabens of the Gobi-Tien Shan and Main Mongolian Lineament rift zones in the east, in southern Mongolia.

The **Gobi-Tien Shan rift zone** (fig. 2) is a broad chain of grabens that extends from northwestern China along the Gobi-Tien Shan ranges across the whole southern Mongolia. The grabens are filled with rocks of a volcanic bimodal complex (basalts, basaltic andesites, comendites, pantellerites, and trachyrhyolites) accompanied by dikes of analogous composition and massifs of alkaline granites. The dikes compose lengthway belts of significant total thickness (up to 1 km and even more), which suggests a regime of large-amplitude overthrusts during their emplacement. The evolution of this rift zone proceeded at 319-280 Ma, as was determined by U-Pb and Rb-Sr dating alkaline granites and volcanics in various portions of the zone [69]. The rift magmatism is thought to occur in two discrete pulses. The earlier took place at approximately 319 Ma within relatively small areas in the central segment of the zone, in which grabens with basalt-comendite associations and alkaline granites were produced. The later pulse manifested itself at 290-280 Ma throughout the whole rift zone [28].

Magmatism in the rift zone is noted for producing both rock of the bimodal association and rocks of the calc-alkaline series: granodiorites and normal biotite granites. Geochemical data testify that the granites were derived from a crustal source by means of crustal anatexis under the effect of mantle magmas [68].

Table 1. Stages and areas of Late Paleozoic–Early Mesozoic within-plate magmatism at the Siberian Craton and folded structures around it in Central Asia (numerals in parentheses indicate rock ages, Ma)

Stages and areas of within-plate magmatic activity	
Late Carboniferous–Early Permian stage	Tarim–Southern Mongolian
<p>Barguzin zonal area</p> <p>Rift zones: Symyr: nepheline and pseudoleucite syenites, putaskites, alkaline granites, syenites, quartz syenites, and granosyenites (295, 290, 285); Uda–Vitim: grabens, depressions, subalkaline gabbro, syenites, granosyenites, alkaline syenites and granites, bimodal basalt–comendite associations (290–275); Saizhen: ultramafic alkaline rocks, alkaline gabbroids, nepheline syenites, and carbonatites (290–285); Eastern Sayan: agpaite and peraluminous granitoids, nepheline syenites, gabbro–syenite associations. Angara–Vitim batholith: Monzonites, monzosyenites, granites of normal alkalinity, quartz syenites, leucogranites, synplutonic subalkaline basites (305–280)</p>	<p>Tarim trap area: high–Ti basalts of the alkaline basalt and tholeiite volcanic series. Surrounding structures: bimodal associations and picrodolerite and picrite intrusions (290–275). Rift zones: Gobi–Tien Shan: grabens, depressions, bimodal basalt–comendite associations, dike belts, subalkaline and alkaline granites (318–280); Li–F granites (285); Main Mongolian Lineament: subalkaline and alkaline granites (315–290).</p>
Permian–Early Triassic stage	Khangai zonal area:
<p>Siberian igneous province</p> <p>Tunguska syncline and Taimyr: basalt lavas, dolerite sills (252–247), alkaline granites (240); Kuznetsk Basin: (250–246) picrites, dolerites, diorites, monzodiorites, kersantites, granites, and leucogranites (269–238); Western Siberian rift system: basalts, trachybasalts, basalt–trachyrhyolite associations (252–247).</p>	<p>Rift zones: Gobi–Altai: grabens, depressions, basalts, comendites, pantellerites, dike belts, alkaline granite and syenite massifs, picrodolerite and picrite intrusions (290, 270); Northern Mongolian: grabens, depressions, basalts, basalt–trachyte–pantellerite associations, alkaline granites, syenites, and gabbro–monzonites (270–250); Khangai batholith: gabbro, gabbro–diorites, granodiorites, granites, subalkaline leucocratic granites and granosyenites (270–240).</p>
Triassic–Early Jurassic stage	Mongolian–Transbaikalian area
<p>Antarctic province: (240–190)</p> <p>magmatic complexes in Taimyr, basalts in the Arctic Basin, dike complexes in the Franz Josef Land.</p>	<p>Rift zones: Western Transbaikalia: grabens, depressions, basalts, trachybasalts, pantellerites, alkaline trachydacites, alkaline granites, granosyenites, Li–F leucogranites (230–195); Northern Gobi Zone: grabens, depressions, basalt–trachyte–trachydacite and basalt–comendite associations, single-feldspar syenites, granosyenites and alaskites, agpaite and Li–F leucogranites (225–205); Kharkhorin Zone: volcanic depressions filled with basalt–trachyte and basalt–trachydacite associations, agpaite and Li–F granites, leucogranites, and granosyenites (215–205); Khentei–Dauria batholith: gabbro, diorites, granodiorites, melanocratic and leucocratic biotite granites, and Li–F granites (230–195).</p>

Note: Age data are compiled from the literature, see corresponding sections of the paper for the references.

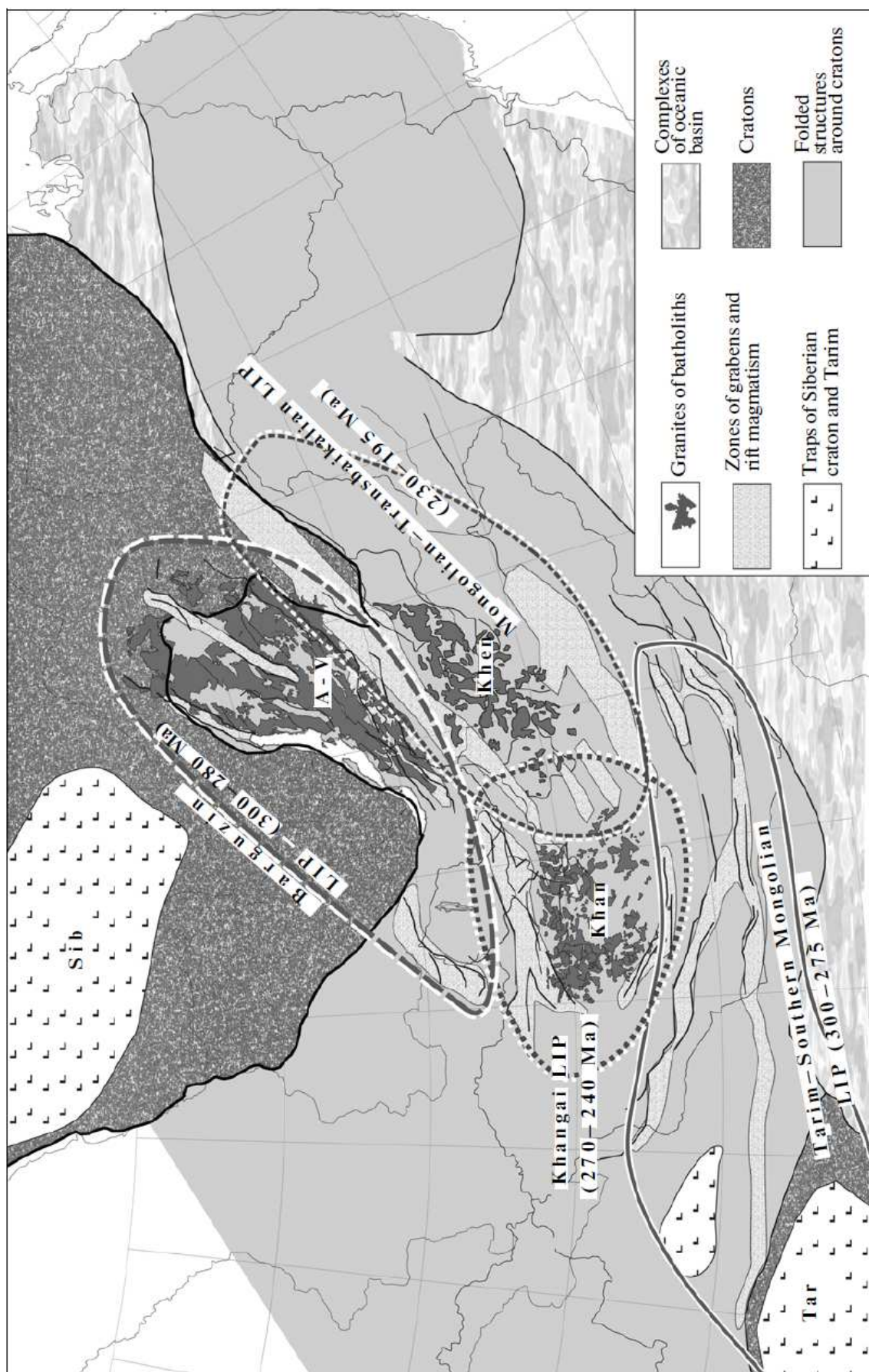


Fig. 1. Schematic map of the distribution of Late Paleozoic–Early Mesozoic large igneous provinces (LIP) in North Asia. Trap provinces: Sib—Siberian, Tar—Tarim; batholiths: A—V—Angara—Vitim, Khan—Khangai, Khen—Khentci.

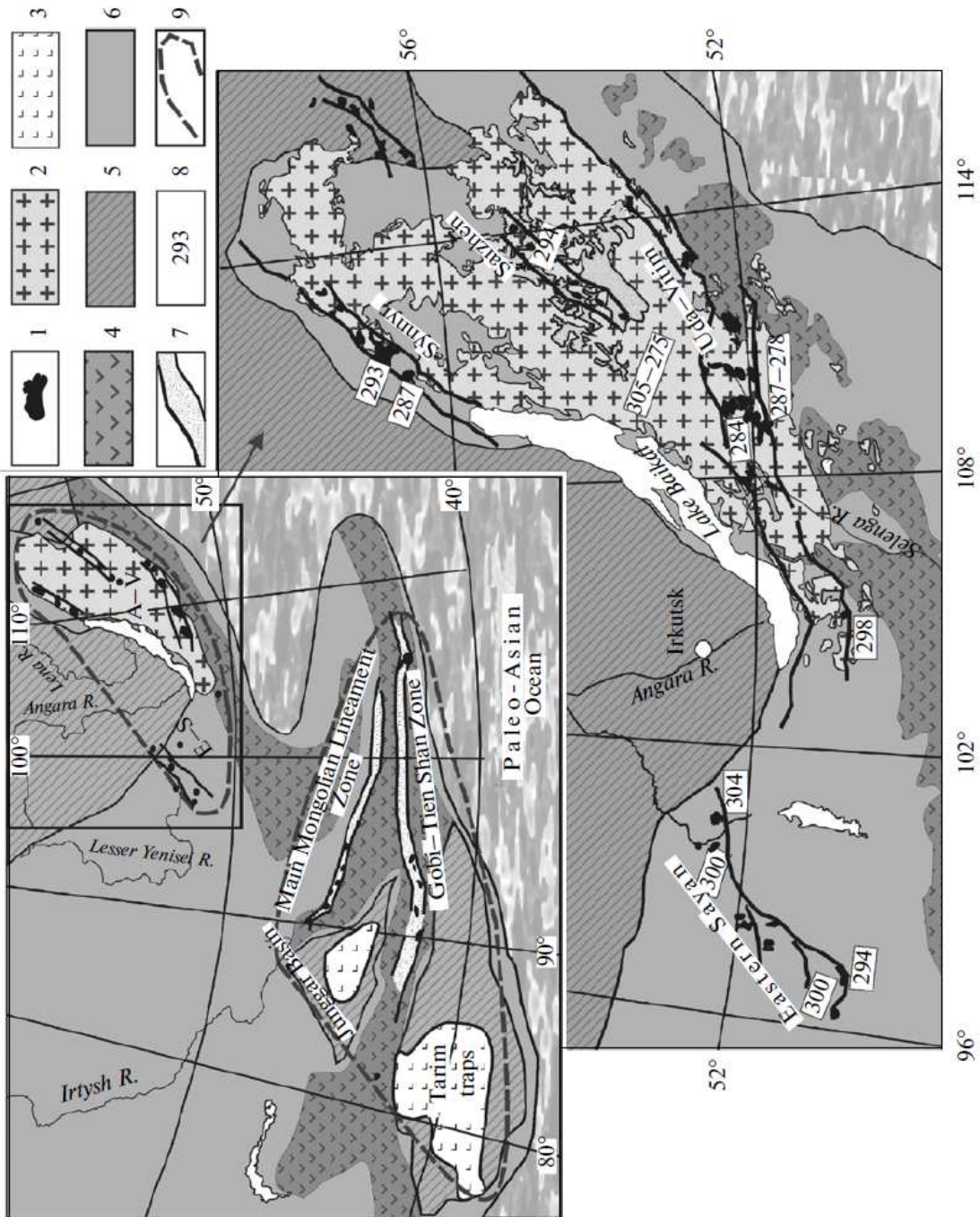


Fig. 2. Schematic map of the Early Permian Barguzin zonal magmatic area. The inset is a location map of the area in the system of magmatic areas produced in the Late Carboniferous–Early Permian at 305–275 Ma. (1) Massifs of alkaline rocks; (2) Angara–Vitim batholith; (3) traps; (4) volcanic complexes of the Early–Middle Carboniferous marginal belt; (5) cratons; (6) Paleozoic folded areas; (7) rift zones; (8) rock ages (Ma); (9) boundaries of magmatic areas.

The ***rift zone of the Main Mongolian Lineament*** (fig. 2) is controlled by the tectonic boundary between Caledonian and Hercynian structures in Mongolia. The zone is traced mostly by exposures of massive alkaline granites, which extend as a discontinuous chain for more than 800 km. The age of these rocks insignificantly varies along the strike of the zone. The U-Pb age of alkaline granites from the Mandakh Massif near the eastern termination of the zone is close to 292 Ma, and the alkali feldspar granites in the Bum Massif in the western part of the central segment of the zone were emplaced at 294 Ma [69]. The Rb-Sr isochron age of analogous rocks in the western part of the rift zone varies from 315 to 285 Ma [18, 59]. The nearby picrite intrusions were emplaced at 288-282 Ma [37, 41]. The rift zone was thus formed within the same time span when the Gobi-Tien Shan zone was produced.

The **Barguzin magmatic area** is located at a distance of more than 2000 km from the Tarim-southern Mongolia area and differs from the latter, first of all, in very widely spread granitoids. The zone hosts the largest Angara-Vitim granitoid batholith and rift zones bounding its flanks.

The ***Angara-Vitim (or Barguzin) batholith*** is one of the world's largest batholiths, which is exposed over an area of more than 150000 km² (fig. 2). According to geophysical data, the batholith is a single lopolith-shaped body 5-7 km in average thickness, with individual swells extending to depths of up to 30 km [55]. The volume of the batholith is likely close to 1 million km³. The batholith is composed of granites, monzonitoids, syenites, granosyenites, and leucogranites [33]. The granites are combined into a number of complexes of various composition, which are thought [33, 52, 53] to differ in age. According to various geochronologic data (U-Pb, Ar-Ar, and Rb-Sr), the age of the batholith ranges from 330 to 280 Ma [52, 53, 67]. At the same time, the U-Pb age (determined using minute amounts of zircons and individual zircon crystals) of rocks from the batholith indicates that all of its numerous complexes were produced within the time span of 303 ± 7 to 281 ± 1 Ma [67, 23], with the ages of individual complexes overlapping within the errors. This led us to conclude [23] that the Angara-Vitim batholith was produced during a time span no longer than 22 Ma, and the differences between its compositions were predetermined first of all by the compositional differences of the source rocks from which the granitoids were derived and by the erosion depths of the complexes.

The **rift zones** (fig. 2) of the area are marked by belts of alkaline rocks [67, 71]. These are the Uda-Vitim zone in the south, the Synnyr zone in the north, the Eastern Sayan zone along the western boundary of the batholith in the Eastern Sayan Range and eastern Tuva, and the Saizhen zone along the axis of the batholith.

The ***Synnyr zone*** comprises exposures of alkaline rocks: nepheline and pseudoleucite syenites, pulas-kites, alkaline granites, and subalkaline rocks:

syenites, quartz syenites, and granosyenites [17, 45, 47]. These rocks, which are collectively referred to as the Synnyr Complex, compose a number of massifs that are traced along an array of northwest-trending faults for approximately 600 km. The rocks of the zone were dated at 295-288 Ma [47, 43, 67].

The *Uda-Vitim zone* hosts numerous gabbro-monzonite, alkaline granite, granosyenite, and syenite massifs, including such large ones as the Khorinskii and Bryanskii massifs [35, 21], dike swarms, and volcanic rocks of bimodal associations, which are dated at 298-275 Ma [34, 35]. The zone is controlled by northwest-trending faults and locally overprints marginal portions of the Angara-Vitim batholith. The relations between the alkaline rocks and granites of the batholith testify that they have similar ages. For example, we have detected mingling textures in gabbro-monzonite in certain parts of the rift zone at contacts with granites of the batholith, and these textures suggest that the rocks were emplaced simultaneously, and the granite and basite melts mingled [34].

The *Saizhen zone* includes massifs of alkaline rocks: alkaline pyroxenites, ijolites, urtites, nepheline syenites, and carbonatites, which are grouped into the Saizhen Complex [17]. Nepheline syenites of some of the massifs intrude the granites of the batholith, and some of the rocks were included in the Zazinskii Complex of granitoids of elevated alkalinity, the second most important granitoid complex of the batholith [17, 33]. The geochronologic data are consistent with geological relations and constrain the age of rocks in this zone to 305-280 Ma [42, 11].

The *Eastern Sayan zone* controls the distribution of massifs of agpaitic and peraluminous granitoids, nepheline syenites, and rocks of the gabbro-syenite association in eastern Tuva. The zone extends along the eastern boundary of Tuva and continues along the Eastern Sayan Range for more than 450 km. The alkaline granitoids were dated at 305-292 Ma [71, 48]. The rocks of the zone typically bear elevated concentrations of rare metals, first of all, Ta, Nb, Zr, REE, and Li and are accompanied by a number of large mineral deposits, such as Ulug-Tanzek, Sol'-Bel'dyr, and Zashikhinskoe.

The data presented above, first of all, the dates, testify that, in spite of differences in the compositions of the rocks and their geological settings, magmatic processes in the marginal and central parts of the Barguzin area occurred virtually simultaneously. It is thought that this roughly simultaneous occurrence of rifting processes and batholith emplacement was predetermined by a common source of regional endogenic activity, namely, a mantle plume [67]. The effect of this plume gave rise to rift magmatism in the marginal portions of the area and induced the anatexis melting of the crust under the effect of mantle magmas in the central part of the area. Relations between anatexis and the activity of the mantle plume also follow, for example, from the fact that the central parts of the batholith includes abundant dikes of alkaline gabbroids [33, 67], which were produced by mantle magmas and were emplaced simultaneously with the granites of the batholith.

Permian-Early Triassic

This stage was responsible for the origin of the large Khangai and Siberian igneous provinces, which show differences similar to those between the Tarim-southern Mongolian and Barguzin magmatic areas.

The **Khangai igneous province** encompasses a territory of more than 150 000 km² and has a zonal concentric structure. Its central portion is occupied by the Khangai batholith, and the peripheries are controlled by the Gobi-Altai and northern Mongolian rift zones (table 1, fig. 3).

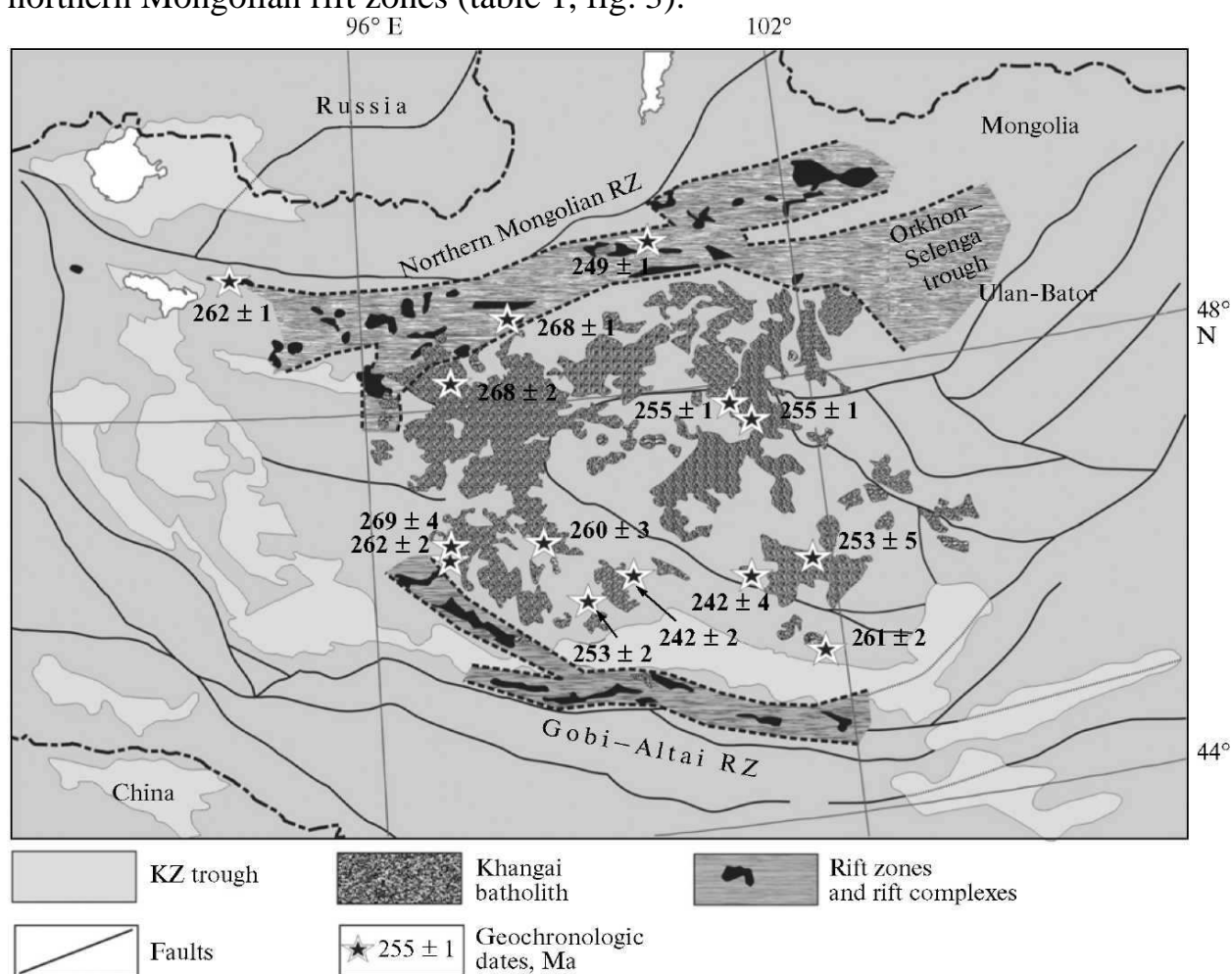


Fig. 3. Schematic map of the Khangai zonal magmatic area.

The **Gobi-Altai** rift zone is a linear array of grabens filled with rocks of a bimodal volcanic complex: basalts, comendites, pantellerites, and spatially related alkaline granites and syenites. The zone extends for more than 800 km along the northern face of the Gobi Altai Range and structurally coincides with the suture that separates the Vendian-Cambrian ophiolites of the Lake Valley and the terrigenous terranes of the Gobi Altai in the basement of the territory. The axial portions of the grabens are traced by dike belts, whose total thickness locally exceeds 1000 m [62]. This led us the conclusion about large enough amplitudes of

extension when the rift zone was formed. Its age estimates rely mostly on paleobotanical data, which suggest that the lavas that fill the grabens were erupted in the second half of the Permian [62].

The *northern Mongolian rift zone* was traced along the northern boundary of the Khangai batholith and is controlled by a latitudinal array of faults that coincides with the Khan-Khukhei, Bolnai, and Butulin-nuru ranges. Structurally, the zone is a wide enough system of echelon grabens filled with basalt and basalt-trachyte-pantellerite volcanics. The zone also hosts numerous massifs of alkaline granites, syenites, and gabbro-monzonites. The zone extends for 500 km and has a width of up to 70 km. Paleobotanical data date the zone at the Late Permian [62]. Our U-Pb (unpublished data) and Rb-Sr isochron data are consistent with this conclusion, and hence, rift-related magmatism occurred in northern Mongolia at 270-250 Ma, mostly in the Late Permian.

Near the eastern termination of the rift zone, it is bounded by structures of the Orkhon-Selenga trough at the northeastern margin of the Khangai batholith. The magmatic associations of the trough compose relatively thin piles of Late Permian-Early Triassic mafic lavas, which were erupted at 260-240 Ma [4, 5]. The basites of these associations exhibit enriched geochemical and isotopic signatures and are in this sense analogous to the basites of bimodal associations in the rift zone [5]. The evolution of the trough was associated with the emplacement of numerous gabbro and gabbro-monzonite sills, dikes, and stocks. Simultaneously the Nomgon layered massif was emplaced near the margin of the batholith. The massif was dated at 256 Ma [19, 20] and hosts Cu-Ni ore mineralization with Pt. The Nariin-Tolburiigol Massif has similar age (249-252 Ma) and composition and also occurs in the Orkhon-Selenga trough [3]. According to [19], analogous massifs are also known in other parts of the zonal area. One of them is the Dzara-ula gabbro-monzonite massif (269-262 Ma) in the southwestern portion of the zonal area. The rock associations of the massifs of this type are comparable with those of layered massifs with ore mineralization in the Tarim-southern Mongolian area, and this suggests certain similarities between magmatism in these areas.

The *Khangai batholith* is the largest fragment of the area. It is situated between the Gobi-Altai and northern Mongolian rift zones and the Orkhon-Selenga trough (fig. 3). The batholith is composed by large granitoid massifs occurring over an area of more than 120000 km² (fig. 1). Geophysical data [56] indicate that the batholith is a giant tabular body 5-7 km thick on average. The volume of granites (>700 000 km³) of the Khangai batholith is comparable with that of the Angara-Vitim batholith. The former consists of a number of rock complexes [14, 16, 51, 8]. The oldest Tarbagatai Complex comprises granodiorites, tonalites, plagiogranites, and, in its older phases, gabbro and gabbro-diorites. The batholith is dominated by rocks of the Khangai Complex, which are medium- to coarse-grained porphyritic hornblende-biotite and biotite granodiorites and granites with mutual facies gradations. The youngest rocks of the batholith are leucocratic granites of the Sharausgol Complex. Synplutonic intrusions (dikes, stocks, and

small bodies) of basites have a fairly unusual setting: they ubiquitously occur in variable proportions and have mingling zones of their melts at contacts with granitoids of the batholith. It is pertinent to mention that the isotopic and geochemical characteristics of these rocks are analogous to those of basalts in rift zones around the batholith.

We have conducted a systematic geochronologic study of rocks collected from various complexes of the Khangai batholith [67, 70] and obtained U-Pb dates for the emplacement of the batholith at 269-242 Ma, which corresponds to the second part of the Permian-Early Triassic. The Rb-Sr isotopic dates are similar: 255 [24], 269, 252, and 248 Ma [50] (table 1). In spite of the giant size of the massif, its evolution was likely constrained within a brief time span of 27 Ma, which is comparable with that of the Barguzin batholith.

The geological and geochronological data presented above unambiguously indicate that the batholith was emplaced simultaneously with magmatic processes in neighboring rift zones.

The **Siberian igneous province** comprises the traps of the Siberian craton and the rift system of central Siberia closely related to them (fig. 4).

The *trap* part of the province is noted for the strong predominance of mafic rocks and their vast volume of more than $1.5 \times 10^6 \text{ km}^3$ [31]. Currently available age estimates [1, 44] testify that the trap province was formed generally within a very narrow age interval of 250-248 Ma. Furthermore, Ar-Ar data [9] indicate that the traps in the Kuznetsk basin were also produced in the earliest Triassic (at approximately 249 Ma).

The *western Siberian rift system* contains bimodal volcanic associations of basalts, subalkaline basalts, and rhyolites. The volcanic processes were controlled by grabens, which are traced for up to 1500 km across the whole West Siberian Plain, from its southern boundary to the Arctic Ocean. Volcanic events (dated at approximately 249 Ma) in this rift system were coeval with the pulse of trap eruptions at the platform [1, 30, 44]. Acid derivatives of these associations were derived by melting the sialic crust under the effect of basaltic magmas [1].

Although the province is obviously dominated by rocks produced within a narrow age interval at the Permian-Triassic boundary, certain data suggest that magmatic processes occurred in this area in a number of stages [10]. For example, U-Pb SHRIMP zircon age values of ore-bearing rocks in the Norilsk intrusion [10] make it possible to distinguish zircon generations dated at 260 ± 5 , 250.7 ± 1.5 (resorbed crystals), and 228.4 ± 1.4 Ma (euhedral crystals). These stages are more strongly pronounced in the evolution of Permian-Triassic magmatism in the Kuznetsk Basin, in which the following endogenic events were distinguished: dolerite and diorite dikes (262-269 Ma) → Tasharinskii picrite-dolerite complex (257-252 Ma) → granitoids of the Priobskii Complex (255-249 Ma) → Kuznetsk Basin traps (250-246 Ma) → dolerites, monzonites, and kersantites of the Tomsk area (243- 238 Ma) → granites and leucogranites of the Barlaskii Complex (240 Ma) [10]. With regard for these data, it is reasonable to conclude that the Siberian

magmatic province was produced within the same age range as the Khangai area. The most important difference between the province and area is that the evolutionary history of the former included a single predominant pulse of magmatism.

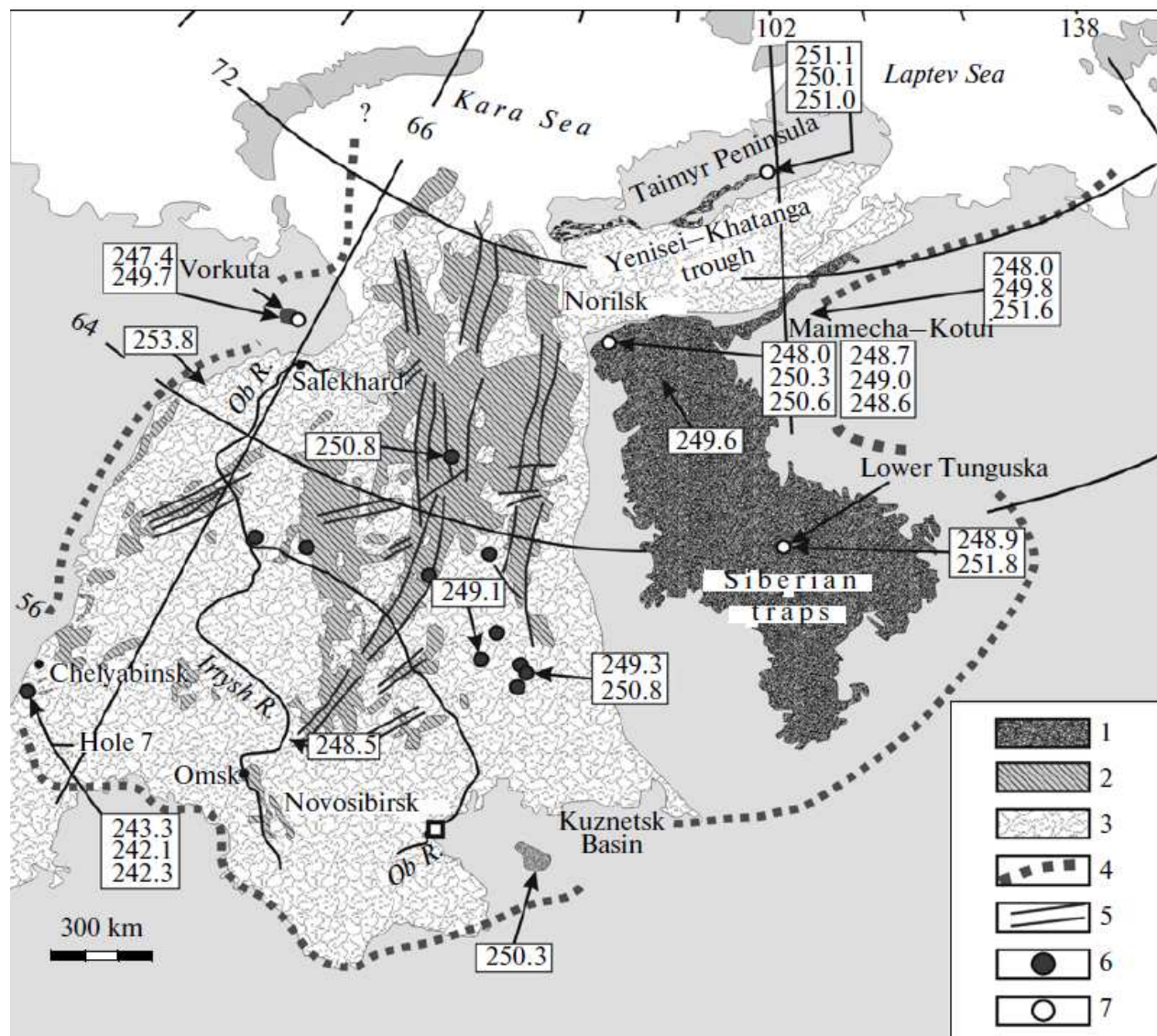


Fig. 4. Schematic map of Late Permian-Early Triassic magmatism at the Siberian craton and Western Siberian Plate [44].

(1) Traps; (2) buried basalts and tuffs; (3) cover of the Western Siberian Plate; (4) boundaries of volcanic provinces; (5) rifts; (6, 7) sampling sites: (6) from borehole core material, (7) from basalt exposures.

Triassic—Early Jurassic Stage

This stage produced the large (800 × 400 km) **Mongolia-Transbaikalia magmatic area** in Central Asia, and the structure of this area resembles that of the Khangai area: it also shows a symmetrically zonal distribution of its magmatic complexes (fig. 5). The core of the magmatic area is composed of the Khentei or

Khentei-Dauria granite batholith, and the outermost zones host alkaline and bimodal associations and are referred to as the Western Transbaikalian (northwestern), northern Gobi (southern), and the Khorkhorin (western) rift zones.

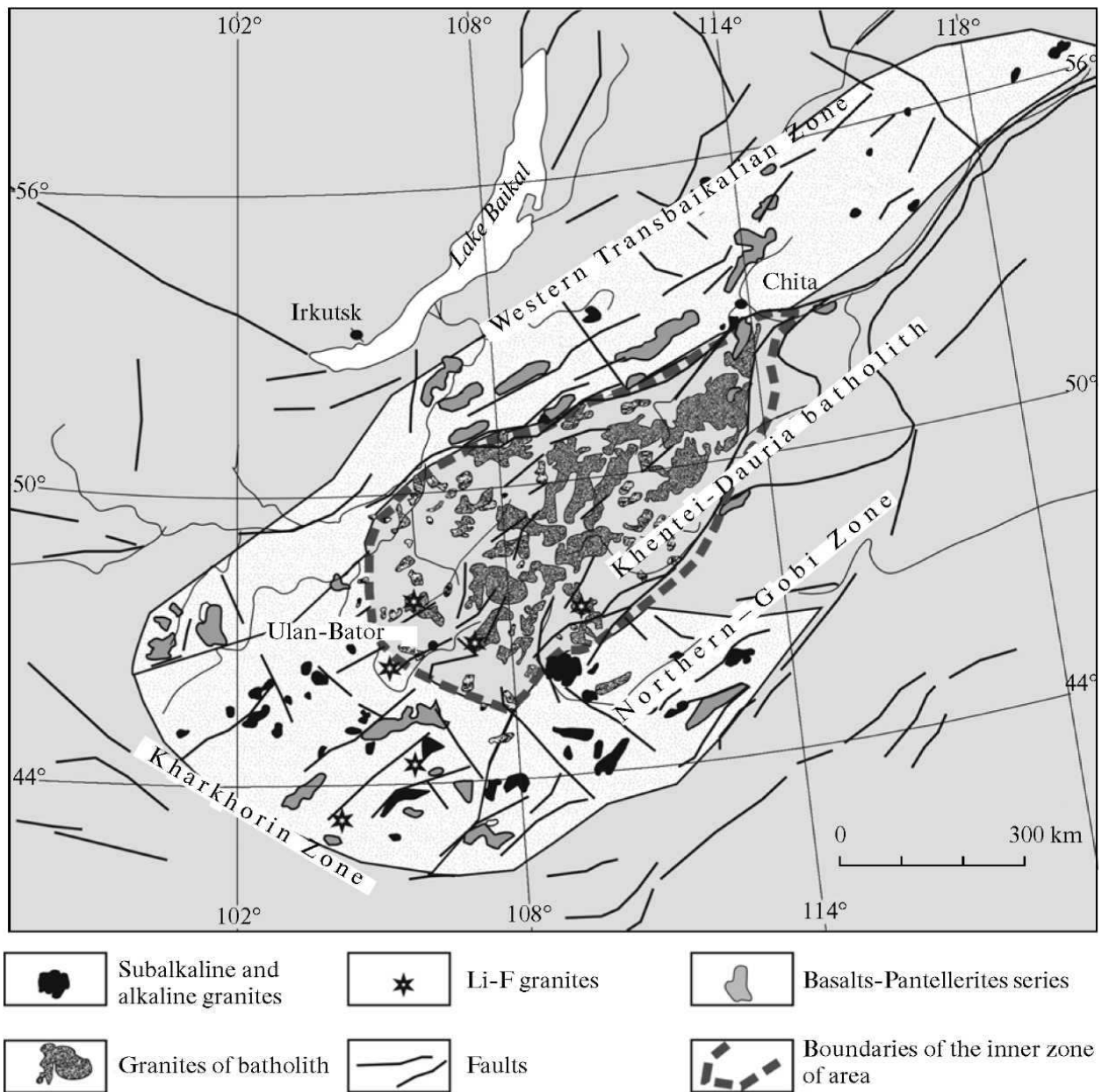


Fig. 5. Schematic map of Mongolia-Transbaikalia Early Mesozoic zonal area.

The *western Transbaikalian rift zone* coincides with troughs in the northern and northwestern surroundings of the Khentei-Dauria Highland, which were traced from the eastern Khangai along the Dzhida, Uda, and Khilok rivers to the upper reaches of the Vitim River. The zone is up to 200 km wide, extends for more than 1000 km [58, 64] and comprises volcanic fields of plateau-basalt and bimodal volcanic associations and numerous hypabyssal massifs of alkaline granites, granosyenites, and Li-F granites. The most widely spread granites belong to the

Kunaleiskii Complex and bimodal volcanic sequences of the Tsagan-Khuntei Formation, which occur as volcano-plutonic associations [58]. Structures of the zone define arrays of lengthway normal faults, grabens, horsts, and dike belts, and this suggests, when considered together with the abundance of alkaline granites, plateau basalts, and bimodal basalt-comendite associations in this zone, that the origin of this portion of the magmatic area was significantly affected by rifting. The zone was formed within a narrow age interval of 230-195 Ma, as follows from U-Pb, Rb-Sr, and K-Ar dates for rocks from the Tsagan-Khuntei Group and the alkaline granites [64, 36, 58, 34].

The ***northern Gobi zone*** includes Early Mesozoic magmatic rocks in the southern surroundings of the Khentei-Dauria Highland, in the Dashibalbar-northern Choibalsan trough system [39]. The zone contains subalkaline rocks of volcanic (basalt-trachyte-trachydacite and basalt-comendite) and plutonic granitoid associations. They compose numerous volcanic fields relatively small in area and hypabyssal and subvolcanic massifs. The occurrence of the rocks is controlled by a belt (up to 200 km wide and up to 300 km long) of faults and related depressions and grabens of northeastern trend. Among the predominant plutonic rocks of the zone, the most widely spread ones are single-feldspar syenites, granosyenites, and alaskites, including their Li-F and agpaitic varieties. The granites and volcanic rocks often compose volcano-plutonic associations, which are prone to fill grabens. An example of these associations is the Dashibalbar association, which is spatially restricted to a large graben filled with Triassic sedimentary and volcanic rocks, and the Dzarthakhuduk association in the Ulziit area [62]. Both associations include swarms of lengthway dikes, which provide evidence of large-amplitude extension during their emplacement. The age of the rift zone was constrained to 221-195 Ma by U-Pb, Rb-Sr, and Ar-Ar dating alkaline rocks from its various parts.

The ***Kharkhorin zone*** comprises alkaline and subalkaline magmatic rocks occurring between the Khangai and Khentei highlands and connects the western Transbaikalia and northern Gobi rift zones. The zone trends generally to the northeast, conformably with the predominant fault array of the so-called Kharkhorin structural step [39]. The inner structure of the zone is, however, determined by small narrow grabens and faults of northeastern trend that cut across the zone. They control the distribution of massifs of leucocratic granite (Li-F, alkaline granite, and granosyenite) associations and individual volcanic fields of rocks of the basalt-trachyte and basalt-pantellerite associations. The relative age of these volcanics is defined by the fact that they unconformably overlay Early Permian rocks. Their U-Pb, Rb-Sr, and K-Ar isotopic ages lie within the range of 220-200 Ma [65, 26].

The ***Khentei-Dauria batholith*** (fig. 5) at the Khentei-Dauria Highland is a group of closely spaced plutons, which merge at a certain depth into a single tabular body approximately 500 km long and up to 300 km wide (geophysical data). Its average thickness is 5 km and locally increases to 20 km [57]. Judging from these values, the body is comparable with the batholiths considered above.

The Khentei-Dauria batholith consists of granitoids of a broad spectrum of compositions from granodiorite to leucogranite, with the predominance of melanocratic and leucocratic biotite granites [24, 39, 65] and a subordinate volume of gabbro and diorites. The latter compose single bodies corresponding to initial intrusion phases and occur as unevenly distributed spherical segregations up to 1 m across in the main-phase granodiorite [24], corresponding to synplutonic basite magma injections. As in other batholiths, the occurrence of such rocks testifies that the granitoid magmas were produced with a contribution of basite (mantle) magmas. The youngest rocks of the batholith are relatively small dike- and stock-shaped leucogranite bodies, including Li-F rare-metal varieties [26].

The age of the rocks composing the batholith has long been a matter of discussion and was estimated within a fairly broad range, from Early Carboniferous to Late Jurassic, according to traditional interpretations of regional geological data and the highly contradictory K-Ar dates of the granitoids [24, 16]. We have conducted systematic U-Pb and Rb-Sr geochronologic studies of rocks of various phases of the batholith [65]. Our results indicate that the rocks crystallized at 230-195 Ma, and hence, similar to the Khangai and Barguzin batholiths, the Khentei batholith was produced within a relatively brief time span.

ZONAL MAGMATIC AREAS AS A MODE OF PLUME-RELATED MAGMATIC ACTIVITY

Late Paleozoic-Early Mesozoic within-plate magmatic activity in North Asia resulted in two trap provinces: the western Siberian and Central Asian rift systems. We believe that this activity has also produced three world's largest batholiths, which are now important structural elements of CARS and compose, together with their bounding rift zones, giant concentrically zoned magmatic areas of unique structure. Moreover, we are also prone to believe that these areas correspond to projections of mantle plumes in the lithosphere. This follows from the analysis of the evolutionary history of magmatism in CARS, according to which the structures were formed by the successive development of a number of magmatic areas of similar structure.

According to geochronologic and geological data, within-plate processes proceeded in this part of CARS during a time span approximately 110 Ma long, between 305 and 195 Ma, and systematically propagated from the paleocontinental margin inward the continent. The first result of this activity was the Tarim-southern Mongolian magmatic area in the margin of the continent. This area comprised the Tarim traps and rift zones (in the Gobi-Tien Shan and the Main Mongolian Lineament). In the middle of Early Permian (between 280 and 270 Ma), the area of within-plate processes shifted from southern to central Mongolia and induced the origin of the Khangai zonal area at 270-240 Ma. In the Early Mesozoic (240-230 Ma), the activity centers shifted farther eastward, into eastern Mongolia, where the eastern Mongolian-Transbaikalian area started to develop beginning at approximately 230 Ma. Thereby the style of magmatism practically

did not change. Similar to the Late Carboniferous-Early Permian Gobi-Tien Shan rift zone, the Late Permian and Early Mesozoic rift zones are dominated by bimodal basalt- comendite and basalt-pantellerite volcanic associations and related alkaline granitoid massifs. This accentuates the obvious similarities between the processes that gave rise to rift zones in Mongolia. Moreover, the "corridors" between magmatic areas of various age host magmatic complexes of common and intermediate age and composition. For example, the Gobi Altai ranges between the Tarim-southern Mongolian and Khangai areas contain alkaline and subalkaline granites dated at 290-270 Ma [27], our unpublished data] that were produced within the time span between the ages of magmatic rocks from that areas.

The territory between the Khatngai and Mongolian-Transbaikalian areas is typified by magmatic complexes in the Orkhon-Selenga trough. These complexes were formed starting in the Late Permian until the Late Triassic inclusive [5], i.e., throughout the whole time span when the magmatic centers migrated between the areas.

We believe that this systematic migration of continental magmatic area over the CAFB territory was related to the movement of the paleocontinent above a mantle plume, which is referred to as the Mongolian plume [66]. The amplitudes of these movements, which were evaluated based on the coordinates of the central portions of magmatic areas of different age, were 400-500 km (at the transition from southern to central Mongolia) and close to 800 km (at the transition to eastern Mongolia). The velocities of these movements ranged between 2 and 4 cm/year, i.e., were comparable with those of lithospheric plates and are thus consistent with the hypothesis that the migration of magmatic areas in the Central Asian Rift System was related to the movements of the continent above a mantle plume.

Another chain of areas of within-plate magmatic activity is traced by the Barguzin area, Siberian trap province, and perhaps, also Triassic eruptions in Arctic part of the continent [22]. We believe that it was related to the passage of the lithosphere above the Siberian plume [30].

Obviously, a distinctive feature of the affects of both plumes was the development of zonal areas with giant batholiths. The batholiths are located between rift zones and mark the central parts of the magmatic areas of certain age. The interrelated development of rift zones and batholiths was predetermined not only the simultaneous occurrence of rift-related (mostly basite and alkaline) magmatism, on the one hand, and granitoid anatectic magmatic, on the other, but also the usual occurrence of synplutonic basite dike in the batholiths, with these dikes showing isotopic and geochemical features analogous to those of basites in the rift zones. The occurrence of these intrusions testify that mantle sources contributed to the generation of the magmas throughout the whole magmatic areas. It can be generally concluded that magmatism in the zonal areas was highly productive. At the same time, practically no simultaneous magmatic processes manifested themselves in structures surrounding these areas, and this led us to suggest that the influence area of the mantle plumes on the lithosphere was

constrained to the zonal magmatic areas and was no less than 500 km in diameter. This size can be regarded as characteristic of the mantle plumes that controlled the magmatic processes.

SOURCES OF MAGMATISM IN THE ZONAL MAGMATIC AREAS

Sources of basite magmatism in the rift zones. Figure 6 summarizes data on the chemical composition of magmatic associations in the Mongolian and Transbaikalian sectors of CARS. The compositions show a clearly pronounced bimodal distribution with maxima at 48-54 and 72-78 wt % SiO₂.

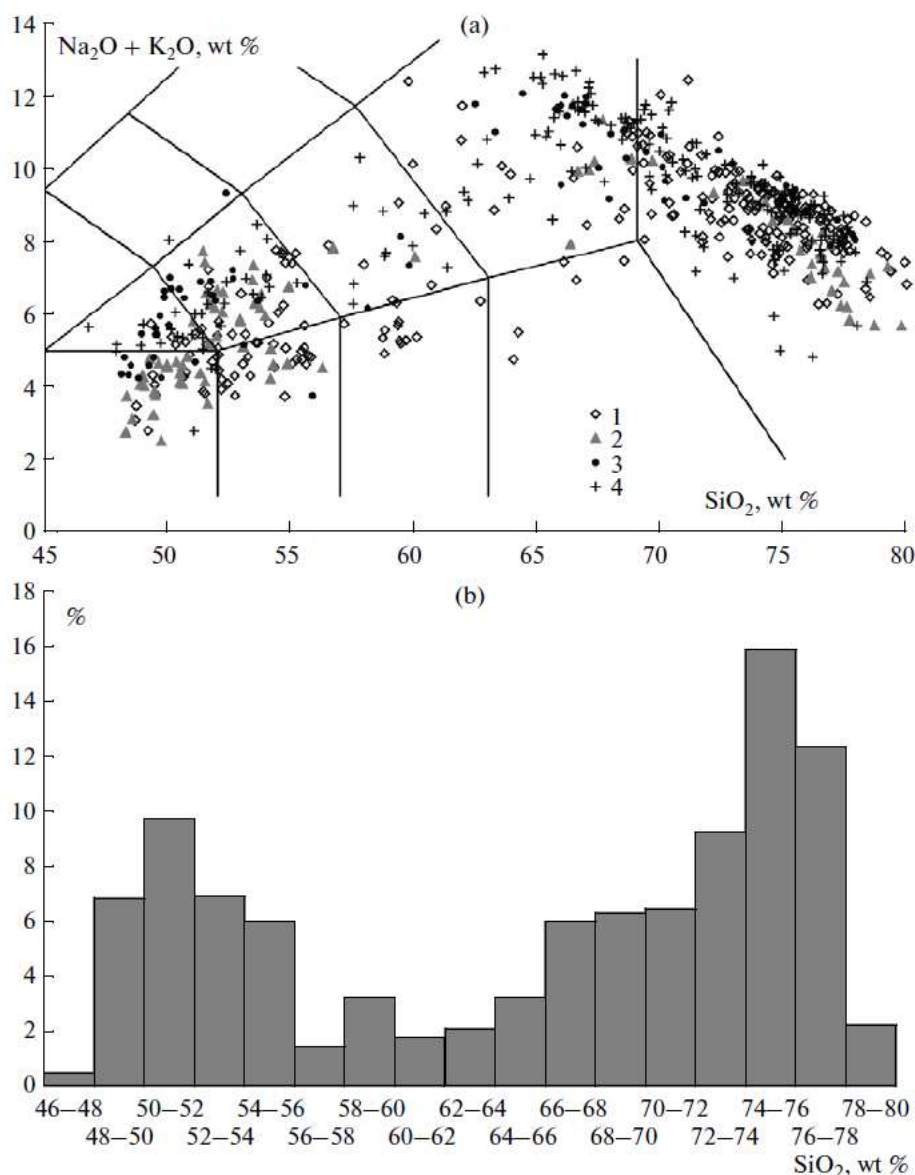


Fig. 6. (a) Chemical compositions of Late Paleozoic-Early Mesozoic rift magmatic rocks and (b) histogram of the abundances of the rocks with various SiO₂ concentrations.

(1-3) Late Paleozoic rift zones: (1) Gobi-Tien Shan, (2) Gobi-Altai, (3) northern Mongolian; (4) Early Mesozoic rift zones in the Mongolian-Transbaikalian area.

In spite of the subordinate amount of rocks of intermediate composition, basite and salic components of the association are usually related through evolutionary transitions controlled by fractionation crystallization with the participation of contamination. Relations of this type are pronounced in the variations in the concentrations of trace elements and their ratios and in the similar isotopic composition of the rocks [25, 29]. According to this conclusion, the bimodal rift associations were produced by mantle magmas. In order to elucidate the compositional specifics and possible variations of the sources in various CARS portions, we have conducted isotopic and geochemical studies of the products of basite magmatism, first of all, those in rift zone related to the development of the Mongolian plume. For comparison, we utilized materials on the composition of magmatic rocks in the Barguzin area [66, 67] and literature data on traps in the Tarim Basin [75, 72], Siberian craton, and mafic volcanics in the western Siberian rift systems [1].

Table 2 and fig. 7 report the average concentrations of trace elements of basites from each of these areas and in the traps in the Tarim Basin and Siberian Platform and basalts in the Western Siberian Rift System. As can be seen in the diagrams, the CARS basites differ from OIB in lower concentrations of HFSE (Zr, Hf, Ti, Th, and particularly, Ta and Nb) and relatively high concentrations of Ba, K, Pb, and, to a lesser extent, Sr and P.

The REE patterns of the rocks are similar to those of OIB at somewhat lower LREE concentrations and lower $(La/Yb)_N$ ratios. These features are generally typical of mafic rocks in within-plate magmatic areas in Siberia and surrounding folded structures. The relatively low HFSE concentrations of the CARS rocks can likely be explained by the origin of these rocks in a territory that evolved as an active continental margin immediately before rifting [62, 8, 69]. The influence of the plume on the upper mantle metasomatized during subduction resulted in the interaction of the plume and subducted (water-enriched) components in the magma source and caused the preservation of minerals concentrating HFSE in the residue. This interaction was illustrated, for example, by the example of basites in the Gobi-Tien Shan Rift Zone, whose source contained, along with a plume component, also a pronounced subduction-related component enriched in water [29].

The comparison of the CARS basalts with traps in the Siberian craton reveals their similarities, and this led us to suggest that the compositions of the sources were similar. Furthermore, with regard for the geological setting of the magmatic areas (at a craton, within microcontinents with a Riphean crust, and in Phanerozoic foldbelts), it should be admitted that geochemical features of the basites are most closely similar, first of all, to the mantle sources. As was mentioned above with reference to the CARS basites, these sources obviously contained subducted metasomatized mantle material, and this predetermined pervasively low Ta and Nb concentrations in the melts. The occurrence of such upper mantle material at the lowermost lithospheric levels beneath Siberia is consistent with paleogeographic reconstructions, according to which the continent

was affected by significant plate-tectonic movements that occurred starting in the Early Paleozoic until the Late Paleozoic [31, 30]. The continent thereby moved above metasomatically recycled upper mantle, which was reworked in subduction zones before the continental margin. Accordingly, it can be suggested that the mantle beneath the continent had generally suprasubduction characteristics. This explains the involvement of this mantle in the source of traps in the Siberian craton.

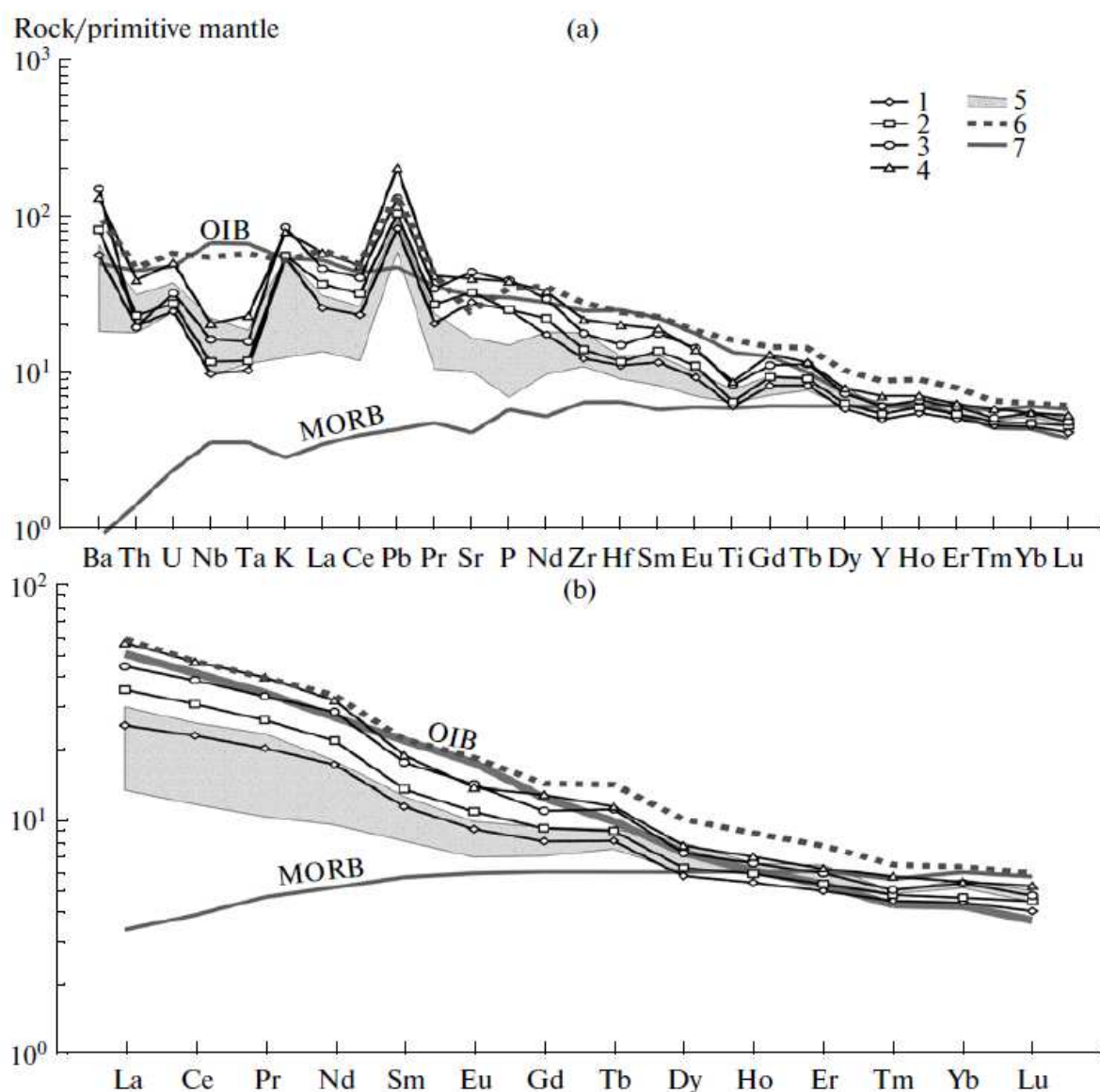


Fig. 7. Primitive mantle-normalized (Sun and McDonough, 1989) trace-element patterns of basaltoids in Late Paleozoic-Early Mesozoic large igneous provinces in North Asia.

(1-3) Basaltoids of Late Paleozoic rift zones: (1) Gobi-Tien Shan, (2) Gobi-Altai; 3. northern Mongolian; (4) basaltoids of Early Mesozoic rift zones in the Mongolian-Transbaikalian area; (5) composition field of traps in the Siberian Platform constrained by the average compositions of tholeiitic and subalkaline basalts [1]; (6) Tarim traps [75, 73]; (7) model basalt compositions of mid-oceanic ridges (MORB) and oceanic islands (OIB) [49].

Table 2.

Average concentrations (ppm) of trace elements in mafic rocks of Late Paleozoic-Early Mesozoic within-plate magmatic associations in North Asia

Element	1	2	3	4	5	6	7	8
Li	17.0	20.5	18.3	22.9	20.3	9	10	n.a.
Be	3.4	1.38	1.52	1.96	3.03	1.3	2.1	n.a.
Sc	26.7	20.3	22.1	16.2	17.8	34	39	23
Ti	11650	7860	8344	10680	11197	9712	6475	20518
V	200	181	193	181	201	n.a.	290	226
Cr	131	78.2	113	108	76.5	150	120	43
Co	41	27.8	31.5	34.1	27.5	40	38	42
Ni	92	50.6	61.8	48.8	46.6	100	110	47
Cu	41	34.7	27.6	30	26.2	n.a.	48	46
Zn	112	87.1	87.4	99.1	128	n.a.	125	153
Ga	21	16.9	17.7	18.6	20.8	n.a.	n.a.	25
Rb	27	16	30	42	38	28	20	27.9
Sr	969	589	695	939	852	360	600	501
Y	28	23.5	25.2	28.4	32.9	27	25	41.3
Zr	184	140	160	203	247	205	120	313.3
Nb	13	7.17	8.5	11.8	14.8	16	9	39.2
Cs	1.5	0.8	1.1	1.3	1.3	n.a.	n.a.	0.7
Ba	800	377	572	1045	915	455	550	704.8
La	31.5	17.2	26.1	32.7	41.3	22	21	43.1
Ce	72.5	41.1	58.9	74.6	89.1	49	40	89.9
Pr	9.5	5.37	7.42	9.37	11.3	6.5	4.4	11.4
Nd	38.6	23.3	30.5	40.5	45.3	25.1	18.8	48.2
Sm	7.9	5.14	6.22	8.05	8.63	5.8	4.4	10.2
Eu	2.3	1.56	1.87	2.41	2.36	1.7	1.3	3.2
Gd	7.3	4.93	5.64	6.68	7.82	5.7	4.6	8.8
Tb	1.0	0.80	0.882	1.09	1.12	0.9	0.7	1.4
Dy	5.6	4.43	4.77	5.5	5.93	6.1	4.4	7.7
Ho	1.0	0.91	0.985	1.1	1.17	1.1	1	1.5
Er	2.9	2.50	2.65	2.94	3.09	3.2	2.6	3.9
Tm	0.4	0.37	0.385	0.4	0.461	0.4	0.4	0.5
Yb	2.5	2.25	2.34	2.7	2.73	2.8	2.9	3.2
Lu	0.4	0.33	0.362	0.38	0.421	0.4	0.5	0.5
Hf	4.1	3.49	3.69	4.72	6.33	4	2.9	7.6
Ta	0.9	0.43	0.491	0.65	0.94	0.77	1.1.	2.3
Pb	5.5	5.28	7.02	8.78	13.8	6.4	7.4	9.0
Th	3.6	1.42	2.07	1.76	3.49	2.8	1.7	4.2
U	0.7	0.46	0.591	0.688	1.07	0.8	0.4	1.2
K	14520	12027	12 464	18844	17688	12 286	7720	11559
$\epsilon_{Nd}(T)$	+3...-2	+8...+1	+6...-3	+4...-3	+3...-3	+4...-8	n.a.	+5...-7

Note: Average compositions of basites from rift zones and within-plate areas: (1) Barguzin-Vitim; (2) Gobi-Tien Shan; (3) Gobi-Altai; (4) northern Mongolia; (5) northern Gobi and western Transbaikalia [67]; (6) Siberian traps [1]; (7) western Siberia; (8) Tarim [75, 72]; n.a. means not analyzed.

Conceivably, a significant role in shaping this isotopic-geochemical anomaly of the mantle magmas was played by the style of subduction. If the lithospheric slab descended into the mantle according to the stagnant slab mechanism [73], then

the slab generated a layer in the transitional mantle zone beneath the moving continent.

In this context, it is pertinent to consider the mechanisms that generated mantle plumes within mantle hot fields as was discussed in [38, 73]. These mechanisms are underlain by the ascent of mantle material from layer D", which was adjacent to the Earth's core. This superplume ascending as a giant mushroom-shaped body reached the transitional zone between the upper and lower mantle, interacted with it, and ascended further in the form of discrete mantle plumes to generate within-plate magmatic areas [38, 73]. According to this hypothesis, subducted stagnant lithosphere was likely involved in the generation of upper mantle plumes, and hence, the mantle of the latter exhibits features typical of both the lower mantle source and the melting products of the subducted lithosphere. This scenario is principally consistent with the estimated Nd model isotopic age (close to 1-1.2 Ga) of the recycled component in the source of mantle within-plate magmatism in North Asia [66]. This estimate enabled us to compare this component with the subducted lithosphere. The elevated water contents in the stagnant slabs should result (in this situation) in certain geochemical features of the within-plate mantle magmas, first of all, pervasively occurring Ta and Nb deficiency of the melts.

The Tarim traps differ from other within-plate magmatic associations in North Asia in having compositions most closely corresponding to the sources of basalts of the OIB type. They are characterized by high concentrations of TiO_2 and most incompatible elements, including Ta and Nb, which makes these rocks remarkably different from basites in other within-plate areas in North Asia. We believe that these features stem from the paleogeographic setting of the Tarim area during the derivation of the traps. Relative to the convergent boundary that controlled the generation of the metasomatized mantle at the lowermost levels of the Siberian continent, the microcontinent was situated on the side of the oceanic plate. Because of this, its upper mantle was not affected by suprasubduction recycling and preserved its unmodified geochemical features. The REE patterns of these traps are generally analogous to those of basites in other within-plate areas of the Siberian paleocontinent, although our rocks contain higher REE concentrations.

Figure 8 shows the distribution of the isotopic compositions of mafic rocks in the considered areas. The basites are generally enriched in radiogenic Sr and relatively depleted in radiogenic Nd [the predominant values are $0.7043 < (^{87}\text{Sr}/^{86}\text{Sr})_0 < 0.708$ and $\epsilon_{\text{Nd}}(\text{T}) < +6$].

Thereby rocks from various rift zones show comparable compositional variations and plot within a common linear field, which extends from the region of the mildly depleted mantle toward elevated $^{87}\text{Sr}/^{86}\text{Sr}$ and relatively low ϵ_{Nd} values. Such isotopic parameters suggest that the leading role in within-plate magmatism in North Asia was played by sources that had similar compositions and corresponded to the enriched mantle of the EMII type [66, 30, 31], and products of its interaction with metasomatized mantle. The involvement of the latter is more clear in CARS basites, which were produced immediately at the active continental

margin. The Tarim traps, whose genesis was not affected by a subduction component, are noted for the most strongly enriched isotopic compositions: the predominant values are $0.7065 < (^{87}\text{Sr}/^{86}\text{Sr})_0 < 0.708$ and $\epsilon_{\text{Nd}}(\text{T}) < -2$. At the same time, the fact that they include rocks with characteristics of the mildly depleted mantle [$(^{87}\text{Sr}/^{86}\text{Sr})_0 < 0.705$ and $\epsilon_{\text{Nd}}(\text{T}) > 2$], which cause the overall elongated configuration of the isotopic composition field, testifies that within-plate magmatism also involved mantle sources of the DM type, perhaps, PREMA.

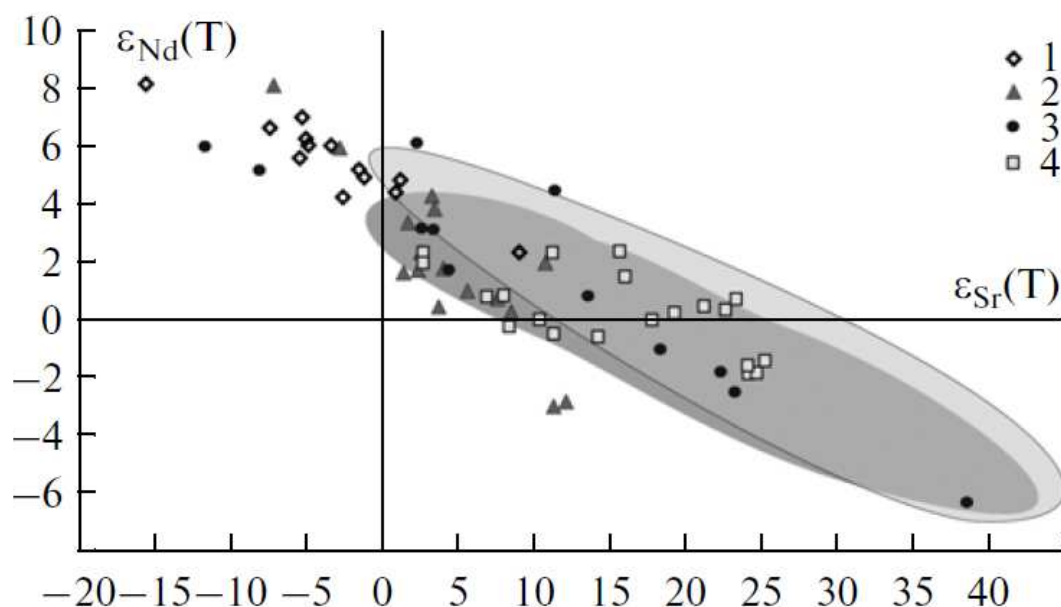


Fig. 8. Sr and Nd isotopic composition of basaltoids in Late Paleozoic-Early Mesozoic rift zones in the Central Asian Foldbelt.

(1-4) Late Paleozoic rift zones: (1) Gobi- Tien Shan, (2) Khangai area, (3) Barguzin area, (4) Early Mesozoic rift zones in the Mongolian-Transbaikalian area. The dark gray field corresponds to traps in the Siberian Platform [12, 13], and the pale gray field corresponds to the Tarim traps [72, 75].

In the Th/Ta-La/Yb plot (fig. 9), which is utilized to distinguish between basalts from different geodynamic environments [7], the compositions of the within-plate weakly differentiated ($\text{MgO} \sim 8 \text{ wt } \%$) basites from CARS plot mostly within the CFB field, which comprises the compositions of trap provinces around the world. At the same time, the overall elongated geometry of the data point swarm toward the enriched mantle composition is consistent with the conclusion that the latter should have been involved in the derivation of the rocks.

The data presented above provide important information that the within-plate activity in North Asia in the Late Paleozoic and Early Mesozoic was controlled by mantle sources whose compositions only insignificantly changed during no less than 110 Ma and preserved little varying isotopic parameters over a vast territory. The nature of these sources was determined by an enriched component of the EMII type and the upper mantle, which was usually modified during subduction.

Sources of the batholith magmatism. The CARS batholiths provide an example of within-plate granite-forming processes not related to plate interaction. Of course, the rocks typically exhibit features testifying to an important role of crustal anatexis. These are migmatization zones, nebulitic textures from the host rocks, strongly recycled xenoliths, etc. At the same time, the inner structure of the zonal areas suggests that these areas were generated above equant mantle sources, and this implies that such sources should have been involved in the processes that produced the batholiths.

These sources could participate in the processes that generated the batholiths by providing not only heat but also material. It is interesting to evaluate how much the compositional parameters of the granitoids do reflect the different nature of their parental magmas.

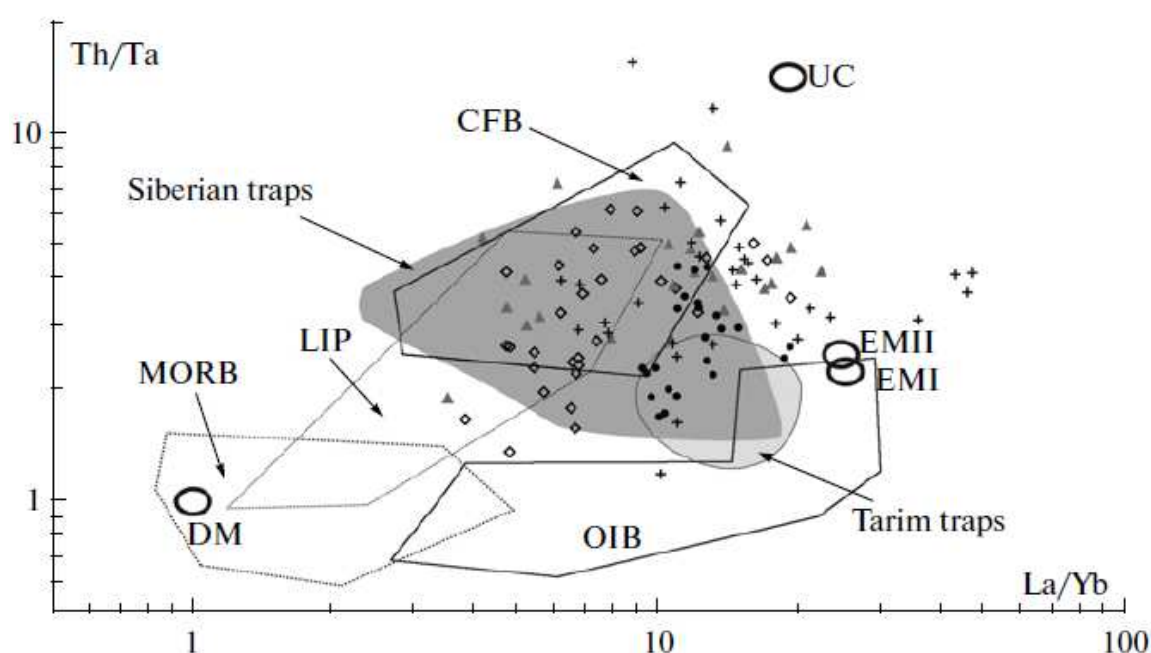


Fig. 9. Th/Ta-La/Yb diagram for basaltoids of Late Paleozoic-Early Mesozoic large igneous provinces in North Asia.

Boundaries between compositional fields and reference mantle compositions are given according to [7]. Mantle source types: DM-depleted mantle, EM-I-mantle enriched in radiogenic Nd, EM-II-mantle depleted in radiogenic Sr, UC- upper crust. Fields of basalt compositions: MORB-mid-oceanic ridge basalts, LIP-basalts at oceanic lava plateaus, CFB- traps (continental flood basalts), OIB-oceanic-island basalts. See Fig. 6 for symbol explanations.

Geochemical data (table 3) and fig. 10 indicate that the average concentrations of trace elements in granitoids from discrete batholiths are similar and close to the average composition of the Earth's crust. The rocks are enriched in elements highly incompatible with the mantle, such as Rb, Ba, Th, U, K, and Rb, and LREE but are depleted in Nb, Sr, P, and Ti. The granites are also close to

Table 3.

Average concentrations (ppm) of trace elements in granites from batholiths in CAFB and host rocks

Element	Granitoids from batholiths			Sedimentary rocks	
	Khentei-Dauria	Khangai	Angara-Vitim	Khentei trough	Khangai trough
Li	47	35	30	48	30
Be	3.3	3	3.4	1.7	1.6
Sc	6	5	3	12	11
Ti	2501	2760	2220	4222	3556
K	32848	33357	39975	38252	16264
P	524	594	436.5	520	670
V	34		41	83	90
Cr	13	12	10	33	77
Co	6	5	3	7	11
Ni	7	7	4	9	26
Rb	143	132	123	119	76
Sr	222	238	401	300	172
Y	24	28	26	26	22
Zr	190	194	185	125	126
Nb	8	13	17	8	11
Cs	8.7	5.6	2.8	10.0	3.9
Ba	478	701	887	1040	446
La	47.5	38.3	42.8	56.1	52.4
Ce	88.1	63.0	72.7	106.5	88.1
Pr	8.7	6.7	9.2	10.9	8.8
Nd	33.6	29.1	31.1	39.2	31.5
Sm	6.2	6.4	5.5	6.8	5.2
Eu	0.8	0.8	1.0	1.5	1.2
Gd	4.9	4.2	4.9	5.9	4.9
Tb	0.8	0.7	0.7	1.0	0.7
Dy	3.9	1.3	3.9	5.2	3.9
Ho	0.8	0.2	0.8	1.0	0.8
Er	2.1	0.5	2.4	2.9	2.4
Tm	0.3	0.1	0.3	0.5	0.4
Yb	2.2	2.3	2.2	2.9	2.4
Lu	0.3	0.3	0.3	0.5	0.4
Hf	3.6	6.4	3.3	3.8	3.7
Ta	1.0	1.4	1.3	0.7	0.9
Pb	15.1	25.3	23.2	20.4	10.4
Th	19.1	22.2	19.9	10.9	10.1
U	3.4	3.2	1.7	2.6	2.0
$\epsilon_{Nd}(T)$	+2...-4	+4...-17	0...-20	0...-4	-2...-25

pelites, which are predominant in the host structures of the granites and differ from the latter mostly in higher U and Th concentrations. These similarities are most clearly pronounced in the REE concentrations and REE patterns (fig. 10). The

differences involve the poorly pronounced Eu minima of the granitoids and their mild enrichment in LREE relative to HREE, which is an indication of certain differentiation of the granite melts or certain selectivity of the melting processes. It should be mentioned that the compositional similarity of the granites with both pelites and the average crust is likely explained by the generation of the batholiths by means of anatexis of vast volumes of crustal material and the averaging of the compositions of all types of melted rocks in the melting products. For comparison, the plot shows data on granitoids from Kamchatka. They differ from the batholiths in Central Asia in containing lower concentrations of most incompatible elements. These differences are thought to stem from the differences in the compositions of the protoliths, which were the subcontinental crust of the island-arc type in island arcs. The facts and considerations presented above led us to conclude that the trace-element composition of the batholiths comprehensively enough reflects the composition of the crust in the territories where these batholiths occur.

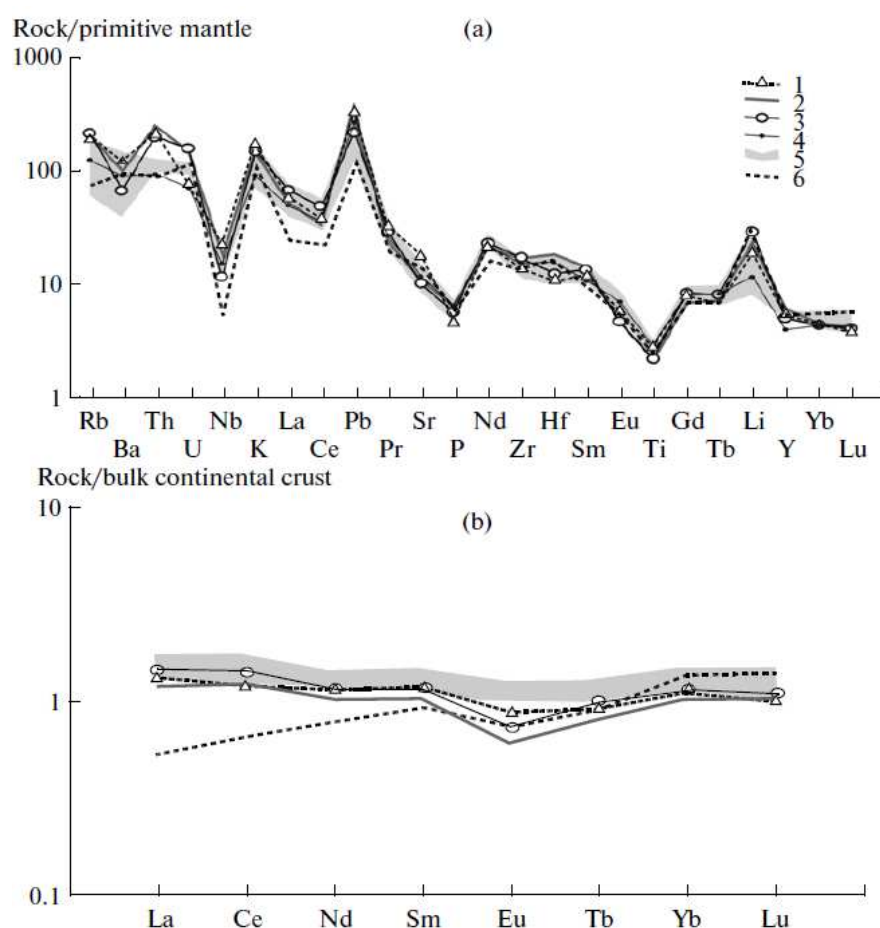


Fig. 10. (a) Primitive mantle [49] and (b) bulk continental crust [15] normalized trace-element and REE patterns of granites from batholiths in the Central Asian Foldbelt.

(1-3) Granites from batholiths: (1) Angara-Vitim, (2) Khangai, (3) Khentei-Dauria; (4) average continental crust composition for China [15]; (5) pelites in the Khangai and Khentei troughs; (6) island-arc granites in eastern Kamchatka [2].

A somewhat different conclusion can be derived from the Nd isotopic composition of the granitoids. Such studies were most systematically conducted at the Khangai batholith and its host crust. The granitoids are hosted in blocks of Early Precambrian (Dzabkhan and Tarbagatai), Neoproterozoic (Songinskii and Khangai), and Caledonian crust (fig. 11). These blocks correspond to heterogeneous Nd isotopic provinces whose $\epsilon_{Nd}(260)$ values vary from - 15 in blocks with Early Proterozoic crust to +1 to +2 in the Caledonides (our unpublished data).

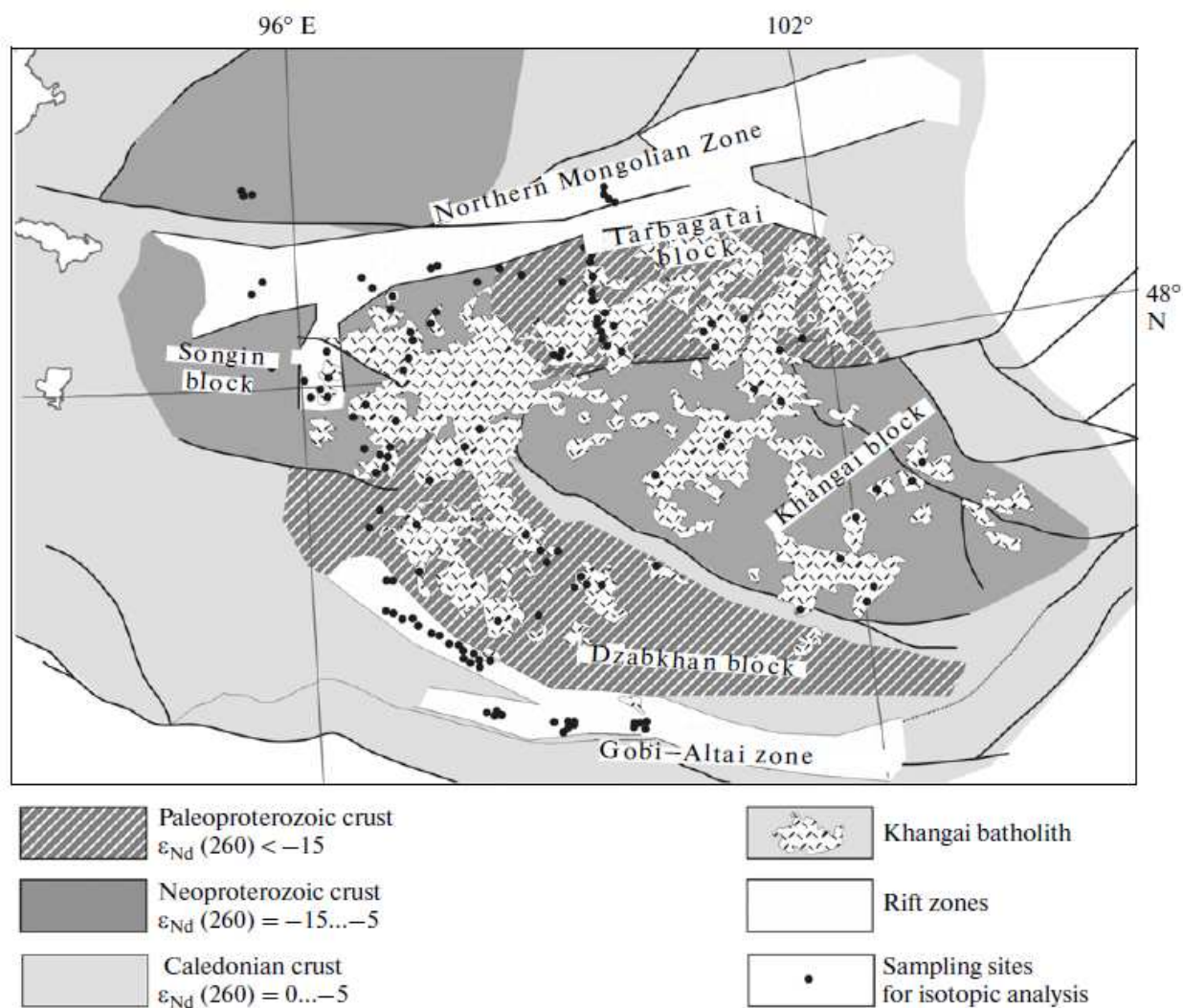


Fig. 11. Distribution of crustal material of various isotopic composition in the generation region of the Khangai batholith.

In spite of the obvious differences of the crustal protoliths in various portions of the Khangai batholith, the compositions of the anatectic derivatives (granites and rhyolites) are not explicitly correlated with the parameters of the host crust. As follows from fig. 12, these compositions vary within a broad range, from the composition of the host crust to that of rift associations during the derivation of the granitoids, whose isotopic parameters fall within the range of $\epsilon_{Nd}(260)$ from - 3 to

+1. The variations are more significant in blocks of Early Precambrian crust, but the lowest $\epsilon_{Nd}(260)$ values are thereby close to the composition of the crustal protoliths.

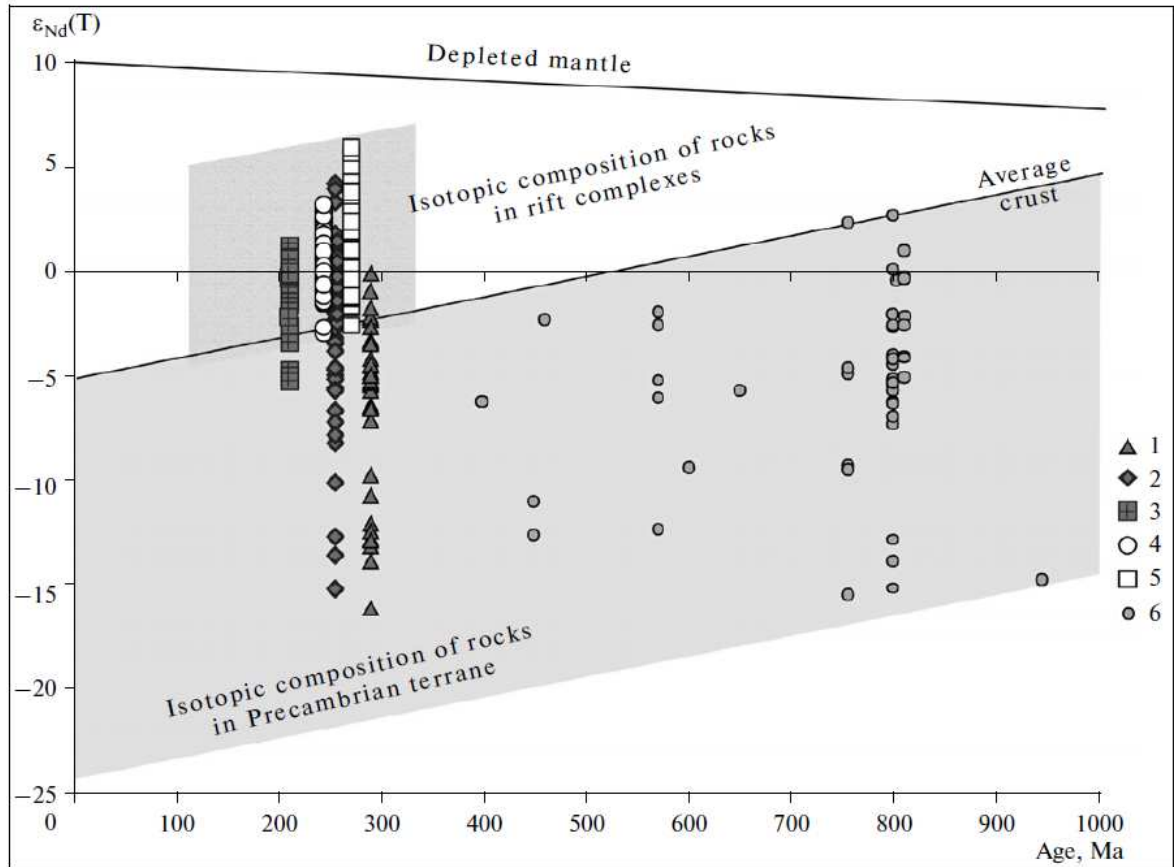


Fig. 12. $\epsilon_{Nd}(T)$ -Age diagram for CAFB granitoids and related rift magmatism zones.

(1-3) Rocks from batholiths: (1) Angara- Vitim, (2) Khangai, (3) Khentei-Dauria; (4, 5) rocks from rift zones: (4) northern Mongolian, (5) Gobi-Altai; (6) host rocks.

The aforementioned variations cannot be explained by the participation of only crustal protoliths in the derivation of the granites. The sources of the granite melts contained another component, which was likely close to the mantle sources of basites in the northern Mongolian and Gobi-Altai rift zones and basites in synplutonic intrusions [$\epsilon_{Nd}(260)$ from -3 to +3] within the batholith. The isotopic data thus suggest that the source of the granite melts should have contained both crustal and mantle components. These data provide support for the hypothesis that a mantle plume was involved in the processes that produced the granites.

Figure 12 presents data on other batholiths in CARS; these data also testify that mantle sources contributed to the origin of the batholiths. Rocks from the Angara-Vitim batholith (table 3) have negative $\epsilon_{Nd}(T)$ from 0 to -8, which correspond to variations in the Nd model age $T_{Nd}(DM-2st)$ from 1000 to 1700 Ma [46]. These isotopic parameters of the granites suggest that the granites were derived from crustal sources in the "Riphean" isotopic province that hosts the

batholith [25, 46] and a juvenile source of composition comparable with basites in rift zones.

In an $\epsilon_{Nd}(T)$ -Age time diagram, the isotopic composition of rocks of the Khentei-Dauria batholith [$\epsilon_{Nd}(T)$ from -4 to +2, Table 2] defines a field corresponding to the isotopic composition of rocks in accretionary prisms in CAFB Caledonides [26] and is close to, for example, the composition of pelites of the Kharinskaya Formation in the Khentei trough [$\epsilon_{Nd}(T)$ from -1 to -3], which hosts the batholith. The higher $\epsilon_{Nd}(T)$ values than those of the pelites unambiguously testify that the melts were derived from "Riphean" sources and those of composition close to the sources of Riphean magmatism in the surroundings of the batholith.

Concluding the isotopic-geochemical characterization of rocks in zonal areas in CARS, it should be mentioned that they were formed by two groups of magmatic melts: crustal and mantle ones. The mantle magmas determined the composition of the magmatic associations, first of all, in the rift zones. The sources of the granitoid melts were not only locally produced crustal rocks, which usually had "Riphean" or "pre-Riphean" Nd isotopic parameters, but also minor amounts of juvenile mantle material that were added to them and predetermined the significant variations in the isotopic composition of the rocks.

EVOLUTIONARY GEODYNAMICS OF CARS

The Late Paleozoic-Early Mesozoic within-plate activity in North Asia resulted in a number of large igneous provinces (LIP) of similar age: trap areas, rift zones, and related giant granite batholiths. This vast area of within-plate magmatism was produced when magmatic centers migrated inward the continent (fig. 13). This migration was likely related to the passage of the paleocontinent above a group of mantle plumes of the African hot mantle field [63, 30, 31, 60].

Role of mantle plumes in the origin of CARS. Within-plate magmatic activity in North Asia began in the Late Carboniferous, when the Tarim-southern Mongolian province and the Barguzin zonal magmatic area were produced in the marginal part of the continent. Their genesis is thought to be related to the overlap of mantle hotspots (Siberian and Mongolian mantle plumes) by a margin of the Siberian continent. The further movement of the continent above these plumes was associated with the migration of the centers of magmatic activity inward the continent [31]. As a result, the Siberian mantle plume was superimposed by the Siberian craton, in which trap eruptions took place at the Permian-Triassic boundary. Starting in the second half of the Triassic, the magmatic centers likely shifted toward the shelf of the Arctic basin, which is consistent with the continuing movement of the continent. Following [22], we believe that the Siberian mantle plume can be compared with the modern Iceland plume, above which the Siberian continent moved in the Late Paleozoic-Early Mesozoic [30, 31].

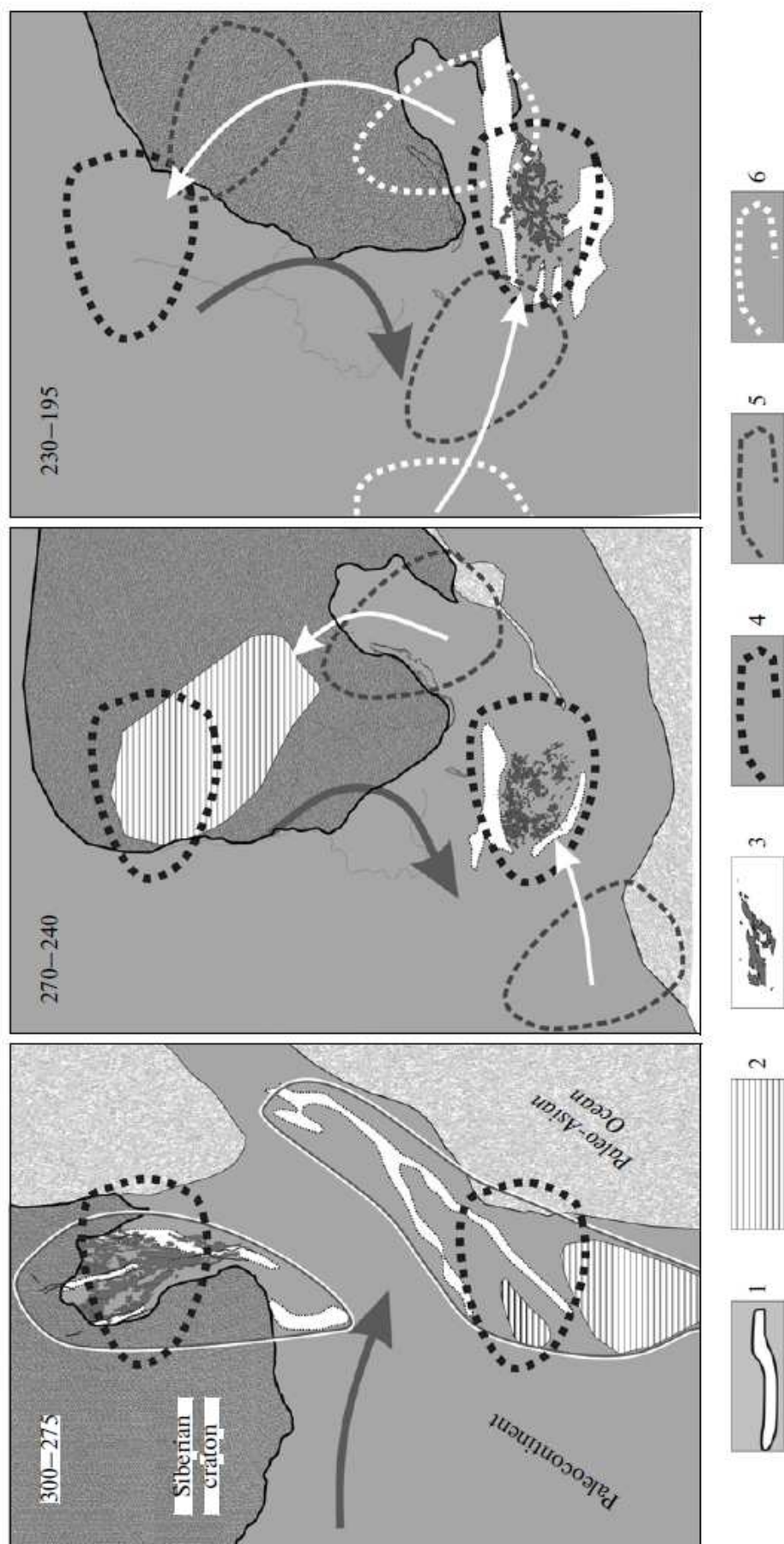


Fig. 13. Schematic representation of the migration of magmatism during the development of the Central Asian Rift System as a result of the rotation of Siberia above the Siberian and Mongolian mantle plumes. (1) Areas of rift magmatism; (2) traps; (3) batoliths; (4) projection of the mantle hotspot (mantle plume); (5, 6) hotspots traces. The dark gray arrow shows the movements of the plate, white arrows show the shift trends of mantle plume projections.

The effect of the Mongolian plume was of paramount importance for the development of the CARS structure. The earliest trace of the plume (at 319- 290 Ma) is marked by traps in the Tarim area and Gobi-Tien Shan rift zone, which were formed near the boundary of the Siberian paleocontinent with the Paleo-Asian Ocean (Fig. 13). Late in the Early Permian (~ 270 Ma), the Khangai magmatic area started to develop and was shifted for approximately 400 km inward the continent relative to the Gobi-Tien Shan zone. The Khentei-Dauria zonal magmatic area of analogous structure was formed in the Late Triassic roughly 800 km east of the Khangai area. We believe that these migrations of the magmatic centers were related to the movement of the lithospheric plate above a relatively motionless plume. According to the sizes of the zonal areas, its sizes were greater than 500 x 500 km.

Geodynamics of the batholith-forming processes. We are prone to believe that conditions favorable for the origin of batholiths within the influence areas of mantle plumes were prepared by the tectonic regime dominating at the convergent boundary of the Siberian continent [66, 26]. This regime was controlled by regional stress induced by the subduction of the oceanic lithosphere beneath the continent and then (starting in the Late Permian) the collision of Siberian and Sino-Korean continents [63, 8]. These processes seem to have been predominant in the area, and hence, extension was restricted to the zone of large strike-slip faults, which shaped the structural framework of the rift system.

Heat was provided for crustal anatexis by basite melts from the mantle plumes. Their involvement in the generation of the zonal areas and batholiths can be explained, for example, within the scope of the under-plating model, according to which mantle magmas were emplaced at lower crustal levels and induced crustal anatexis. The sizes (>0.7-1 million square kilometers) and morphologies of the batholiths are similar, and this testifies to a comparable contribution of a mantle heat source to their generation. The heat was provided by the emplacement of basite melts into the bottom part of the crust. According to [9], the volumes of these melts should have been comparable with the volumes of the batholith themselves, and this makes it possible to regard zonal magmatic areas as equivalents of large igneous provinces (LIP).

The occurrence of mantle plumes at the bottom part of the Late Paleozoic Siberian continent was discussed in much detail in [63, 30, 31, 60] and was thought to be related to the migration of Siberia above the African hot mantle field throughout the whole Paleozoic. The continent thereby interacted with a number of mantle plumes in the hot field and successively overlapped them when moving to the north. The occurrence of corresponding hotspots in the Paleo-Asian Ocean in front of the continent follows from the occurrence of OIB-type basalt complexes in the Hercynian structures accreted to the continent [70].

CONCLUSIONS

The Late Paleozoic-Early Mesozoic was marked by widespread magmatic within-plate activity in North Asia and the origin of a number of large igneous areas of different structure and composition. Among them, the Central Asian Rift System has the most complicated inner structure, was the longest lived, and combined the origin of the Tarim traps and large zonal magmatic areas with batholiths in their cores. In its integral expression, it is, first of all, a large (3000 x 600 km) latitudinally oriented belt of rift zones with a trap province at its western termination and batholiths in the central portion. The rift system started to develop in the Late Carboniferous. The rifting processes systematically expanded inward the continent, terminated in the Early Jurassic, and evolved for approximately 110 Ma.

The most conspicuously pronounced feature of the evolution of this rift system was its relation to a number of vast batholiths, whose location was controlled by the space between two simultaneously developing rift zones. Together with these zones, the batholiths formed zonal magmatic areas, which were characterized by crustal (granitoid) magmatism in their central portions and mantle (rift) magmatism in troughs and grabens in peripheral zones. The granitoids of the batholiths typically show geological and isotopic-geochemical indications that they were formed via the anatexis of the host rocks at an active participation of mantle magmas (including the involvement of their material).

The isotopic parameters [$\epsilon_{Nd}(T)$ from -3 to +7 and $\epsilon_{Sr}(T)$ from -5 to + 25] of basites in the zonal magmatic areas suggest that the sources of the parental melts involved subducted upper mantle material of the DM type and enriched mantle material of the EMII type with an isotopic model age of 1-1.2 Ga [66, 30]. The mafic rocks of various areas have comparable incompatible-element patterns and similar geochemical and isotopic parameters. These similarities testify that the mantle feeding regions of the plumes were homogeneous in composition.

Large within-plate magmatic provinces were produced in North Asia in relation to the subduction-driven overlap of at least two mantle plumes by an active continental margin of the Siberian paleocontinent, with these plumes generated in the oceanic sector of the Paleo-Asian Ocean. Within the continental lithosphere, the mantle plumes induced activity of the within-plate type and facilitated the development of rifts and the origin of alkaline basaltic and alkaline-sialic associations. In stressed environments produced during collision of various types within the continental margin, the mantle melts did not ascend above the lowermost crustal levels. The thermal effect of these melts on crustal rocks induced anatexis and eventually predetermined the origin of the batholiths.

The authors thank Dr. A.E. Izokh (Institute of Geology and Mineralogy, Siberian Branch, Russian Academy of Sciences) for discussion of the manuscript and constructive criticism. This study was financially supported by Program 10 of the Earth Science Division of the Russian

Academy of Sciences, the Russian Foundation for Basic Research (project nos. 11-05-00264 and 11-05-92200), and Project 87 of the Siberian Branch of the Russian Academy of Sciences.

REFERENCES

1. **Almukhamedov A.I., Medvedev A.Ya., and Zolotukhin V.V.** Chemical Evolution of the Permian-Triassic Basalts of the Siberian Platform in Space and Time. *Petrology*, 2004, vol. 12, no. 4, pp. 297-311.
2. **Antipin V.S., Perepelov A.B., Mitichkin M.A., and Odgerel D.** Geochemical Types and Petrogenesis of Granitoids in Within-Plate and Subduction Geodynamic Environments: An Example of Phanerozoic Granitoids in Siberia, Mongolia, and Kamchatka, in *Materialy X Vserossiiskogo petrograficheskogo soveshchaniya "Petrografiya XXI veka* (Proceedings of 10th All-Russian Petrographic Conference "Petrography in the 21st Century"), Apatity, 2005, vol. 2, pp. 18-20.
3. **Arakelyants M.M., Polyakov G.V., Izokh A.E., and Krivenko A.P.** New Data on the Age of the Gabbro-Montzodiorite Association in Mongolia, *Dokl. Akad. Nauk SSSR*, 1989, vol. 305, no. 3, pp. 690-694.
4. **Berzina A.P. and Sotnikov V.I.** Character of Formation of the Erdenet-Ovoo Cu-Mo Magmatic Center (Northern Mongolia) in the Zone of Influence of a Permo-Triassic Plume, *Russ. Geol. Geophys.*, 2007, vol. 48, no. 2, pp. 141-156.
5. **Berzina A.P., Gimon V.O., Nikolaeva I.V., et al.** Basites of the Polychronous Magmatic Center with the Erdenetiyn-Ovoo Porphyry Cu-Mo Deposit (Northern Mongolia): Petrogeochemistry, $^{40}\text{Ar}/^{39}\text{Ar}$ Geochronology, Geodynamic Position, and Related Ore Formation, *Russ. Geol. Geophys.*, 2009, vol. 50, no. 10, 827-841.
6. **Borisenko A.S., Sotnikov V.I., Izokh A.E., Polyakov G.V., and Obolenskii A.A.** Permo-Triassic Mineralization in Asia and its Relation to Plume Magmatism, *Russ. Geol. Geophys.*, 2006, vol. 47, no. 1, pp. 170-186.
7. **Condie K.C.** *Mantle Plumes and Their Record in Earth History*, Cambridge: Cambridge University Press, 2001.
8. **Dergunov A.B., Kovalenko V.V., Ruzhentsev S.V., and Yarmolyuk V.V.** *Tectonics, Magmatism, and Metallogeny of Mongolia*, London-New York: Routledge Taylor and Francis Group, 2001.
9. **Dobretsov N.L.** 250-Ma Large Igneous Provinces of Asia: Siberian and Emeishan Traps (Plateau Basalts) and Associated Granitoids, *Russ. Geol. Geophys.*, 2005, vol. 46, no. 9, pp. 847-868.
10. **Dobretsov N.L., Borisenko A.S., Izokh A.E., and Zhmodik S.M.** A Thermochemical Model of Eurasian Permo-Triassic Mantle as a Basis for Prediction and Exploration for Cu-Ni-PGE and Rare-Metal Ore Deposits, *Russ. Geol. Geophys.*, 2010, no. 9, pp. 903-924.
11. **Doroshkevich A.G., Ripp G.S., and Izbrodin I.A.** Alkaline Rocks of the Vitim Province (Western Transbaikalia): Stages, Conditions of Formation, and Sources, in *Geodinamicheskaya evolyutsiya litosfery Tsentral'no-Aziatskogo podvizhnogo poyasa: ot okeana k kontinentu* (Geodynamic Evolution of the Lithosphere of the Central Asian Mobile Belt: From Ocean to Continent), Irkutsk: IZK SO RAN, 2011, issue 9, pp. 81-83.
12. **Fedorenko V.A., Lichtfoot P.C., Naldrett A.J. et al.** Petrogenesis of the Flood-Basalt Sequence of Norilsk, North Central Siberia, *Int. Geol. Rev.*, 1996, vol. 38, pp. 99-135.
13. **Fedorenko V.A.** Results of New Field and Geochemical Studies of the Volcanic and Intrusive Rocks of the Maymecha-Kotuy Area, Siberian Flood Basalt Province, Russia, *Int. Geol. Rev.*, 1997, vol. 39, pp. 479-553.

14. **Fedorova M.E.** *Geologicheskoe polozhenie i petrologiya granitoidov Khangaiskogo batolita* (Geological Setting and Petrology of Granitoids in the Khangai Batholith), Moscow: Nauka, 1977.
15. **Gao Sh., Luo T.-C., Zhang B.-R., et al.** Chemical Composition of the Continental Crust as Revealed by Studies in East China, *Geochem. Cosmochem. Acta*, 1998, vol. 62, no. 11, pp. 1959-1975.
16. **Geologiya Mongol'skoi Narodnoi Respubliki (Geology of the Mongolian People's Republic)** Moscow: Nedra, 1973, vol. 2.
17. **Gordienko I.V., Andreev G.V., and Kuznetsov A.N.** *Magmaticheskie formatsii paleozoya Sayano-Baikal'skoi gornoj oblasti* (Paleozoic Magmatic Formations of the Sayan-Baikal Mountainous Area), Moscow: Nauka, 1978.
18. **Han B. F., Wang S.-G., Jahn B.-M. et al.** Depleted-Mantle Source for the Ulungur River A-Type Granites from North Xinjiang, China: Geochemistry and Nd-Sr Isotopic Evidence, and Implications for Phanerozoic Crustal Growth, *Chem. Geol.*, 1997, vol. 138, pp. 135-159.
19. **Izokh A.E., Vishnevskii A.V., Polyakov G.V., and Shelepaev R.A.** Age of Picrite and Picrodolerite Magmatism in Western Mongolia, *Russ. Geol. Geophys.*, 2011, vol. 52, no. 1, pp. 7-23.
20. **Izokh A.E., Polyakov G.V., Anoshin G.N., and Golovanova N.P.** Geochemistry of PGE in the Nomgon Troctolite-Anorthosite-Gabbro Massif, *Geokhimiya*, 1991, no. 10, pp. 1398-1405.
21. **Jahn B.M., Litvinovsky B.A., Zanvilevich A.N., and Reichow M.** Peralkaline Granitoid Magmatism in the Mongolian-Transbaikalian Belt: Evolution, Petrogenesis and Tectonic Significance, *Lithos*, 2009, vol. 113, pp. 521-539.
22. **Kharin G.S.** Magmatic Pulses of the Iceland Plume, *Petrology*, 2000, vol. 8, no. 2, pp. 97-112.
23. **Kovach V.P., Sal'nikova E.B., Rytsk E.Yu., et al.** Duration of the Formation of the Angara-Vitim Batholith: Results of U-Pb Geochronological Studies, *Dokl. Earth Sci.*, (in press).
24. **Koval' P.V.** *Regional'nyi geokhimicheskii analiz granitoidov* (Regional Geochemical Analysis of Granitoids), Novosibirsk: NITs OIGM, 1998.
25. **Kovalenko V.I., Yarmolyuk V.V., Kovach V.P., et al.** Sources of Phanerozoic Granitoids in Central Asia: Sm-Nd Isotope Data, *Geochem. Int.*, 1996, vol. 34, no. 8, pp. 628-640.
26. **Kovalenko V.I., Yarmolyuk V.V., Sal'nikova E.B., et al.** Sources of Igneous Rocks and Genesis of the Early Mesozoic Tectonomagmatic Area of the Mongolia-Transbaikalia Magmatic Region: 2. Petrology and Geochemistry, *Petrology*, 2003, vol. 11, no. 3, pp. 205-229.
27. **Kozakov, I.K., Kovach, V.P., Bibikova, E.V., et al.** Age and Sources of Granitoids in the Junction Zone of the Caledonides and Hercynides in Southwestern Mongolia: Geodynamic Implications, *Petrology*, 2007, vol. 15, no. 2, pp. 126-150.
28. **Kozlovsky A.M., Yarmolyuk V.V., Travin A.V., et al.** Stages and Regularities of the Manifestation of the Late Paleozoic Anorogenic Magmatism in the Hercynides of Southern Mongolia, *Dokl. Earth Sci.* (in press).
29. **Kozlovsky A.M., Yarmolyuk V.V., Savatenkov V.M., and Kovach V.P.** Sources of Basaltoid Magmas in Rift Settings of an Active Continental Margin: Example from the Bimodal Association of the Noen and Tost Ranges of the Late Paleozoic Gobi-Tien Shan Rift Zone, Southern Mongolia, *Petrology*, 2006, vol. 14, no. 4, pp. 337-360.

30. **Kuzmin M.I., Yarmolyuk V.V., and Kravchinsky V.A.** Phanerozoic Within-Plate Magmatism of North Asia: Absolute Paleogeographic Reconstructions of the African Large Low-Shear-Velocity Province, *Geotectonics*, 2011, vol. 45, no. 6, pp. 415-438.
31. **Kuzmin M.I., Yarmolyuk V.V., and Kravchinsky V.A.** Phanerozoic Hot Spot Traces and Paleogeographic Reconstructions of the Siberian Continent Based on Interaction with the African Large Low Shear Velocity Province, *Earth-Sci. Rev.*, 2010, vol. 102, no. 1-2, pp. 29-59.
32. **Li Z.L., Yang S.F., Li Z.L., Yang S.F., et al.** Chronology and Geochemistry of Taxinan Basalts from the Tarim Basin: Evidence for Permian Plume Magmatism, *Acta Petrologica Sinica*, 2008, vol. 24, no. 5, pp. 959-970.
33. **Litvinovsky B.A., Zanvilevich A.N., Alakshin A.M., and Podladchikov Yu.Yu.** *Angaro-Vitimskii batolit-krupneishii granitoidnyi pluton* (Angara-Vitim Batholith-the Largest Granitoid Pluton), Novosibirsk: Nauka, 1992.
34. **Litvinovsky B.A., Yarmolyuk V.V., Vorontsov A.A., et al.** Late Triassic Stage of the Formation of the Mongolo-Transbaikalian Alkaline-Granitoid Province: Data of Isotope-Geochemical Studies, *Russ. Geol. Geophys.*, 2001, vol. 42, no. 3, pp. 445-455.
35. **Litvinovsky B.A., Tsygankov A.A., Jahn B.M., et al.** Origin and Evolution of Overlapping Calc-Alkaline and Alkaline Magmas: The Late Palaeozoic Post-Collisional Igneous Province of Transbaikalia (Russia), *Lithos*, 2011, vol. 125, pp. 845-874.
36. **Lykhin D.A., Kovalenko V.I., Yarmolyuk V.V., et al.** The Yermakovsky Deposit, Western Transbaikal Region, Russia: Isotopic and Geochemical Parameters and Sources of Beryllium-Bearing Granitoids and Other Rocks, *Geol. Ore Dep.*, 2010, vol. 52, no. 4, pp. 289-301.
37. **Mao J.W., Pirajno F., Zhang Z.H., et al.** A Review of the Cu-Ni Sulphide Deposits in the Chinese Tianshan and Altay Orogens (Xinjiang Autonomous Region, NW China): Principal Characteristics and Ore-Forming Processes, *J. Asian Earth Sci.*, 2008, vol. 32, pp. 184-203.
38. **Maruyama S., Santosh M., and Zhao D.** Superplume, Supercontinent, and Postperovskite: Mantle Dynamics and Anti-Plate Tectonics of the Core-Mantle Boundary, *Gondwana Res.*, 2007, vol. 11, no. 1-2, pp. 7-37.
39. ***Mezozoiskaya i kainozoiskaya tektonika i magmatizm Mongolii (Mesozoic and Cenozoic Tectonics and Magmatism of Mongolia)*** Moscow: Nauka, 1975, p. 305.
40. **Mossakovskii A.A.** *Orogennye struktury i vulkanizmpaleozoid Evrazii* (Orogenic Structures and Volcanism of Paleo-zoids of Eurasia), Moscow: Nauka, 1975.
41. **Pirajno F., Jingwen M., Zhaochong Z., et al.** The Association of Mafic-Ultramafic Intrusions and A-Type Magmatism in the Tian Shan and Altay Orogens, NW China: Implications for Geodynamic Evolution and Potential for the Discovery of New Ore Deposits, *J. Asian Earth Sci.*, 2008, vol. 32, pp. 1165-183.
42. **Pokrovsky B.G. and Zhidkov A.Ya.** Sources of the Ultrapotassic Alkaline Rocks of the Synnyr and Southern Sakun Massifs of Transbakalia Based on Isotope Data, *Petrologiya*, 1993, vol. 1, no. 2, pp. 195-204.
43. **Polyakov G.V., Izokh A.E., and Borisenko A.S.** Permian Ultramafic-Mafic Magmatism and Accompanying Cu-Ni Mineralization in the Gobi-Tien Shan Belt as a Result of the Tarim Plume Activity, *Russ. Geol. Geophys.*, 2008, vol. 49, no. 7, pp. 455-467.
44. **Reichow M.K., Pringle M.S., Al Mukhamedov A.I. et al.** The timing and extent of the eruption of the Siberian Traps large igneous province: implications for the end-Permian environmental crisis. *Earth Planet.Sci*, 2008, V.32, pp.9-20.
45. **Ripp G.S., Vladykin N.V., Doroshkevich A.G., and Sotnikova I.A.** Akit Alkaline Massif and Associated Mineralization, in *Glubinnyi magmatizm, ego istochniki i plyumy*

- (Deep-Seated Magmatism, Its Sources and Plumes), Mirnyi-Irkutsk: IGKh SO RAN, 2006, pp. 285-304.
46. **Rytsk E.Yu., Kovach VP., Yarmolyuk V.V., et al.** Isotopic Structure and Evolution of the Continental Crust in the East Transbaikalian Segment of the Central Asian Foldbelt, *Geotectonics*, 2011, vol. 45, no. 5, pp. 349-377.
 47. **Sotnikova I.A. and Vladykin N.V.** Petrogeochemical and Mineralogical Features of Rare-Metal Massifs of Northern Baikal Region, *Izv. Sibirsk. Otd. Sekts. Nauk o Zemle RAEN. Geol., Poiski i Razvedka Rudn. Mestorozhd.*, 2009, vol. 9, pp. 100-110.
 48. **Sugorakova A.M., Yarmolyuk V.V., Lebedev V.I., and Lykhin D.A.** Late Paleozoic Alkali-Granitic Magmatism of Tuva and Its Relation to Intraplate Activity within the Siberian Paleocontinent, *Dokl. Earth Sci.*, 2011, vol. 439, no. 5, pp. 1070-1075.
 49. **Sun S., S. and McDonough W.F.** Chemical and Isotopic Systematics of Oceanic Basalts: Implications for Mantle Composition and Processes, in *Magmatism in the Ocean Basins*, Saunders, A.D. and Norry, M.J., Eds., Geol. Soc. Am. Sp. Publ., 1989, vol. 42, pp. 313-345.
 50. **Takahashi Y., Arakawa Y., Oyungerel S., and Naito, K.** Geochronological Data of Granitoids in the Bayankhongor Area, Central Mongolia, *Bull. Geol. Soc. Japan*, 2000, vol.51, pp. 167-174.
 51. **Tektonika Mongol'skoi Narodnoi Respubliki (Tectonics of the Mongolian People's Republic)**, Moscow: Nauka, 1974.
 52. **Tsygankov A.A., Matukov D.I., Bepezhnaya N.G., et al.** Late Paleozoic Granitoids of Western Transbaikalia: Magma Sources and Stages of Formation, *Russ. Geol. Geo-phys.*, 2007, vol. 48, no. 1, pp. 120-140.
 53. **Tsygankov A.A., Litvinovskii B.A., Dzhan' B.M., et al.** Sequence of Magmatic Events in the Paleozoic of Transbaikalia, Russia (U-Pb Isotope Data), *Russ. Geol. Geo-phys.*, 2010, no. 9, pp. 972-994.
 54. **Jiang Changyi Li Youzhu Zhang Pengbo and Ye Shufeng.** Petrogenesis of Permian Basalts on the Western Margin of the Tarim Basin, China, *Russ. Geol. Geophys.*, 2006, vol. 47, no. 2, pp. 237-248.
 55. **Turutanov E.Kh., Grebenshchikova V.I., and Noskov D.A.** Shape and Sizes of the Angara-Vitim Batholith, in *Geodinamicheskaya evolyutsiya litosfery Tsentral'no-Aziatskogo podvizhnogo poyasa: ot okeana k kontinentu* (Gepdynamic Evolution of the Lithosphere of the Central-Asian Mobile Belt: from the Ocean to Continent), Irkutsk: IZK SO RAN, 2006, vol. 2, no. 4, 183-187.
 56. **Turutanov E.Kh., Grebenshchikova V.I., and Ogloblin R.V.** Deep Structure and Geochemistry of Rocks in the Khangai Granitoid Batholith, Mongolia, in *Geodinamicheskaya evolyutsiya litosfery Tsentral'no-Aziatskogo podvizhnogo poyasa: ot okeana k kontinentu* (Geodynamic Evolution of the Lithosphere of the Central Asian Mobile Belt: from the Ocean to Continent), Irkutsk: IZK SO RAN, 2007, vol. 2, no. 5, pp. 133—135.
 57. **Turutanov E.Kh. and Stepanenko A.V.** Deep Geometry of the Khentei Granitoid Batholith (Mongolia), in *Geodi-namicheskaya evolyutsiya litosfery Tsentral'no-Aziatskogo podvizhnogo poyasa: ot okeana k kontinentu* (Geodynamic Evolution of the Lithosphere of the Central Asian Mobile Belt: from the Ocean to Continent), Irkutsk: IZK SO RAN, 2008, vol. 2, no. 6, pp. 134-135.
 58. **Vorontsov A.A., Yarmolyuk V.V., and Baikin D.N.** Structure and Composition of the Early Mesozoic Volcanic Series of the Tsagan-Khurtei Graben, Western Transbaikalia: Geological, Geochemical, and Isotopic Data, *Geochem. Int.*, 2004, vol. 42, no. 11, pp. 1046-1061.

59. **Wang Sh. and Han B.** Geochemistry and Tectonic Significance of Alkali Granites Along Ulungur River, Xingan, *Sci. Geol. Sinica*, 1994, vol. 29, no. 4, pp. 373-383.
60. **Yarmolyuk V.V. and Kuzmin M.I.** Rifting and Silicic Large Igneous Province of the Late Paleozoic-Early Mesozoic in the Central Asia, *Large Igneous Provinces Commission. December 2011 LIP of the Month*. (www.largeigneous-provinces.org).
61. **Yarmolyuk V.V.** *Pozdnepaleozoiskii vulkanizm kontinental'nykh riftogennykh struktur Tsentral'noi Azii* (Late Paleozoic Volcanism of Continental Rift Structures of Central Asia), Moscow: Nauka, 1983.
62. **Yarmolyuk V.V. and Kovalenko V.I.** *Riftogennyi magmatizm aktivnykh kontinental'nykh okrain i ego rudonosnost'* (Rift Magmatism at Active Continental Margins and Its Ore-Generating Potential), Moscow: Nauka, 1991.
63. **Yarmolyuk V.V., Kovalenko V.I., and Kuz'min M.I.** North Asian Superplume Activity in the Phanerozoic: Magmatism and Geodynamics, *Geotectonics*, 2000, vol. 34, no. 5, pp. 343-366.
64. **Yarmolyuk V.V., Litvinovsky B.A., Kovalenko V.I., et al.** Formation Stages and Sources of the Peralkaline Granitoid Magmatism of the Northern Mongolia-Transbaikalia Rift Belt during the Permian and Triassic, *Petrology*, 2001, vol. 9, no. 4, pp. 302-328.
65. **Yarmolyuk V.V., Kovalenko V.I., Sal'nikova E.B., et al.** Tectono-Magmatic Zoning, Magma Sources, and Geodynamics of the Early Mesozoic Mongolia-Transbaikal Province, *Geotectonics*, 2002, vol. 36, no. 4, pp. 293-311.
66. **Yarmolyuk V.V. and Kovalenko V.I.** Deep Geodynamics and Mantle Plumes: Their Role in the Formation of the Central Asian Fold Belt, *Petrology*, 2003a, vol. 11, no. 6, pp. 504-531.
67. **Yarmolyuk V.V. and Kovalenko V.I.** Batholiths and Geodynamics of Batholith Formation in the Central Asian Fold Belt, *Russ. Geol. Geophys.*, 2003b, vol. 44, no. 12, pp. 1260-1274.
68. **Yarmolyuk V.V., Kovalenko V.I., Kozlovsky A.M., et al.** Crust-Forming Processes in the Hercynides of the Central Asian Foldbelt, *Petrology*, 2008, vol. 16, no. 7, p. 679-709.
69. **Yarmolyuk V.V., Kovalenko V.I., Sal'nikova E.B., et al.** Geochronology of Igneous Rocks and Formation of the Late Paleozoic South Mongolian Active Margin of the Siberian Continent, *Stratigr. Geol. Correlation*, 2008, vol. 16, no. 2, pp. 162-181.
70. **Yarmolyuk V.V., Kozlovsky A.M., Sal'nikova E.B., et al.** Age of the Khangai Batholith and the Problem of Duration of the Formation of the Largest Batholiths of Asia, in *Geodinamicheskaya evolyutsiya litosfery Tsentral'no-Aziatskogo podvizhnogo poyasa: ot okeana k kontinentu* (Geodynamic Evolution of the Lithosphere of the Central Asian Mobile Belt: from the Ocean to Continent), Irkutsk: IZK SO RAN, 2011b.
71. **Yarmolyuk V.V., Lykhin D.A., Shuriga T.N., et al.** Age, Composition of Rocks, and Geological Setting of the Snezhnoe Beryllium Deposit: Substantiation of the Late Paleozoic East Sayan Rare-Metal Zone, Russia, *Geol. Ore Dep.*, 2011a, vol. 53, no. 5, pp. 390-400.
72. **Yu X., Iang Sh-F., Chen H-L., et al.** Permian Flood Basalts from the Tarim Basin, Northwest China: SHRIMP Zircon U-Pb Dating and Geochemical Characteristics, *Gondwana Res.*, 2011, vol. 20, pp. 485-497.
73. **Yuen D.A., Maruyama S.H., Karato S.I., and Windley E.F.** *Superplumes: Beyond Plate Tectonics*, New York: Springer, 2007.
74. **Zhong C.L., Li Z.X., Li Z.H., et al.** A Permian Layered Intrusive Complex in the Western Tarim Block, Northwestern China: Product of a ca. 275-Ma Mantle Plume?, *J. Geol.*, 2008, vol. 116, pp. 269-287.

75. **Zhou M.-F., Zhao J.-H., Jiang Ch.-Y, et al.** OIB-Like, Heterogeneous Mantle Sources of Permian Basaltic Magmatism in the Western Tarim Basin, NW China: Implications for a Possible Permian Igneous Province, *Lithos*, 2009, vol. 113, pp. 583-594.
76. **Zonenshain L.P., Kuzmin M.I., Kovalenko V.I., et al.** Structural-Magmatic Zoning and Metallogeny of the Western Part of the Pacific Belt, *Geotektonika*, 1973, no. 5, pp. 3-21.

FUNDAMENTAL PROBLEMS OF THE EARTH EVOLUTION AND THE NATURE OF D" LAYER AS ONE OF THEM

Pushkarev Y. D.

*Institute of Precambrian Geology and Geochronology, St.-Petersburg, Russia.
(ydcanon@rambler.ru)*

This article contains the summarized results obtained from the projects supported by the Russian Foundation for Basic Research: # 04-05-64462, # 07-05-00527 and current project # 12-05-00523, which were aimed at studying the evolution of the Earth. Our approach is different from the traditional. Such an approach is not based on the summarized data for the mantle igneous rocks, but uses a more rare material (mantle xenoliths from different depth). As a result two co-existing different ideas are available.

One idea (articles by Y.A. Kostitsyn published between 2004 and 2012 [5, 6, 7]) suggests mixing of the substance in the mantle that results in the averaging of sources of mantle igneous rocks. Another idea is based on studies of xenoliths of the initial mantle substratum (in particular, the present article).

It is essentially important to understand that the Earth could not lose elements which were heavier than helium after it had been formed. If it lost them, it, most likely, occurred in the course of the Earth's growth because when it reached the present size effective losses were already impossible. Thus, they were either not available on its orbit from the very beginning as, they were initially irregularly distributed on radius from the Sun, or the initial subchondritic substance had been already differentiated, and had lost them prior to intensive planet-formation.

At the same time there is a very important component of this problem. The definition of paleotemperatures of igneous rocks of the first megastage of the exogenous nature does not bear any information on a physical condition of the Earth formation as a whole. There is still unclear whether the Earth had been completely melted or not.

As a whole this article is devoted to a brief discussion of those processes which could proceed in first 500 Ma, i.e. during the first megastage of its evolution mainly of exogenic activity; the result of that megastage is not completely evident. At the same time the article is devoted to one of the most interesting problems i.e. the problem of the origin of D" layer.

However, before discussing the results obtained from the studies of the mantle xenoliths, we will list the most actual geodynamic problems, which are still subject for intense debate despite isotope investigations that have been lasting for over 50 years.

We have to begin such a list with the most important problem of the Earth's origin: **Was the Earth melted or not? If it was melted where was the oceanic water contained and how it could be preserved? These problems are still open. Another geodynamic problem which is as important as the first one is what was the initial composition of the Earth and what was its primary structure. Was it a homogenous chondritic (CHUR) or heterogeneous depleted reservoir (HDR)?**

There is a series of other actual geodynamic problems the solution of which will most likely demand a lot of time. Below are the most significant among them.

How and when did a solid metal core appear in the planet's centre? Whether this core had been a protoplanetary germ; whether it had been initially solid or had been a product of partial crystallization of a liquid core, melted out of the mantle and then lowered?

Why an external core is liquid? What is nature of its heating and isolation? What if D" layer is not the formation which lowered outside like in the model put forward by I.N. Tolstikhin and E. Hofmann [19] but is the silicate component separating from inside during the crystallization of a liquid core? The non-spherical upper border of layer D" points out to it.

What is a general energy of planetary evolution? Where does the observable heating of bowels come from and what its nature? When was the maximum of this process reached? When did the culmination of the endogenous heating take place? Or will it happen in the future? Is the temperature that is thought to be the temperature of the substance at the core-mantle interface real? If it is real, what is the nature of such overheating?

What is nature of the lack of such elements as K, Rb and ^{36}Ar , ^{204}Pb isotopes? What is this lack of elements relative to chondrites stipulated for? What does the initial isotope composition of the mantle substance ($^{87}\text{Sr}/^{86}\text{Sr}$)_o = 0.703, instead of 0.780 that should be reached on the Earth at the average primary chondrite composition) mean? What is the reason of a very low Rb/Sr value in the mantle: Rb lack or Sr surplus? Did this feature come into existence when the planet was formed? Or does it result from the Earth's evolution? What is the nature of Rb lack? Is it identical to K deficit?

When and in what state did the water come to the Earth? When did it give rise to the ocean? I.e. when was the temperature on the surface lower than the temperatures of intensive boiling and water evaporation (about 100°C-120°C)? At present it is well known that the temperature of mantle magmatic melts in big faults exceeds 1000°C. However, a general modern heating of the Earth cannot provide a complete evaporation of an ocean.

And, at last, there is one more significant feature in the evolution of the Earth - specificity of the first megastage – exogenous, covering almost the whole first 0.5 Ga. Had been all four major reservoirs (proto-crust with the ocean, mantle, liquid core and solid core) in existence by the beginning of the endogenous geodynamic evolution? It is not inconceivable that if the Earth had died by 4 Ga all

these reservoirs could have been already in existence. The knowledge of such initial state is of crucial importance for deciphering the endogenous evolution. There are two modern ideas about the nature of the initial Earth: the model of initially melted homogeneous Earth and the model of heterogeneous accretion.

MODEL OF INITIALLY MELTED HOMOGENEOUS EARTH

According to this model the chondrite Earth underwent the impact with the Moon, was completely melted and as a result of such melting was differentiated. It is still unknown where, when and at what temperature the water ocean came into the existence on the Earth; whether it existed from the very beginning or came into the existence after the earth had been already melted. After such general melting all major reservoirs had to be produced during the crystallization. However, it could happen without a complete melting.

MODEL OF HETEROGENEOUS ACCRETION

A complete planetary melting did not take place. From the very beginning water ocean was available on the surface and a strong melting similar to the recent one took place at the depth. Moreover, all four planetary reservoirs were formed during the heterogeneous accretion of the Earth, i.e. they appeared at the first megastage but at the exogenous stage.

The further part of this article includes the compilation of results and preliminary publications for the last five years.

As stated above, the present character of the initial development of the Earth has not been completely defined. There are two mutually exclusive viewpoints. One includes a complete melting of the Earth and accordingly simultaneous differentiation. Another idea is that at the beginning of the planet-formation the surface temperature did not exceed 100 °C as the water was contained in the oceans. Thus, the temperature of deep-seated melts brought through the faults could be higher than 1000 °C, like we observe today at the bottom of the Atlantic ocean and in volcanoes on islands along the continents' margins.

What is a reality? Unfortunately, the detailed studies to understand the nature of planetary activity in the first 0.5 Ga are still scarce. Strictly speaking, to solve such problems it is difficult to understand, what major reservoirs existed on the Earth by the beginning of endogenous megacycles. It is a very important component of the initial evolution of the Earth in order to understand planetary features of its development at the first stage.

The strongest argument which is in contradiction to the chondrite model is that this model is not in the agreement with U/Pb value in the mantle being one order higher. Concentrations and ratios of other elements do not also agree with the chondrite model (CHUR). The major among them is the modern Sr isotope composition of the mantle which is significantly depleted by the radiogenic Sr (0.703-0.705) as compared with the chondrite substance (0.720-0.800).

To check this statement we have analyzed U/Pb value in the substance which is brought to the surface as mantle xenoliths. It turned out that by Pb isotope characteristics such substance is similar to the major mantle reservoir, lying in Pb-Pb isotope coordinates on crossing of a mantle evolution line and the geochrone. It well agrees with the ideas that the major mantle reservoir is not related to the non-altered chondrites, but starting from the very beginning of the Earth's evolution it has been developing in the system which has U/Pb values being one order higher than that in CHUR, and the Sr isotope composition is more primitive than the chondritic one.

The seismic tomography revealed the layer D" at the core–mantle boundary. This layer shows specific physical features. Thus, one of the most actual problems of modern geology is to understand the nature of this layer. About 3% of the Earth's mass fell within this layer having the maximum thickness of 300 km. Though it is quite often interpreted as a part of the lower mantle, there are grounds to believe that by chemical and isotope composition the layer D" can differ from the overlapped mantle substance. There are two hypotheses: (1) the substance of the layer D" was dissolved in a liquid core, fractionated, separated and uplifted during its crystallization [11]; (2) the layer D" is the multi-component substance which was produced at the Earth's surface at the very beginning of its evolution (due to mixing of the proto-crust with the space material) and sank to the core–mantle interface [19].

Technical difficulties with a mass spectrometer didn't allow accomplishing Sr isotope analysis in iron meteorites which show the increased Th and U concentrations. Nevertheless, it didn't affect the results for the project on the whole as we found literature data concerning the composition of accessory phosphates in such meteorites which were supplemented to our results. All of them point out the presence of lithophile elements in the liquid core prior to its crystallization. At the same time it was found out that the lithophile elements, like the accessory minerals that host them are irregularly distributed in iron meteorites, and iron as a mineral phase is "sterile" as regard to impurities. Thus, the more representative samples are required to obtain correct total concentrations of such elements, which were used for ICP-MS analysis.

We wanted to find isotope effects which should take place due to the removal of surplus elements to the layer D" during the crystallization of the liquid core. It could be related to the contribution of the substance from this layer to the formation of mantle magmatic derivatives. However in order to define, in what isotope systems we could expect those effects, we have to find out which elements when they become in abundant amount could be removed from the core to the bottom of the lower mantle. Also we have to find out which trace lithophile elements could be melted in the liquid core prior to its crystallization. Only those high-temperature elements (REE, Th, U, Hf, etc.) which were not lost due to high volatility during the accretion and which are used in radiogenic isotope geochemistry were of particular interest.

By now the share of such elements in the silicate Earth's shell or, in the primitive mantle (PM), was identified with the chondrite that suggested a complete "sterility" of the core as regard to REE and any trace lithophile elements. The hypothesis under study presumes that such an assumption is incorrect and the liquid core was separated due to melting of the low-temperature eutectic component of the protoplanetary substance which should include trace lithophile elements at the first exogenous megastage.

The aim of the present study was to identify the PM substance in mantle xenoliths and to reveal the deficiency of elements relative to chondrite. Having known the concentrations of non-volatile high-temperature elements in the primitive mantle and following the principle of balance between the primitive mantle and the complementary core we can understand which lithophile elements were brought into the liquid core. Among 58 mantle xenoliths we managed to identify varieties corresponding to PM in terms of the major rock-forming elements. Moreover, the most promising result was the identification of the deficit of LREE (relative to chondrite) and a complete agreement between Nd isotope composition and isotope composition in the MORB source.

So, despite the traditional ideas the deficit of LREE in the MORB source is not related to crust-growing but reflects the feature of the silicate Earth's shell which is either caused by LREE removal into the complementary core, or suggests the heterogeneity solar nebular (by the distribution of rare-earth elements). However, during the discussion of the obtained results we came to the necessity to find out the following problem: did the PM substance in the studied xenoliths undergo the partial melting? At the initial stage the partial melting does not effect the concentrations of major elements, but can cause depletion by trace elements. Besides, it was necessary to find out, whether the petrochemical characteristics of xenoliths which are similar to the primitive mantle in terms of major elements result from the metasomatic enrichment of the depleted mantle substratum or not.

1. IDENTIFICATION OF GEOCHEMICALLY ISOLATED PM SUBSTANCE IN MANTLE XENOLITHS

It seems that identification of PM substance should not represent special difficulties because the petrochemical and isotope characteristics of the primitive mantle are known and by those characteristics we have to find the substance itself. However, it is far not so because the most complicated task here is to reveal the geochemical isolated PM substance.

In addition to a potential contribution of the mantle substance to the crust-generation it was subject to the numerous secondary processes which could disturb its geochemical isolation.

Detailed studies of foreign scientists [10] show there are at least five various factors which can be responsible for the composition of trace elements in the bulk samples of mantle xenoliths. (peridotites), and thus for their isotope composition. The most essential difficulty is the presence of accessory apatite in xenoliths,

because the major part (from 25 to 75 %) thorium, uranium, strontium and LREE is due to apatite. Therefore, if apatite is primary or appears in the conditions of geochemical isolation of the rock as a whole, its dissolution by the acid treatment of samples (to remove the contamination) is so strongly that it breaks the isolation of U-Th-Pb, Sm-Nd and Rb-Sr isotope systems. As a result, it almost completely excludes their use for identifying the PM substance.

Hence, to avoid errors in identifying the isotope composition due to the contamination by the acid treatment we have to find such xenoliths which still preserve the central parts uncontaminated. The most perspective turned out to be xenoliths from alkaline volcanoes of Mongolia and Vitim plateau. Unfortunately, the sample preparation made them impossible for solving the problem under discussion because prior to the analysis the xenoliths were processed with the acid. For this reason in the present study we used the bulk xenolith samples which were mechanically freed of the contamination. We also used the published data concerning the non-contaminated and non-metasomatized mantle substance.

There are number of features by which the xenoliths can be regarded as PM, but only a certain combination of these features can provide a reliable identification of this substance. Among them we have to distinguish between the necessary and the sufficient. The necessary (but not sufficient) include the chondrite-like ratio of the major rock-forming elements (Al/Mg, Al/Si, Mg/Si, Ca/Al). However, as it was already stated, the major elements are almost tolerant to low degree of the partial melting and primitive substance (as regard to the ratios of these elements) could lose a considerable part of highly incompatible trace elements.

The REE content similar to chondrite is not a reliable indicator that the substance belongs to PM. When the core had been separated it could not remain unchanged as the concentration of all refractory elements which were not contained in the core, had to increase as many as the mass of the Earth is higher than that of the Earth's silicate shell. Secondly, as stated above the chondrite distribution of LREE in the PM casted serious doubts and it was necessary to find out what is an actual LREE distribution. At last, one more complication to identify geochemically isolated PM substance in the mantle xenoliths is the contamination by the host volcanics. Thus, it is better to identify the geochemical isolated PM substance in several stages: first to choose the most suitable xenoliths as regard to major elements, then to verify that they do not show any signs of metasomatism and exhibit low degree of melting and at last, to analyze their isotope composition.

1.1. Identification of primitive mantle xenoliths as regard to major elements: Al/Si-Mg/Si system

At the first stage of PM identification it is convenient to use the system which was proposed by Jagoutz et al., used for revealing mantle xenoliths which are the most similar to the primary substance of the Earth in terms of the composition [16]. (fig. 1). On Al/Si-Mg/Si diagram they plotted the chemical composition

changes in different chondrites and the differentiation of the Earth's substance. Assuming that Al, Si and Mg were not brought into the core the crossing of these plots define the BE (Bulk Earth) composition.

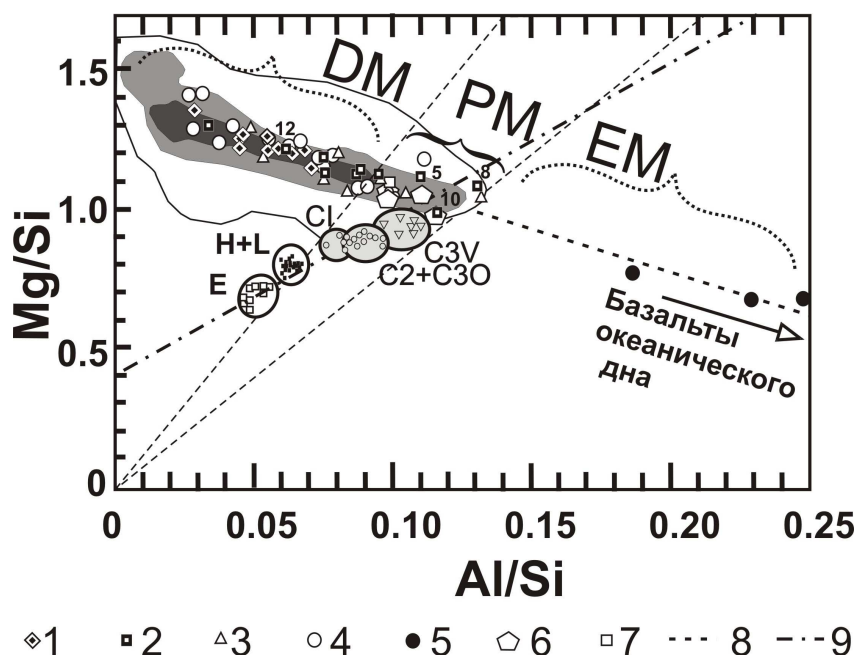


Fig. 1. Diagram Mg/Si - Al/Si (wt. %) for revealing the xenoliths being similar to the primitive mantle as regard to Al, Mg and Si ratios

Xenoliths, investigated in the present study: 1 - Mongolia, 2 - Vitim plateau; xenoliths from literature sources; 3 - Vitim plateau [1]; 4 – xenoliths, used by Jagoutz et al. [16] for defining the PM composition and 5 – comatiites from the same publication; 6 - PM compositions from models of different researchers; 7 – pyrolite composition; 8 - trend of fractionation of the Earth's substance, 9 - trend of cosmo-chemical fractionation; 10 – chondrite compositions. Isolines - projection to a plane of the three-dimensional histogram for 593 xenoliths, based on the compilation from Pearson et al. [17]. Two lines from the beginning of co-ordinates (dotted line) correspond to the minimum and maximum Al/Mg values in coal-bearing chondrites (C1, C2+C3O, C3V) and divide the trend of evolution of the mantle substance composition into three parts: PM - primitive mantle, EM - enriched mantle, DM- depleted mantle.

As there are grounds to consider that the core can contain up 7.3 % Si [9], BE lies under this crossing, slightly closer to the chondrite field. The crossing of two trends most likely correspond to BSE (Bulk Silicate Earth) or PM (Primitive Mantle). The comparison of five xenoliths, laying on the diagram closer the crossing of trends shows that their compositions are similar irrespective of the sampling site. So, Jagoutz et al. suggested to take their average composition as the PM composition. To develop this approach two lines which divide the evolution trend into three parts corresponding to the depleted (DM) mantle, enriched (EM) mantle and primitive mantle (PM) were added to the diagram.

Fig. 1 shows the PM compositions obtained by different researchers and chemical composition of 593 mantle xenoliths from [17]. The latter are interpreted in isolines of points density. The summary suggests that the samples corresponding

to PM as regard to Al, Mg and Si ratios are very scarce. However, mantle xenoliths do not include the enriched varieties. It contradicts the conclusion that the composition of the primitive mantle resulted from the metasomatic alteration of the depleted mantle substances. If such a composition was the result of metasomatic alteration, the xenoliths should contain the enriched varieties with positive ENd and primitive Sr isotope composition. Only two spinel lherzolites collected in the south-east China exhibit the increased content of radiogenic Sr (^{87}Sr). It is most likely due to the contamination or metasomatic alteration that is verified by amphibole and phlogopite present in those samples.

1.2. Identification of xenoliths of the primitive mantle which was not subject to mantle metasomatism: Ca/Al-Al/Si system

One of the major conditions to find the xenoliths of the geochemically isolated primitive mantle is that Ca/Al value in it has to be similar to that observed in the chondrite. The variations of this value in mantle xenoliths which are regarded to be similar to the primitive mantle have been discussed by different researchers. Let's analyze the character of these variations Ca/Al ratio in the mantle substance subjected to metasomatic element redistribution (fig. 2) is given to understand that the main reason of those variations was the mantle metasomatism.

With this purpose we used diagram Ca/Al - Al/Mg (fig. 2) which in addition to the samples collected earlier gives the chondrite compositions [21]. To illustrate variations in Ca/Al value we plotted (fig. 2) all xenoliths. Moreover, on this figure the agreement with chondrites is reflected by Al/Mg value. The plot (fig.2) shows that 12 samples are similar to chondrites as regard to Ca/Al and Al/Mg values and, hence, are potentially identical to the PM. Those samples include five from the Vitim plateau (Vt-5, Vt-8, Vt-10, 313-3, 313-6); five samples from China [23] and only two samples from Hart, Zindler, [14].

1.3. Revealing of xenoliths of the primitive mantle which was not subjected to weak differential melting: Al/Mg-Sr/Mg-End system

To exclude the samples which were altered as a result of small degree of partial melting we used the ratio between any highly incompatible element and one of the rock-forming elements vs. the Al/Mg ratio. In order to use a wide scope of mantle xenoliths studied by Sm-Nd and Rb-Sr methods, but not studied for the concentrations of other minor and trace elements, we have chosen Sr/Mg value as an indicator of a low degree of partial melting.

Fig. 3 gives Al/Mg-Sr/Mg-End system in which Sr/Mg values do not depend on Sm/Nd value. A distinct cosmochemical trend for different chondrites in this system allows identification of the substance of the primitive mantle which was not subjected to low degree partial melting. To display the trend of evolution of the mantle substance on Sr/Mg-Al/Mg diagram we plotted compositions of upper-

mantle peridotites of ultramafic rocks, Hokkaido [18]. The analytical results obtained by Takazawa et al., are preferable for two reasons. First, all samples were not chemically treated.

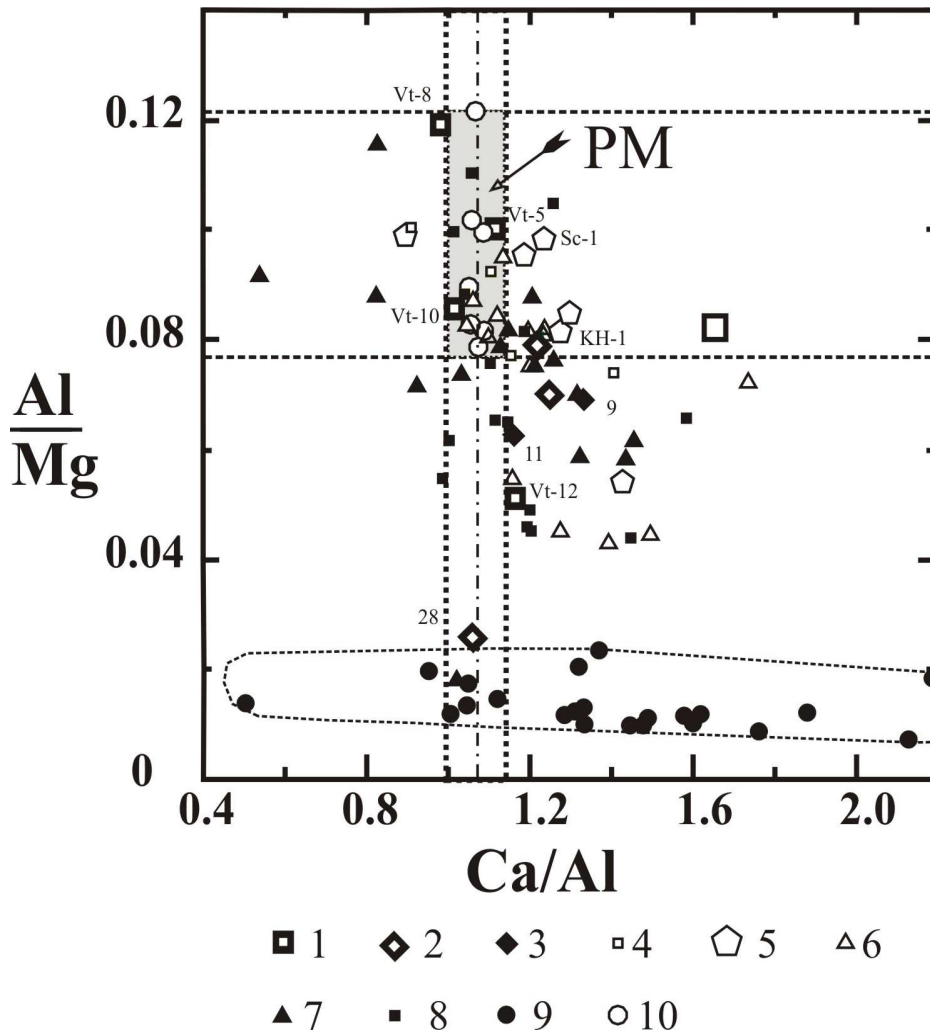


Fig. 2. Diagram Mg/Si - Ca/Al (wt. %) for selecting mantle xenoliths with non-disturbed chondrite Ca/Al ratio

Xenoliths, used in this study: 1- Vitim plateau, 2 - Mongolia (numbers near points correspond to numbers of samples given in Table 1); xenoliths from literature sources: 3 - Mongolia, Tariat [4], 4 - Vitim plateau [1], 5 - xenoliths, used for definition of the PM composition (Jagoutz et al, 1980); 6- xenoliths from lherzolites, South-East China [23], 7- xenoliths of lherzolites and 8 - orogenic lherzolites from Hart, Zindler, 1986; 9 - xenoliths of lherzolites, Canary Islands, subjected to mantle metasomatism [Neumann, 2004]; 10 - chondrites of different types [21].

Secondly, as opposed to the mantle xenoliths the mantle substance which was subjected to partial melting of different intensity, was not affected by the contamination with the melt as it doesn't include xenoliths but orogenic peridotites.

Those samples which demonstrate Ca surplus and which were studied by Sm-Nd and Rb-Sr methods were plotted on the diagram, given on Fig. 3. Seven of them (Vt-5 and six samples from south-east China) lie close to the field of

chondrite or PM composition. These xenoliths are similar to the substance with high positive End values and primitive isotope Sr composition. The increased concentrations of the radiogenic Sr (^{87}Sr) is observed only in two spinel lherzolites from south-east China, that were most likely affected by selective contamination or metasomatic alteration, that is confirmed by amphibole and phlogopite in those samples.

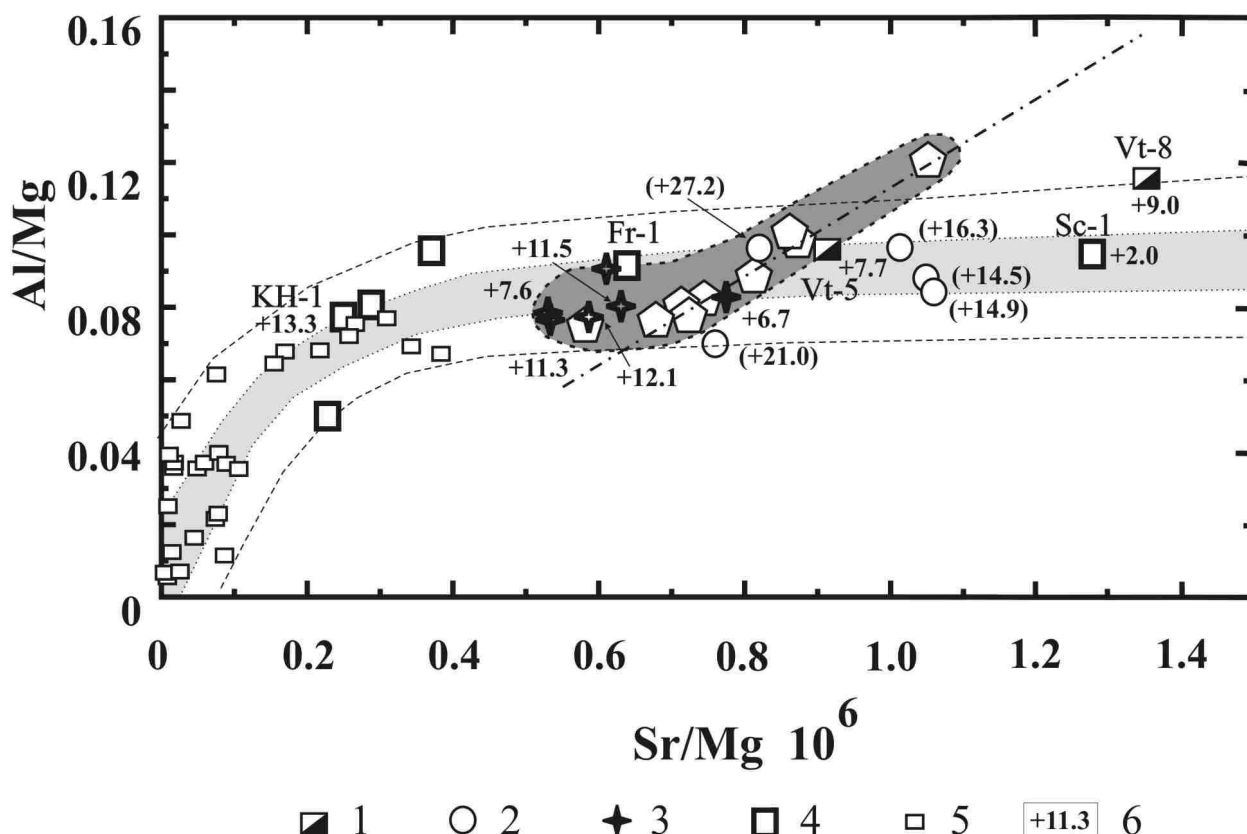


Fig. 3. Diagram Sr/Mg - Al/Mg-END (wt. %) for selecting mantle xenoliths which were not subjected to the partial melting

Xenoliths, used in this study: 1 – Vitim plateau; xenoliths from literature sources: 2 – Vitim plateau [1, 3], 3 – xenoliths of Nyushan volcano, south-east China [23, Xu et al, 2003]; 4 – xenoliths used for analysis of primitive mantle composition by Jagoutz [16]; 5 – orogenic lherzolites, Hokkaido, Japan [18], metazomatized xenoliths, Canary islands, 6 – ENd values for bulk samples, in brackets - the same for clinopyroxene. The thin dotted line with light grey axial part limits zone of magmatic differentiation, dark grey field - chondrite and PM composition. If the samples are similar to the PM as regard to Al, Mg, Si and Ca and are similar to chondrite Sr/Mg value, they are most likely similar to PM by other trace elements.

Fig. 3 shows also six xenoliths taken from Jagoutz et al, [16], which were used by them for analyzing PM composition but which didn't pass the test for chondrite Ca/Al ratio (see fig. 2). As regard to Sr/Mg values all of them except for sample Fr-1 do not correspond to non-altered PM substance.

2. Sm/Nd AND Rb-Sr VALUES IN THE PRIMITIVE MANTLE OBTAINED FROM Nd AND Sr ISOTOPE COMPOSITION

Results for mantle xenoliths from the Vitim plateau combined with the data from literature sources for southeast China, show ENd value in the non-altered PM ranging from +7.6 to +11.5 with the average value as $+9.5 \pm 2.0$ that corresponds to $\text{Sm/Nd} = 0.351 \pm 0.006$. Thus, $^{87}\text{Sr}/^{86}\text{Sr}$ value in PM scatters from 0.70282 (sample NuSh-2) to 0.70333 (sample Vt-5) that on average corresponds to $(\text{Rb/Sr})_{\text{PM}} = 0.0215$ value. These values completely agree with those obtained by Sm-Nd isotope method for the mantle derivatives, mainly MORB basalts [5]. Thus, Nd isotope composition in the geochemically isolated primitive mantle confirms the preliminary conclusion that it is characterized by the increased (relative to chondrite) Sm/Nd values, and thus demonstrates a primary Nd deficit, that is neither related to the partial melting nor mantle metasomatism.

3. Pb-Pb AGE OF XENOLITHS FROM THE PRIMITIVE MANTLE AS AN ADDITIONAL EVIDENCE OF GEOCHEMICAL ISOLATION

Pb-Pb method was used to determine the age of the primitive mantle substratum. As compared with other methods of isotope dating its major advantage is the insusceptibility to the disturbance of geochemical isolation of the system caused by the removal of parental and child elements and uranium supply. It is in particular important for the investigated mantle xenoliths from Mongolia and Vitim plateau as the age of the host volcanics is the Cenozoic. Thus, the contamination by uranium from these volcanics cannot break the geochemical isolation of Pb-Pb isotope system. Four samples (all from basalts of the Vitim plateau) were collected; by petrochemical characteristics (Al_2O_3 , CaO, Al/Mg, HREE) the bulk samples are similar to PM. The Pb-Pb age of four samples is estimated as 4457 ± 12 Ma.

Strictly speaking, the identification of PM substance in the mantle xenoliths is equivalent to the age determination because PM origin is considered to be one of the most ancient processes on the Earth. By time it corresponds to separation of the protoplanetary substance into the core and the silicate shell which includes the primitive mantle. However, there is a paradoxical situation as regard to the age of this process. On one hand, surplus of ^{182}W isotope in the silicate shell of the Earth can evidence the supply of siderophile tungsten in the core prior to the decay of short-lived isotope ^{182}Hf , limiting the core formation by 30 Ma after the accretion had began [Kleine et al., 2002; Yin et al., 2002]. On the other hand, in U-Th-Pb isotope system which should also respond to Pb removal into the core by the significant increase in U/Pb value in the silicate shell, formation of the core and PM could proceed during 100 Ma after the Earth's accretion had begun [13]. Hence, the minimum PM age in U-Th-Pb isotope system is estimated as 4460 Ma.

It seems that such discrepancy is a result of the simplified interpretation of isotope effects in Hf-W system. At the same time W isotope composition in the

silicate shell of the Earth results from both the in-situ ^{182}Hf decay and the homogenization of isotopes in the substance of the protoplanets. If the substance is not completely homogenized the surplus of isotope ^{182}W in silicate rocks can be observed even in the case if the shell started to be formed after a complete decay of the short-lived ^{182}Hf isotope. Therefore, a more correct is the age of the core and the primitive mantle, calculated from isotope effects in U-Th-Pb system. The agreement between the ages estimated as 4460 Ma and Pb-Pb age (4457 ± 12 Ma) which was obtained by us for PM xenoliths indicate that they are very close to real.

Os isotope composition in xenoliths with petrochemical characteristics identical to those in PM turned out to be similar to chondrite [17]. In other words, Os isotope composition is similar to that of the primitive substance in which the silicate part was not subjected to partial melting since the accretion had started i.e. throughout 4560 Ma. It is an additional confirmation of geochemical isolation of PM substance in the bulk xenoliths samples. The major among them is the possibility to use the concentrations of trace elements in PM and first of all U and Th concentrations. The obtained concentrations of these elements are the maximum as some contamination by the substance from the host volcanics is possible. The host volcanics are enriched by REE, Sr, Pb, U, Th.

The influence of such contamination on concentrations of different elements xenoliths is different. If the contamination took place quite recently, it is not recorded in Pb isotope composition, but is capable to change strongly Sm/Nd, Rb/Sr and U/Pb values. The contamination of the xenoliths from the Vitim plateau by Sr can vary from 0.05 to 0.4 %.

4. RARE AND RARE-EARTH LITHOPHILE ELEMENTS IN IRON METEORITES AND IN THE CORE SUBSTANCE

As iron and stony-iron meteorites are considered to be the products of destruction of cores of planetesimal and can serve as material analogue of the Earth's core, there is a possibility to check the assumption that scarce LREE and U are found in the core itself. 39 meteorites and three phosphides were analyzed by ICP-MS. The results obtained suggest that iron meteorites contain such lithophile elements as Th, U and REE, occurring mainly as accessory phosphates. Some samples show the concentrations which are comparable with the chondrite, but they are usually lower than those which the liquid core should exhibit in order to provide the balance when the protoplanetary substance was divided into the core and silicate shell.

However, when discussing these results one keep in mind that observable concentrations are similar to those typical of the crystallized substance of the core free of any impurities. It follows from Wood's calculations [22]. The results for iron meteorites obtained by ICP suggest that such lithophile elements as REE, U and Th are brought into the core.

Analyzing the composition of the investigated samples showing the distribution of HREE which is similar to chondrite one can make sure that by Al,

Mg and Si ratios there are varieties identical to the samples, which Jagoutz et al. were used to analyze the average PM composition. Nevertheless, such an agreement with PM composition is not sufficient for selecting perspective samples as regard to major elements as the considered system does not solve a problem of possible disturbance of geochemical isolation due to mantle metasomatism. Therefore the following stage of xenolith identification of the non-altered PM was to be done in Ca/Al-Al/Si system.

5. HIMU COMPONENT AS A POSSIBLE DERIVATIVE OF LAYER D''

Identification of PM substance in mantle xenoliths can create the basis for revealing isotope effects that show the contribution of layer D'' in generation of mantle derivatives. In the course of studies we assumed that if any ratio of hard-volatile elements (or their concentrations) for the Earth as a whole differs from that in the primitive mantle it can be caused by supply of a scarce element into core. In accordance with this approach we paid attention to lack of uranium in xenoliths of the primitive mantle. Real concentrations of this element in the xenoliths (5-18 ng/g) turned out to be similar or slightly lower in comparison with that in chondrites (8-17 ng/g). It is especially noticeable when we compared it with the uranium concentration in CV-chondrites (17 ng/g) whose composition is similar to the Bulk Earth. On the other hand we have found the increased concentrations of uranium and thorium in some iron meteorites and in troilites from them. It suggests that scarce uranium in PM is found in the liquid core. Moreover, in order to keep the balance the uranium and thorium concentration in the liquid core have to be similar to the chondrite contents or be slightly higher. So, this can provide a new viewpoint as regard to HIMU component origin.

When the liquid core is crystallized the solid phase should be free of impurities, and the surplus of uranium and thorium is brought into the bottom of the lower mantle. As a result high $\mu = {}^{238}\text{U}/{}^{204}\text{Pb}$ value is found in the layer of the silicate substance close to the core, i.e. the HIMU-component which in time demonstrates increased concentrations of radiogenic Sr isotopes is formed. Thus, a well-known ${}^{207}\text{Pb}/{}^{206}\text{Pb}$ age of HIMU component of about 1800 Ma [8], defined by isochrone of mixing reflects the time of real process and the beginning of the core crystallization. The HIMU-component becomes the most effective isotope signal from the layer D'', which is formed during the liquid core crystallization. Abundant HIMU-component observed in the volcanics which are regarded to be derived from the mantle plumes is good evidence of the above hypothesis.

6. THE «SILICATE ROCKS - MASSIVE SULPHIDIC ORES» INTERFACE IN DEPOSITS OF NORILSK TYPE AS ANALOGUE OF THE MANTLE-CORE INTERFACE

The hypothesis that the layer D'' was formed due to the crystallization of the

liquid core can be checked partly on natural modeled object. Such an object is silicate rocks-sulfide melt interface as the crystallization of the sulfide melt leads to the formation of huge accumulation of massive ores at the bottom of intrusive bodies (e.g. Norilsk deposit). Unfortunately, this idea came to us a month before the accomplishing of the present project and we couldn't analyze all material. At the same time even an ordinary study of the cores of two largest deposits Talnakh and Kharaelakh provides the valuable information. Both deposits show a very exotic layer of the silicate substance located at the igneous rocks- massive ores interface. This layer is significantly different both from the overlying non-olivine gabbro in the Kharaelakh complex and from olivine-bearing gabbro of the Talnakh intrusion. In both cases the rocks from this layer are regarded as "hornblende". Their thickness in the Kharaelakh complex is 2 meters, and that in the Talnakh intrusion makes up 3 meters. The detailed isotope-geochemical and petrographic studies of rocks from this layer can shed light on differentiation which occur at the "mantle-core" interface and can provide the information concerning the origin of the layer D".

7. RESULTS FROM THE PROJECT IN CONNECTION WITH PROSPECTING OF MASSIVE ORES IN DEPOSITS OF NORILSK TYPE

When large deposits are formed the sulfide melt being heavier in comparison with silicate one, lowered to the bottom of the magmatic chamber where it produced a layer of ore substance of 30-40 m thick with a total area up to 4 km. (Kharaelakh deposit). Because of lower crystallization temperature the sulfides are crystallized after silicates. As a result the interface "solid silicates-sulfide liquid" is formed. In a certain sense a final crystallization stage of such an intrusive body with the ore melt at the bottom is a tiny model of process occurring at the "core-lower mantle interface" but at significantly lower pressure. In the same way like the crystallizing core gets rid of dissolved impurities of incompatible elements the sulfide solution removes them into the bottom of the intrusion's silicate part.

As opposed to the situation occurring at core-mantle interface the ores couldn't crystallized hundred million years after the "liquid-solid" interface had been produced. Therefore, isotope compositions of daughter elements in ore and in the silicate part of the intrusion have no chance to become different due to the radioactive in-situ decay of parental elements. However if the ore melt is primarily "labeled" by the isotope composition of any element distinct from that in the silicate melt, the gradient should arise from the crystallization of ore and removal of this element over the deposit. Owing to ore dilution the share of the element under removal could be decreased and the isotope composition of the mixture could become similar to the isotope composition of an element in the silicate substance.

If an expected effect is found for such ore-bearing intrusions of Norilsk type as Kharaelakh and Talnakh, it can be used as an isotope criterion for prospecting

massive sulfide ores in other intrusions. The isotope-geochemical studies of industrially ore-bearing intrusions of Norilsk type [Arndt et al., 2003] suggest the significant difference in the initial isotope composition of some lithophile elements in ore and silicate substance (e.g. Sr and Nd isotope composition).

8. RESULTS OF THE PROJECT IN CONNECTION WITH A PROBLEM OF PLANETARY DIFFERENTIATION OF INITIAL SUBSTANCE AND POSSIBLE ENDOGENOUS NATURE OF LAYER D"

The novelty of obtained results, results first of all from the identification of PM substance which is considered to be an analogue of MORB source. The substance which is called the depleted mantle in all modern isotope systems is actually BSE (Bulk Silicate Earth), i.e. the substance which is similar to the non-depleted mantle. This confused situation emerged about 30 years ago. But by now is it difficult to understand what actually is responsible for BSE depletion relative to chondrite if it is not related to the crust generation. At the same time, in order to keep the balance, LREE should be concentrated in the core. Such not trivial conclusion agrees with results from studies of iron-stone meteorites, published in Nature [12]. These data indicate that they contain the phosphates enriched in REE. This conclusion is also in agreement with the results obtained by us for iron meteorites and troilites and schreibersites from them.

Xenoliths with chondrite ratio of minor and rare-earth elements typical of the primitive mantle have been earlier discovered. Practically all of them include lherzolites. Nevertheless, Sr-Nd isotope characteristics which indicate that these xenoliths belong to the mantle being depleted due to the crust generation were crucial. It induced researchers to interpret the chondrite ratios of major elements as random resulting from the metasomatic alteration of the depleted mantle substance. However, the results obtained from our projects supported by the Russian Foundation for Basic Research suggest that the chondrite ratio of major elements in the mantle xenoliths with high ENd positive values is not the only evidence that they belong to non-altered primitive mantle.

Earlier the similarity to chondrites was demonstrated by Al_2O_3/SiO_2 and MgO/SiO_2 values and HREE distribution we have confirmed it by CaO/Al_2O_3 value serving as indicator of the intensity of the mantle metasomatism and by Sr/Mg ratio used as the indicator of weak partial melting. In addition, the conformity to PM is confirmed by Pb isotope composition which corresponds to the BSE most ancient substance.

Other new result is the lack of uranium relative to its distribution in chondrites. It gives both the chance to offer nonconventional interpretation of nature of HIMU component and to use it as the indicator of the contribution of layer D" in the mantle petrogenesis, but also show new perspectives "for discussing the geodynamic activity in the system "crust-mantle-core".

The matter is that the hypothesis about the presence of thorium and uranium

in the core of the Earth is widely discussed. The calculations of heat balance at the "core-mantle" interface [Doornbos et al., 1986, Anderson 2002] suggest that core temperature at this interface is 1000 °C higher than that for the silicate shell. If the heat is released due to the radioactive decay it could explain both the reason of such overheating, and why the most part of the core is still kept liquid. Note once again that the recent temperature of magmatic melts that reach the surface is in cases higher than 1000 °C and those magmatic melts coexist with the ocean with a constant water temperature.

Recently there is a number of experimental works which show basic possibility of presence of some amount of uranium in the Earth's core. In particular the experiments of the Canadian scientists [Bao et. al., 2005] demonstrate that at pressure higher than 3GP uranium starts to change its lithophile features into chalcophile. Thus, the hypothesis that relates energy of the core with decay of uranium and thorium has been recently confirmed by experiments. We hope that such studies will continue in the near future.

The obtained results are of interest, first of all because they provide new information concerning one of the most actual problems of modern geodynamics.

The current state of the problem results from the coexistence of two competing hypotheses, one of which [11] does not take into account those limits which the chondrite model uses. Another one [19, 20] suggests the ancient subduction of heterogeneous substance from the Earth's surface to the core-mantle interface and thus the formation of layer D" about 4.5 Ga.

COMMENTS

An attempt to find more natural explanation of the layer D" from the viewpoint of the evolution of Sr, Pb and Nd isotope compositions in the system "crust-mantle-core" leads to isotope-geochemical modification of the model similar to B. Buffet's one [11]. According to this model the layer D" generated as a result of the substance differentiation during the crystallization of the liquid core.

The isotope-geochemical approach for checking of such model has been recently formulated. This approach includes: (1) to identify non-altered geochemically isolated PM substance in the mantle xenoliths; (2) to compare with the chondrite protoplanetary substance and to define the deficit elements; (3) to confirm the occurrence of these lithophile elements in the Earth's core via analyzing their concentration in analogue of the core, i.e. in the iron meteorites; (4) to define those isotope effects which can result from the removal of such elements into the layer D" during the crystallization of the liquid core; (5) to find the corresponding isotope effects in the mantle derivatives.

The possibility to obtain an isotope signal from core has been recently discussed as regard to siderophile and chalcophile elements that is connected with their studies in Hf-W and Re-Pt-Os isotope systems. Isotope effects resulting from the extraction of nonvolatile high-temperature lithophile elements by substance of the liquid core, and their removal to the layer D" during the core crystallization

have not been studied, and such a problem is put forward for the first time.

The xenoliths of the garnet-spinel composition in the host mafic rocks are an effective source of the planetary geodynamic information. The Sr isotope composition suggests that the investigated xenoliths with deep-seated garnet-spinel mineral association includes the most ancient not differentiated mantle substance. This composition reflects the final stage of the Sr general isotope evolution in the main mantle reservoir.

Table 1

Results of isotopic analyze of Pb xenolites and accomodating magmatic rocks (обп.Vt-39β)

Паб. №	Sample	206/204*	Err, %**	207/204*	Err, %**	208/204*	Err, %**
309-13	48/3 ЮП-2008	18,007	0,04	15,551	0,04	37,989	0,04
310-13	Vt-39/3 ЮП-2008	17,870	0,08	15,515	0,08	37,760	0,08
311-13	Vt-39/4 ЮП-2008	17,972	0,06	15,551	0,06	37,945	0,06
314-13	Vt-39β	18,137	0,005	15,538	0,004	38,305	0,006
315-13	Vt-37/4	17,900	0,03	15,535	0,03	37,795	0,03
316-13	Vt-27/3	18,009	0,02	15,553	0,02	37,942	0,02
318-13	Vt-57/3	18,012	0,17	15,559	0,17	37,938	0,17
319-13	Vt-57/4	18,042	0,08	15,590	0,08	37,964	0,08

* - Корректированы на изотопное фракционирование (0,13% на а.е.м.) и холостой опыт

** - Measurement error.

Паб. №	Sample	206/204*	Err, %	207/204*	Err, %	208/204*	Err, %	Pb, ppb
315-13	Vt-37/4	17,899	0,07	15,536	0,096	37,797	0,12	147,5

So, it can be concluded that two processes are combined: primary differentiation of the mantle substance and its mixing in the subducted material. It is most likely that these mantle xenoliths with a maximum representation of the component from layer D" without adding the subducted component. It is most likely that in time one can observe higher concentrations of He-3 isotope.

Note, that Sr isotope composition corresponding to non-differentiated substance xenoliths from the main mantle reservoir are given in table 1 and on fig.4.

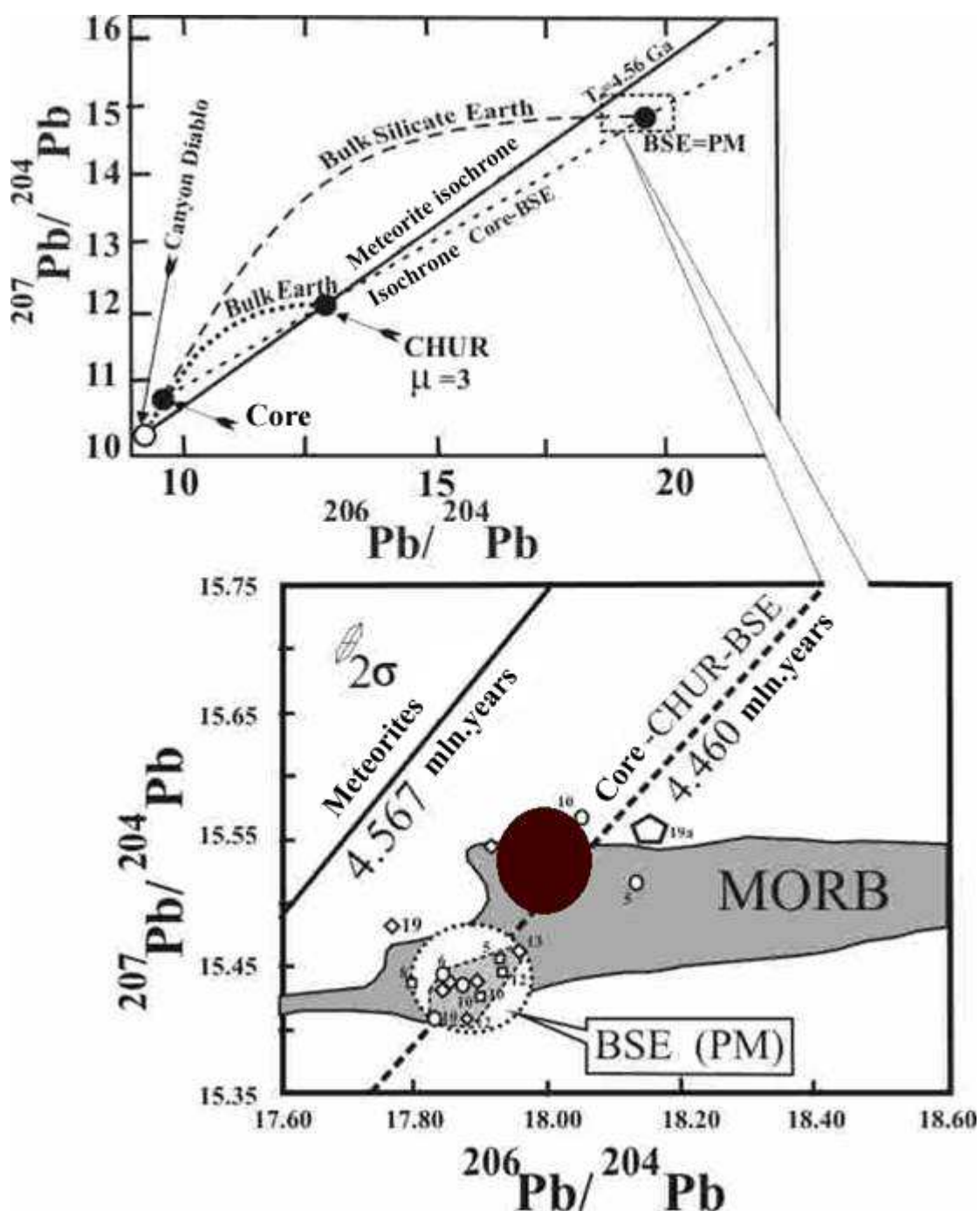


Fig. 4. The fields of Sr isotope composition in xenoliths of the non-differentiated mantle substance from two sampling sites.

Light signs and the corresponding field show Mongolia, black field - schematic area of isotope composition of samples from Siberia collected close to Irkutsk and given in table 1.

CONCLUSION

Summarizing the above, it is necessary to define four main problems for their further studies. One of them is directly connected with the nature of the layer D'' and discussed herein.

1. The most considerable component of unsolved geodynamic problems contain two mutually exclusive options of initial planetary substance and its state:

(i) initially the Earth of the chondritic composition was completely melted or (ii) high-temperature melts (originating at the depth) of subchondritic differentiates co-existed with the solid proto-crust in the combination with oceanic water.

2. Other geodynamic problems are: what was the primary composition of the Earth? Was it initially chondritic by the composition or was it a heterogeneous depleted planetary reservoir?

3. We discuss the similarity between the core-mantle interface and silicate rocks-ore interface.

4. We discuss that the layer D" is not of exogenous, but endogenous nature as it originated as a result of liquid core crystallization and differentiation.

We are grateful to the co-authors of the projects supported by Russian Foundation for Basic Research. We are also thankful to I.V. Ashchepkov, E.S. Bogomolov, A.G. Goncharov, T.F. Zinger, R.S. Krymsky, N.G. Rizvanova, S.A. Sergeev, V.I. Skiba, Doctors of Sciences L.P. Nikitina and S.V. Starchenko for the fruitful discussion. We also thank V.F. Guseva and N.A. Sergeeva for the analysis.

The studies were supported by Russian Foundation for Basic Research (# 04-05-64462 –a (2004-2006), 07-05-00527-a (2007-2009) and 12-05-00523-a (2012-2014).

REFERENCES

1. **Ionov D.A., Aschepkov I.V., Shtosh X. G., Zek X.A., Vitt-Aykshen G.** Xenoliths of Vitim garnet peridotites in the volcanic field of Zabaykal: petrology and geochemistry of garnet-spinel peridotites in the subcontinental mantle transitional zone // *Magmatism of the rift and fold belts*. Moscow. Science. 1993a. P. 169-211 (Russian).
2. **Ionov D.A., Krumm I., Štoš A., Kovalenko V.I.** Evolution of the upper mantle of the South part of Baikal rift zone according to the Sr and Nd isotope composition in the xenoliths of Bartoi volcanos and others // *Magmatism of the rift and fold belts*. Moscow. Science. 1993b. P. 211-234 (Russian).
3. **Ionov D.A., Iaguts E.** Isotopes of Sr and Nd in minerals of garnet and špinel-peridotite xenoliths of the Vitim plateau: First evidences for the mantle inclusions // *Dokl of the USSR Academy of Sciences*. 1992. V. 301. №5. P. 1195-1199 (Russian).
4. **Kovalenko V., Yarmolyuk V. V., Ionov D.A et al.** Evolution of the central Asia mantle and development of the crustal tectonic structures // *Geotectonic.*, 1990. № 4. P. 3-16 (Russian).
5. **Kostitsyn Y.A.** Sm-Nd and Lu-hf isotopic systems of the Earth: are they identify to chondrites // *Petrology*. 2004. V.12. №15. P. 451-466 (Russian).
6. **Kostitsyn Y.A.** Intercommunication between chemical and isotopic (Sr, Nd, Hf, Pb) heterogeneity of the mantle. // *Geochemistry* 2007. V.45. №12. P. 1267-1291 (Russian).
7. **Kostitsyn Y.A.** Time of the Earth core formation according to the isotopic data: concordance of Hf-W and U-Pb systems // *Deep magmatizm, its sources and plums*. Irkutsk, 2012. 4. (Russian).
8. **For G.** Basis of the isotope geology // M. Mir, 1989 (Russian).
9. **Allegre C.J., Poirier J.P., Humber E., Hoffman A.W.** The chemical composition of the Earth // *Earth Planet. Sci. Lett.* 1995. V. 134. P. 515-526.

10. **Bedini J.-L., Bodinier J.-L.** Distribution of incompatible trace elements between the constituents of spinel peridotite xenoliths: ICP-MS data from the East African rift // [Geochim. et Cosmochim. Acta](#), 1999, V 63, N 22, pp. 3883-3900.
11. **Buffett B.A.** The thermal state of Earth's core // *Science*, 2003. V.299. P. 1675–1677.
12. **Davis A.M., Olsen E.J.** REE Patterns in Pallasite Phosphates -A Window on Mantle Differentiation in Parent Bodies, 1996. *Meteoritics & Planet. Sci.* 31, A34-A35.
13. **Galer S. J. G. and Goldstein S. L.** Influence of accretion on lead in the Earth. // In *Earth Processes: Reading the Isotopic Code* (eds. A. Basu and S. R. Hart). 1996. American Geophysical Union, Washington, DC. P. 75-98.
14. **Hart S.R., Zindler G.A.** In search of a bulk-earth composition // *Chem. Geol.* 1986. V. 57. P. 247-267.
15. **Ionov D.A.** Chemical variations in peridotite xenoliths from Vitim, Siberia: inferences for REE and Hf behaviour in the garnet-facies upper mantle // *J. Petrol.* 2004. V. 45. P. 343-367.
16. **Jagoutz E., Palme H., Baddenhausen J., et al.** (1979), The abundance of major and trace elements in the Earth's mantle as derived from primitive ultramafic nodules, *Geochim. Cosmochim. Acta*, 1979, 11, 2031-2050.
17. **Pearson D.G., Irvine G.J., Ionov D.A., Boyd F.R., Dreibus G.E.** Re-Os isotope systematics and platinum group element fractionation during mantle melt extraction: A study of massif and xenoliths of peridotite suites // *Chem. Geol.* 2004. V. 208. P. 29-59.
18. **Takazawa E., Frey E.A., Shimizu N., Obata M.** Whole rock compositional variations in an upper mantle peridotite (Horoman, Hokkaido, Japan): Are they consistent with a partial melting process // *Geochim. Cosmochim. Acta*. 2000. V. 64. №4. P.695-716.
19. **Tolstikhin I.N., Hofmann A.W.** Early crust on top of the Earth's core // *Phys. Earth Planet. Inter.* 2005, **148**, 109-130.
20. **Tolstikhin I.N., Kramers J.D., Hofmann A.W.** A chemical Earth model with whole mantle convection: The importance of a core–mantle boundary layer (D") and its early formation // [Chemical Geology](#), vol. 226, №. 3, pp. 79-99, 2006.
21. **Wasson J.T., Kallemeyn W.** Compositions of chondrites // *Phil. R. Soc.Londjn.* 1988. A325. P. 535-544.
22. **Wood J. A.** *Meteorites and the Origin of Planets.* Earth and Planetary Science Series, 1968, McGraw-Hill Book Co., New York, 117 pp.
23. **Xu X., O'Reilly S.Y., Griffin W.L., Zhou X.** Genesis of young lithospheric mantle in SE China // *J. Petrol.* 2000. V. 41. P. 111-148.

MODEL OF FORMATION OF THE Khibiny- LOVOZERO OREBEARING VOLCANIC-PLUTONIC COMPLEX

Arzamastsev A. A.¹, Arzamastseva L. V.¹, Zhirova A. M.², and Glaznev V. N.³

¹*Institute of Precambrian Geology and Geochronology, Russian Academy of Sciences,
Petersburg, Russia*

²*Geological Institute, Kola Science Center, Russian Academy of Sciences, Russia*

³*Voronezh State University, Russia*

The paper presents the results of a study of the large Paleozoic ore-magmatic system in the north eastern Fennoscandian Shield comprising the Khibiny and Lovozero plutons, the Kurga intrusion, volcanic rocks, and numerous alkaline dike swarms. As follows from the results of deep drilling and 3D geophysical simulation, large bodies of rocks pertaining to the ultramafic alkaline complex occur at the lower level of the ore-magmatic system. Peridotite, pyroxenite, melilitolite, melteigite, and ijolite occupy more than 50 vol % of the volcanic-plutonic complex within the upper 15 km accessible to gravity exploration. The proposed model represents the ore-magmatic system as a conjugate network of mantle magmatic sources localized at different depth levels and periodically supplying the melts belonging to the two autonomous groups: (1) ultra mafic alkaline rocks with carbonatites and (2) alkali syenites–peralkaline syenites, which were formed synchronously having a common system of outlet conduits. With allowance for the available isotopic datings and new geochronological evidence, the duration of complex formation beginning from supply of the first batches of melt into calderas and up to postmagmatic events, expressed in formation of late pegmatoids, was no less than 25 Ma.

INTRODUCTION

The northeastern Baltic Shield is a classical region of continental magmatism manifested in Paleozoic alkaline and ultramafic alkaline intrusions with carbonatites. The Khibiny and Lovozero plutons, which are in the group of the world's largest alkaline intrusions, occupy the central position in the Kola province. Contemporary estimation of the ore potential of igneous complexes, as well as elaboration of prospecting guides, is based on multidisciplinary research providing insights into deep structure of intrusive bodies, systems of feeding conduits, and zones of magma generation; the lifetime of magmatic systems; and the migration and concentration of ore elements. Solving the problems arising during investigation of giant alkaline plutons is complicated by the following factors.

First, study of the morphology and deep structure of large intrusions requires a great deal of initial geophysical data and complexing of gravity measurements with seismic surveying necessary to develop high resolution 3D models. The

network of geophysical observations in the area of Khibiny and Lovozero plutons is sufficient for creating their density and seismic 3D models and estimating the basic elements of their internal structure down to a depth of 10-12 km.

Second, estimation of the lifetime of complex plutons characterized by staged evolution over a long time, in particular, dating of initial stages, is hampered by disturbance of isotopic systems under effect of late intrusive phases.

Third, to ascertain the formation mechanisms of such giant volcanic–plutonic complexes as the Khibiny and Lovozero and related mineralization, it is necessary to study all their constituents from the onset of caldera origination (filling of early ring faults with the first batches of alkaline melt) to the completing events, expressed in the formation of dikes and explosion pipes, which cut through all alkaline complexes, and late pegmatoid veins in the contact zones with the basement.

Fourth, the discovery of carbonatites [25] broadening of the area and the set of ultramafic alkaline rocks in the Khibiny [16] and Lovozero [3] and revealing rocks of miaskite series [30] have lead to a substantial revision of the model describing the formation of this large ore-magmatic cluster. Specification of knowledge on the large P, Sr, REE, Zr, and Nb deposits hosted in these plutons is an obvious consequence of the completed work.

This paper presents the results of a comprehensive study of the large Paleozoic ore-magmatic system formed in central part of the Kola region as a combination of the pivotal Khibiny and Lovozero plutons, the adjacent minor ultramafic and syenite intrusions, alkaline dikes, and diverse subalkaline and alkaline volcanic rocks. The study is based on the results of drilling and detailed geophysical surveying.

RESEARCH METHODS

To study the deep structure of the plutons, we used the technique of 3D simulation based on a joint interpretation of gravity and seismic data [7, 21]. The computation algorithms include original programs assigned to solve the inverse gravity field problem [20] based on the principles of equivalent redistribution [26] and the FIR-STOMO software package to solve the inverse seismic tomography problem [36]. To visualize the results in graph form, the GL3DShow software package [19] was used. The joint consideration of the results of seismic survey and density simulation based on more precise factual data made it possible to specify the internal structure of plutons.

A $^{40}\text{Ar}/^{39}\text{Ar}$ isotopic geochronological study was carried out at the Institute of Geology and Mineralogy, Siberian Branch, Russian Academy of Sciences, in Novosibirsk. The phlogopite and biotite grains assigned for dating were picked out under a binocular microscope from the 0.25-0.15 mm fraction of the comminuted sample. Argon was released from samples by stepped heating [34, 35]. The sample charges, together with muscovite MCA11 (K-Ar age is 313 Ma) and biotite LP6 (age is 128.1 Ma) used as monitors, were wrapped in aluminum foil and placed in

the quartz ampoule, which was sealed after air exhaust. Then the samples were irradiated in the cadmium-plated channel of the scientific VVR-K-type reactor at the Research Institute of Nuclear Physics in Tomsk. The gradient of the neutron flow did not exceed 0.5 % of sample size. Experiments on stepped heating were performed in the quartz reactor with an external heating element. The blank run to determine ^{40}Ar (10 min at 1200°C) did not exceed $5 \times 10^{-10} \text{ ncm}^3$. Argon was cleaned with Ti and Zr-Al-SAES getters. The argon isotopic composition was measured on a VG5400 Noble Gas mass spectrometer (Micromass, England). The uncertainty of measurements corresponds to a range of $\pm 1\sigma$. Preliminary degassing of samples before measurements was implemented at 300°C. Special attention was paid to control the factor of isotopic discrimination by measuring a portion of cleaned atmospheric argon. The average $^{40}\text{Ar}/^{36}\text{Ar}$ ratio during measurements was 296.5 ± 0.5 . The criteria proposed by Fleck et al. [15] and Gustafson et al. [22], were used for interpretation of age spectra.

The Rb-Sr method was also used for age determination. The charges of wholerock samples and mineral fractions 100-200 mg in mass were decomposed applying the technique described by [11]. The Rb and Sr isotopic compositions and concentrations were measured with isotopic dilution on a Finnigan MAT-261 solidphase eight-collector mass spectrometer in the static mode at the Institute of Precambrian Geology and Geochronology, Russian Academy of Sciences. The $^{87}\text{Rb}/^{86}\text{Sr}$ isotope ratios were measured with an accuracy not worse than $\pm 0.5\%$ (2σ), and element concentrations, with an accuracy of ± 0.5 - 1% (2σ). During measurements, the $^{87}\text{Sr}/^{86}\text{Sr}$ isotope ratio was 0.705037 ± 50 ($n = 4$) for BCR-1 standard and 0.7102249 ± 18 ($n = 23$) for SRM-987 standard. The level of the blank run was 0.03 ng Rb and 0.1 ng Sr. The isochron parameters were calculated with a 95 % confidence interval; uncertainty in determining the point coordinates was taken as 0.5 % and 0.005 % along the x and y axes, respectively.

GEOLOGY

The Paleozoic volcanic-plutonic complex comprises the Khibiny and Lovozero plutons, volcanic rocks, the Kurga intrusion, and swarms of dikes and explosion pipes localized within the plutons and in their frameworks (fig. 1). According to geological observations, the initial, main, and final phases of the volcanic-plutonic complex formation are distinguished.

Initial Phase of Complex Formation

The formation of the volcanic-plutonic complex began with the origination of a series of faults in the Neoproterozoic complex of tonalite, trondhjemite, and granodiorite; ascent of ultramafic and subalkaline melts along these faults; merging of the melts into the Kurga intrusion; and volcanic eruptions in the north eastern part of the future Lovozero structure.

The Kurga intrusion, situated 3 km of the northeastern contact of the

Lovozero pluton, is a multiphase intrusion composed largely of peridotite and pyroxenite (fig. 2a). Two nearly vertical nepheline syenite bodies are localized in its central and southwestern parts. The 3D density simulation shows that the intrusion is lopolith-like in morphology and traced to a depth of 4.5 km (fig. 2b).

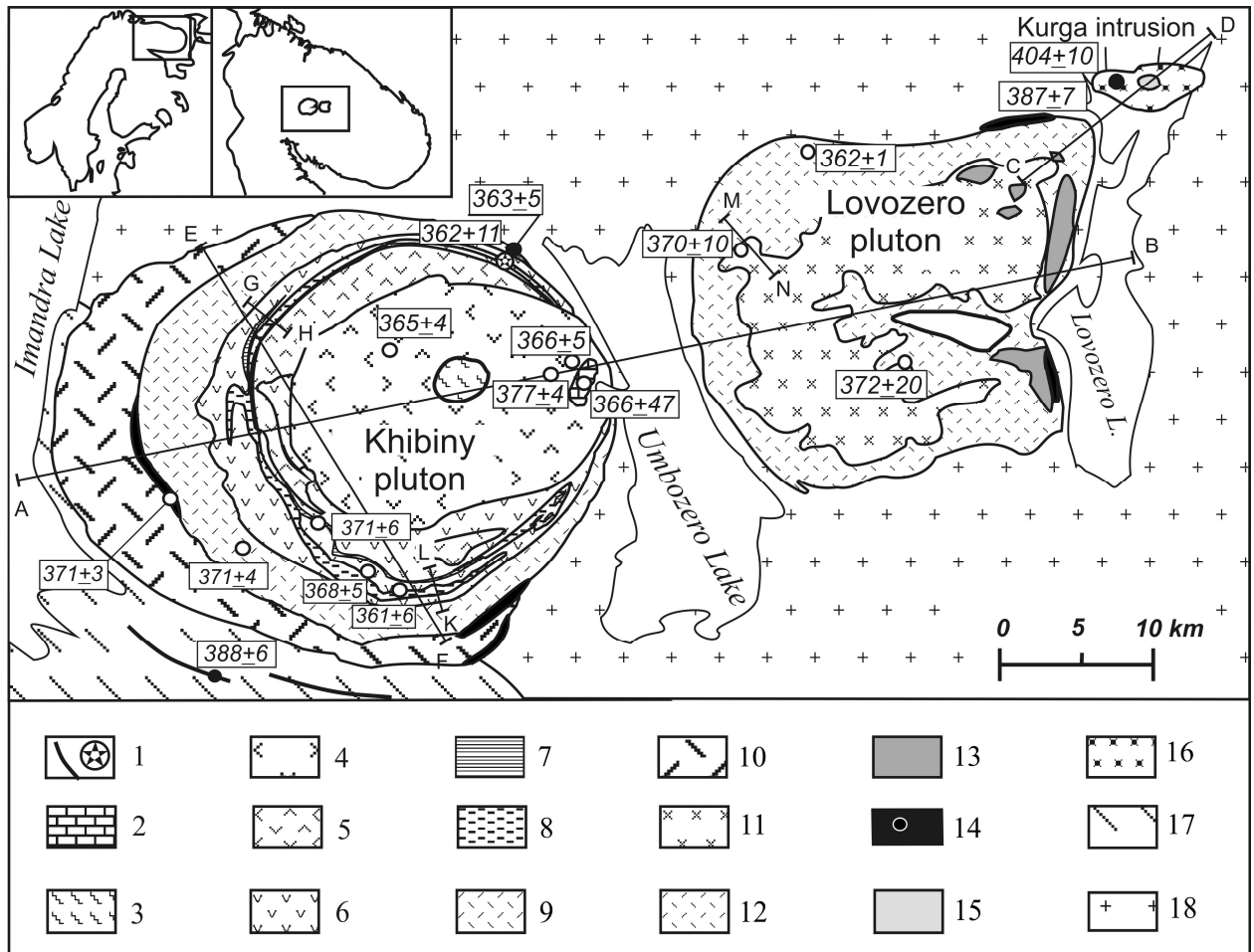


Fig. 1. Schematic geological map of Khibiny-Lovozero ore-bearing volcanic-plutonic complex. (1) Dike and explosion pipe.

1 - dikes and explosion pipe; 2 - carbonatite; 3 - pulaskite; 4 - foyaite; 5 - inequigranular foyaite; 6 - K-nepheline syenite; 7 - apatite-nepheline rock; 8 - ijolite and melteigite; 9 - trachytoid khibinite; 10 - massive khibinite; 11 - eudialyte lujavrite; 12 - differentiated lujavrite-foyaite-urtite complex; 13 - volcanic rocks of Lovozero Formation; 14 - ultramafic alkaline rocks; 15 - syenite of Kurga intrusion; 16 - peridotite of Kurga intrusion; 17 - Proterozoic basalt, porphyry, and dolerite; 18 - Archean tonalite and trondhjemite. Location of complex in Baltic Shield and Kola Peninsula is shown in inset. Age of rocks, Ma, is shown in boxes: filled circles, author's data; open circles, after Kramm et al. [32], Kramm and Kogarko [33], Zaitsev et al. [38], Bayanova [9, 10], and Wu et al. [37]. Section lines across contact zones are shown.

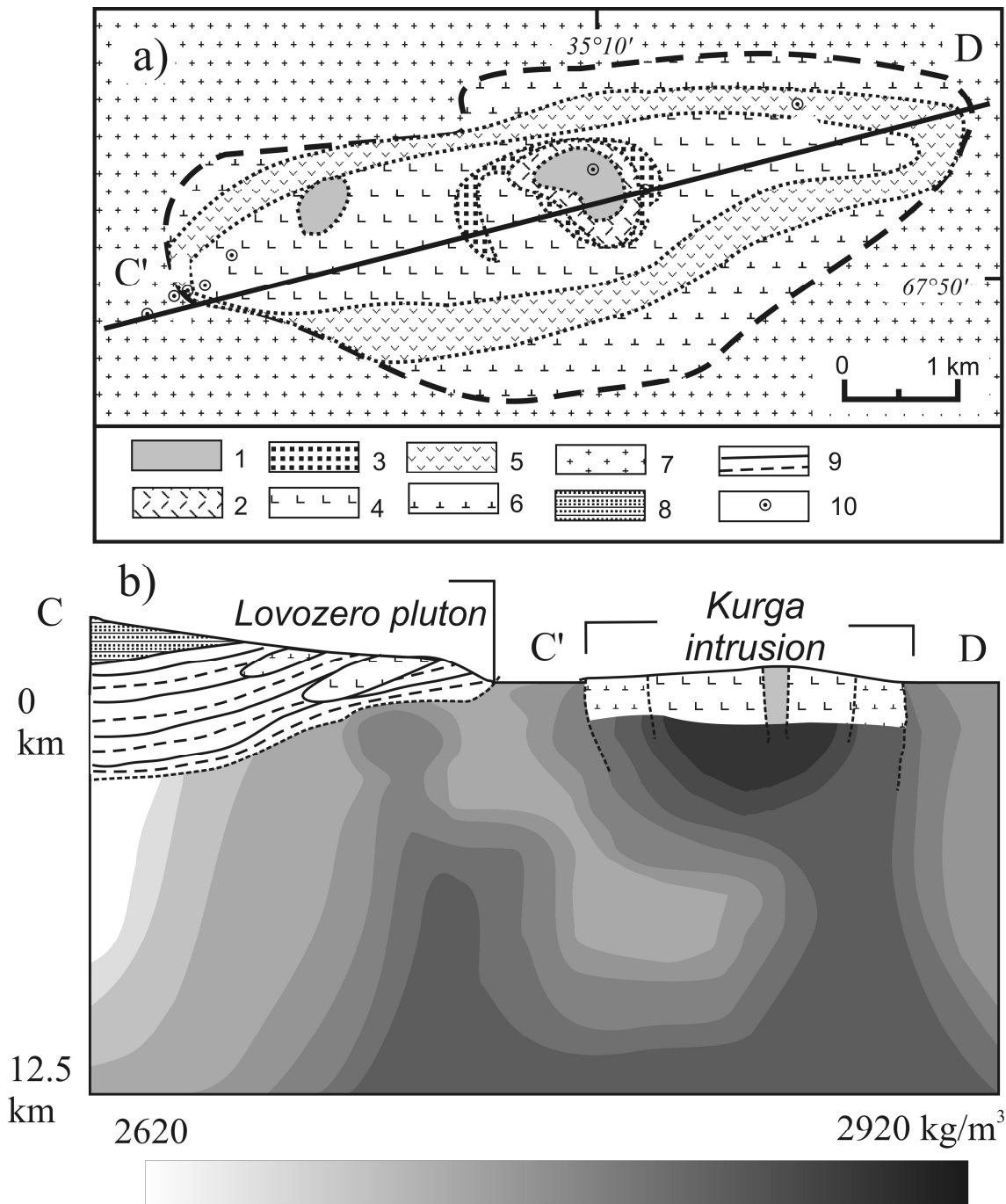


Fig. 2. (a) schematic geological map of Kurga intrusion, simplified after Kalinkin [24], and (b) density section of conjugated Lovozero and Kurga intrusions.

1 - Alkali syenite, larvikite, lardalite; 2 - amphibole-pyroxene-plagioclase rock; 3 - pyroxenite with titanomagnetite; 4 - olivinite; 5 - peridotite; 6 - olivine pyroxenite; 7 - biotite-amphibole gneiss of Precambrian basement; 8, 9 - rocks of Lovozero pluton: 8 - eudialyte lujavrite; 9 - lujavrite, foyaite, and urtite of differentiated series; 10 - borehole.

An anomaly that marks a feeding conduit is related to a large positive anomaly in the northeastern Lovozero pluton, which indicates a body of high-density rocks at a depth of 3 km in this part of the alkaline pluton. The Kurga intrusion is composed of several groups of rocks, which correspond to the

following intrusive phases from earlier to later: (1) peridotite and olivinite, (2) pyroxenite, and (3) alkali syenite (larvikite, lardalite) and nepheline syenite. A zone of metasomatic biotite–kaersutite and kaersutite-pyroxene-plagioclase rocks extends along the contact between ultramafic rocks and syenites. The U-Pb age of zircon from pyroxenite and larvikite estimated at 387 ± 7 Ma [4] indicates that the Kurga intrusion should be referred to the initial stage of Paleozoic tectono-magmatic reactivation. The Rb–Sr isochron age (two whole-rock samples of alkali pyroxenite and alkali syenite along with apatite, biotite, and amphibole fractions from these rocks) yielded 404 ± 10 Ma [4]. The geological data show that the massif was formed in parallel with comagmatic volcanic rocks pertaining to the early phase of the Kontozero caldera. Estimation of Rb–Sr isochron age of these rocks gave an unsatisfactory result because of the thermal effect of intrusive phases. The regression equation based on five points yielded 446 ± 56 Ma ($I_{Sr} = 0.70301 \pm 0.00009$; MSWD = 0.64) [5].

The volcanic rocks formed at the early stage of caldera evolution largely occur in the northeastern part of the Lovozero pluton, where large blocks of volcanic rocks up to 200 m thick are hosted in the differentiated lujavrite-foyaite-urtite complex and spatially associated with sedimentary rocks of the Lovozero Formation. The elements of zoning are revealed in the distribution of various volcanic rocks. Ankaramite remnants dominate in the extreme northeast of the pluton; alkali basanite occurs farther to the south, giving way to phonolite porphyry close to Mts. Apuaiv and Kuamdespahk. Reconstruction of this sequence is possible only for the ultramafic part of the section. The study across the strike and down the dip shows that ankaramites alternating with basanites are predominant in the large remnants of volcanic rocks. The thickness of each flow does not exceed a few meters. The basaltoids contain small xenoliths of picrites and ankaramites and were probably related to another phase of volcanic activity. In the Khibiny Mountains, subvolcanic and volcanic rocks pertaining to the early phase of caldera development occur as dikes related to ring tectonic structures in the framework at a distance of up to 5 km of the contact of the pluton, as well as numerous xenoliths of volcanic rocks in the least eroded areas in the high-mountain part of the pluton (fig. 3). The $^{40}\text{Ar}/^{39}\text{Ar}$ dating of one dike (age of plateau 388 ± 6 Ma, see fig. 4) corresponds to the minimal age of the infill of the Khibiny caldera with ultra mafic alkaline melts. The largest outcrop of volcanic rocks, up to 10 km in extent and with a maximum apparent thickness reaching 100 m, was mapped in the western part of the pluton at the contact of the massif and trachytoid nepheline syenites (khibinites) occupying the marginal zone of the intrusion. The lower part of the sequence consists of metamorphosed volcano-sedimentary rocks, and phonolite porphyry dominates in its upper part. In addition to leucocratic volcanics, [12] noted porphyritic rocks with augite phenocrysts in the Chasnachorr-Yudichvumchorr Block of the Khibiny.

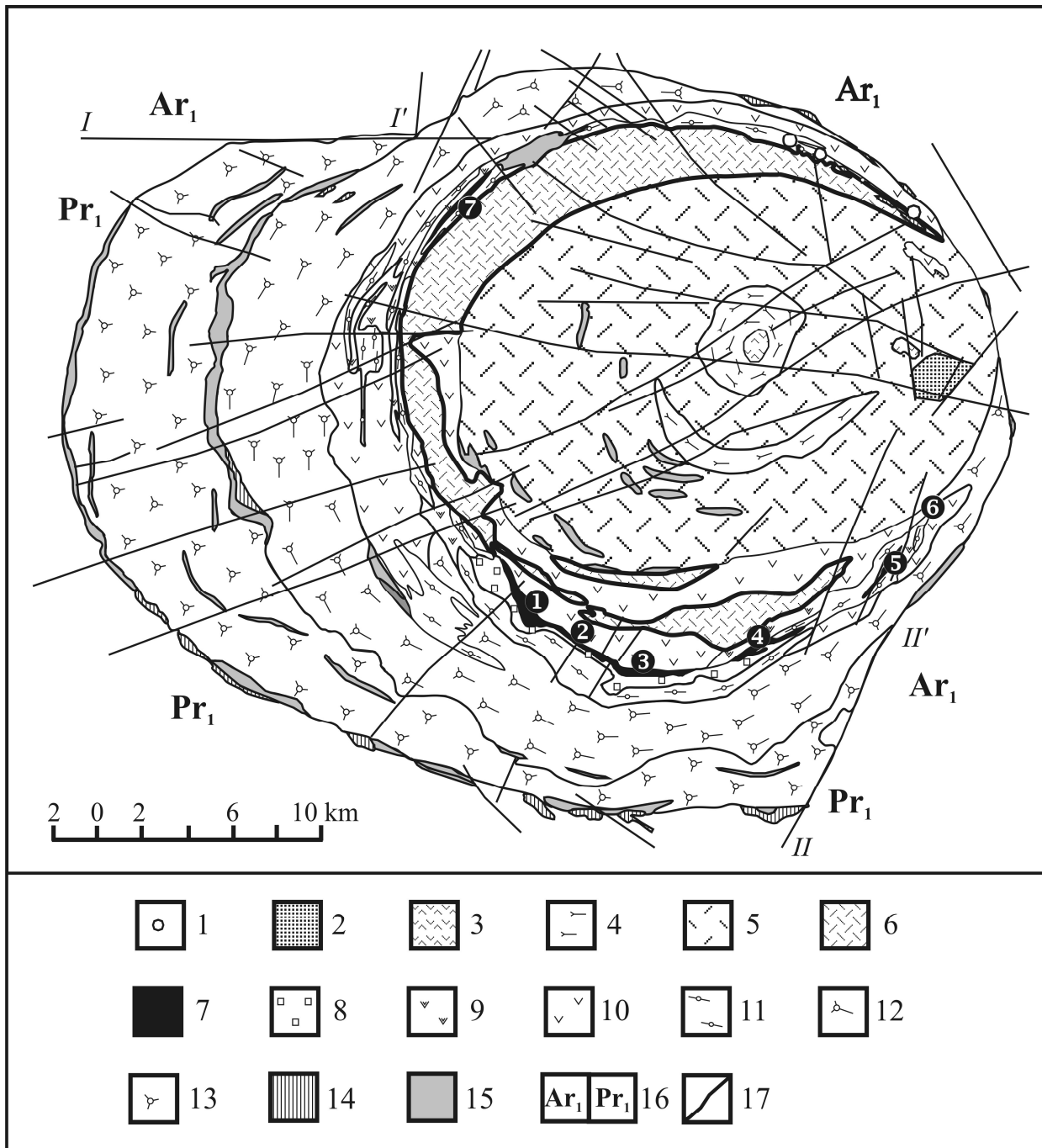


Fig. 3. Schematic geological map of Khibiny pluton, after map prepared by Murmansk Geological Exploration Expedition, Sevzapgeologiya Regional Geological Survey.

1 - explosion pipe; 2 - carbonatite; 3 - pulaskite; 4 - trachytoid foyaite; 5 - massive foyaite; 6 - inequigranular foyaite; 7 - apatite-nepheline rock; 8 - massive urtite; 9 - massive juvite; 10 - K-nepheline syenite (rischorrite); 11 - melteigite, ijolite; 12 - trachytoid nepheline syenite (khibinite); 13 - massive nepheline syenite (khibinite); 14 - peridotite, pyroxenite, melilitolite; 15 - fenite in contact zone and fenitized rocks of roof; 16 - Archean (Ar_1) and Proterozoic (Pr_1) basement rocks; 17 - fault. Deposits (numerals in circles): 1 - Kukisvumchorr; 2 - Jukspor; 3 - Rasvumchorr; 4 - Koashva; 5 - Njorkpahk; 6 - OleniiRuchei (Deer Creek); 7 - Partomchorr. $I-I'$ and $II-II'$ are faults in contact zone of massif.

Main Phase of Complex Formation

The main phase of endogenic activity was expressed in the formation of the ring fault system, subsidence of the Lovozero and Khibiny cauldron, and multistage filling of the calderas with alkaline melts. The age of the main rock associations in the plutons varies close to 365 ± 5 Ma [32, 33, 38, 9, 10, 37]. According to earlier data [16, 17, 1, 2], the calderas were filled with ultramafic alkaline and peralkaline melts derived from two sources. In the course of the investigations, it was established that the Khibiny and Lovozero plutons are separated by a screen, whose density and seismic wave velocity correspond to country granite gneiss. The results of magnetic surveying also indicate that rocks with petrophysical characteristics inherent to nepheline syenite are absent in the zone of conjugation. Thus, the Khibiny and Lovozero plutons have autonomous internal structures down to a depth of 12.5 km and have no common feeding conduit. The geological structure of each group of rocks occurring in the Khibiny and Lovozero plutons has been described in detail in many publications, so we dwell only on newly obtained data.

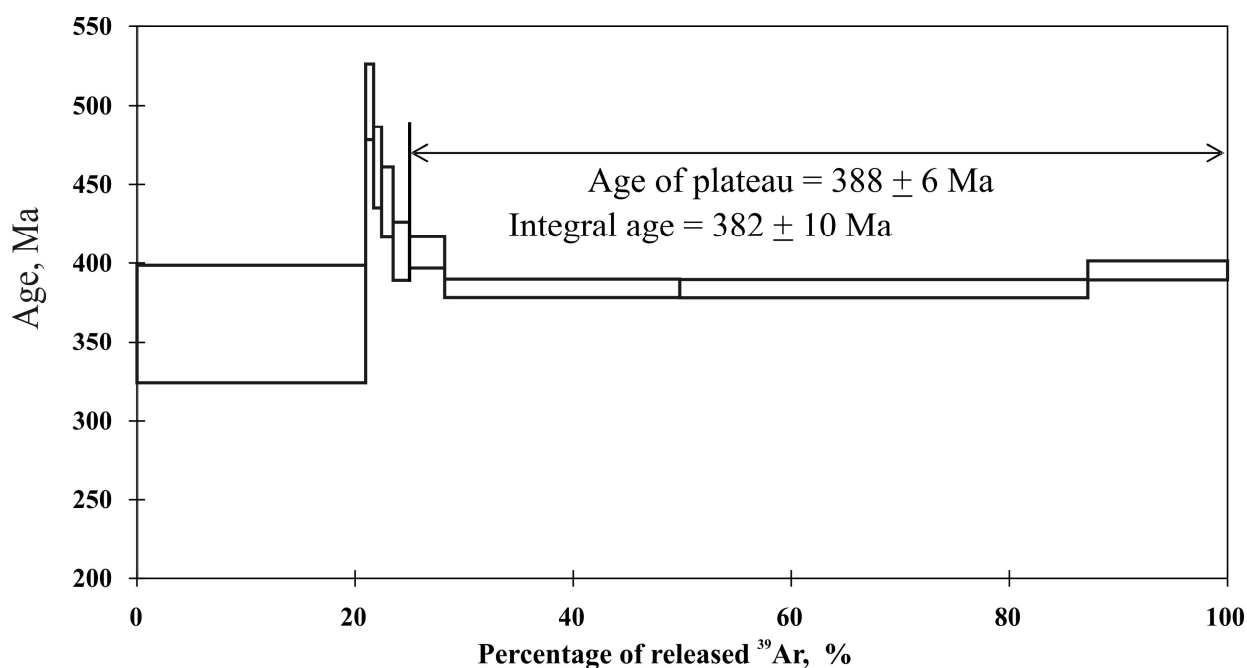


Fig. 4. Results of $^{40}\text{Ar}/^{39}\text{Ar}$ study of amphibole fraction from dike 991 in southern framework of Khibiny massif using steppedheating.

Khibiny pluton. The conic and ring structure of the pluton is retained to a depth of 12.5 km. The western contact dips inward at angles of $30\text{-}40^\circ$ down to 5 km and becomes steeper ($50\text{-}60^\circ$) at a depth of 5-10 km (fig. 5). The eastern contact close to the carbonatite stock dips steeply toward the center and is traced to a depth of 13 km. In the southwest, the contact of the pluton with Proterozoic volcanic rocks is nearly vertical and flattens at a depth of about 4 km. The Proterozoic volcanic rocks of the Imandra-Varzuga Zone are expressed as

anomalies of elevated density (up to 3250 kg/m³) and velocity (up to 7.0-7.4 km/s), which are traced to a depth of 12-13 km. In the southern frame work of the Khibiny pluton, Proterozoic rocks are also marked by a high-density anomaly, which plunges beneath plutonic rocks. In the depth interval of 5-11 km, the contacts flatten and the pluton diminishes in size, forming a feeding conduit a few kilometers in diameter at a depth of >12 km. Its center shifts to the east toward the Lovozero pluton relative to its position at the surface.

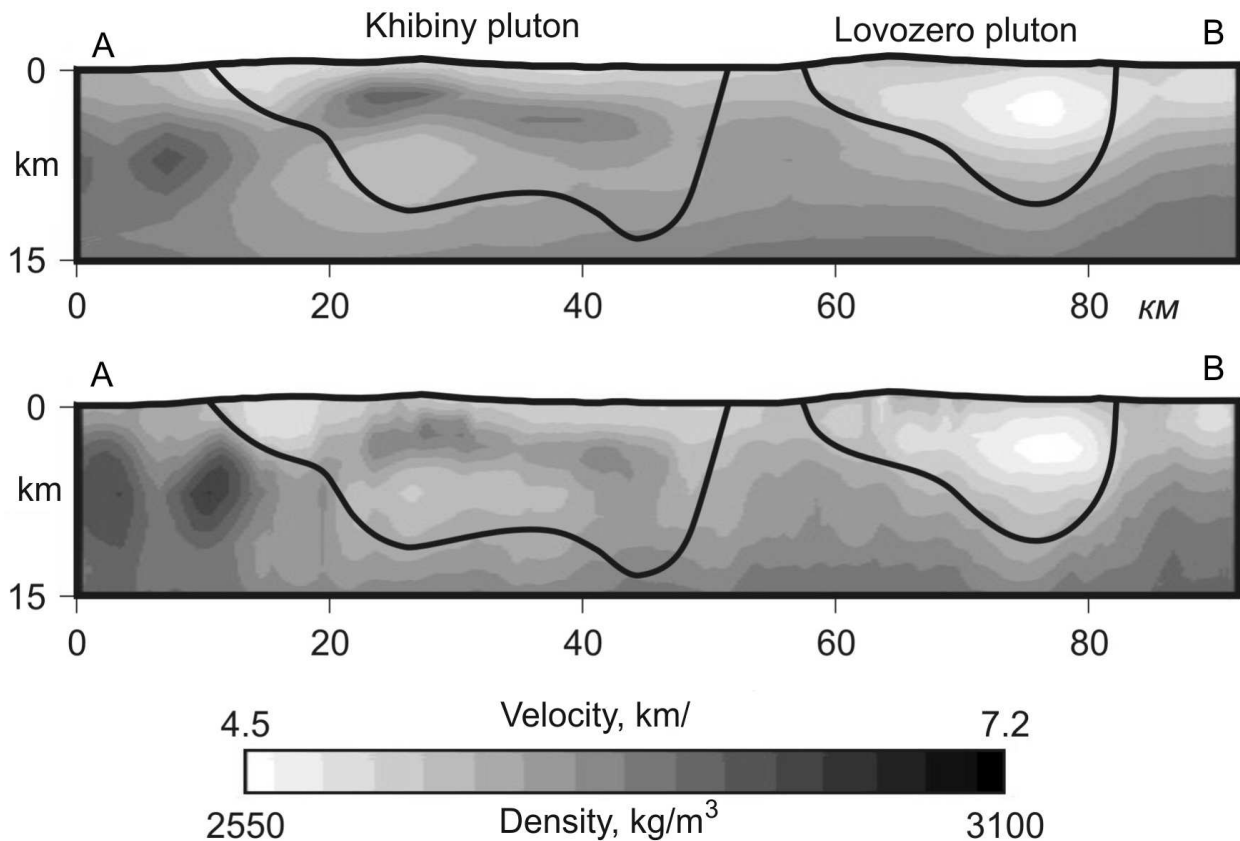


Fig. 5. (a) velocity and (b) density sections of 3D complex model of the Khibiny-Lovozero volcanic-plutonic complex.

See fig. 1 for section line.

The geological survey accompanied by drilling allowed us to reveal new groups of rocks and substantially specify geological relationships between rock series. According to up to date evidence, the pluton consists of the following rocks (from older to younger): (1) ultramafic alkaline rocks; (2) peralkaline nepheline syenite in marginal part of the pluton (khibinite); (3) K-nepheline syenite; (4) differentiated ijolite-melteigite series; (5) juvite, urtite, and related apatite-nepheline ore; (6) peralkaline nepheline syenite of central part of the pluton (foyaite); (7) pulaskite; and (8) carbonatite.

The density simulation shows that maximum thickness of ultramafic alkaline series is attained in the northern part, where a large ring body of high-density rocks

occurs at a depth of >3 km beneath nepheline syenite (fig. 6). The zones of xenoliths composed of peridotite, pyroxenite, melilitolite, and ultramafic foidolites penetrated by boreholes are direct evidence for the occurrence of ultramafic alkaline rocks with depth. In the western sector of the pluton, a zone of numerous xenoliths of ultramafic intrusive and volcanic rocks extends for 15 km along the contact between the massif and trachytoid nepheline syenites (khibinites) (fig. 3). No significant geophysical anomalies were revealed in this tract, indicating that bodies of the aforementioned rocks most likely are rootless remnants of the roof. Small outcrops of ultramafic alkaline rocks are also known at the southeastern and north western contacts of the pluton.

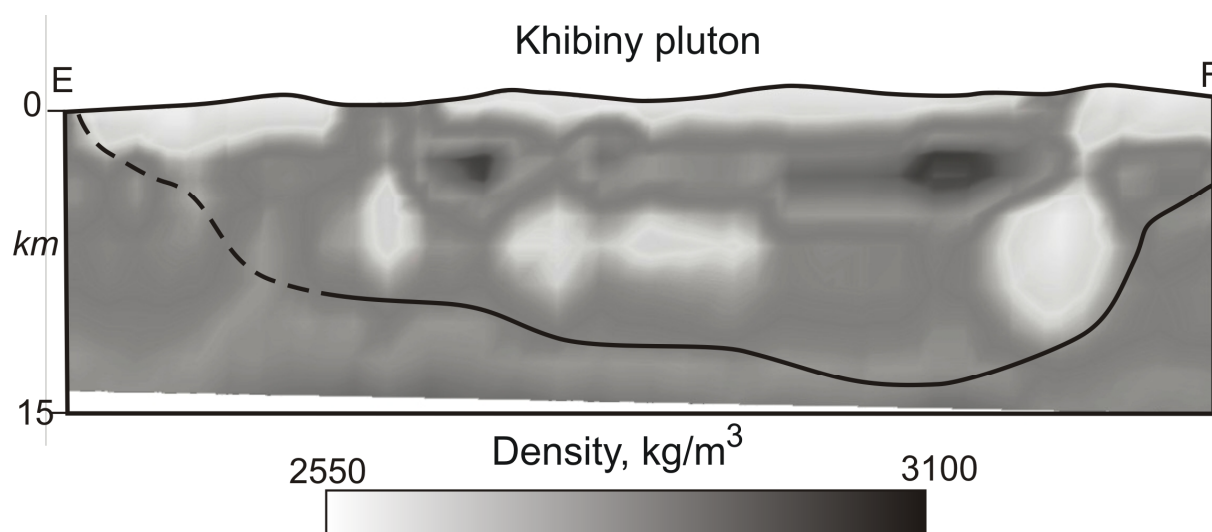


Fig. 6. Density section of 3D complex model of Khibiny pluton.

See fig. 1 for section line.

The rocks of the ijolite-melteigite series in their presentday position form a body ring in plan view, which separates nepheline syenites of the marginal and central parts of the pluton. The ijolite-melteigite intrusion is characterized by the internal structure and texture, which are inherent to the layered igneous complexes. The correlation of sections of the layered series shows that key layers gently dip at angles of 15-30° inward the pluton. The absence of positive gravity anomalies below 3.5 km in the southwestern part suggests that the ijolite-melteigite series is cut off by per alkaline nepheline syenite in central part of the pluton at a depth of 1-2 km in compliance with drilling results (figs. 7, 8).

According to the complex 3D simulation, the rocks of elevated density and velocity corresponding to the foidolite series occur immediately beneath peralkaline nepheline syenite at a depth of 3-5 km in the central part of the pluton (fig. 6). In this connection, the numerous ijolite and melteigite xenoliths found in the central part of the pluton indicate that foidolite series occurs beneath foyaite.

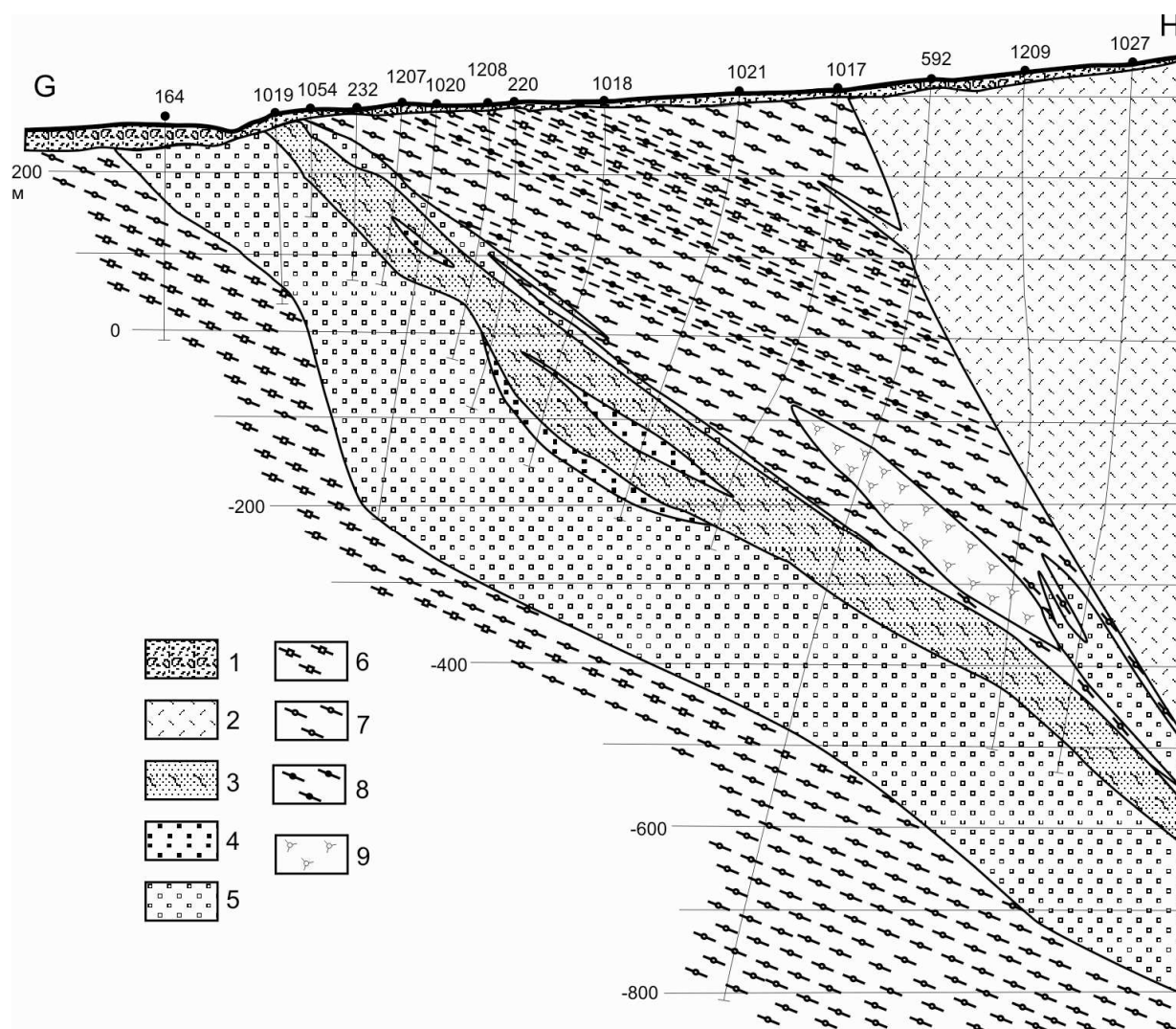


Fig. 7. Geological section along line G-H across central part of Partomchorr deposit.

1 - Quaternary sediments; 2 - inequigranular foyaite; 3 - apatite-nepheline rock; 4 - massive urtite; 5 - massive feldspathic urtite; 6 - trachtyoid feldspathic ijolite; 7 - ijolite; 8 - melteigite; 9 - nepheline syenite (khibinite). See fig. 1 for section line.

K-nepheline syenite (rischorrite), juvite, and urtite, which combined into the common on the basis of petrological and geochemical evidence [8], and related apatite–nepheline ore occupy a crosscutting position relative to both the per alkaline nepheline syenite of marginal part of pluton and the layered ijolite-melteigite series. These rocks make up a consecutive series with a gradual increase in K-feldspar content from urtite to juvite and further to K-nepheline syenite (rischorrite). The lodes of apatite-nepheline ore are related to massive urtite as a feldspar-free member of this series.

The relationships of rocks unambiguously show that ijolite-melteigite series is older than massive urtite, apatite-nepheline ore, and juvite-rischorrite. This is confirmed by zones of brecciation, where fragments of trachtyoid ijolite are cemented by massive juvite. At several deposits, the rhythms of layered urtite-ijolite-melteigite series are cut off by the upper contact of ore zones and trachtyoid

rocks abut the low-angle contact with overlying juvite-rischorrite series. Xenoliths and large remnants of ijolite and melteigite are incorporated into massive juvite-rischorrite in the northwestern sector of the arc. A more complex pattern is observed at the southeastern closure of the ijolite-urtite arc. It can be suggested that the formation of the ore lode at this site predated the emplacement of the foidolite intrusion. The main ore-controlling fault responsible for localization of ore lodges at the lower level of the Njorkpahk and Olenii Ruchei (Deer Creek) deposits and the major deposits in the Khibiny was formed after consolidation of this intrusion. The geological features and relationship between the textural patterns of ore at the Njorkpahk site are also indirect evidence for their formation conditions in contrast to other deposits.

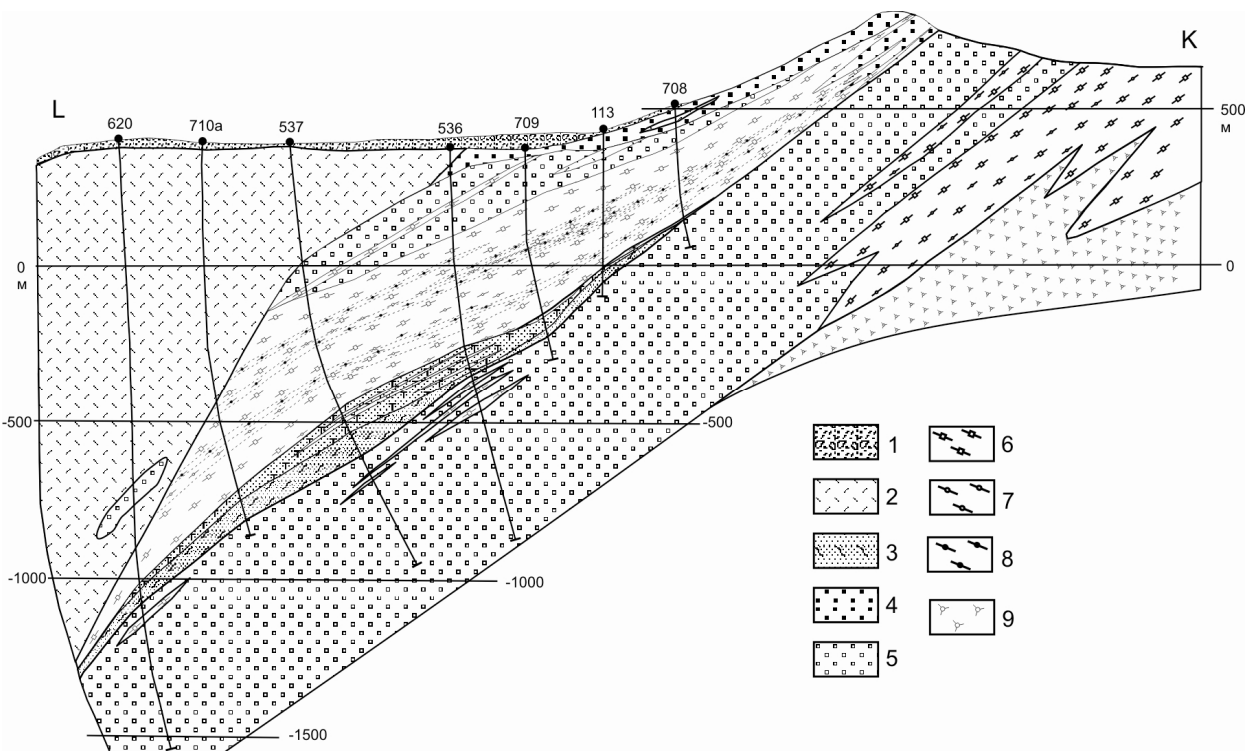


Fig. 8. Geological section along line K-L across central part of Upper Rasvumchorr-Eveslogchorr deposit.

1 - quaternary sediments; 2 - inequigranular foyaite; 3 - apatite-nepheline rock; 4 - massive urtite; 5 - massive feldspathic urtite; 6 - trachtyoid feldspathic ijolite; 7 - ijolite; 8 - melteigite; 9 - nepheline syenite (khibinite). See section line in fig.1 and fig. 6 for legend.

The results of drilling in the poorly exposed central part of the pluton allowed us to establish that large negative density anomalies in the field of foyaite are caused by carbonatite (eastern anomaly) [25] and pulaskite (anomaly at the center of complex) [30]. In addition, nepheline syenite in the central part of the pluton contains numerous large remnants of fenitized roof and xenoliths of foidolites similar in composition to the rocks of differentiated ijolite-melteigite series.

Lovozero pluton (fig. 9). The complex 3D simulation shows (fig. 5) that down

to a depth of 10 km, the pluton looks like an asymmetric lopolith, the feeding conduit of which is projected onto the southeastern part of its presentday erosion level. In contrast to the nearly vertical southern contact, in the western and northwestern parts of the caldera, the contacts dip at angles of 60-70° down to a depth of 3 km with a tendency toward flattening. The eastern and northern contacts are traced vaguely because of many xenoliths composed of alkaline volcanic rocks.

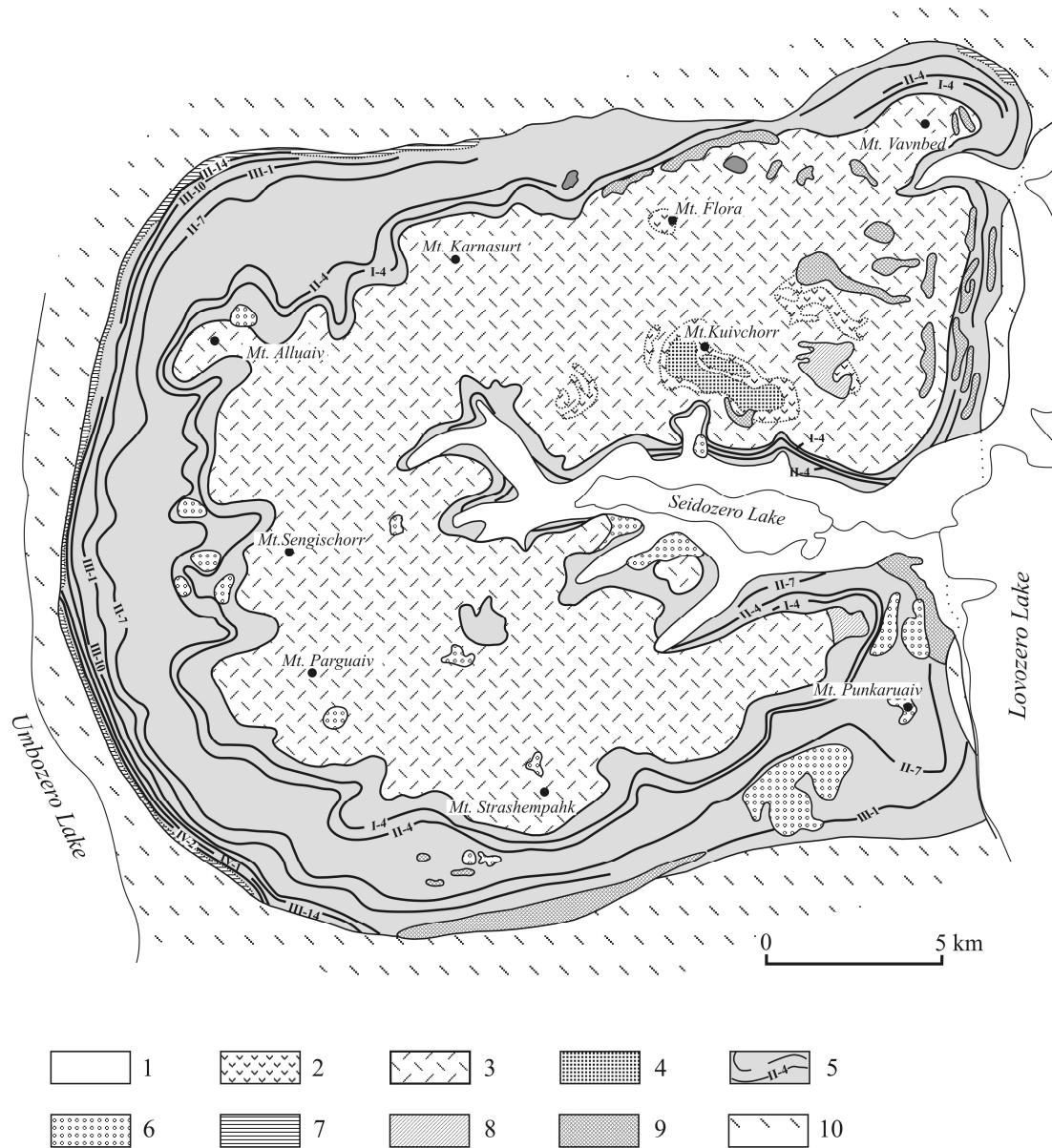


Fig. 9. Schematic geological map of the Lovozero pluton.

Compiled after data published by Gerasimovsky et al. [18], Bussen and Sakharov [13]. 1 - quaternary sediments; 2 - foyaite-lujavrite; 3 - eudialyte lujavrite, lovozerite–murmanite lujavrite; 4 - ijolite with apatite and titanite; 5 - differentiated lujavrite-foyaite-urtite series; 6 - poikilitic nepheline-sodalite syenite; 7 - pegmatoid foyaite, lujavrite, and alkali syenite of contact zone; 8 - phonolite porphyry; 9 - alkali picrite, limburgite; 10 - rocks of Precambrian basement. Roman numerals denote numbers of key layers in differentiated complex.

The petrophysical parameters of peralkaline syenites making up several

intrusive series are rather uniform and do not allow reliable reconstruction of the internal structure of the pluton. Nevertheless, it was established that at a depth of more than 2 km, the pluton consists of two zones sharply distinct in density (fig. 10). Taking into account observations at the surface and drilling results, it is accepted that the intrusive body, except for its southeastern part, is composed of the differentiated lujavrite-foyaite-urtite series down to a depth of 8 km. In the central part of the pluton, near Seidjavr Lake, a local negative gravity anomaly corresponds to a body of alkali and analcime syenites with a density of 2580-2630 kg/m³. In the northeast, the pluton has a two-stage structure (fig. 2). The upper zone is traced to a depth of 1-2 km and, like in the southwestern part, is composed of eudialyte lujavrite and differentiated lujavrite-foyaite-urtite series (fig. 11).

The density of underlying rocks exceeds 2800 kg/m³. Thus, in accordance with the data published by Gerasimovsky et al. [18], Bussen and Sakharov [13], Kogarko et al. [27], and Arzamastsev et al. [3], the Lovozero pluton consists of the following rock groups.

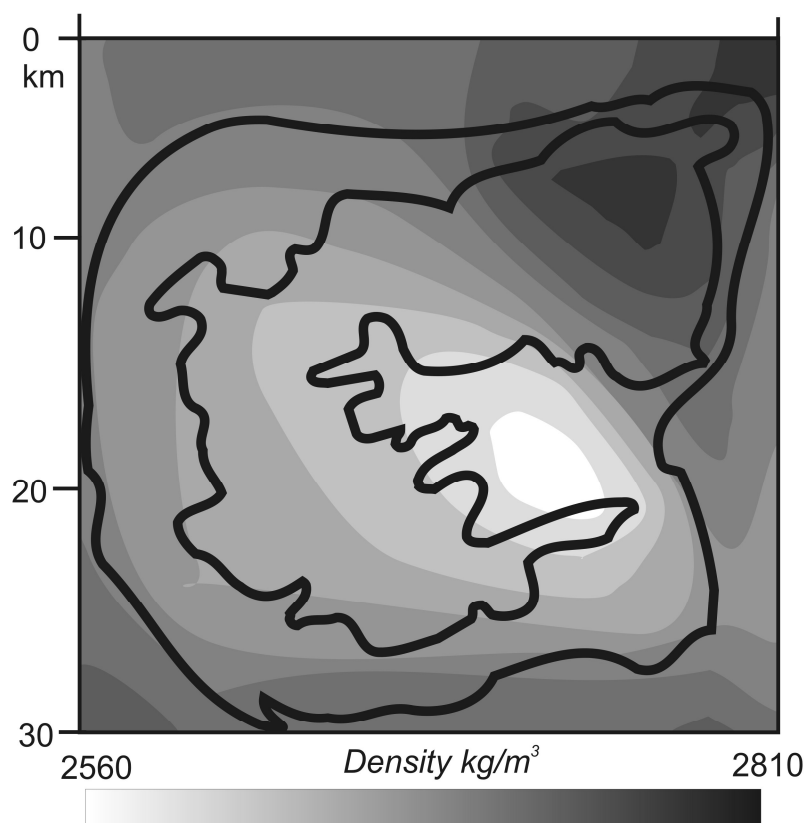


Fig. 10. Density distribution in area close to Lovozero pluton at depth of 5 km.

Contour lines indicate location of main rock groups at surface.

(1) Remnants of alkaline volcanic and sedimentary rocks of the roof, which are abundant in the northeastern and eastern parts of the calderas.

(2) Ultramafic alkaline rocks that occur in the northeastern part of pluton as a relatively large intrusive body at a depth below 2 km beneath differentiated lujavrite-foyaite-urtite complex. Xenoliths of melteigite, pyroxenite, and

melilitolite revealed in bore holes suggest that an ultramafic alkaline intrusion exists deep down as in other intrusions of the province. It should be noted that the northeastern zone of high density rocks reveals links to the Kurga intrusion of ultramafic subalkaline rocks at a depth of 7-8 km (fig. 2).

(3) Poikilitic nepheline-sodalite syenite retained only as remnants and xenoliths (?) in rocks of the lujavrite-foyaite-urtite series.

(4) Loparite-bearing differentiated lujavrite-foyaite-urtite series fills the main volume of caldera and attains maximum thickness in the southwestern part of the pluton, where it is traced to a depth of no less than 8 km.

(5) Eudialyte lujavrite forms, according to drilling results, a sheet-like body up to a few hundred meters in thickness, which is conformable with underlying lujavrite, foyaite, and urtite (fig. 11).

(6) Alkali syenite with density of 2580-2630 kg/m³ occurs as a low-density stock up to 5 km in diameter in central part of the pluton.

The borehole near Seidjavr Lake penetrated zircon-bearing alkali syenite similar to pulaskite in the central part of the Khibiny pluton at a depth of 700 m.

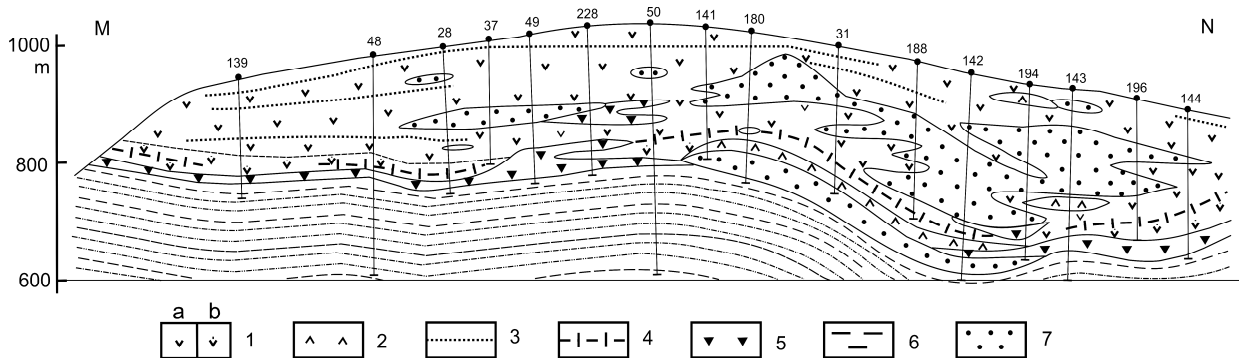


Fig. 11. Geological sections along line M–N across northwestern part of Lovozero pluton.

1 - eudialyte lujavrite: a - coarse grained and b - inequigranular; 2 - eudialyte foyaite; 3 - eudialyte; 4 - loparite juvite; 5 - eudialyte lujavrite porphyry; 6 - lujavrite and foyaite of differentiated series; 7 - poikilitic sodalite and nosean syenites. See fig. 1 for section line.

Final Phase of Complex Formation

The latest igneous rocks in the calderas comprise carbonatite, alkali picrite, melanephelinite, phonolite, and alkaline gabbroic dike swarms, as well as alkali picrite and picrite-carbonatite explosion pipes. Large swarms are located near the southeastern group of the Khibiny apatite deposits (Njorkpahk deposit) and in country gneisses in the zone of the northern junction of the Khibiny and Lovozero plutons. A separate ring and radiate melanephelinite dikes mark faults in the southwestern Khibiny pluton and are traced at a distance of up to 5 km from its southwestern contact. To estimate the age of final magmatic activity, the explosion pipes and splaying melanephelinite dikes cutting through the juvite and K-nepheline syenite were chosen. The ⁴⁰Ar/³⁹Ar age of phlogopite from the sample of olivine melanephelinite was estimated at 363±5 Ma (fig. 12). This date was

confirmed by the Rb-Sr isochron age (362 ± 11 Ma) (table). Taking into account the crosscutting relationship of the explosion pipe with respect to the main rock groups of the Khibiny pluton, the above age may be interpreted as the time of completion of magmatic activity in the Khibiny and Lovozero plutons.

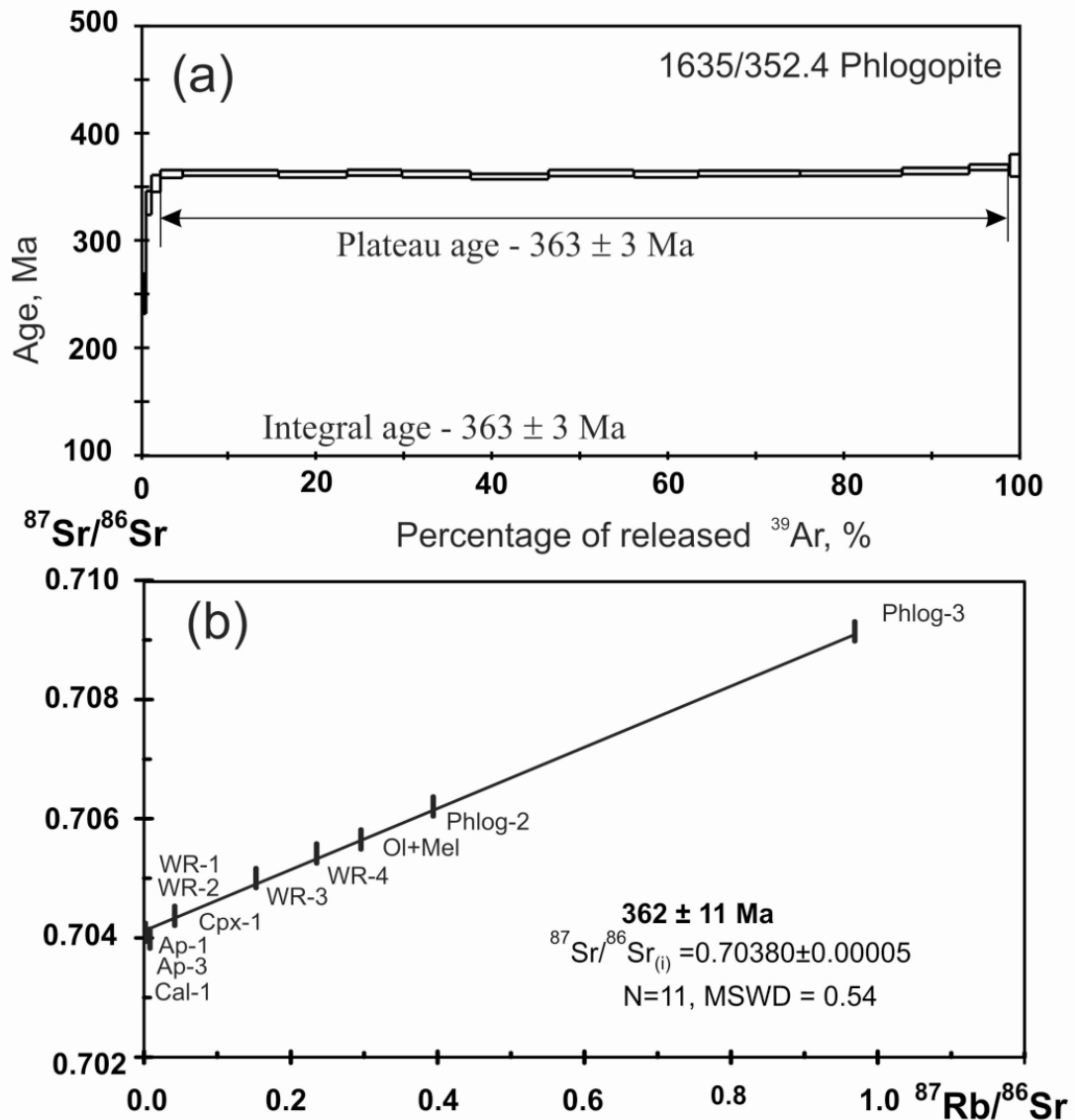


Fig. 12. Data of isotope studies of rocks from explosion pipes at Mount Namuaiv.

(a) - results of $^{40}\text{Ar}/^{39}\text{Ar}$ study of phlogopite fraction with stepped heating; (b) - Rb-Sr isochron. WR, wholerock sample; Phlog., phlogopite; Ap., apatite; Ol, olivine; Mel, melilite; Cpx, clinopyroxene; Cal, calcite.

Late and postmagmatic rocks include diverse alkaline pegmatites and veins with unique rare-metal mineralization, which, as a rule, are facies pegmatoid varieties of the main rock groups. The late igneous rocks are controlled by young faults [14].

Table

Rb-Sr isotopic characteristics of rocks from Namuaiv explosion pipe, Khibiny-Lovozero volcanic-plutonic complex

Sample	Material	Rb, ppm	Sr, ppm	$^{87}\text{Rb}/^{86}\text{Sr}$	$^{87}\text{Sr}/^{86}\text{Sr} \pm 2\sigma$	$^{87}\text{Sr}/^{86}\text{Sr}(t)$
16351	WR1	0.7	2185	0.00092	0.703847 \pm 12	0.703842
16351	Cpx1	4.6	332	0.03962	0.704010 \pm 21	0.703806
16351	Ol+Mel	4.3	42.8	0.29329	0.705335 \pm 15	0.703823
16351	Calc1	0.8	5135	0.00043	0.703742 \pm 18	0.703740
16351	Ap1	0.7	3965	0.00047	0.703862 \pm 13	0.703860
16352	WR2	0.6	3557	0.00044	0.703801 \pm 18	0.703799
16352	Phlog2	333	2478	0.38872	0.705803 \pm 16	0.703800
1635/352.4	WR3	137	2669	0.14837	0.704588 \pm 19	0.703823
1635/352.4	Phlog3	263	783	0.96981	0.708820 \pm 14	0.703822
1635/352.4	Ap3	2.2	10448	0.00060	0.703835 \pm 15	0.703832
1635/197.8	WR4	132	1602	0.23891	0.704918 \pm 11	0.703687

Samples: 1635/352.4, carbonate-free olivine melanephelinite (phase I); samples 16351, 16352, 16352, 1635/197.8, carbonate-bearing alkali picrite (phase II). WR, whole-rock sample; Cpx, clinopyroxene; Ol, olivine; Mel, melilite; Calc, calcite; Ap, apatite; Phlog, phlogopite; Bt, biotite.

DISCUSSION

Ultramafic Alkaline Rocks

The high-velocity and high-density sheet-like anomaly up to 3 km in thickness, which occupies the central part of the Khibiny pluton at a depth of more than 4 km, confirms the statement that only a small marginal part of the differentiated ijolite-melteigite series, which once filled the entire caldera, has been retained now in the section. During subsequent sinking, the central part of the differentiated series was broken up and displaced downward 2.5-3.0 km along the ring fault. The following batch of peralkaline melts has filled the central part of the caldera and overlain the disturbed sheet-like body of differentiated foidolite series. Thus, a differentiated series is recognized in the Khibiny pluton, but in contrast to the Lovozero pluton, where the peralkaline lujavrite-foyaite-urtite series was formed, a layered series of ultramafic foidolites was formed in the Khibiny pluton. This interpretation allows us to explain the extremely persistent section of the Khibiny ijolite-melteigite series, which hardly could have been formed within an inclined narrow conic chamber, where these rocks are currently localized.

The data obtained compel us to reestimate the proportions of volumes occupied by peralkaline and ultra mafic alkaline series. The estimation performed on the basis of geophysical data shows that the main volume of peralkaline syenites in the Khibiny pluton falls on the marginal zone of the pluton, where these rocks (khibinites) form a conic body no more than 2-3 km thick and occupy less

than 25 % of the total volume. The contribution of peralkaline syenites that occur in central part of the Khibiny pluton above the sheet-like jolite-melteigite body also does not exceed 15-20 %. In the Lovozero pluton, ultramafic alkaline rocks occur largely in its northeastern part and in the Kurga intrusion adjoining this pluton. Their share is more than 30 % of the total pluton volume within the 12 km depth interval accessible to reliable gravity 3D simulation. In general, it is supposed that ultramafic alkaline rocks occupy more than 50 % of the total volume in the Khibiny-Lovozero volcanic-plutonic complex.

Thus, the model proposed for the Paleozoic magmatic system in the central Kola Peninsula assumes the existence of two autonomous groups of (1) ultra mafic alkaline rocks with carbonatites and (2) alkali and peralkaline syenites in the Khibiny and Lovozero plutons. The available data on Sr and Nd isotopes indicate different mantle sources for the Khibiny nepheline syenites and ultramafic alkaline rocks with carbonatites [33, 38]. The latter are enriched in radiogenic Sr, and their data points are shifted toward positive ϵ_{Sr} relative to the mixing line established for the Kola carbonatite complexes [32]. Information on the composition of the isotope reservoir corresponding to the mantle source of ultramafic alkaline rocks in the Khibiny and Lovozero plutons, ultrabasic foidolites, carbonatites, and alkali picrites–olivine melanephelinite dike is based on data concerning mantle xenoliths found in olivine nephelinite pipes cutting through older rocks of the pluton [6]. The formation of major volumes of alkali and peralkaline syenites, as well as alkali trachyte and phonolite dikes, is related to the activity of the second source. Proceeding from the concept of an autonomous source of nepheline syenites, the origin of phonolitic melt may be assumed to be a product of dynamic crystallization of nepheline benmoreite [33] or basanite [23] magma under mantle conditions. In this connection, we call attention to significant volumes of miaskite syenites revealed in the plutons under consideration. Pulaskite, which occurs among these rocks, is in fact a plutonic counterpart of nepheline benmoreite. The participation of basaltic magma as a parental melt for nepheline syenite in the Khibiny and Lovozero melts is hardly possible, taking into account the absence of geochemical evidence for plagioclase fractionation [28, 29].

The autonomous evolution of the mantle sources synchronously functioning during the formation of heterogeneous Khibiny and Lovozero intrusive complexes implies that different levels of the upper mantle were reactivated in the Paleozoic. If it is assumed that, in terms of the concept of plume-lithosphere interaction, the zones of magma generation are regarded as a conjugated system of magma sources located at different depth levels and supplying various melts from these levels. If this concept is applicable to the Paleozoic magmatism of the Baltic Shield, then we can suggest that the ultramafic alkaline and phonolitic rock associations of the Khibiny and Lovozero plutons were formed during synchronous evolution of distinct magma sources having a common system of outlet channels.

Difference in Internal Structure of the Khibiny and Lovozero Plutons

Despite the spatial conjugation of the plutons separated only by a narrow screen of Precambrian basement rocks and the close composition of rocks, the Khibiny pluton is an assembly of ring and conic intrusions, whereas the Lovozero pluton consists of strati form sheet-like intrusive bodies. The difference in the internal structure of these alkaline plutons and related orebodies is caused by the following factors.

Formation of the Paleozoic magmatic system in the center of the Kola region began with subsidence of the Lovozero caldera superposed on the Archean basement of the Kola-Norwegian Terrane, relatively homogeneous in tectonic structure and density of rocks. The initial fill of the caldera with ultramafic alkaline melts was limited by the northeastern part of the Lovozero caldera and formation of the Kurga intrusion related to a hypabyssal compact body localized at a depth of 0.5-2.0 km beneath the rocks of differentiated series in the northeast of the pluton. The supply of alkaline ultramafic melt did not disturb the lopolith-like structure of the Lovozero caldera. The peralkaline magma was emplaced in a chamber approaching an ideal lopolith in shape, and this predetermined the formation of the marginal and major differentiated magmatic series of the Lovozero pluton, i.e., the loparite-bearing lujavrite–foyaite–urtite complex as classic layered intrusions.

On the contrary, the Khibiny caldera is localized at the boundary between the Archean and Paleoproterozoic basement complexes (fig. 1). As follows from geophysical data, the magmatic reservoir of the peripheral part of the pluton, where peralkaline melt has intruded, is considered a lenticular cavity, the depth of which abruptly changes in the lateral direction, forming a number of segments. At the present day erosion surface, this is indicated by large faults, along which the bottom of the caldera is displaced with complication of its morphology. Such faults are traced in the recent structure of the pluton along the Gol'tsovoe Lake–Imandra railway station line at the northern contact (fig. 3, line *II'*) and along line *III'* at the southeastern contact. The nepheline syenite complexes of the marginal zone, which reveal only slightly expressed rough layering [16], were formed as a result of filling of a relatively narrow segmented zone with peralkaline melt. The emplacement of a significant mass of ultramafic alkaline rocks further complicated the shape of the magma chamber, which afterward was repeatedly filled with peralkaline syenites. The multiple pulsatory supply of melt from an ultrabasic source into the caldera was an important factor that hampered formation of distinctly delineated layering of peralkaline syenites. This process was accompanied by substantial tectonic dislocations. At the same time, the foidolite melts were supplied under conditions favorable for the development of layering. Correlation of the ijolite-melteigite sections confirmed the persistence of every key layer (mica melteigite, urtite, etc.) at all sites in the central productive zone of the pluton [8]. Thus, it can be supposed that the formation of the magmatic reservoir in the homogeneous stable block of the Precambrian basement facilitated the development of intra-chamber differentiation observed in peralkaline syenites in

the Lovozero pluton. In the Khibiny pluton, the development of this process was hampered by unstable conditions within relatively narrow conical chambers. At the

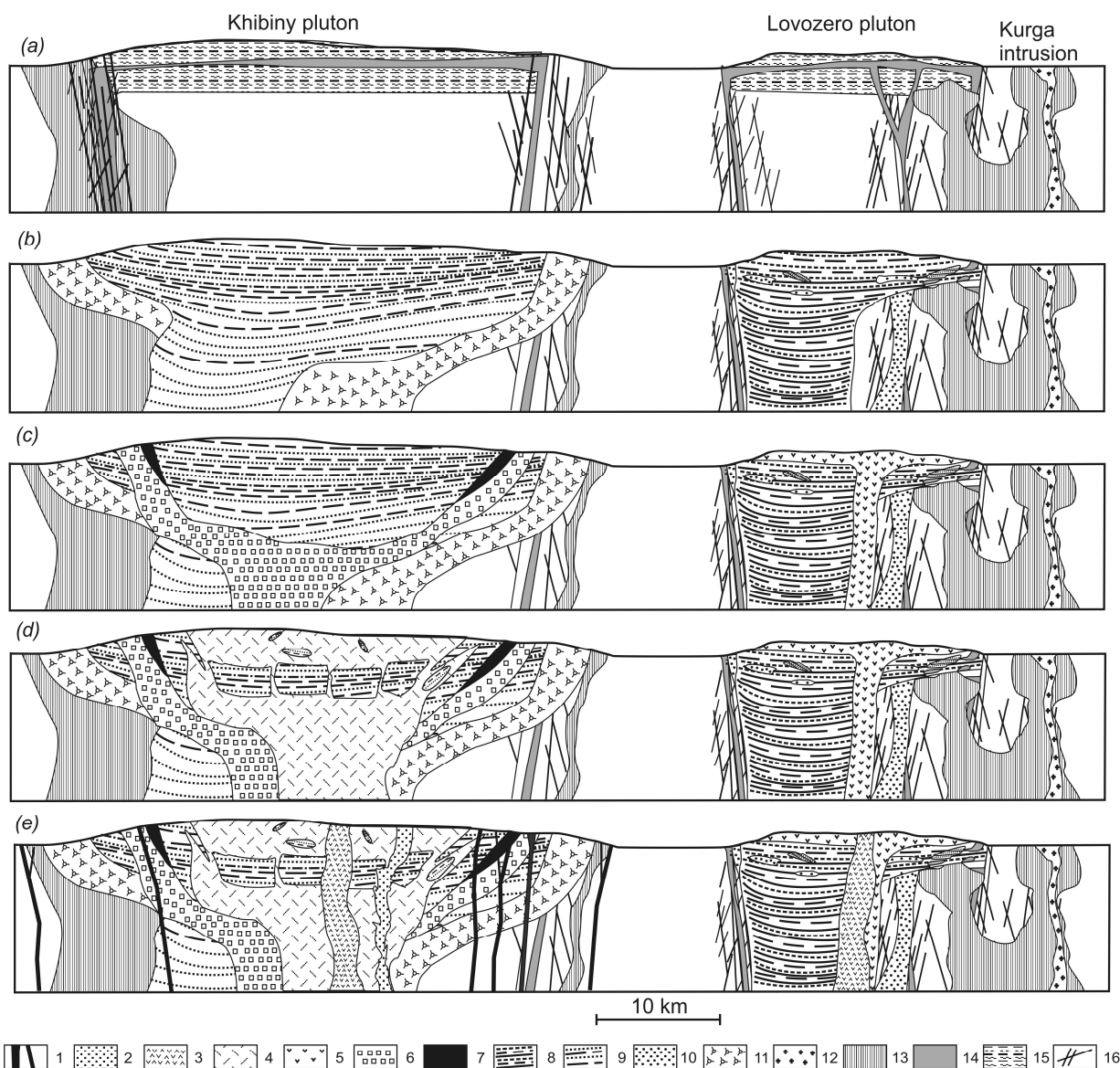


Fig. 13. Hypothetical model of formation of Khibiny-Lovozero volcanic-plutonic complexes.

1 - olivine melanephelinite dikes and explosion pipes; 2 - carbonatite; 3 - pulaskite, alkali syenite; 4 - nepheline syenite (foyaite) in central part of Khibiny pluton; 5 - eudialyte lujavrite; 6 - K-nepheline syenite, juvite, urtite; 7 - apatite nepheline rock; 8 - rocks of loparite-bearing differentiated lujavrite-foyaite-urtite series; 9 - rocks of differentiated ijolite-melteigite series; 10 - poikilitic sodalite syenite; 11 - nepheline syenite of marginal part of Khibiny pluton (khibinite); 12 - larvikite, lardalite; 13 - alkaline ultramafic rocks (peridotite, pyroxenite, melilitolite, foidolite); 14 - subalkaline ultrabasic volcanics of Lovozero Formation; 15 - sedimentary rocks of Lovozero Formation and xenoliths; 16 - rocks of Precambrian basement and faults therein.

same time, differentiation in the Khibiny pluton developed in full measure during the formation of the foidolite series, large fragments of which have been retained as a discontinuous ring that separates peralkaline syenites of the marginal and

central parts of the pluton.

CONCLUSIONS

With allowance for the obtained data and the available isotopic age determinations of rocks pertaining to various magmatic series, it is concluded that the considered magmatic system was formed as a sequence of magmatic events. The magma emplacement at the initial stage was accompanied by the formation of the self-dependent Kurga intrusion. The late stages occurred in both plutons within a short time interval. The volcanic-plutonic complex evolved in the following sequence.

Premagmatic stage:

Manifestation of mantle metasomatism predated the vigorous Paleozoic magmatic cycle [4].

Early magmatic stage:

Faulting in the Neoproterozoic tonalite-trondhjemite-granodiorite (TTG) complex; emplacement of intrusive bodies (Kurga intrusion) and volcanic eruptions (early Lovozero sequence of ultramafic and subalkaline volcanic rocks) at the northeastern place of the future Lovozero ring structure (fig. 3a).

Main magmatic stage:

(1) Formation of ring fault system and subsidence of the Khibiny cauldron at the contact between the Neoproterozoic TTG complex and Paleoproterozoic Pechenga-Imandra-Varzuga Rift Belt; emplacement of the first batches of melanephelinite melt as ring dikes in the framework.

(2) Emplacement of alkaline ultramafic melts in the northern Khibiny and northeastern Lovozero calderas with the formation of intrusive bodies composed of olivine pyroxenite, melilitolite, and olivine melteigite (fig. 13a).

(3) Formation of the main Khibiny and Lovozero plutonic complexes of peralkaline syenites.

In the Khibiny caldera:

– emplacement of peralkaline nepheline syenite along outer conic faults (khibinite intrusion);

– further subsidence of the cauldron and formation of the layered ijolite–melteigite complex in the central zone of the caldera (fig. 13b);

– formation of conic faults in the ijolite–melteigite complex and emplacement of phosphate-bearing urtite-juvite-kalcilite-syenite along these faults (fig. 13c);

– formation of a new conic fault system in the central part of the ijolite-melteigite complex; breakup of its central zone and emplacement of nepheline syenite melt as a core of pluton (foyaite intrusion);

– emplacement of carbonatite and pulaskite stocks in the eastern part of caldera.

In the Lovozero caldera:

- formation of conic faults and subsidence of the southwestern part of the caldera accompanied by emplacement of the first batches of peralkaline magma and its crystallization as poikilitic sodalite syenite;
- further subsidence of the southeastern part of the caldera. According to the results of density simulation, the amplitude of subsidence (present-day position of the bottom of the caldera) is 7-8 km; during this period, peralkaline magma filled the entire depression with the formation of the loparite-bearing layered lujavrite-foyaite-urtite complex (fig. 13b);
- breakup of the central part of the differentiated loparite-bearing complex and emplacement of hypabyssal eudialyte lujavrite intrusion along the breakup zone;
- emplacement of the alkali syenite (pulaskite) intrusion into the central part of the Lovozero caldera (fig. 13d).

(4) Formation of a dike complex in the Khibiny and Lovozero composed of alkali picrite, olivine melanephelinite, nephelinite, and phonolite dikes and explosion pipes (fig. 13d).

Late magmatic stage:

- formation of late microcline-albite pegmatoids with ilmenite and zircon in the framework of the Lovozero pluton;
- late magmatic processes in alkali syenite in the central part of the Lovozero pluton as a manifestation of waning magmatic activity in the Khibiny and Lovozero calderas.

Taking into account new geochronological data and previously published isotopic evidence, the duration of the above-listed events, beginning from supply of first batches of melts into calderas and up to finishing postmagmatic events expressed in the formation of late pegmatoid veins, is estimated at >25 Ma.

The isotopic dating was carried out by B.V. Belyatsky (VNIIO keanologiya, St. Petersburg) and A.V. Travin (IGM Siberian branch RAS, Novosibirsk). This study was supported by the Russian Foundation for Basic Research (project no. 12-05-00244).

REFERENCES

1. **Arzamastsev A.A. and Arzamastseva L.V.** Evolution of foidolite series of alkaline massifs in the Kola province: mineralogical and geochemical attributes, *Petrologiya*, 1993, vol. 1, no. 5, pp. 524-535.
2. **Arzamastsev A.A. and Arzamastseva L.V.** Alkaline ultra basic plutonic series of the Lovozero massif, Kola Peninsula, *Dokl. Earth. Sci.*, 1996, vol. 348, no. 4, pp. 533-536.
3. **Arzamastsev A.A., Arzamastseva L.V., Glaznev V.N., and Raevsky A.D.** Petrologic-geophysical model for the structure and composition of deep levels of the Khibiny and Lovozero complexes, Kola Peninsula, *Petrology*, 1998, vol. 6, no. 5, pp. 434-450.
4. **Arzamastsev A.A. and Belyatsky B.V.** Evolution of the mantle source of the Khibiny massif: Evidence from Rb-Sr and Sm-Nd data on deep-seated xenoliths, *Dokl. Earth Sci.*, 1999, vol. 366, no. 4, pp. 562-565.

5. **Arzamastsev A.A., Belyatsky B.V., and Arzamastseva L.V.** The Kola alkaline province in Paleozoic: estimation of duration of processes and evolution of mantle sources, in *Trudy nauchnoishkoly "Shchelochnoi magmatizm Zemli"* (Proceedings of scientific school: Alkaline magmatism of the Earth), Moscow: GEOKHI RAN, 2001, pp. 8-9.
6. **Arzamastsev A.A. and Dahlgren S.** Deep mineral assemblages in dikes and explosion pipes of the Baltic Shield, *Geokhimiya*, 1993, vol. 31, no. 8, pp. 1132–1142.
7. **Arzamastsev A., Glaznev V., Arzamastseva L., and Raevsky A.** Morphology and internal structure of the Kola alkaline intrusions, NE Fennoscandian Shield: 3D density modeling and geological implications, *J. Asian Earth Sci.*, 2000, vol. 18, no. 2, pp. 213-228.
8. **Arzamastsev A.A., Ivanova T.N. and Korobeinikov A.N.** *Petrologiya iiolit-urtitov Khibin I zakonomernosti razmeshcheniya v nikh zalezhei apatita* (Petrology of ijolites-urtites of the Khibiny and localization of apatite lodes therein), Leningrad: Nauka, 1987.
9. **Bayanova T.B.** Vozrast repernykh geologicheskikh kompleksov Kol'skogo regiona idlitel'nost' protsessov magmatizma (Age of reference geological complexes in the Kola region and duration of magmatic processes), St. Petersburg: Nauka, 2004.
10. **Bayanova T.B., Elizarov D.V., and Ikorsky S.V.** Isotopic RbSr dating of pegmatites in the Khibiny massif, Kola region, in *Rudnyi potentsial shchelochnogo, kimberlitovogo I karbonatitovogo magmatizma: TezisyMezhdunar. konf.*(Abstracts of International Conference: Ore potential of alkaline, kimberlite, and carbonatite magmatism), Moscow–Minsk, 2011, pp. 8-9.
11. **Belyatsky B.V., Vinogradova L.G., Krymsky R.Sh., et al.** Sm-Nd and Rb-Sr isotopic dating of the Zabytoewolframite–rare-metal deposit, Primorye, *Petrologiya*, 1994, vol. 2, no. 3, pp. 243-250.
12. **Borutsky B.E.** *Porodoobrazuyushchie mineraly vysokoshchelochnykh kompleksov* (Rockforming minerals of hyperalkaline complexes), Moscow: Nauka, 1988.
13. **Bussen I.V. and Sakharov A.S.** *Petrologiya Lovozerskogo shchelochnogo massiva* (Petrology of the Lovozero alkaline massif), Leningrad: Nauka, 1972.
14. **Dudkin O.B. and Savitsky A.V.** Late orthoclasites of the Lovozero massif and its framework, *Dokl. Akad. Nauk SSSR*, 1979, vol. 247, no. 6, pp. 1441–1443.
15. **Fleck R.J., Sutter J.F., and Elliot D.H.**, Interpretation of discordant $^{40}\text{Ar}/^{39}\text{Ar}$ age spectra of Mesozoic tholeiites from Antarctica, *Geochim. Cosmochim. Acta*, 1977, vol. 41, pp. 15-32.
16. **Galakhov A.V.** *Petrologiya Khibinskogo shchelochnogo massiva* (Petrology of the Khibiny alkaline massif), Leningrad: Nauka, 1975.
17. **Galakhov A.V.** The Khibiny alkaline massif as a complex central-type intrusion related to several sources, *Dokl. Akad. Nauk SSSR*, 1988, vol. 302, no. 3, pp. 673-675.
18. **Gerasimovsky V.I., Volkov V.P., Kogarko L.N., et al.** *Geokhimiya Lovozerskogo shchelochnogo massiva*(Geochemistry of the Lovozero alkaline massif), Moscow: Nauka, 1966.
19. **Glaznev V.V. and Glaznev E.V.** Computer simulation of 3D geological and geophysical media, in *Sb. materialov 34 sessii Mezhdunar. seminaraim. D.G.Uspenskogo "Vopros yteorii I praktiki interpretatsii gravitatsionnykh, magnitnykh ielektricheskikh polei"* (Proceedings of the 34th Uspensky International Seminar: Theory and practice of interpretation of gravity, magnetic, and electric fields, Moscow, 2007, pp. 77-78.
20. **Glaznev V.N., Raevsky A.B., Balagansky V.V., et al.** 3D model of the upper crust in the Kittilá-Sodankyla, Finnish Laplandia (northern Baltic Shield), in *Sbornik materialov, posvyashch. 40letnemu yubileyu kafedry geofiziki VGU* (Col lection of papers dedicated to the 40th anniversary of Department of Geophysics, Voronezh State University), Voronezh: Voronezh State Univ., 2002, pp. 11-20.

21. **Glaznev V.N., Zhirova A.M., and Raevsky A.B.** New data on the deep structure of the Khibiny and Lovozero massifs, Kola Peninsula, *Dokl. Earth Sci.*, 2008, vol. 422, no. 7, pp. 1150-1152.
22. **Gustafson L.B., Orquera W., Mcwillan M., et al.** Multiple centers of mineralization in the Indio Muerto district, El Salvador, Chile, *Econ. Geol.*, 2001, vol. 96, pp. 325-350.
23. **Irving A.J. and Price R.C.** Geochemistry and evolution of lherzolite-bearing phonolitic lavas from Nigeria, Australia, East Germany and New Zealand, *Geochim. Cosmochim. Acta*, 1981, vol. 45, no. 8, pp. 1309-1320.
24. **Kalinkin M.M.**, New data on deep structure and tectonics of the Lovozero alkaline massif, in *Regional'nayageologiya, metallogeniya i geofizika* (Regional geology, metallogeny, and Geophysics), Apatity: Kola Branch, Acad. Sci. USSR, 1974, pp. 56-75.
25. **Karbonatity Khibin** (Khibiny carbonatites), Apatity: Kola Branch, Acad. Sci. USSR, 1984.
26. **Kobrunov A.I. and Varfolomeev V.A.** A method of ϵ equivalent redistribution and its application to interpretation of gravity fields, *Izv. Akad. Nauk SSSR, Ser. Fizika*, 1981, no. 10, pp. 25-44.
27. **Kogarko L.N., Kononova V.A., Orlova M.P., and Woolley A.R.** *Alkaline rocks and carbonatites of the world, part 2: Former USSR*, London: Chapman and Hall, 1995.
28. **Kogarko L.N.** Microcomponents as indicators of the differentiation of alkaline magmatic series, in *Origin and distribution of the elements*, L.H.Ahrens, Ed., 1979, pp. 217-222.
29. **Kogarko L.N.** *Problemy genezisa agpaitovykh magm* (Genesis of peralkaline magmas), Moscow: Nauka, 1977.
30. **Korobeinikov A.N. and Arzamastsev A.A.**, Pulaskites in the Khibiny alkaline massif: New evidence for polyserial igneous complex, *Dokl. Ross. Akad. Nauk*, 1994, vol. 338, no. 5, pp. 638-640.
31. **Kramm U.** Mantle components of carbonatites from the Kola alkaline province, Russia and Finland: a Nd-Sr study, *Eur. J. Mineral.*, 1993, vol. 5, pp. 985-989.
32. **Kramm U., Kogarko L.N., Kononova V.A., et al.** The Kola alkaline province of the CIS and Finland: precise Rb-Sr ages define 380-360 age range for all magmatism, *Lithos*, 1993, vol. 30, pp. 33-44.
33. **Kramm U. and Kogarko L.N.** Nd and Sr isotope signatures of the Khibina and Lovozero agpaitic centres, Kola alkaline province, Russia, *Lithos*, 1994, vol. 32, pp. 225-242.
34. **Lepezin G.G., Travin A.V., Yudin D.S., et al.** Age and thermal history of the Maksyutovo metamorphic complex: $^{40}\text{Ar}/^{39}\text{Ar}$ evidence, *Petrology*, 2006, vol. 14, no. 1, pp. 98-114.
35. **Ponomarchuk V.A., Lebedev Yu.N., Travin A.V., et al.** Use of magnetic separation technology in K-Ar, $^{40}\text{Ar}/^{39}\text{Ar}$, and Rb-Sr methods of rock and mineral dating, *Geol. Geofiz.*, 1998, vol. 39, no. 1, pp. 55-64.
36. **Roslov Yu.V., Vinnik A.A. and Kopylova A.V.** Recovery of complexly built velocity models on the basis of integrated seismic tomography and kinematic migration, in *Model I zemnoi koryi verkhnei mantii: Mater. Mezhdunar. Nauchnopr akticheskogo seminar*a (Proceedings of international scientific and practical seminar: Models of the Earth's crust and upper mantle), St. Petersburg, 2007, pp. 177-180.
37. **Wu FuYuan, Yang YueHeng, Marks M.A.W., et al.** In situ U-Pb, Sr, Nd, and Hf isotopic analysis of eudialyte by LA (MC)ICP-MS, *Chem. Geol.*, 2010, vol. 273, pp. 8-34.
38. **Zaitsev A.N., Bell K., Wall F. and Le Bas M.J.** Alkaline rare-earth element carbonates from carbonatites of the Khibiny massif: mineralogy and genesis, *Dokl. Earth Sci.*, 1997, vol. 355, no. 5, pp. 786-790.

SALT (CARBONATITE) MELTS OF THE BOL'SHAYA TAGNA MASSIF, THE EASTERN SAYAN REGION: EVIDENCE FROM MELT INCLUSIONS

Andreeva I. A.

Institute of Geology of Ore Deposits, Petrography, Mineralogy, and Geochemistry (IGEM), Russian Academy of Sciences, e-mail: andreeva@igem.ru

The calcite-fluorite and fluorite rocks together with cognate carbonatites are commonly associated with alkaline ultrabasic complexes. The magmatic or metasomatic (postmagmatic) origin of carbonatites has been actively discussed for almost half a century. Nevertheless, no certain view on this subject has been settled to date, especially concerning the usual carbonatites and fluorite rocks formed at the late stage of the evolution of the alkaline ultramafic complexes. Many petrologists refer to these rocks as products of metasomatic or hydrothermal processes. The findings of melt inclusions in minerals from the aforementioned rocks [1-4] served as conclusive evidence for their magmatic origin. However, an attempt to estimate the composition of the respective melts in quantitative terms was made only in [1, 3]. These data remain insufficient, and it is necessary to furnish additional data on the state and composition of mineral-forming medium of such objects as a basis for understanding the genesis of carbonatitic complexes.

In this communication, we report the results of a detailed study of melt inclusions and coexisting crystalline inclusions in minerals of the calcite-fluorite carbonatites from the Bol'shaya Tagna Massif in the eastern Sayan region. This investigation allowed us to reveal natrocarbonatitic melts responsible for the formation of this rock and to estimate for the first time their quantitative composition.

The Bol'shaya Tagna Massif is situated in the eastern Sayan province of alkaline ultrabasic rocks and carbonatites. This massif is a rounded and concentrically zonal-ring complex structure (4 km in diameter) that demonstrates the consecutive formation of ijolite-melteigite, nepheline and subalkali syenite (microcline), picritic porphyritic rock (alnoite), and carbonatite rocks [5]. The abundance of syenites and microclinites and the intense development of fluorite mineralization related to the formation of carbonatite rocks are distinguishing features of this massif. Three types of fluorite carbonatites are recognized: (1) fine-grained calcite carbonatites with fine- and very fine-crystalline fluorite, hematite, and apatite; (2) massive or banded ore consisting of fluorite (0.1 mm-1 cm in size), calcite, K-feldspar, and aegirine (fluorite crystals vary from fractions of millimeter

to 1 cm in size); and (3) stringer-disseminated ore with fluorite crystals from 3-4 mm to 1 cm in size.

The studied sample is a coarse-grained fluorite carbonatite of the second type composed of carbonate (~60 vol %), fluorite (~30 %), K-feldspar (<up to 5 %), pyrite (2-3 %), and barite (up to 1-2 %). The chemical composition of the sample and the rock-forming minerals is given in table 1. Carbonate is represented by calcite with elevated contents of Mn (as much as 2.3 wt %) and an admixture of FeO (<up to 0.60 wt %). The two-phase exsolution structure is often observed (Table 1, analyses 5 and 6). One phase is Mn-calcite, while another phase is kutnahorite (carbonate of dolomite group) that contains 38 wt % CaO, 15 wt % MnO, 10 wt % FeO, and 5 wt % MgO. It should be noted that kutnahorite was reported from carbonatites of the Khibiny Massif [6] and carbonatites of Brazil [7]. Fluorite is characterized by an admixture of SrO (<up to 0.15 wt %) and REEs (the total content of Ce₂O₃ and La₂O₃ is up to 0.2 wt %). As much as 0.5 wt % SrO is detected in barite.

The chemical composition of minerals, crystalline inclusions, and daughter mineral phases in melt inclusions was studied with a Camebax-Microbeam microprobe with the following conditions: accelerating voltage 15 kV, current 30 nA, and scanning area 5 × 5 and 2 × 2 μm.

The primary melt inclusions and syngenetic crystalline inclusions were revealed in fluorite, K-feldspar, and pyrite from fluorite carbonatite. The inclusions contain carbonates, fluorite, K-feldspar, aegirine, columbite, and pyrite. The chemical composition of inclusions is presented in table 1.

The crystalline inclusions in carbonates are represented by calcite, Na-Ca-carbonate, and kutnahorite. The rounded calcite inclusions (30-40 μm in diameter) have been found in fluorite and pyrite. Like the rock-forming calcite, this mineral from the calcite inclusions contains as much as 2.8 wt % MnO and 1.6 wt % FeO. Sporadic columbite ingrowths in calcite have been identified. Columbite is observed as an extremely rare phase commonly replacing pyrochlore in carbonatites. Nonetheless, columbite in carbonatites of the Bol'shaya Tagna Massif is an accessory mineral that fits mangano-columbite in composition (table 1, analysis 14) and contains as much as 11 wt % MnO, 9.5 wt % FeO, and 4.6 wt % TiO₂.

The Na-Ca-carbonate inclusions in fluorite are colorless euhedral prismatic crystals 20-30 μm in size (table 1, analysis 15). The studied carbonate contains up to 44.6 wt % CaO, 18 wt % Na₂O, and 4.5 wt % F, 3.7 wt % MnO, and as much as 1 wt % FeO. The occurrence of carbon and all other identified carbonate phases in this mineral has been supported qualitatively by microprobe analysis. This mineral is conditionally named Na-Ca-fluorcarbonate, because we failed to class this phase with any known carbonate group. The empirical formula of this mineral was calculated from the chemical analysis as Na^sCCa^v, Mr[^], Fe_{0.14})_{8.96}[CO₃]_{7.00} (F₂₄₉OH₁₅₁)₄₀₀. The calculated H₂O and CO₂ contents are 1.31 and 29.66 wt %, respectively, and the total is 101.09 wt %.

Table 1.

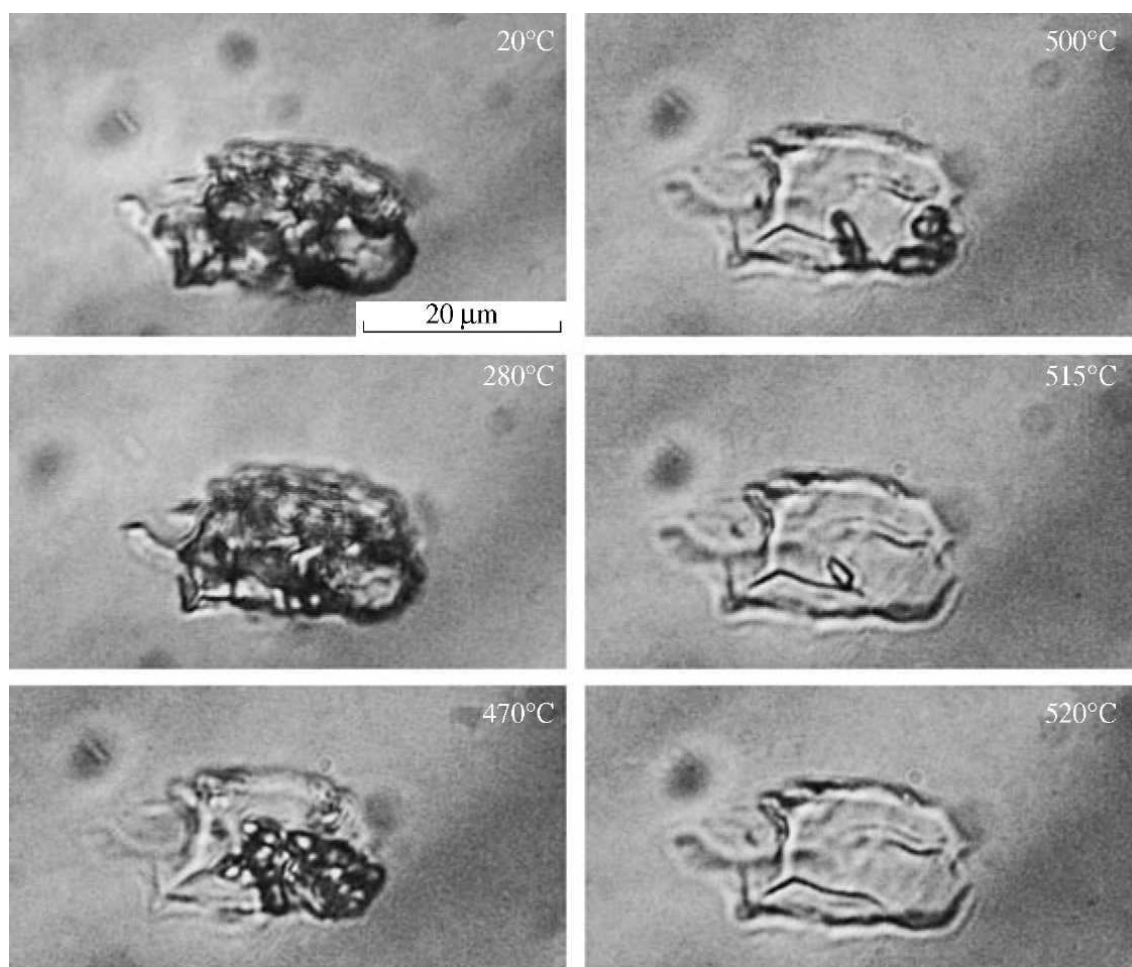
Chemical composition of rock, minerals, and crystalline inclusions in minerals of fluorite carbonatite (wt %)

Component	1	2	3	4	5	6	7	8	9	10	11	12	13	14	15	16	17
SiO ₂	3.10	64.53	0.06	0.01	0.01	0.08	0.12	0.06	0.07	64.15	53.96	0.03	0.05	0.06	0.00	0.49	0.37
TiO ₂	0.16	0.00	0.01	0.00	0.00	0.00	0.00	0.00	0.02	0.03	2.08	0.00	0.00	4.63	0.00	0.00	0.00
Al ₂ O ₃	0.82	18.41	0.03	0.00	0.03	0.01	0.02	0.86	0.01	19.19	0.33	0.02	0.01	0.08	0.02	0.08	0.12
FeO	2.76	0.22	0.02	0.29	0.60	10.11	18.29	0.14	47.56	0.06	28.57*	1.63	1.11	9.48	0.94	8.84	48.02
MnO	3.21	0.03	0.00	2.29	1.76	15.09	15.47	0.00	0.04	0.01	0.10	2.79	2.20	11.04	3.76	11.68	0.34
MgO	2.35	0.00	0.00	0.01	0.11	5.22	5.11	0.00	0.04	0.02	0.30	0.15	0.02	0.05	0.01	5.46	0.00
BaO	1.36	0.06	0.06	0.01	0.00	0.06	0.05	65.76	0.01	0.02	0.13	0.04	0.00	0.16	0.01	0.03	0.00
SrO	0.42	0.00	0.14	0.16	0.12	0.11	0.05	0.52	0.00	0.00	0.00	0.49	0.13	0.03	0.11	0.06	0.00
CaO	48.88	0.22	51.26	59.71	62.67	38.76	32.57	0.04	0.10	0.04	0.86	59.23	59.47	0.62	44.65	28.01	0.03
Na ₂ O	0.13	0.10	0.00	0.00	0.01	0.15	0.29	0.19	0.02	0.06	13.52	0.00	0.01	0.03	18.05	0.06	0.00
K ₂ O	0.80	16.02	0.00	0.01	0.00	0.16	0.44	0.00	0.01	16.47	0.00	0.00	0.01	0.01	0.00	0.24	0.02
P ₂ O ₅	0.28	0.01	0.00	0.01	0.01	0.01	0.02	0.00	0.03	0.03	0.02	0.02	0.03	0.04	0.07	0.04	0.00
^c 2O ₃	0.18	-	0.14	0.00	0.12	0.01	-	0.00	0.08	-	-	0.15	-	-	0.00	0.05	-
La ₂ O ₃	0.14	-	0.07	0.03	0.00	0.00	-	0.00	0.02	-	-	0.05	-	-	0	0.06	-
^{Nb} 2O ₅	0.04	-	-	0.02	0.03	0.02	-	-	-	-	-	-	-	72.88	0.00	0.00	-
F	4.13	-	47.75	0.07	0.05	0.05	-	-	-	-	0.29	-	-	-	4.55	0.00	-
Cl	-	-	0.00	0.00	0.00	0.14	-	-	-	-	-	0.02	-	-	0.00	0.00	-
S	0.47	0.02	0.00	0.01	0.00	0.19	0.20	31.07	51.57	0.01	0.01	0.00	0.00	-	0.00	0.01	51.85
Total	100.55*	99.62	99.54	62.63	65.52	70.17	72.63	98.64	99.58	100.09	100.17	64.62	63.02	99.11	72.17	55.10	100.75

Note: (1) Rock (total includes 0.36 wt % H₂O and 30.96 wt % CO₂); (2-9) rock-forming minerals; (10-17) crystalline inclusions in fluorite (10-15, 17), K-feldspar (16), and pyrite (13, 14). (2, 10) K-feldspar; (3) fluorite; (4, 5, 12, 13) calcite; (6, 7, 16) kutnahorite; (8) barite; (9, 17) pyrite; (10-12, 15, 17) crystalline inclusions in fluorite; (10) K-feldspar, (11) aegirine, (12) manganocolumbite, (15) Na-Ca-fluorocarbonate, (17) pyrite; (13) calcite and (14) manganocolumbite inclusions in pyrite; (16) kutnahorite inclusion in K-feldspar. FeO is total iron (here and in Table 2); (*) total iron given as Fe₂O₃.

Kutnahorite $\text{Ca}(\text{Mn,Mg,Fe})(\text{CO}_3)_2$ was identified as rhombic inclusions (20-25 μm in size) in K-feldspar. These inclusions are close in composition to the rock-forming kutnahorite.

In addition to carbonate phases, the crystalline inclusions of clinopyroxene, K-feldspar, and opaque ore mineral were detected in fluorite of the studied carbonatites. Fluorite inclusions were found in K-feldspar of the carbonatites. Greenish acicular crystals of clinopyroxene (up to 60 μm long) correspond to aegirine in composition. Prismatic crystalline inclusions of K-feldspar range from 30 to 50 μm in size and contain as much as 16.5 wt % K_2O . The opaque ore inclusions were identified as pyrite.



Behavior of salt inclusion in fluorite from fluorite carbonatites during a thermometric run at 1 atm.

The irregular melt inclusions (30-50 μm in size) are disposed chaotically in fluorite (figure). The inclusions are completely crystallized and they contain a residual gas phase and daughter mineral phases (carbonate, fluoride, and chloride) (table 2). Carbonates are predominant and represented by calcite, kutnahorite, Na-fluor-carbonate, nyerereite, and burbankite. Compositions of the daughter phases (calcite, kutnahorite, and Na-fluor-carbonate) are identical to the compositions of these minerals observed as crystalline inclusions. Nyerereite (Na-Ca-carbonate)

and burbankite (Ba-Sr-carbonate) are rather rare minerals. They have been identified as daughter phases in melt inclusions for the first time. Nyerereite is characterized by elevated contents of K_2O , FeO, and MnO (6.0, 1.3, and 1.3 wt %, respectively). Burbankite contains 12 wt % SrO and 2 wt % Ce_2O_3 . Fluorite and villiaumite are fluoride minerals contained in the melt inclusions. The presence of fluorite as a daughter mineral of melt inclusions in carbonatite is quite natural. However, villiaumite NaF is atypical of such a mineral assemblage. It should be noted that the daughter fluorite is moderately enriched in SrO (<up to 0.7 wt %). Qualitative microprobe analyses have indicated the presence of halite (45.57 wt % Na_2O and 36.31 wt % Cl) and sylvite (52.82 wt % K_2O and 31.74 wt % Cl) as daughter chlorides.

In general, the mineral assemblage of melt inclusions in fluorite from carbonatites of the Bol'shaya Tagna Massif is consistent with mineral composition of carbonatitic lavas of the Oldoinyo Lengai Volcano (Tanzania), where Na-Ca-carbonate (nyerereite), Na-carbonate (gregoryite), Ba-carbonate, fluorite, and sylvite have been identified as phenocrysts and ground-mass minerals in the lavas [8].

The thermometric experiments with melt inclusions were carried out on a Linkam TS 1500 microscopic heating stage with visual control. The first indications of melting of crystalline phases were observed at 280 °C; thereby, the gas bubble acquired a perfect spherical shape. At 500 °C, the inclusions contained melt and one or two relict crystalline phases. The complete homogenization of inclusions into salt melt was attained at 520-525 °C. During the subsequent cooling, the melt completely crystallized into a microgranular aggregate of quenched crystals. The phase transformation of the fluorite-hosted melt inclusions in fluorite in the process of heating is illustrated in the figure.

A complete scanning of the chemical composition of homogenized melt inclusions in fluorite analyzed by scanning over the whole area allowed us to estimate the composition of the salt melt (table 2) that produced the fluorite carbonatite (table 2). The melt is characterized by extremely high contents of Na_2O (up to 22 wt %) and CaO (up to 10 wt %), as well as by elevated contents of FeO (up to 7 wt %), MnO (up to 4-5 wt %),

K_2O (up to 3-8 wt %), SrO (up to 0.6-0.8 wt %), and Ba (up to 0.6 wt %), F, and Cl. The natrocarbonatitic melts have been determined previously only once as inclusions in melilite from melilitolites of the Gardiner alkaline ultrabasic complex in eastern Greenland [9]. It should also be mentioned that a microprobe analysis of inclusions was performed during two stages. First, we determined the major components, BaO, SrO, S, and Cl. Then, F and REEs were analyzed. The mineral phases within inclusions are unstable under electron beam and burn down completely in the process of microprobe analysis. Hence, determinations of F, Ce, La, and Cl can be incomplete. Therefore, we checked only these elements in several inclusions (table 2, analysis 12). It has been established that the studied salt melts are substantially enriched in the aforementioned trace elements (e.g., F up to

Table 2
**Chemical composition (wt %) of daughter minerals and homogenized melt inclusions
 in fluorite from fluorite car-bonate (wt %)**

Component	1	2	3	4	5	6	7	8	9	10	11	12	13	14
SiO ₂	0.06	0.04	0.06	0.02	0.02	0.11	0.09	0.02	0.77	0.80	0.37	-	0.16	0.21
TiO ₂	0.00	0.02	0.15	0.00	0.00	0.00	0.00	0.00	0.40	0.41	0.08	-	0.02	0.02
Al ₂ O ₃	0.03	0.02	0.00	0.00	0.04	0.00	0.03	0.01	0.04	0.05	0.66	-	-	-
FeO	0.00	0.44	5.45	4.30	4.45	1.98	0.12	0.04	6.85	5.48	1.34	-	0.28	0.48
MnO	0.06	2.00	9.24	5.39	5.51	2.93	0.10	0.05	5.54	4.31	1.32	-	0.38	0.60
MgO	0.00	0.15	10.28	0.02	0.00	0.00	0.02	0.01	0.18	0.16	0.40	-	0.38	0.50
BaO	0.05	0.06	0.06	0.02	0.03	0.11	41.31	0.04	0.63	0.37	1.00	-	1.66	2.17
SrO	0.74	0.16	0.10	0.09	0.11	0.00	11.45	0.00	0.82	0.69	0.59	-	1.42	1.43
CaO	51.10	59.20	29.00	43.66	43.97	31.80	6.63	0.06	9.95	8.09	8.95	-	14.02	12.86
Na ₂ O	0.00	0.00	0.08	15.21	15.69	22.59	3.17	54.44	22.54	19.65	19.41	-	32.22	30.42
K ₂ O	0.03	0.00	0.01	0.13	0.10	6.04	0.02	0.01	2.66	2.68	8.75	-	8.38	9.14
P ₂ O ₅	0.00	0.03	0.02	0.04	0.00	0.30	0.02	0.01	0.10	0.08	0.05	-	0.85	0.75
Ce ₂ O ₃	-	-	0.00	0.03	0.18	0.10	1.97	0.02	0.13	-	0.27	1.28	0.07	0.11
La ₂ O ₃	-	-	0.00	0.00	0.02	0.09	0.60	0.00	0.02	-	0.07	0.10	0.06	0.09
F	48.30	0.00	0.00	5.90	7.18	0.04	0.99	45.90	1.65	-	0.80	1.04	2.50	4.10
Cl	0.00	0.01	0.00	0.00	0	-	-	0.01	0.36	-	0.66	1.10	3.40	5.18
S	0.01	0.01	0.01	0.00	0.00	0.18	0.00	0.00	0.13	0.14	0.20	-	3.72*	5.58*
Total	100.38	62.14	54.46	74.81	77.30	66.27	66.52	100.62	52.77	42.91	44.92	-	65.80	68.06

Note: (1-8) Daughter minerals in melt inclusions: (1) fluorite, (2) calcite, (3) kutnahorite, (4, 5) Ca-Na-fluorocarbonate, (6) nyereite, (7) burbankite, (8) villiaumite; (9-12) homogenized melt inclusions; (13, 14) carbonatitic lavas of the Oldoinyo Lengai Volcano; (*) contents given as SO₃.

1.65 wt %, Ce₂O₃ up to 1.3 wt %, and Cl up to 1.0 wt %). This is consistent with the occurrence of chlorides, fluorides, and REE-bearing Ba-Sr-carbonate as daughter minerals in the melt inclusions.

The studied carbonatitic melts reveal obvious compositional similarity with carbonatitic lavas of the Oldoinyo Lengai Volcano in Tanzania (table 2). However, it should be noted that the analyzed melt inclusions have a lower sum total of components (without the consideration of CO₂) in the analyzed melt inclusions (table 2, analyses 9-11) in comparison with the sum total of chemical analyses of the Oldoinyo Lengai lavas (table 2, analyses 13, 14). This may be caused by loss of Na in the process of microprobe analysis. The physicochemical similarity of the studied melts and the Oldoinyo Lengai carbonatitic lavas is also supported by the following fact: the homogenization temperature of fluorite-hosted melt inclusions in fluorite (520-525 °C) is almost the same as the magma temperature (544 °C) measured during the eruption of the Oldoinyo Lengai Volcano in 1988 [8].

Thus, the detailed study of fluorite-hosted melt inclusions in fluorite from fluorite carbonatites of the Bol'shaya Tagna Massif has shown that this rock crystallized from a natrocarbonatitic melt markedly enriched in Mn, Fe, Ba, Sr, Ce, F, and Cl. This melt reveals physicochemical similarity with lavas from the Oldoinyo Lengai Volcano. A compositional difference between these rocks and melts (particularly, in terms of CaO and Na₂O contents) may be accounted for by instability of sodium carbonates and chlorides and their removal with fluid phase at the late stage of magma crystallization. The sodic phases could also have been leached by water from the rock, but this process is less probable because leached cavities are absent in the rock.

The authors are grateful to P.M. Kartashov for useful consultations during the preparation of the manuscript.

REFERENCES

1. I. A. Andreeva, V. B. Naumov, V. I. Kovalenko, and N. N. Kononkova, **Petrologiya** **6**, **307** (1998) [**Petrology** **6**, **284** (1998)].
2. I. P. Solovova, I. D. Ryabchikov, and L. N. Kogarko, **Geokhimiya** **36**, **435** (1998) [**Geochem. Int.** **36**, **377**, (1998)].
3. B. E. Nesbitt and W. C. Kelly, **Contrib. Mineral. Petrol.** **63**, **271** (1977).
4. L. S. Puzanov, **Dokl. Akad. Nauk SSSR** **233**, **463** (1977).
5. A. A. Frolov and S. V. Belov, **Geol. Rudn. Mestorozhd.** **41** (2), **109** (1999) [**Geol. Ore Deposits** **41** (2), **94** (1999)].
6. S. Sindern, A. Zaitsev, A. Demeny, et al., **Mineral. Petrol.** **80**, **215** (2004).
7. C. B. Gomes, E. Rubert, and L. Morbidelli, **J. South Am. Earth Sci.** **3** (1), **51** (1990).
8. K. Bell and J. Keller, *Carbonatite Volcanism Oldoinyo Lengai and the Petrogenesis of atrocarbonatites* (Springer, Berlin, 1995).
9. T. F. D. Nielsen, I. P. Solovova, and I. V. Veksler, **Contrib. Mineral. Petrol.** **126**, **341** (1997).

BEHAVIOR OF F AND Cl IN AGPAITIC ACID MELTS

Solovova I. P., Girnis A.V.

¹*Institute of Geology of Ore Deposits, Petrography, Mineralogy, and Geochemistry, Russian Academy of Sciences, Russia*

Many deposits of rare elements (Be, Zr, Nb, REE, Y, and others) are genetically related to acid agpaitic (with the mole ratio $(\text{Na}_2\text{O} + \text{K}_2\text{O})/\text{Al}_2\text{O}_3 > 1$) magmas [2]. The concentration of these elements most likely results from crystallization differentiation leading to their accumulation in the residual melts at the expense of low coefficients of minor element partitioning between silicate minerals and melts Kovalenko et al., [4]. Gradual accumulation of incoherent minor elements in melts may be violated by separation of salt melts from magma. According to the experimental data [5], minor elements are most effectively extracted by fluoride melts. Because of this, silicate-salt liquid immiscibility is an important factor of geochemical and metallogenic evolution of magmas. The formation of chloride melts during the evolution of magmatic systems was established for some objects [6]. The presence of fluoride melt in acid magmatic systems was described in individual cases [7], and each new finding is of intense interest. In this paper, we discuss the results of the study of melt inclusions in phenocrysts from magmatic rocks of Pantelleria Island (Central Mediterranean, Italy) [9], in which liquid immiscibility of alkaline acid magmas with the formation of salt melt was observed. Chloride melts in inclusions and glasses from rocks of Pantelleria Island were first discovered in 1987 [10] and hereafter were described in glasses of the rock groundmass [11].

The melt and fluid inclusions were studied in phenocrysts from ignimbrite and pantellerite collected in different parts of Pantelleria Island and related to the precaldera and postcaldera stages of volcanism evolution. Salt globules in glasses of melt inclusions were observed in phenocrysts of alkaline feldspar and rare quartz phenocrysts. The compositions and behavior of melt inclusions from different minerals and rocks are quite similar; that is why in this paper we will consider inclusions in phenocrysts of alkaline feldspar from pantellerite. Inclusions in precaldera pantellerite (Sample 16, Cala dei Cinque Denti) and postcaldera pantellerite (Sample 19, Contrada Gadir) are most well studied.

Feldspar phenocrysts are presented by anorthoclase with low concentrations of CaO. Partially crystallized melt inclusions in them contain glass, rims of daughter anorthoclase on walls of vacuoles, and microcrystalline salt globules. These inclusions contain unusual skeletal and vermiform fluorite segregations. The portion of daughter anorthoclase crystallizing on inclusion walls is 18-55 vol %. The composition of the daughter anorthoclase rim differs strongly from the composition of the host mineral by the Fe_2O_3 concentration (up to 10 and 0.5 wt %,

respectively), which increases toward the center of the inclusion. Such alkaline feldspars (up to 18.4 wt % Fe₂O₃) were described in some lamproites of the United States [12] and Spain [13] with a high Fe/Al ratio that is also typical for glasses of the considered melt inclusions (table 1, analysis 1).

Таблица

Compositions of coexisting silicate and salt melts (wt %)

	1	2	3
SiO₂	71.25	-	-
TiO₂	0.77	0.0	0.0
Al₂O₃	3.62	0.0	0.0
FeO	8.71	0.86	0.4
MnO	0.54	0.15	0.0
MgO	0.16	0.90	0.0
CaO	0.26	2.27	1.9
Na₂O	3.83	65.86	52.0
K₂O	3.82	0.0	0.0
ZrO₂	0.33	0.96	0.4
F	0.18	25.9	1.4
Cl	0.55	10.2	43.8
Сумма	92.47	100	100

Note: (1) Silicate melt; (2) fluoride-chlor(3) chloride melt.

Melt inclusions contain salt globules of two types: mostly halite (NaCl) and halite-villiaumite (NaCl + NaF). A CaF₂ admixture is registered in both types. These are polycrystalline spherical aggregates (diameter up to 10-15 μm) or segregations along the boundary of gaseous isolation. One inclusion may contain up to 20-30 globules, and their total amount may reach a few percent of the inclusion volume, up to 10 vol % in some cases. Analogous salt aggregates were also found in the glassy groundmass of some acid volcanic rocks (Cala dell'Altura, Punta Scauri, Cuddia Gadi). The chemical composition of globules of the first type corresponds to practically pure NaCl (average from 22 analyses): 98.7 mol % NaCl + 1.3 mol % NaF. Ca and Fe are strongly dependent (table 1, analysis 3). Globules of the second type are characterized by strongly negative optical relief because of the prevalence of villiaumite crystals (fig. 1). The composition of globules corresponds to a mixture of NaCl and NaF with an admixture of Ca, Mg, and Fe. The concentration of NaF ranges from 36 to 99 mol %. It is important that globules of both types are registered separate in silicate melt inclusions, although direct contact between them was never observed. Thus, in one inclusion three mixed NaCl-NaF globules containing 35, 8, and 99 mol % NaF were analyzed.

Figure 1 shows one melt inclusion in alkaline feldspar phenocryst (Sample 57 collected in the region Cala dei Cinque Denti) containing two saline globules. One of them is mainly presented by villiaumite, the other one halite. The study of their compositions on the scanning ion microprobe "Cameca" IMS-4f (Institute of Microelectronics and Informatics, Russian Academy of Sciences, Yaroslavl, analyst S.G. Simakin) provided evidence for clear enrichment of the salt fluoride

melt in Be, Nb, Zr, Y, Ce (fig. 2), Nd, Rb, and Li in comparison with the coexisting silicate pantellerite melt. As is evident from table 1 (analysis 2), the Fe-

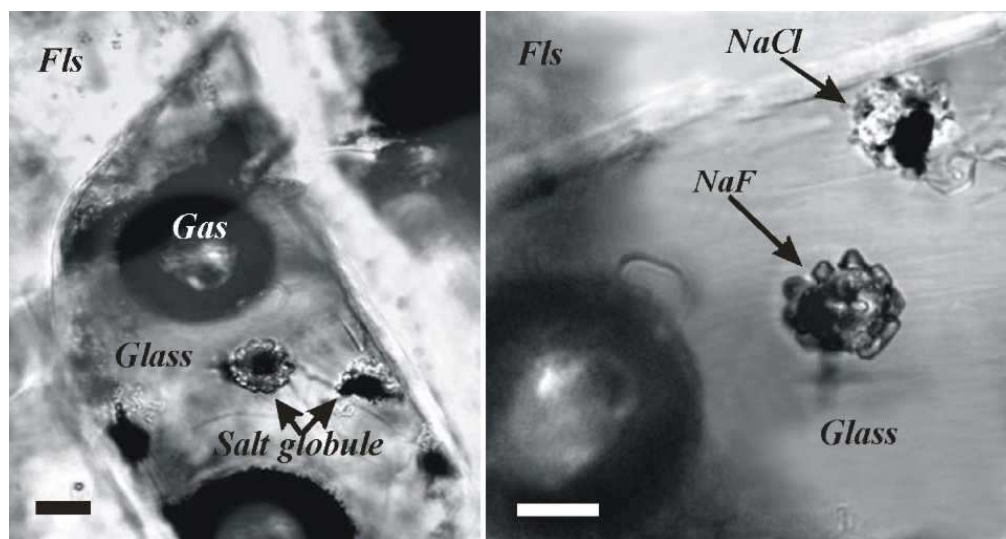


Fig. 1. Microphotograph of silicate melt inclusion in feldspar (a) and fragment of this inclusion with two globules of predominantly NaF and NaCl composition (b).

Transmitting light, parallel nicols. Fls is the alkaline feldspar. Scale bar is 10 μm .

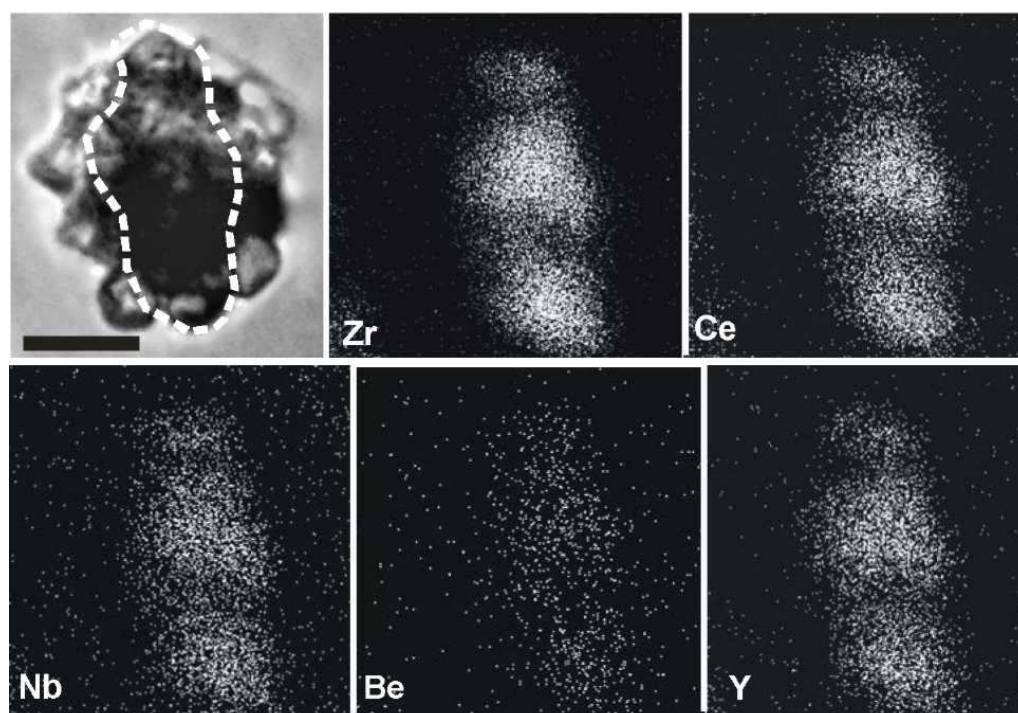


Fig. 2. Distribution of minor elements in the salt globule obtained by the Camebax scanning ion microprobe.

The dashed line in the microphotograph in transmitting light shows the part of the globule exposed on the surface. The black field around salt material on the images of concentration distributions is presented by silicate glass. Scale bar is 5 μm .

bearing saline globule is enriched in Zr by almost three times relative to the silicate melt, whereas the essentially chloride melt of globules (analysis 3) is not

characterized by such enrichment: the coefficient of Zr partitioning between chloride and silicate melts is close to 1.

Complete melting of material of globules of the first type was observed at heating up to 740-760 °C. Dissolution of salt matter and fluorite crystals in the silicate melt was observed in a wide temperature range, from 760 to 930 °C. In some experiments we managed to simulate the primary appearance of inclusions by their rapid cooling to 580-560 °C. Vermiform CaF₂ crystals and NaCl globules were precipitated synchronously in them. Complete homogenization of inclusions was reached at 930-1020 °C. Inclusions treated to complete homogenization (with melting of the daughter anorthoclase rim on inclusion walls) did not extract salt melt with a temperature decrease. Such behavior is most likely explained by the strong dependence of F solubility on the (Na₂O + K₂O)/Al₂O₃ ratio in the melt [14] or kinetic factors.

Melting of salt crystals in globules from the glassy groundmass of ignimbrite and pantellerite with subsequent homogenization of the salt melt (disappearance of gaseous bubbles) occurred at a temperature close to 730 °C.

The first signs of phase changes (most likely recrystallization) in globules of the second type were observed at 250 °C. Further temperature increase resulted in melting of all crystals (500-650 °C) and the appearance of gaseous bubbles. Homogenization of the salt melt with dissolution of the gaseous phase in it (680-780 °C) was observed at temperatures close to homogenization of NaCl globules. At this moment, melt inclusions contained daughter anorthoclase, silicate and salt melts, and the gaseous phase. Inclusions were completely homogenized at 1035-1070 °C.

Thus, we obtained the first direct evidence for the existence of high temperature sodium chloride and fluoride melts enriched in microelements and formed as a result of pantelleritic magma differentiation. Essentially fluoride melts were previously described in comendite of Central Mongolia [7] and ongonite of Eastern Transbaikalia [8]. In all cases the compositions of salt melts were characterized by significant variations. I. Peretyazhko and E. Savina noted the presence of several immiscible fluoride melts with different cation compositions. In this connection our observations of the association of essentially fluoride and essentially chloride melts in inclusions are quite interesting. Interpretation of such observations is ambiguous, because there is one eutectic and complete solubility in the liquid state in the pure NaCl-NaF system. It may be assumed that the presence of salt phases with contrasting compositions results from kinetic factors. Alternatively, the data by Z.A. Kotel'nikova and A.R. Kotel'nikov [15] demonstrate that the behavior of fluoride systems is strongly dependent on the presence of silicates because of the high silicon solubility in NaF solutions. That is why the behavior of chloride-fluoride phases in the presence of silicate minerals and melts, especially those containing additional components (for example, Ca, Fe, Mg, and water), may strongly differ from the behavior of the simple NaCl-NaF

system and it is impossible to exclude the possibility of immiscibility between essentially chloride and fluoride melts.

The obtained qualitative data on the distribution of minor elements (fig. 2) confirm experimental data of I.V. Veksler [5] on the high extractive ability of fluoride melts regarding REE. In addition we demonstrated that fluoride melts were also enriched in Zr, Ba, Nb, and other incompatible elements. The coefficient of Zr partitioning between fluoride and silicate melts is significantly higher than 1 (~3), but lower than the coefficients of REE partitioning obtained by I.V. Veksler [5] (10-200). This provides evidence for the fact that separation of small amounts of fluoride melts may result in significant fractionation of minor elements and influence metallogenic specialization of deposits related to alkaline rocks.

Работа выполнена при поддержке гранта РФФИ 13-05-00499а, программ ОНЗ и проекта Ведущих школ

REFERENCES

1. **Kovalenko V. I.**, in Petrology and Geochemistry of Rare Metal Granitoids (Nauka, Novosibirsk, 1977) [in Russian].
2. **Kovalenko V. I., V. B. Naumov, A. V. Girnis, et al.** *Petrologiya* 17, 437-456 (2009) [*Petrology* 17, 410 (2009)].
3. **Antipin V. S., V. I. Kovalenko, and I. D. Ryabchikov**, Distribution Coefficients of Rare Elements in Magmatic Rocks (Nauka, Moscow, 1984) [in Russian].
4. **Kovalenko V. I., R. L. Hervig, and M. F. Sheridan**, *Am. Mineral.* 73, 1038-1045 (1988).
5. **Veksler I. V., A. M. Dorfman, M. Kamenetsky, et al.**, *Geochim. Cosmochim. Acta* 69, 2847-2860 (2005).
6. **Roedder E. and D. S. Coombs**, *J. Petrol.* 3, 417-451 (1967).
7. **Andreeva I. A., V. I. Kovalenko, V. V. Yarmolyuk, et al.**, *Dokl. Akad. Nauk* 414, 528-534 (2007) [*Dokl. Earth Sci.* 414, 655 (2007)].
8. **Peretyazhko I. S. and E. A. Savina**, *Petrologiya* 18, 237-256 (2010).
9. **Civetta L., M. D'Antonio, G. Orsi, et al.**, *J. Petrol.* 39, 1454-1487 (1998).
10. **Solovova I. P., V. B. Naumov, V. I. Kovalenko, et al.**, *Dokl. Akad. Nauk* 297, 1449-1452 (1987).
11. **Lowenstern J. B.**, *Am. Mineral.* 79, 353-369 (1994).
12. **Kuehner S. M. and A. J. Joswiak**, *Am. Mineral.* 81, 229-237 (1996).
13. **Linthout K. and W. J. Lustenhouwer**, *Mineral. Mag.* 57, 289-299 (1993).
14. **Webster J. D.**, *Contrib. Mineral. Petrol.* 104, 424-438 (1990).
15. **Kotel'nikova Z. A. and A. R. Kotel'nikov**, *Geokhimiya*, No. 1, 54-68 (2008) [*Geochem. Int.* 46, 48 (2008)].

GEOLOGY, PETROGRAPHY AND MINERALOGY OF THE ZARYA PIPE KIMBERLITES

Spetsius Z.V.¹, Polyanichko V.V.², Xarlamova E.I.¹, Tarskix O.V.¹, Ivanov A.S.³

¹*Scientific Investigation Geology Enterprise (NIGP), "ALROSA" OJSC, Mirny;*

²*Amakinskaya geological prospecting expedition, "ALROSA" OJSC, Mirny;*

³*Botuobinskaya geological prospecting expedition, "ALROSA" OJSC, Mirny*

The paper summarizes the available data on the chemical composition, petrography and mineralogical characteristics of kimberlite rocks from the Zarya pipe. There have been used the original data for the investigation of the content and distribution of the debris of sedimentary rocks and ultramafic xenoliths in kimberlitic core from exploration bore holes, the presence of olivine and pseudomorphoses by them as well as autolytic formations in different varieties of kimberlites. It shows results of the study chemistry of kimberlite rocks and content of minerals as composition of the bulk according to the X-ray study of groundmass.

Petrography and mineralogical evidences suggest that the kimberlites of the Zarya pipe are characterized by relatively low content of indicator minerals with the predominantly garnet indicator minerals association, predominance of crimson pyropes lherzolite paragenesis, low frequency of occurrence titan rich garnets, two types of the compositions ilmenites and very low content of chromites. It can be to believe that these parameters are characteristic of the relatively low diamonds grade kimberlite body.

Research results of garnets chemistry and data on the ratio of eclogitic and peridotitic paragenesis of garnets, in the concentrate of this pipe, given the number of paragenetic associations diamond paragenesis show low occurrence of eclogitic garnets among the indicator minerals. It shows a low contribution of eclogitic paragenesis diamonds in diamond population of this pipe that, in our opinion causes low content and quality of diamonds from the Zarya pipe.

INTRODUCTION AND GEOLOGICAL WORKS OBSERVATIONS

The Zarya pipe is located in Alakit-Markha kimberlite field within the area of Aikhal mining processing of «ALROSA» OJSC. The Zarya kimberlite pipe is located on the distance 5 km from Aikhal town and is a steeply dipping body with sharp contacts with the host rocks. Zarya pipe was discovered in 1973 when there were conducted exploration works on the network 500×500 m by geologists Amakhinsky geological exploration expedition under the guidance of I. Y. Bogatyh. In the same time, it was delineated on the network bore holes 160x80 m and opened to a depth 50 m. According to a non-representative core sampling it was established it's miserable diamond grade. There is no data in the literature on the geology of this kimberlite pipe; its description is not given even in the monograph of the overview of kimberlite deposits [6] that prompted us to prepare

this article.

In 2007 within the exploration object Sokhsolooch-Markha by the Amakhinsky geological expedition on the Zarya pipe was carried out additional testing of kimberlites with the using of large diameter drilling, whereby representativeness of kimberlites grade testing significantly increased, average weight of samples was 260-450 kg. Wherein within the limits of pipe was identified central ore body with rather high diamond content (0.2 ct/t). According to the drilling data it is found that the pipe size is 410x255 m, and the size of a central ore body – 410× (150-100) m.

In connection with the fact that the kimberlite Zarya pipe is considered by the «ALROSA» company as an additional source of mining ores after working off Komsomolskaya pipe, it have been decided to continue the study its morphology and diamond grade. In 2009-2012 was continued study of the Zarya kimberlite pipe geology. Search and evaluation works carried out Amakhinsky geological expedition by the network of bore holes 80×40 and 40×40 m with the deepening them to kimberlites 300-400 m (to horizon +200 ÷ 100 m). Carried out work is confirmed by a central ore body and two phases the introduction of kimberlite. According to the research carried out geologists Amakhin geological exploration expedition, kimberlites I phase of the introduction is predominantly porphyritic kimberlites and central pillar body complex mainly autolytic kimberlite breccias. Average diamond content in the ore body, according to testing, is 0.24 ct/t, and porphyritic kimberlites – 0,05 ct/t. According drilling data it is found that the pipe size is 465x260 m and ore body - 350-160 m.

GEOLOGY OF THE ZARYA KIMBERLITE PIPE

The Zarya kimberlite pipe has ellipsoidal form in plan. It is stretch northeast on azimuth 56°. The particularities of the geological construction of this pipe are reflected on the schematic plan and section (Fig. 1). The Zarya kimberlite pipe completely overlapped thick layer of the rocks presented by the dolerites and tuffs with the large blocks of sedimentary rocks of the aykhalsky suite. The average thickness of overlaying rocks is 103 m. Surface of the ore body under overlaying rocks not even, but slightly wavy, northwest flank of the pipe is elevated comparatively south-east on 7 - 16 m. Pipe size under overlaying rocks is 465 × 260 m (fig. 1a). With the depth ore body becomes of nonsymmetrical dumbbell form with the expansion in northeast part and its size is powerfully decreases. The ore body is built by the autolytic kimberlite breccias and porphyritic kimberlites. Autolytic kimberlite breccias form the central ore body and intruding the porphyritic kimberlites. The industrial interest presents only central ore pole.

According to the data of geologists from the Amakhinsky expedition V.V. Ivanov and F.F. Tyurin (2012), contacts of ore body with surrounding rocks are clear and sharp. The fall angles of the ore body vary over a wide range: in northwest part corner of the pipe fall angles are vary from 55 - 65° to 76° - 82° for the horizon +400 - +350 m and between horizons +300 - + 350 m they plateau up

+400 - +350 m and sub vertical below these level. The south-west board of the ore body is characterized by the sub vertical contacts ($82 - 84^\circ$) till horizon +400 m and below horizon +300 m and plateau angles $-48^\circ - 52^\circ$ between horizons +400 - +300 m. The northeast board of the ore body falls to the center of the pipe at the angle 86° till horizon +360 m and below this level fall angles inverse to the center of the pipe and become $67^\circ - 76^\circ$. In kimberlites close of contact zones are noted xenoliths of surrounding carbonate rocks by the size from the first meters up 10 x 30 m that are most characteristic for the south-west part of ore body. In ore pole, except rare debris surrounding rocks exist cut-in a porphyritic kimberlites with the size from the first meters up to 35 m. In the contact zone of kimberlite body with containing rocks are noted zones of the crushing carbonate rocks from the first meters up to the tenth of the meters. In these zones are noted kimberlite veins from 1.2 m up 8.8 m. In most cases zones of the crushing and deformation are connected with the horizons of limestones and marls of the lower Silurian baytahsky suite or to dolomite horizon of the lower Ordovician oldodinsky suite. As a whole, surrounding rocks in zone of the contact with the kimberlite body are characterized by raised fracturing and presence of mirror slides; there quite often are noted calcification and sulphidization of rocks.

As it was noted above, the Zarya kimberlite pipe is built by two kimberlite types that are formed on different stages of its formation and are differ on the level diamond grade and contents to heavy faction. On the first stage were formed the low grade porphyritic kimberlites that composing northwest, south-east and south-west flanks of the ore body and on the second stage were formed industrial diamond grade Autolytic kimberlite breccias of the central ore pole. The contacting hybridization zone between these types of kimberlitic rocks is accompanied by elevated content of xenogenic material.

Autolytic kimberlite breccia's and porphyritic kimberlites greatly differ on their diamond grade, the content of diamonds in the first is nearly in 4 times above than in the second and content of heavy fraction minerals on 13% above.

PETROGRAPHY OF KIMBERLITES FROM THE ZARYA PIPE

Petrographic features of kimberlite, executing the Zarya pipe, is based on result of the study 180 samples, selected from the core of thirty nine exploration bore holes.

The Zarya kimberlite pipe is built by two petrographic types of kimberlitic rocks: porphyritic kimberlites (PC) and autolytic kimberlite breccias (AKB) with broad variations forming their component (Table 1). Kimberlite of the Zarya pipe inherent certain image blur of the structured signs, there are no clear contacts of the rockforming minerals with the groundmass that was noted on sections of all bore holes. Particularly this image blur reveals itself in surface zones that vastly obstruct the count of rockforming components; with the depth the drawing of rocks becomes more distinct.

Table 1.

Component composition of kimberlite rocks from Zarya pipe (the results of calculation of components in core, line.%)

№	Xenoliths			Sferotakskity	Garnet	Ilmenite	Pseudomorphoses after olivine				
	Sedimentary rocks	Ultra basic rocks	Metamorphic rocks				Total content	Grain size, mm			
								1-2	2-4	4-8	8-16
1	2	3	4	5	6	7	8	9	10	11	12
Porphyritic kimberlite											
1	3,74	5,62	0	0	0,79	0,63	26,19	8,89	11,62	5,18	0,5
2	3,73	0	1,34	0	0,19	0,39	25,8	8,65	10,45	4,35	2,35
3	7,26	0	0,83	0	0	0,45	19,49	7,32	7,59	3,32	1,26
4	0,28	1,55	1,94	0	0,28	1,21	16,38	4,3	5,35	3,31	3,42
5	8,29	0	1,05	0,29	1,35	0,48	19,48	5,72	7,58	5,13	1,05
6	1,4	0	13,08	0	0,49	0,25	21,36	8,1	9,68	2,52	1,06
7	4,87	2,44	0	0,09	0,45	0,41	15,01	6,49	6,6	1,61	0,31
8	2,02	0	3,11	0	0,15	0,34	24,36	7,58	9,8	5,6	1,38
9	1,91	7	0	0	0,07	0,57	25,22	7,79	13,65	2,77	1,01
10	2,01	0	1,72	0	0,58	0,58	25,63	7,21	9,66	6,52	2,24
11	4,89	1,22	8,53	2,71	0,92	0,57	25,32	9,47	9,37	6,48	0
12	6,84	0	2,65	0	0,63	0,37	20,06	6,64	8,63	2,49	2,3
13	5,38	0,3	2,49	1,61	1,67	1,66	25,17	9,66	12	3,51	0
14	11,83	0,56	0,31	0	1,26	0,23	26,28	11,59	9,62	4,49	0,58
15	3,21	0	3,35	0,4	0,18	1,28	23,64	6,51	8,6	5,32	3,21
Autolitic kimberlite breccia											
16	24,48	0	0	18,87	0	0,21	10,37	4,69	4,04	1,64	0
17	6,1	0,75	6,9	2,12	0,54	1,04	24,12	8,33	10,12	2,55	3,12
18	29,5	0	0	12,24	0	0,32	13,56	3,41	5,65	3,5	1
19	7,39	0	2,36	0	0	0,37	27,44	9,29	9,06	7,62	1,47
20	2,1	0	0	33,57	0	0,11	2,37	1,19	1,18	0	0
21	5,09	0	0	3,06	0,29	0,31	14,02	7,47	6,55	0	0
22	41,08	0	0	0	0	0,28	12,93	5,41	5,18	2,34	0
23	15,08	0	0,35	19,5	0	0,15	19,74	5,78	8,73	4,33	0,9
24	26,98	0	0	13,4	0	0,75	14	7,5	5,35	1,15	0
25	36,01	0	0	11,19	0	0,25	16,76	6,19	5,97	4,6	0
26	14,3	0	0	8,19	0,33	0,73	15,21	5,54	5,99	2,48	1,2
27	10,15	0	1,2	5,84	1,39	0,56	18,64	7,06	7,74	3,84	0
28	22,82	0	0	6,26	0	0,35	15,06	5,38	6,47	3,21	0
29	42,08	0	0,96	0	0,2	0,36	11,19	4,97	4,28	1,35	0,59
30	8,26	0	0	1,39	0,43	0,61	21,92	6,92	8,19	5,28	1,53

Porphyritic kimberlites present itself rocks of gray and light-gray colour, sometimes with pale-blue or brown tones. The structure is fine- and middle-

porphyritic, texture massive and fluidal in some places. Coarse-grained porphyritic kimberlites, characterizing dominating amount of olivine pseudomorphoses with the size up to 5 mm, are presented only in single samples. The olivine separations are completely serpentized and have oval, angular-round and much seldom angular form. Their contents vary from 13 to 38%, at the average content is 23 %. Distribution of phenocrysts in the rocks is comparatively even. Serpentine pseudomorphoses sharply stand out on the background of the kimberlite matrix and are executed light-, dark-green and light-brown serpentine. On the place of some phenocrysts are noted emptiness's and cavities of serpentine dump leaching, which are safe in the manner of serpentine rinds on the sides of the emptiness's. Pseudomorphoses on II generation of olivine that are <1 mm in size by their composition similar to pseudomorphoses of the first generation. In the majority they are oval and are executed the same serpentine. Variation in the contents of pseudomorphoses and the other components are rather essential (see table 1).

The porphyritic kimberlites are characterized by of low content of xenogenic material that is presented by the single debris of sedimentary rocks (on average 4 %) and xenoliths of crustal and very seldom of the mantle rocks (0.6 %). Their distribution is uneven as on separate samples as on the different bore holes (fig. 2a). The average content of metamorphic rocks xenoliths in porphyritic kimberlites is 0.98%. Basically, these are small single debris, diameter which does not exceed 1 cm.

Autolytic kimberlite breccias, composing given pipe are presented by the rocks gray in color, containing at the average 11% of the sedimentary rocks debris. In majority, these debris are of the oval or angular-rounded forms dark- and light-gray (less dark-green) of the color and are presented by carbonate-clay rocks that vary in sizes from 0.5 to 2-3 cm; portioned in kimberlite breccia comparatively evenly. The texture of the rocks in a whole is brecciated and of kimberlitic cement is fine- or middle-porphyritic. The ball texture of the ground mass is displayed enough clearly, spheroidal shells are situated on peripheries of pseudomorphoses and debris of the sedimentary rocks in the manner of small spherical isolations fine-grained constructions and variable power, more dark of the color, than the main matrix and comprises of itself pseudomorphoses on olivine II generation. Pseudomorphoses by olivine of the I-st generation are basically executed greenish-gray and brown serpentine and subordinated calcite. Their contents noticeably lower in contrast with porphyritic kimberlites and forms at the average about 18 %. Most clearly difference of the described types of the rocks is tracked in contents of pseudomorphoses by olivine and debris of the sedimentary rocks (fig. 2a).

The clear difference between PC and AKB exists in the same way and in percent ratio of olivine (pseudomorphoses) of different sieve classes (fig. 2b). Amount of grains class 1-2mm always dominates in porphyritic kimberlites, at the average forming 56 % (in the calculation of total olivine 1 generation content in size > 1 mm in every sample was taken for 100 % and, thereby, did not depend on the other rocks forming components). The olivine content of class 4-8 mm in AKB

is low than such in PC. The constancy of the olivine different sieving class relations within one petrographic kimberlite type, probably, is conditioned its genetic individuality, reflecting thermodynamic conditions of crystallizations.

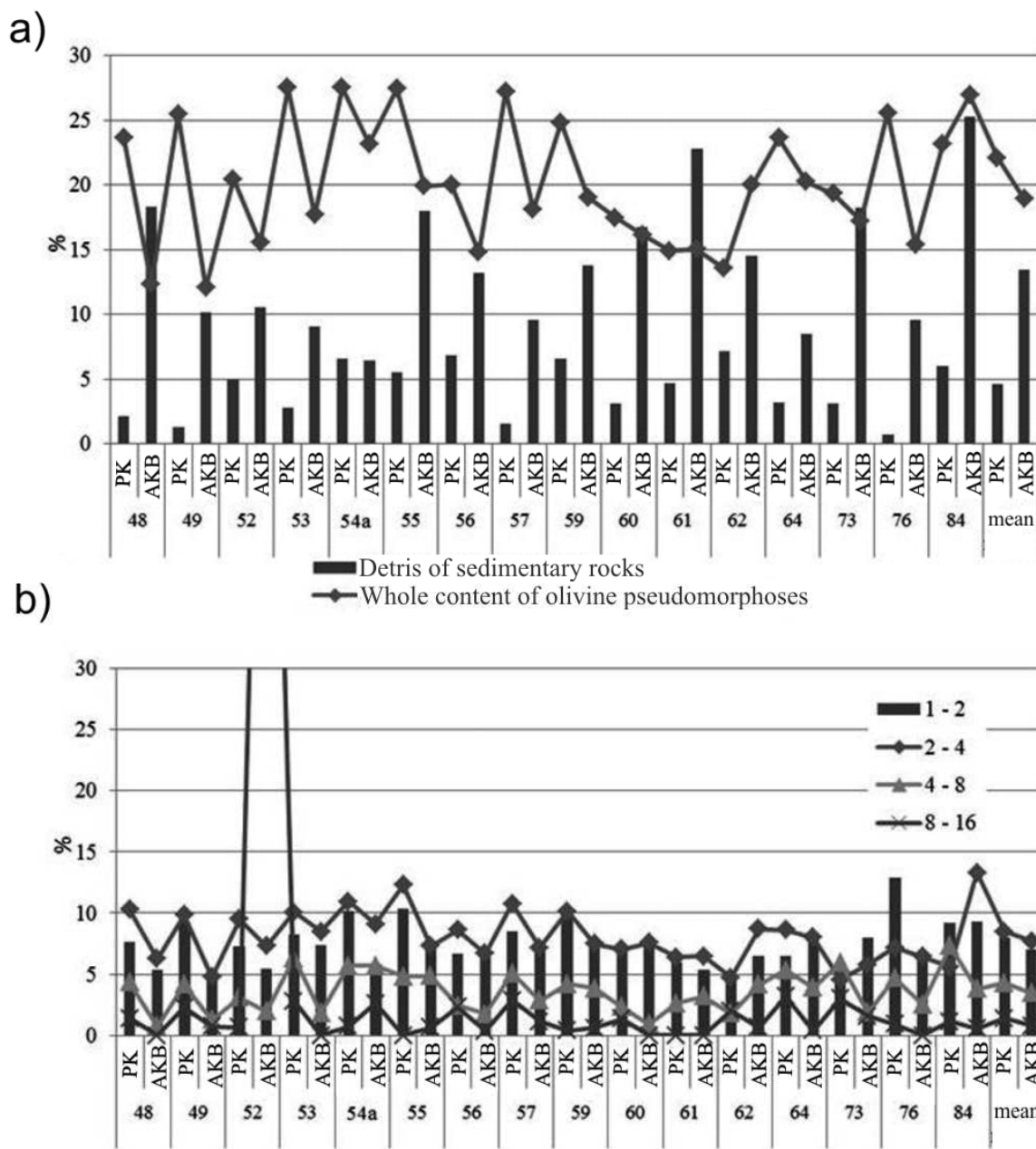


Fig. 2. Distribution of sedimentary rock debris and olivine pseudomorphoses in kimberlites of the Zarya pipe.

a) on separate bore holes, in PK and AKB, b) distribution olivine pseudomorphoses in different sieving classes.

The difference in olivine relations between different kimberlite types, probably, is indicative of difference in T-conditions of the diverse stages of kimberlite formation, and on a certain deficit of olivine (MgO) component in the final intruding phases. The stable proportion in contents of different sieve class

olivine is one of the most stable sign, which is kept practically in all studied pipe. This relation can serve priority at the typification of kimberlite rocks and dividing of different intruding phases.

PARTICULARITIES OF THE CHEMICAL COMPOSITION OF THE ZARYA PIPE KIMBERLITES

The chemical composition the Zarya pipe kimberlites was analyzed on the same samples, on which was realized macro petrographic analysis of the rocks (105 samples was analyzed). The results of the chemical studies of the kimberlitic groundmass of the Zarya pipe have shown that porphyritic kimberlites are characterized by increased FeO content and raised contents of oxides TiO_2 and P_2O_5 , in contrast with autolytic kimberlite breccias. For the explored samples are typical broad variations of chemical composition even within one petrographic kimberlitic type, as evidenced by data (table 2) and corresponding graphic construction (fig. 3). The maximum contents of silica noted in autolytic kimberlite breccias of the bore holes 54a, 62, 64 and in porphyritic kimberlites bore holes 55, 56, 57, 59. As a rule, for these samples are typical also raised contents of magnesium and lowered contents of calcium. The MgO content is broadly vary in different samples and separate bore hole in porphyritic кимберлитах and, particularly, in autolytic kimberlite breccias (refer to fig. 3), under similar average contents - 23 wt. % MgO.

It should be noted comparatively high TiO_2 content of kimberlitic rocks of the Zarya pipe. The maximum contents of titanium oxide is noted in porphyritic kimberlites from bore holes 53 and 57 (up to 1.9 wt. % TiO_2), as well as in autolytic kimberlite breccias of the bore holes 60 and 62 (up to 3.2 wt. % TiO_2). The average contents of TiO_2 are close in both types of the rocks and form 1,6 wt. % TiO_2 in porphyritic kimberlites and 1.5 wt.% - in autolytic. Raised TiO_2 content of kimberlites is a negative factor for their diamond grade and is indicative of aggressive nature corresponding to upstanding kimberlite magma [1, 8] that usually conditioned of the presence of corroded and rounded crystals in diamond product. It should be emphasize that high grade pipes, as a rule, differ by the lowered TiO_2 content of kimberlites [6, 8].

For both kimberlite types of the Zarya pipe is typical nearly alike average content of Fe_2O_3 (6.4 wt. %). The maximal Fe_2O_3 contents are noted in porphyritic kimberlites bore holes 55, 54a and autolytic kimberlite breccias of the bore hole 54a, reaching up to 9.5 wt. %. The maximal content of the aluminum oxide is noted in kimberlite of the bore hole 61 (autolytic breccia) and 62 (porphyritic kimberlite), at the average it is slightly higher in the autolytic breccias. For studied kimberlites it is typical very narrow variations in manganese contents. Particularly uniform distribution of manganese is fixed in porphyritic kimberlites, standard deviation make up 0.01 wt. % MnO.

Table 2.

Chemical composition of kimberlites from Zarya pipe (wt. %)

N ₂	SiO ₂	TiO ₂	Al ₂ O ₃	Fe ₂ O ₃	MnO	MgO	CaO	Na ₂ O	K ₂ O	P ₂ O ₅	Ppp	Total
Autolytic kimberlite breccia												
1	21,0	1,2	2,9	5,6	0,1	18,3	24,0	0,0	0,3	0,2	26,3	99,9
2	27,0	1,4	1,3	5,8	0,1	26,8	15,8	0,1	0,1	0,3	21,9	100,7
3	23,2	1,7	2,6	8,5	0,1	21,7	18,7	0,1	0,6	0,5	22,3	100,2
4	25,8	1,5	1,3	7,0	0,1	25,1	16,4	0,2	0,4	0,3	22,6	100,8
5	16,8	2,0	3,0	11,7	0,1	13,5	24,8	0,0	0,6	0,7	26,5	99,7
6	24,4	1,0	1,4	6,0	0,1	22,6	21,6	0,0	0,5	0,4	22,3	100,3
7	24,6	2,2	3,0	9,2	0,1	23,6	15,9	0,2	0,4	0,7	20,5	100,3
8	22,6	1,3	1,9	4,3	0,1	19,7	22,7	0,0	0,3	0,5	26,9	100,4
9	30,8	3,0	3,1	8,7	0,2	32,9	5,3	0,3	0,0	0,8	15,3	100,4
10	24,3	1,0	2,9	5,9	0,1	18,9	20,9	0,0	0,1	0,4	25,6	100,0
11	23,9	1,2	2,3	5,2	0,1	20,1	21,0	0,1	0,1	0,2	25,9	100,1
12	21,1	0,7	3,9	4,4	0,1	22,3	21,5	0,1	0,3	0,3	26,1	100,7
13	27,5	1,4	1,7	4,1	0,1	29,3	14,3	0,3	0,2	0,3	21,5	100,7
14	24,6	1,8	2,7	6,5	0,1	31,0	10,1	0,4	0,7	0,5	22,6	101,0
15	20,3	0,9	2,8	4,1	0,1	20,5	22,8	0,1	0,6	0,3	27,8	100,4
16	25,6	1,8	2,9	5,7	0,1	24,3	16,7	0,2	0,5	0,4	22,4	100,5
17	23,8	1,5	1,2	7,1	0,1	20,6	21,0	0,1	0,0	0,2	25,0	100,6
18	22,5	0,9	1,0	5,9	0,1	19,3	23,2	0,0	0,1	0,2	27,2	100,5
19	25,4	1,3	1,9	5,6	0,1	25,9	17,1	0,2	0,3	0,4	22,8	100,9
20	22,6	1,7	2,3	5,1	0,1	15,6	25,1	0,0	0,4	0,6	25,9	99,4
Porphyritic kimberlite												
21	24,7	0,3	4,5	4,2	0,1	20,9	19,7	0,2	0,1	0,1	25,3	100,3
22	28,3	1,8	2,0	7,5	0,1	24,8	14,0	0,3	0,5	0,5	20,0	99,8
23	23,9	1,6	2,0	5,9	0,1	21,0	19,8	0,3	0,6	0,5	24,4	100,2
24	28,0	1,6	1,7	7,5	0,1	27,0	13,5	0,3	0,5	0,3	20,0	100,5
25	29,3	1,7	1,9	8,2	0,1	25,7	13,3	0,3	0,3	0,4	19,6	100,8
26	26,9	1,5	1,8	7,5	0,1	26,6	14,7	0,3	0,3	0,5	20,2	100,4
27	24,3	2,0	3,7	6,5	0,1	20,5	19,2	0,3	0,8	0,6	22,2	100,2
28	27,1	2,0	1,7	9,2	0,1	27,9	12,2	0,2	0,5	0,4	19,2	100,6
29	22,9	2,0	1,9	9,3	0,1	21,1	19,0	0,1	0,2	0,5	23,5	100,6
30	23,2	1,0	2,3	4,1	0,1	21,2	21,8	0,0	0,1	0,4	26,1	100,4
31	23,2	1,5	2,0	4,1	0,1	22,7	20,8	0,2	0,3	0,6	24,9	100,3
32	22,3	1,7	2,8	5,3	0,1	15,2	25,0	0,0	0,8	0,8	25,9	100,0
33	23,7	1,3	1,4	3,9	0,1	22,8	20,2	0,2	0,1	0,1	26,5	100,4
34	24,4	1,6	1,9	8,1	0,1	24,0	17,1	0,2	0,5	0,6	21,7	100,3
35	23,2	1,6	2,6	8,1	0,1	20,4	19,3	0,2	0,4	0,5	23,8	100,3
36	27,6	2,0	1,8	5,3	0,1	27,5	14,3	0,2	0,2	0,4	21,2	100,8
37	20,3	2,0	2,0	6,9	0,1	18,3	23,7	0,1	0,1	0,7	26,2	100,4
38	28,7	1,9	1,8	7,6	0,1	31,6	9,0	0,3	0,3	0,5	18,8	100,6
39	26,4	1,2	1,7	4,9	0,1	23,3	18,3	0,1	0,2	0,4	24,0	100,7
40	24,0	1,8	1,8	5,7	0,1	22,4	19,4	0,2	0,1	0,6	24,2	100,6

Note. Chemical analysis of kimberlite samples are made in Institute of geology and mineralogy SB RAS (Novosibirsk) under the guidance of V.B.Vasilenko on the X-ray fluorescence analyzer BRA-20R.

It is possible to note the higher sodium contents in porphyritic kimberlites (the average content Na₂O – 0.2 wt. %) in contrast with breccias (0.1 wt. %). For

studied samples of AKB is characteristically raised potassium contents, maximal contents of potassium are noted in autolytic breccias of the bore hole 61, which are obliged this to the presence of phlogopite in the composition of the ground mass. The raised contents of phosphorus are also typical for AKB type.

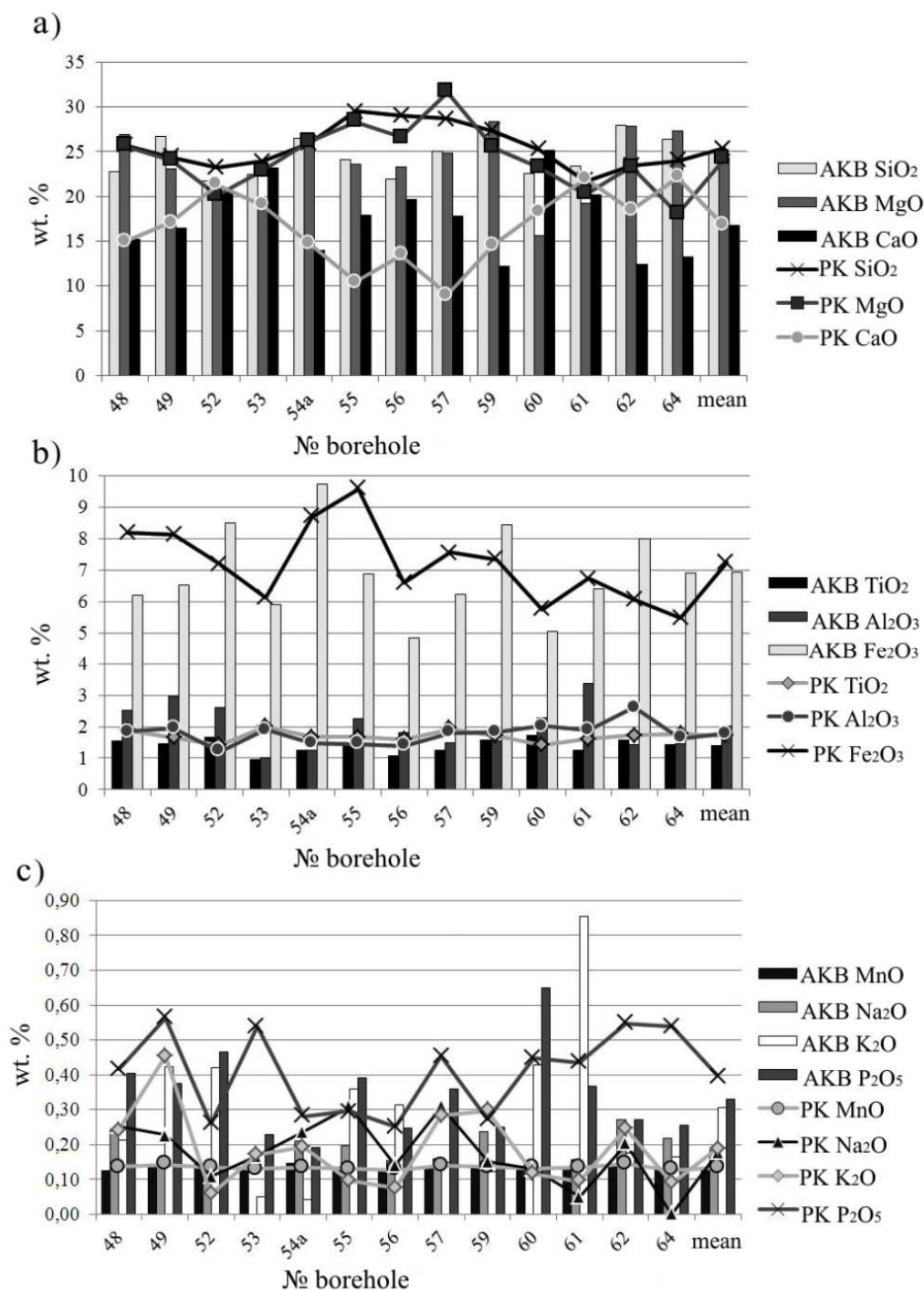


Fig. 3. Variations of the kimberlite chemistry in bore holes and types of the rocks from the Zarya kimberlite pipe.

There exists the well-marked negative correlation between contents of oxide magnesium and calcium, which is noted for kimberlitic rocks of the majority pipes

of the Yakutian province [8]. For PK are typical raised contents of silicon and magnesium and lowered - calcium. Also for this type of the rocks is typical raised content of titanium and ferric and lowered of the aluminum oxide. For the AKB are typical raised contents of potassium and phosphorus in contrast with porphyritic kimberlites.

The broad variations in PK and AKB rocks of calcium contents can be explained by the difference in degree of the rocks carbonatization (see table 2), raised contents of titanium are probably connected with broad manifestation of ilmenite and titan magnetite in the kimberlite matrix. Thereby, coming from available data on the rocks chemistry, an AKB is more perspective in respect of diamondiferousity in comparison with the PK that corresponds to their testing results.

The essential differences in the chemistry of kimberlitic rocks from different bore holes and their varieties are confirmed by the difference in the mineral composition of their ground mass and comparatively broad variations of the main minerals concentration such as serpentine, calcite and chlorite even in samples selected from different depths of one the same bore holes (table 3). From these tabular data it is obvious raised variability of minerals distribution in AKB and more intensive degree of their carbonization.

MINERAL PARTICULARITIES OF THE ZARYA PIPE KIMBERLITES

Indicator minerals of this pipe are presented mainly by picroilmenite (the average contents 2.7 kg/t) and garnet (430.5 g/t); there are met rater less content of chromespinelides and noted single grains of chrome-diopside.

The **garnets** content in different core samples varies over a wide range. For kimberlite bore hole 7A the range of the fluctuations forms 50 - 6610 g/t (average 481 g/t), for the bore hole 9A: 100-2130 g/t (average 313 g/t).

The garnets in studied samples (12346 grains) are presented by grains with size $-5+0.5$ mm, dominates sieving class $-1+0,5$ mm. Garnets are characterized by low degree of wholeness, in studied sample dominate the debris (49.9%), broken off grains (11.0%), damaged (0.6%), splinter (38.3%). In studied samples dominate orange-red garnets (34.8%), on the second place on frequency are violet garnets (27.7%). The form of the garnet most often angular, noted also angular-round and round grains. Garnet grains with the crystallographic relic forms are not found.

On garnets surfaces are fixed two main types of the relief: endogenic matting (53.3%) and pyramid- tiled relief of the dissolution (45.9%). The garnets with inclusions in studied samples make up 15.0%, amongst them dominated garnets with plural inclusions, most often garnets with inclusions meet amongst red garnets. Most often inclusions have needle and rounded forms, they are presented mainly by rutile and other ore minerals.

Table 3.

Mineral composition of kimberlites from the pipe Zarya (%)

№	Olivine	Serpentine	Phlogophite	Chlorite	Talc	Smectite, saponite	Calcite	Dolomite	Anatase	Apatite, halite	Magnetite	Hematite, pyrite, perovskite	Quartz	Mica	Spinel
Autolytic kimberlite breccia															
1	0	13	0	4	0	0	83	0	0	0	0	0	0	0	0
2	0	14	0	0	0	0	5	75	4	0	2	0	0	0	0
3	0	7	0	1	0	0	72	20	0	0	0	0	0	0	0
4	2	19	0	3	0	0	74	0	0	1	3	0	0	0	0
5	0	21	0	5	0	0	70	0	0	0	2	0	2	0	0
6	0	13	3	1	1	0	76	1	0	0	1	0	4	0	0
7	1	19	3	1	0	0	73	0	0	2	2	0	0	0	0
8	0	18	6	2	0	0	69	0	0	1	1	0	3	0	0
9	0	26	1	5	0	0	65	0	0	0	2	0	1	0	0
10	0	3	43	4	0	0	46	0	0	2	2	0	0	0	0
11	0	31	8	8	0	0	49	0	0	0	4	0	0	0	0
12	2	42	7	4	0	0	42	0	0	0	4	1	0	0	0
13	0	9	2	4	3	0	80	0	0	1	0	1	0	0	0
14	0	17	0	0	0	0	82	0	0	1	0	0	0	0	0
15	0	23	1	0	0	0	28	47	0	1	0	0	0	0	0
16	0	35	4	4	0	0	40	0	2	2	2	2	9	0	0
17	0	50	0	0	0	9	41	0	0	0	0	0	0	0	0
18	0	65	0	0	0	0	35	0	0	0	0	0	0	0	0
19	0	56	0	8	0	0	21	0	0	0	0	0	4	11	0
20	0	56	0	0	0	0	13	30	0	0	0	0	0	0	0
Porphyric kimberlite															
21	1	14	0	2	0	0	82	0	0	1	1	0	0	0	0
22	0	17	0	2	0	0	77	0	2	1	0	1	0	0	0
23	0	14	0	7	0	0	73	0	3	0	2	1	0	0	0
24	0	29	0	9	0	0	60	0	0	0	2	0	0	0	0
25	0	88	0	0	0	0	12	0	0	0	0	0	0	0	0
26	0	52	0	17	0	10	21	0	0	0	0	0	0	0	0
27	0	74	0	0	0	0	25	0	0	1	0	0	0	0	0
28	0	61	0	7	0	0	30	0	0	0	0	0	0	2	0
29	0	58	0	0	0	5	28	0	0	0	0	9	0	0	0
30	0	54	0	14	0	6	23	0	0	2	0	0	0	1	0
31	0	39	0	17	0	0	42	0	0	1	0	0	0	1	0
32	0	79	0	0	0	0	21	0	0	0	0	0	0	0	0
33	0	73	0	2	0	0	25	0	0	0	0	0	0	0	0
34	0	13	0	1	0	0	74	0	0	2	0	0	1	6	3
35	0	22	0	5	0	0	73	0	0	0	0	0	0	0	0
36	0	6	0	3	0	0	88	2	0	1	0	0	0	0	0
37	0	12	0	1	0	0	75	0	0	0	0	0	0	12	0
38	0	11	0	0	0	0	89	0	0	0	0	0	0	0	0
39	0	10	0	2	0	0	83	0	0	0	0	0	0	5	0
40	0	11	0	8	0	0	78	0	0	3	0	0	0	0	0

Note: X-ray analysis of the groundmass of kimberlite rocks determined on diffractometer DRON-2 in NIGP "ALROSA" OJSC, Mirny. Analytical conditions: Cu K α - emanation, V=40 kv, J=20 mA, analyst: Liskovaya L.V.

On garnet grains are fixed coats and kelephytic rims of the different composition and thickness, most often relics of coats are noted on violet garnets. The coats are presented mainly serpentine-carbonate aggregates, kelephytic rims meet seldom.

It was determined the chemical composition of 157 garnets. The broad scatter is fixed in contents окислов MgO, CaO, FeO and Cr₂O₃ (table 4). On chemical composition among studied samples dominate the garnets of lherzolite paragenesis (69.7 %).

The garnets of the lherzolite paragenesis on accordance with D. Dowson and V. Stephens [2] are characterized broad variations of the chemical composition, amongst them most widespread are the high titanium pyropes (46.2 %), and on the second place on frequency are titaniferous pyropes (33.3 %). Low calcium chrome pyropes compose 14.8% amongst the garnet lherzolites, uvarovite-pyropes – 3.7 %. The rarest are calcium pyrope-almandines.

The garnets of eclogitic paragenesis compose 17.4 % among the studied samples and are presented by magnesian almandines (92.6 %), titaniferous pyropes (3.7 %) and calcium pyrope-almandines (3.7 %). The diamond association garnets compose 7.4 % from all amount of eclogitic garnets and are presented titaniferous pyropes and calcium pyrope-almandines.

The dunite-harzburgite paragenesis garnets form 10.9% from the studied amount and are presented low calcium chrome pyropes (94.1%) and titaniferous pyropes (5.9 %). To the garnets of diamond association belong 7.7% from studied samples of this paragenesis (fig.4).

The rarest in studied sample are garnets of wehrlitic paragenesis (1.9 %). They are presented by titaniferous and uvarovite-pyropes (subsequently 33.3 % and 14 %).

Thereby, chemical composition of garnets from kimberlites is indicative of prevalence in the Zarya pipe of the ultramafic material on the eclogitic. High frequency of diamond association garnets of dunite-harzburgite paragenesis can be estimated as positive indicator-mineral sign of diamondiferousity. We should point that the garnets of the Zarya pipe are close to the garnets from the Sytykanskaya pipe as by distribution of different paragenises and by their diamond associations (see fig. 4).

Ilmenite is presented by separations -2+0,5mm in size. There are described 3800 grains. Ilmenite from the Zarya kimberlite pipe is presented mainly splinter (54.6 %), it is enough often meet the debris and broken off grain (30.7 and 12.1 % accordingly). In studied sample dominate angular-round grain (76.2 %), rather less are meet the angular forms (22.5 %).

There often are fixed coats of the different composition and thickness around ilmenites. The amount of grains with relic coats forms 78.8 % of the studied amount. The wide-spread coats are presented by the kimberlite matrix. On the ilmenite grains surface are noted two main types of endogenic relief: matting and aculeiform, the first is dominating (81.5 %).

Table 4.

Representative analyses of garnets from the kimberlite pipe Zarya

№	SiO ₂	TiO ₂	Al ₂ O ₃	Cr ₂ O ₃	FeO	MnO	MgO	CaO	Na ₂ O	NiO	Total
Garnets of eclogitic paragenesis											
1	39,63	0,19	22,06	0,05	18,28	0,36	11,01	8,32	0,12	0,01	100,03
2	38,62	0,09	21,66	0,02	27,62	0,66	9,00	2,32	0,03	0,03	100,04
3	39,28	0,01	22,06	0,08	24,10	0,44	12,07	1,94	0,05	0,01	100,04
4	38,98	0,09	21,43	0,09	27,03	0,58	9,16	2,70	0,00	0,00	100,05
5	38,62	0,08	21,77	0,07	24,87	0,51	11,93	2,12	0,04	0,00	100,01
Garnets of diamond association of eclogitic paragenesis											
6	39,63	0,19	22,06	0,05	18,28	0,36	11,01	8,32	0,12	0,01	100,03
7	41,45	0,36	22,44	0,19	10,09	0,28	18,84	6,27	0,07	0,04	100,03
Garnets of vherlrite paragenesis											
8	41,76	0,22	21,63	1,20	9,30	0,32	18,09	7,36	0,10	0,01	100,00
9	40,77	0,52	16,07	8,36	8,07	0,47	17,98	7,62	0,12	0,00	99,98
10	41,62	0,37	22,12	0,23	9,89	0,29	18,95	6,49	0,07	0,00	100,04
Garnets of dunite-harzburgite paragenesis											
11	41,32	0,44	18,32	6,00	7,73	0,46	21,33	4,24	0,12	0,00	99,96
12	42,06	0,00	20,85	3,71	7,53	0,43	23,75	1,67	0,01	0,00	100,03
13	42,05	0,06	19,25	5,56	7,00	0,40	21,57	4,05	0,07	0,00	100,02
14	41,76	0,02	19,28	5,43	7,05	0,41	21,99	3,96	0,07	0,00	99,97
15	41,73	0,06	19,32	5,59	7,20	0,41	21,60	4,01	0,06	0,03	100,02
Garnets of diamond association of dunite-harzburgite paragenesis											
16	41,24	0,04	14,91	11,24	7,59	0,45	22,82	1,62	0,04	0,00	99,96
17	41,12	0,00	14,76	11,53	7,65	0,49	22,67	1,66	0,00	0,00	99,88
18	41,37	0,01	15,01	11,06	7,66	0,44	22,67	1,80	0,00	0,01	100,02
19	41,32	0,21	16,47	9,35	6,85	0,41	20,29	5,04	0,05	0,00	100,00
20	41,76	0,02	19,28	5,43	7,05	0,41	21,99	3,96	0,07	0,00	99,97
21	41,47	0,18	15,62	9,97	7,00	0,48	21,00	4,27	0,08	0,00	100,07
Garnets of lherzolitic paragenesis											
22	41,77	0,31	20,83	3,08	8,00	0,38	21,43	4,11	0,04	0,02	99,97
23	42,08	0,66	21,23	1,49	7,95	0,27	21,95	4,29	0,04	0,01	99,97
24	41,77	1,10	19,19	2,43	9,81	0,36	20,30	4,85	0,12	0,01	99,93
25	42,27	0,39	21,93	1,15	8,86	0,39	20,97	3,94	0,05	0,00	99,94
26	42,04	0,34	19,86	4,19	6,86	0,36	21,76	4,44	0,09	0,02	99,96
27	41,53	0,34	15,69	8,72	7,33	0,32	19,84	5,97	0,08	0,03	99,84
28	40,38	1,34	13,85	9,59	8,19	0,38	19,14	6,92	0,07	0,00	99,87
29	42,18	0,24	19,18	4,78	6,93	0,36	21,68	4,55	0,04	0,01	99,96
30	40,94	1,45	14,21	9,00	7,77	0,36	19,71	6,50	0,05	0,00	99,98
31	41,99	0,56	20,42	2,39	7,90	0,32	21,89	4,46	0,07	0,00	99,99
32	41,73	0,22	20,33	4,15	8,34	0,47	19,64	4,97	0,07	0,00	99,91
33	40,74	1,30	14,11	9,49	7,44	0,34	19,46	6,86	0,09	0,04	99,87
34	40,81	0,41	14,45	10,56	7,63	0,47	18,57	6,86	0,14	0,00	99,89
35	42,35	0,54	21,22	1,73	8,21	0,30	21,52	4,02	0,05	0,03	99,97
36	42,31	0,69	19,86	2,57	7,56	0,30	22,02	4,61	0,10	0,00	100,02
37	41,57	0,77	17,81	5,12	7,68	0,30	21,14	5,54	0,03	0,04	99,99
38	41,28	0,97	16,89	6,17	8,46	0,26	20,56	5,28	0,07	0,01	99,95

Note: Analyses are carried out by using electron microprobe Superprobe JXA-8800R in CAL BGRE "ALROSA" OJSC, Mirny, analyst A.S. Ivanov.

There were determined chemical compositions of 119 ilmenite grains. As a result of studies is installed that ilmenite from kimberlites of the Zarya pipe is characterized by the narrow composition range and is presented by picroilmenite (the contents MgO are found within 7.8-12.5 wt.%), also for it is typical broad variations in content of Cr_2O_3 (table. 5).

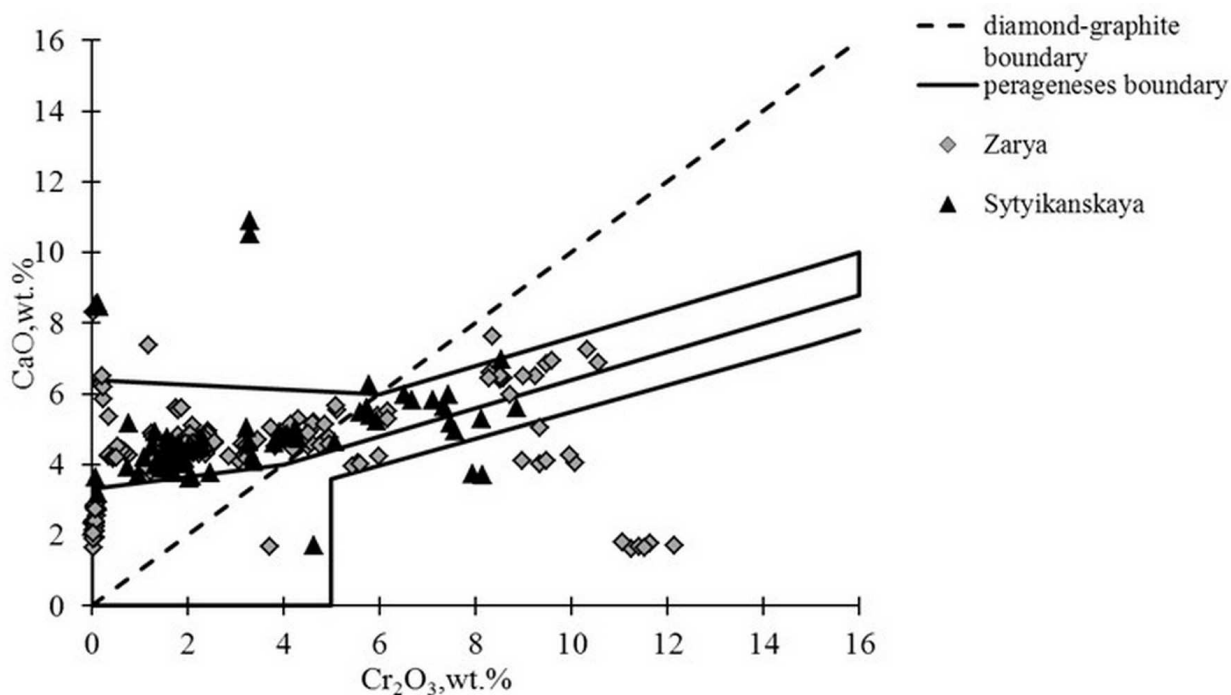


Fig. 4. Figurative composition points of garnets from the Zarya kimberlite pipe in coordinates Cr_2O_3 -CaO (accordingly [7]).

For a comparison garnets from the Sytykanskaya pipe concentrate are shown.

On diagram in coordinates Cr_2O_3 - MgO (fig. 5) figurative composition points displaced to the right left branch of the Haggerty parabola [3, 4]. Picroilmenite from kimberlites of the Zarya pipe is characterized broad variations of the of titanium and chromium contents and by raised content of manganese (refer to the table 5).

On diagram of J.Gurney [5] the figurative ilmenite compositions points are located in transition area, corresponding to the index 2-3 that answers to the high aggressive kimberlitic melt, accordingly, to middle degree of diamonds safety. It is necessary to note that in tested samples dominate grains with high content of ferric iron ($\text{Fe}_2\text{O}_3 > 26\%$ wt.%, table 5) that also suggests of raised aggressiveness of corresponding kimberlitic magma.

The chemical composition of garnet and ilmenite is indicative of the prevalence of ultramafic rocks on eclogitic substratum of the upper mantle under this pipe. As a whole, the indicator minerals association in the studied testing core samples is enough peculiar to the kimberlitic bodies of the Alakit-Marhinsky field.

Representative analyses of Ilmenite from the kimberlite pipes Zarya

№	SiO₂	TiO₂	Al₂O₃	Cr₂O₃	FeO	MnO	MgO	CaO	Na₂O	NiO	Total
1	0,00	49,77	0,39	0,88	40,27	0,27	9,13	0,01	0,04	0,06	100,81
2	0,00	49,51	0,45	0,90	39,91	0,25	8,96	0,05	0,07	0,08	100,17
3	0,02	48,86	0,43	0,90	39,98	0,31	9,15	0,00	0,00	0,09	99,75
4	0,05	50,75	0,75	2,35	33,46	0,25	11,81	0,03	0,04	0,22	99,72
5	0,02	48,99	0,52	0,91	39,88	0,26	8,81	0,01	0,00	0,09	99,48
6	0,02	49,27	0,39	1,03	40,18	0,26	8,92	0,00	0,07	0,07	100,21
7	0,01	48,66	0,44	1,12	40,13	0,26	8,60	0,00	0,00	0,04	99,27
8	0,04	50,33	0,50	0,47	36,78	0,24	10,63	0,00	0,00	0,08	99,06
9	0,02	51,26	0,58	0,97	34,18	0,36	11,66	0,02	0,00	0,12	99,16
10	0,01	46,01	0,19	4,60	40,71	0,27	7,98	0,00	0,00	0,11	99,87
11	0,01	49,60	0,47	0,92	39,68	0,31	8,86	0,01	0,04	0,05	99,93
12	0,07	49,05	0,47	0,91	39,78	0,26	9,31	0,00	0,14	0,03	100,02
13	0,09	49,26	0,52	0,95	39,49	0,27	9,60	0,01	0,11	0,13	100,40
14	0,06	49,19	0,49	0,87	39,05	0,29	9,02	0,00	0,07	0,09	99,12
15	0,00	49,25	0,45	1,01	38,75	0,29	9,33	0,01	0,08	0,05	99,21
16	0,04	50,38	0,41	1,89	35,90	0,31	10,40	0,03	0,01	0,11	99,48
17	0,04	49,17	0,47	0,92	39,32	0,31	8,82	0,01	0,03	0,03	99,12
18	0,05	49,81	0,47	0,96	39,90	0,30	8,76	0,02	0,00	0,03	100,29
19	0,05	48,28	0,56	0,82	40,22	0,36	9,39	0,05	0,07	0,05	99,85
20	0,03	50,85	0,53	0,48	36,88	0,27	10,64	0,02	0,00	0,04	99,74
21	0,04	47,51	0,33	2,75	41,19	0,32	7,97	0,00	0,01	0,10	100,20
22	0,02	48,50	0,43	2,05	40,91	0,29	8,19	0,02	0,00	0,14	100,54
23	0,04	49,31	0,48	0,93	39,57	0,30	8,97	0,01	0,02	0,09	99,71
24	0,05	49,52	0,45	0,99	39,71	0,26	9,12	0,00	0,08	0,08	100,26
25	0,03	49,15	0,43	0,89	39,82	0,34	9,06	0,02	0,06	0,07	99,85
26	0,02	49,40	0,41	0,94	40,09	0,28	8,83	0,00	0,00	0,05	100,01
27	0,03	49,45	0,47	0,98	39,83	0,25	9,03	0,01	0,15	0,07	100,27
28	0,05	49,04	0,55	0,82	38,93	0,28	9,88	0,04	0,00	0,06	99,64
29	0,00	48,09	0,37	1,71	40,83	0,30	8,48	0,01	0,00	0,13	99,92
30	0,04	49,11	0,47	1,03	40,50	0,30	8,86	0,01	0,03	0,08	100,43
31	0,01	48,80	0,47	1,02	39,99	0,31	8,77	0,00	0,06	0,09	99,50
32	0,06	52,36	0,56	0,49	35,81	0,26	11,28	0,03	0,09	0,07	101,00
33	0,00	51,08	0,43	3,51	32,33	0,31	11,81	0,01	0,00	0,15	99,64
34	0,04	50,34	0,60	5,05	31,81	0,23	11,90	0,04	0,07	0,15	100,23
35	0,05	51,81	0,66	0,60	34,87	0,26	11,38	0,06	0,07	0,10	99,86
36	0,02	48,58	0,44	1,36	40,25	0,38	8,71	0,01	0,05	0,10	99,91
37	0,02	50,88	0,50	2,84	34,75	0,30	10,47	0,00	0,02	0,26	100,04
38	0,01	49,34	0,47	0,70	39,06	0,29	9,22	0,00	0,02	0,10	99,20
39	0,02	50,65	0,44	2,82	34,39	0,36	10,89	0,01	0,13	0,19	99,90
40	0,04	50,34	0,60	5,05	31,81	0,23	11,90	0,04	0,07	0,15	100,23

Note: Analyses are carried out by using electron microprobe Superprobe JXA-8800R in CAL BGRE "ALROSA" OJSC, Mirny, analyst A.S. Ivanov.

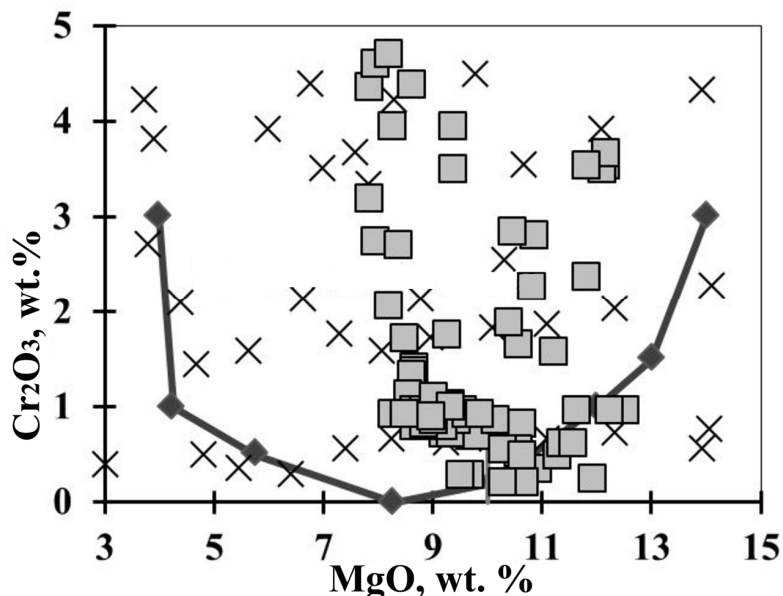


Fig. 5. Figurative composition points of ilmenites from the Zarya pipe in coordinate Cr₂O₃ - MgO (accordingly [3]).

By the crosses are marked the average compositions of statistical clusters of ilmenites that are divided on the data of 10000 analyses from different pipes.

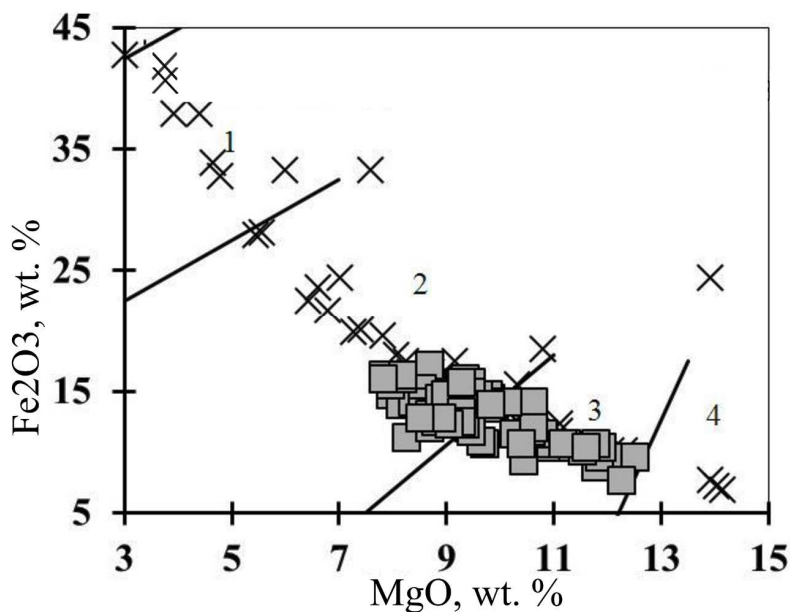


Fig. 6. The diagram of the ilmenite composition from the Zarya kimberlite pipe in coordinate Fe₂O₃ -MgO (accordingly [5]).

CONCLUSION

Findings by thereby, for kimberlites of the Zarya pipe are typical following features their material composition: a) a comparatively low contents of indicator minerals of the diamond, b) mainly garnet indicator mineral association, c) prevalence of lherzolite paragenesis garnets, d) high frequency of titaniferous

garnets, e) two types of ilmenite compositions, f) nearly full absence of chromespinelides, g) subordinated amount of eclogitic paragenesis garnets, including diamond association. It is possible to suppose that these parameters are typical for the low or middle grade kimberlitic pipes.

The garnet chemistry and data on ratio of eclogitic and ultramafic garnets in concentrate of the Zarya pipe with the provision for amount of corresponding paragenic diamond associations are indicative of low contents of the eclogitic type garnets among indicator minerals and, accordingly, about low contribution of eclogitic paragenesis diamonds in the whole diamond population of this pipe. On our opinion, this, as well as raised titaniferousness of kimberlites, wide abundance of titaniferous garnets and nearly full absence of chromespinelides explain the low content and comparatively low quality of the Zarya pipe diamonds.

In conclusion, consider its pleasing debt to thank M.V.Shalkina, for the execution of macro petrography and counts of components in kimberlite core samples, N.A. Kuz'mina and L.N. Dovbush for mineralogical analysis.

REFERENCES

77. **Chepurov A.I., Fedorov I.I., Sonin V.M.** Experimental modeling of the processes of diamonds formation. Novosibirsk, SB RAS, SIC OIGGM, 1997, 196 p.
78. **Dawson J.B and Stephens W.E.** Statistical analysis of garnets from kimberlites and associated xenoliths // *J. Geol.*, 1975, v. 83, p. 589 - 607.
79. **Haggerty S.E.** The chemistry and genesis of opaque minerals in kimberlites // *Phys. Chem. Earth*, 1975, vol. 9, p. 295-307.
80. **Haggerty S.E.** Spinel and ilmenite in high pressure regimes: an empirical analysis // In G.R. Boyd and H.O.A. Meyer (eds) *The Mantle sample*. Washington, 1979.
81. **Gurney J.J.** 1989. Diamonds. In: Ross J et al. (eds) *Diamonds, Kimberlites and Related Rocks*, Volume 2. *Geol. Soc. Aust. Spec. Publ.*, 14, Blackwell Scientific Publications, Melbourne, p. 935-965.
82. **Kharikov A.D., Zinchuk N.N., Kryuchkov A.I.** Diamond primary deposits of the world. M.: Nedra, 1998, 555p.
83. **Sobolev N. V.** Deep-seated Inclusions in Kimberlites and the Problem of the Composition of the Upper Mantle. American Geophys. Union, Washington, DC, 1977, 279 p.
84. **Spetsius Z.V, Kornilova V.P., Tarskih O.V., Ivanov A.S.** Mineralogical-petrographic features of kimberlites of deep horizons from the Internationalnaya pipe. In: *Deep magmatism, its sources and plumes*. Irkutsk, 2012, p. 168-191

ORIGIN OF THE MANTLE XENOLITHS WITH GREEN GARNETS FROM KIMBERLITES (DIKE NEWLANDS, SOUTHERN AFRICA AND NYURBINSKAYA PIPE, YAKUTIA)

Sablukov S.M.¹, Sablukova L.I.¹, Stegnitskiy Yu.B.², Karpenko M.A.³

¹ *RUSGEO Ltd, Moscow, Russia; sablukoff@rambler.ru*

² *NIGP ALROSA Co. Ltd., Mirny, Russia;*

³ *Nyurbinskaya Mine ALROSA Co. Ltd., Mirny, Russia*

ABSTRACT

Absolutely fresh samples of mantle rocks containing green garnet in the kimberlites of Newlands dike and separate grains of green garnet from kimberlites and the placer of Nyurba pipe as well as the comparison and the comprehensive studies of these samples using high-precision isotope-geochemical methods helped to elucidate the origin of these exotic mantle “wehrlites”. Xenoliths of rocks containing green garnet from kimberlites demonstrate a very changeable modal composition: from garnet-bearing rocks, to almost mono-olivine rocks containing individual small inclusions of garnet and «chromite ores»; clinopyroxene in the xenoliths is extremely scarce. The textures of rocks with green garnet are diverse: xenomorphic, poikilitic, in cases panidiomorphic. The structures of rocks are also diverse massive, schlieren, parallel-banded. The green garnet demonstrates both subidiomorphic and irregular shape, a zonal distribution of inclusions of other minerals, as well as the heterogeneous composition of its grains which sometimes exhibit a zonal texture. At same time even if the chemical composition and the contents of major components are similar the green garnet shows sharply increased concentrations of light (LREE) and medium (MREE) REE, as well as Sc. Moreover, the content of titanium in the garnet from different samples can differ in 20 times, and that of zirconium – can be different even in 80 times (!), reaching very high values (from 0,09 to 1,75 % of TiO₂ and from 13 to 1042 ppm of Zr). The isotope oxygen composition in green garnet ($\delta^{18}\text{O} = 4,05\text{-}4,25 \text{ ‰}$) and in olivine ($\delta^{18}\text{O} = 4,91 \text{ ‰}$) is significantly different from mantle values. By these characteristics the samples containing green garnet from kimberlites are similar to the layered gabbro from ophiolite complexes. The age of rocks with green garnet is relatively young, probably Meso-Proterozoic ($T_{\text{NdDM}} = 1,78 \text{ Ga}$) that can be hardly typical of “usual” rocks of the mantle substratum. The rocks with green garnet exhibit a non-equilibrium character of ol+sp+gar paragenesis that is an evidence of the formation at moderate depth in the mantle (80-90 km) in the conditions of a high heat flow (52-55 mW/m²), that is probably connected with plume-formation. By the structure and the composition the rocks containing green garnet from kimberlites are not “wehrlites” and most likely are metasomatic units of uvarovite-chromite veins or schlieren formed at moderate depth in the upper mantle - likewise uvarovite-chromite veins or schlieren of the metasomatic origin in the crustal serpentinites.

INTRODUCTION

Green garnets occur very rarely in the concentrates of diamond-bearing kimberlite bodies: Yakutia (Udachnaya, Sytykanskaya, Dalnyaya, Mir, Internatsional'naya, Aikhal, Zimnyaya pipes); Southern Africa (Newlands and Bellsbank dikes, Premiere, Bellefontaine, Campferstadam, etc. pipes); Venezuela (Guanamo); Canada (kimberlites of Mud Lake, Slave craton) [2, 10, 14, 20, 34].

Green (emerald-green) garnets in kimberlites have very bright, absolutely unusual, unnatural, almost improbable color as the most widespread are violet, crimson, red and orange garnets and thus green garnets are always of particular interest. Scarce findings and unusual color led to different viewpoints concerning the origin of green garnet in kimberlites: hypotheses concerning the origin of such exotic formations as green garnets are also rather unusual and exotic. «The specific features of their composition suggest their special genesis which is still a subject of intense debate» [7].

Clarke and Carswell [20] discovered the macrocrysts of green garnet in kimberlites from Newlands dike during the field geological excursion at the 1st International Kimberlite Conference (1973, Cape Town) and proposed four models of formation of such garnets at a great depth:

1) Green garnets are considered to be a part of "normal", i.e. non-depleted mantle peridotites from great depth where pyroxenes are dissolved in a garnet solid solution (possibly at the depth of > 350 km).

2) Green garnets could be formed in the residual during the partial melting at the depth of > 350 km.

3) Green garnets are products of fractional crystallization of magma (not necessarily kimberlite one), formed from the partial melting of mantle peridotites at a depth of > 250 km.

4) Green garnets can be products from fragmentation of xenoliths of garnet wehrlites, formed from subsolidus recrystallization of primary spinel wehrlites (products of fractional crystallization of magma at a depth of > 200 km). Moreover, the reaction: diopside + Cr-spinel = uvarovite + olivine takes place.

Clarke and Carswell [20] consider the 4th hypotheses as the most probable hypothesis concerning an origin of green garnets from kimberlites because of: 1 – iron content in green garnets is too high, that they could be a liquidus phase of the primary melt; 2 - Cr-spinel are very frequent in diamonds, and as opposed to chrome-containing garnet Cr-spinel is most likely a liquidus phase of high pressure; 3 - both uvarovite-bearing xenoliths from Yakutia contain chrome spinel [10]; 4 - the association of uvarovite garnets with wehrlites nodules, and knoringite garnets with lherzolite or harzburgite nodules agree with the reaction of subsolidus recrystallization of spinel wehrlites ($2\text{Cpx} + \text{Crsp} = \text{Uvar} + \text{Ol}$) and spinel lherzolites ($4\text{Opx} + \text{Crsp} = \text{Knorr} + \text{Ol}$), accordingly.

Following Clarke and Carswell, [20] who stated that “high-uvarovite garnets from kimberlites and xenoliths originated from subsolidus exsolution of Cr-clinopyroxenes in high pressure conditions.

M. Kopylova et al. [7], describing microscopic (3×40 microns) lamellae of high-calcium garnet in clinopyroxenes and orthopyroxenes from deep-seated inclusions from Obnazhennaya pipe is also in favor of the 4th hypothesis.

Kharkiv [14] also considered that «... the xenoliths of the wehrlites paragenesis belong to ***especially deep-seated rocks of the mantle*** (given bold by us, C.M.C.) and during the transportation upwards could be subjected to an intensive decomposition, and a green garnet, being the most difficult to be decomposed part of these rocks, has remained». At the same time there is a possibility of «... crystallization of a considerable part of green garnet from the melt during one of stages of its deep evolution» [15].

On the other hand it was also suggested [38] that the kimberlitic green garnets, most likely were produced during the subduction and prograde metamorphism of uvarovite-bearing crustal serpentinites.

All models of origin of green garnets were proposed from studies of separate grains because xenoliths with green garnets are very scarce in kimberlites [14] and are usually strongly altered. Therefore, the studies of absolutely fresh xenoliths of peridotites with green garnet from Newlands dike (Republic of South Africa) which were found by us during the field geological excursion at the 7th International Kimberlite Conference (1998, Cape Town), and studies of mineral accumulations and separate green garnet grains from kimberlites of new area (the Nakyn field of Yakutia) are of particular interest.

«One good sample is better than ten hypotheses» - E.Ehelson.

SAMPLES AND ANALYTICAL METHODS

Two xenoliths of “peridotite” with green garnet and a green garnet grain found by us “in situ” in kimberlites from Newlands dike were studied. In addition one more xenolith of “peridotite” with green garnet was discovered under the microscope in kimberlites from Newlands dike (that may be an evidence of a wide distribution of green garnets in this dike).

As to kimberlites and placer of Nyurba pipe (Nakyn field, Yakutia) are concerned, green garnets have been discovered only during studies of the mineral composition of crushed samples. We have found 1 garnet grain with the size of 0.3 mm in kimberlites, 4 green garnet grains of 0.7-2.0 mm in the terrigenous sediments of the placer including 1 intergrowth gar+sp (3 garnet grains have been found by us when observing the selected monofractions of chrome-diopside from the concentrates and 1 grain has been discovered when studying crushed samples). Besides, 9 small (0.15-0.3 mm) fragments of green garnet grains have been revealed when studying of the mineral composition of bulk samples (enrichment “tails”) of kimberlites and placer.

Comprehensive studies of samples with green garnet included the description and studies of samples and minerals via the microscope, studies of the chemical composition of minerals and trace element composition of garnets as well as Sm-

Nd and Rb-Sr isotope composition of samples and oxygen isotope composition of garnet and olivine.

The samples and minerals were described via the MBS-10, NIKON SMZ1500 and polarization NIKON ECLIPSE E600 POL microscopes. The samples were taken photos by digital camera PENTAX Optio 550, microphotographing of samples and minerals was done with the help of NIKON SMZ1500 microscope and digital NIKON DIGITAL SIGHT DS-L1 camera. Totally we studied 4 samples of «peridotites» (3 samples with green garnet and one sample of "usual" non-altered garnet lherzolite for comparison) as well as 15 separate green garnet grains. X-ray microanalysis of minerals (25 analyses) was done at the laboratory of "Gintsvetmet" via "Camebax SX-50" device at accelerating voltage of 20 kV, current 15-20 nA. Sm-Nd and Rb-Sr isotope characteristics were obtained via mass spectrometer Finnigan MAT-261 at the Laboratory of the Institute of Precambrian Geology and Geochronology, Russian Academy of Sciences (St.-Petersburg). The trace element composition of garnets (8 analyses) was studied at the Center of Isotope Researches FGUP CSEGEI (St.-Petersburg). LA-ICPMS, laser ablation DUV-193 with excited-state dimer laser COMPex-102, mass spectrometer Element-II were used. The diameter of a beam is ~ 200 micron; impulse frequency of the laser is 10 hertz. Oxygen isotope composition of garnet (3 analyses) and olivine (2 analyses) was studied via fluoridation on mass spectrometer DELTA plus. TP-parameters of mineral parageneses were defined by means of PT-Quick software.

SHAPE AND MINERALOGY

GREEN GARNETS FROM NEWLANDS DIKE

The kimberlite dike Newlands is located in 60 km to the northwest from Kimberley, Cape Province, the Republic of South Africa. The Newland dike is composed of a series of kimberlite veins stretching over 600 m with five small bulges of 15-40 m in diameter. The kimberlites from Newlands dike belong to non-ilmenite kimberlites of group 2, South Africa [36]. The rocks from the dike are diverse in shape and textural features. We studied two varieties of kimberlites from this dike: 1) the kimberlite lava with magnophyric texture ("porphyritic kimberlite" [8]) of black color, unusually fresh, with almost non-altered olivine, this rock also contained "peridotites" with green garnet (samples NL-11 and NL-21). From the same rock we collected the non-altered garnet lherzolite (sample NL-51) for comparison; 2) Strongly altered, carbonatized xenolava of magnophyric kimberlites («xenolith eruptive kimberlite breccia by [8]) of light brown color with phlogopite matrix and completely altered olivine, this rock also contained "peridotite" with green garnet (sample NL-41) and separate green garnet grains (sample NL- 31).

The xenoliths of "peridotites" are of irregular-flat-like shape and have similar modal composition: they contain olivine, green garnet and chrome-spinellid.

Clinopyroxene or pseudomorphs in clinopyroxene have not been observed. The texture is mainly middle-crystalline (size of grains- 2-4 mm), the structure is taxitic or schlieren. The xenoliths of “peridotites” are altered according to alteration degree of the host kimberlites.

Of particular interest is the xenolith sample NL-11 (fig. 1A), with the size of 4,5*1,7 cm and containing large emerald-green garnet grains, absolutely fresh, transparent olivine and small isometric inclusions chrome-spinellids (including that in the garnet): gar (70) +ol (28) +sp (2). This sample demonstrates transversal veins of 2 mm thick being of metasomatic origin, and the crystalline aggregate gar+phlog+sp.

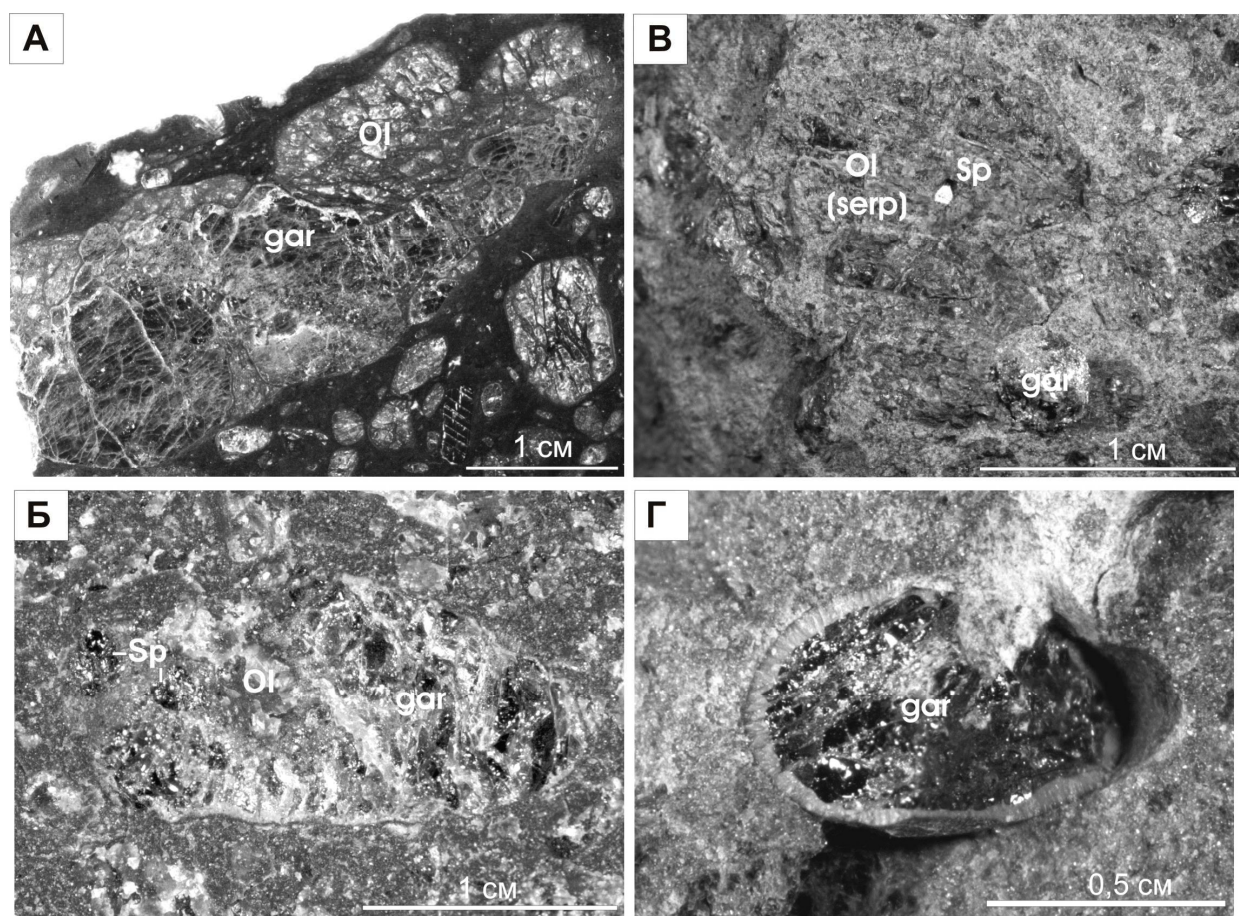


Fig.1. Samples with green garnet from kimberlites of Newlands dike, South Africa.

A - xenolith of “peridotite”, sample NL-11; - xenolith of «peridotite», sample NL-21; B – xenolith of “peridotite”, sample. NL-41; G – green garnet macrocryst, sample NL-31.

The sample NL-21 (fig. 1B) has the size of 1,7*07 cm, contains large emerald-green garnet grains, of strongly serpentinized, transparent olivine and isometric chrome-spinellid grains: gar (50) +ol (30) +sp (20).

The sample NL-41 (fig. 1B) has the size of 1,7*1,5 cm, contains completely serpentinized olivine with large isometric emerald-green garnet inclusions and individual octahedron-like chromespinellid grains: gar (8) +ol (82) +sp (0,2). A distinctive feature of this sample is panidiomorphic-granular medium-crystalline

texture with straight-like contours of separate mineral grains.

Green garnet grain (sample NL-31, fig. 1D) of 0,7*0,5 cm exhibits a monocrystalline texture and is surrounded by a thin (0,5 mm) pale-green kelyphytic rim containing (judging by the composition) the cross-section-radiant aggregate of amphibole and phlogopite. The composition of garnet from the studied samples of Newlands dike is relatively stable (table 1, fig. 3, 4), garnets show high Cr₂O₃ (10,94-11,99 %) and low TiO₂ (0,24-0,52 %) and FeO (3,73-5,33 %) contents. CaO (19,52-24,94 %) concentration is the most variable and depends inversely on MgO (10,20-6,66 %) content. The share of the uvarovite component ranges from 33,2 to 36,7 %; that of grossular component scatters from 13,3 to 26,1 %; and the share of the pyrope component varies within 25,6-38,9 %.

Table 1.

Chemical (wt. %) and oxygen isotope composition of green garnets grains from Newlands dike

Samples	HJI-11			HJI-21			HJI-31		HJI-41	HJI-51
	Grt	Sp	Ol	Grt	Sp	Ol	Grt	Kel	Grt	Ol
Minerals	Grt	Sp	Ol	Grt	Sp	Ol	Grt	Kel	Grt	Ol
SiO₂	38,47	-	40,85	38,48	-	40,65	38,85	35,33	38,85	40,82
TiO₂	0,52	0,47	0,00	0,48	0,57	0,00	0,24	0,42	0,45	0,04
Al₂O₃	12,37	14,59	0,02	12,57	13,24	0,06	13,94	12,09	12,98	0,00
Cr₂O₃	11,99	55,36	0,03	11,76	53,45	0,06	10,94	6,27	11,88	0,00
FeO	3,73	14,75	5,81	5,15	18,98	6,61	4,90	7,71	5,33	7,27
MnO	0,22	0,23	0,08	0,25	0,3	0,07	0,29	0,12	0,47	0,10
MgO	6,66	14,15	51,78	8,02	13,10	50,84	10,20	22,45	9,49	50,85
CaO	24,94	-	0,09	22,79	-	0,08	19,52	2,38	19,61	0,03
Na₂O	0,03	-	0,05	0,00	-	0,09	0,00	0,03	0,00	0,04
K₂O	-	-	-	-	-	-	-	6,31	-	-
NiO	-	-	0,48	-	-	0,37	-	-	-	0,46
Total	98,93	99,55	99,19	99,50	99,64	98,83	98,88	93,11	99,06	99,61
Fo, %	-	-	94,6	-	-	93,6	-	-	-	92,9
Uvar, %	36,7	-	-	35,9	-	-	33,2	-	36,0	-
δ¹⁸O, ‰	4,20	-	4,91	4,25	-	-	-	-	4,05	5,11

The composition of chrome-spinellid is constant; chrome-spinellid exhibits high Cr₂O₃ (53,45-55,36 %) and low TiO₂ (0,47-0,57 %) contents. The olivine is high-magnesian (Fo_{93,6} - Fo_{94,6}). However, there is an increased CaO (0,08-0,09 %) content; that is higher than the olivines from deep-seated peridotites have. It is most likely due to high calcium content in the system. Moreover, the olivine from "usual" garnet peridotite of Newlands dike shows CaO content (0,03 %) typical of deep-seated olivine; at the same time the magnesia content is slightly lower (Fo_{92,9}).

The data from earlier publications [20] show that 5 green garnet grains with

the size of up to 1 cm (including an intergrowth of two grains) were discovered in Newlands dike. The composition of these garnet grains as a whole is similar to composition of garnet from Newlands dike studied by us: TiO₂ content scatters from 0,40 to 0,52 %, the share of the uvarovite component ranges within 30,2-43,4 %; that of grossular component is in the spread from 10,1 to 31,5 %; the share of the pyrope component varies from 24,0 to 37,7 %. Thus, only one sample being an intergrowth of two garnet grains (with sharp uneven contact between grains) has as a whole much higher TiO₂ concentration and demonstrates a heterogeneous texture of one of the grains so the concentrations of a number of components significantly vary in these two grains: TiO₂ (1,04-1,27 %), MgO (6,36-10,13 %), CaO (25,94-19,18 %). It can be a convincing evidence of unstable conditions when those garnets were produced.

GREEN GARNETS FROM THE NYURBA PIPE AND PLACER

The Nyurba pipe is located in the Nakyn field of Sredne-Markhinsky area of the Yakutian diamond-bearing province [19, 13, 5, 4], in three hundred kilometers to northeast Mirny city. The pipe is composed of unique ilmenite-free kimberlites, by composition they are partly similar both to the kimberlites from the group 1 and to kimberlites of group 2, South Africa [36]. The Nyurba pipe is related to the placer, moreover the rocks of four stratigraphic units (from top to bottom) are considered to be the productive and potentially productive. They include units of the weathering crust (T₂₋₃), Dyakhtar sequence (T₃-J₁dh), Ukugut unit (J₁uk), Tyunga unit (J₁tn).

We found only one fine green garnet grain (one grain in 28 crushed samples!) in the kimberlite pipe proper (tuffizites of kimberlites of 3rd intrusion phase). The garnet grain has the size of 0,3 mm and is a protofragment of irregular, angular shape (fig. 2).

Only 4 grains of green garnet of 0,7-2,2 mm, including 1 intergrowth gar+sp have been found by date in the placer of the Nyurba pipe. 3 garnet grains from the placer are non-rounded, of irregular shape with uneven edges, are replaced in cracks by the light brown microscaly aggregate of secondary minerals (fig. 2, left bottom).

They include one garnet grain in the sample from the Tyunga unit (J₁tn) sample, two grains in the sample from the Early Jurassic Ukugut unit (J₁uk). These garnet grains, including 1 intergrowth gar+sp, are most likely microfragments of the mantle xenoliths. One (the largest) garnet grain of the irregular shape was found in the sediments of the Dyakhtar unit (T₃-J₁dh). This grain is also non-rounded, but is homogenous in texture, shows signs of the hypergene dissolution of the surface and is possibly a fragment of the garnet macrocryst which was involved into weathering crust of kimberlites (fig. 2, bottom right). Nine small (0,2-0,3 mm), non-rounded fragments of green garnet grains were found when we studied the "tails" of enrichment of kimberlites and placer.

The chemical compound of the studied garnet grains is quite usual and

constant (table 2, fig. 3, 4); they show high Cr_2O_3 (7,49-14,17 %) and increased FeOt (5,40-8,10 %) contents. CaO (17,34-22,87 %) content is the most variable and depend inversely on MgO (11,21-7,56 %). The share of the uvarovite component ranges within 22,3-43,8 %; that of grossular component is in the scatter from 0 to 21,2 %; the share of the pyrope component varies from 28,7 to 43,1 %. However, the majority of garnet grains demonstrate higher TiO_2 content, 1,38 % as an average (from 1,05 to 1,75 %). Only one garnet grain from the intergrowth with chrome-spinellid exhibits TiO_2 content as «normally» decreased (0,35 %); this TiO_2 concentration is similar to TiO_2 content in green garnet grains from Newlands dike. The chrome-spinellid from this intergrowth also demonstrates the decreased TiO_2 (0,35 %) and low Cr_2O_3 (36,71 %) contents. Moreover, one garnet grain from the placer of the Dyakhtar unit has a very low TiO_2 (0,09 %), decreased Cr_2O_3 (7,49 %), increased Al_2O_3 (16,63 %) contents. At the same time this grains also exhibits a very high share of the grossular component (21,2 %).

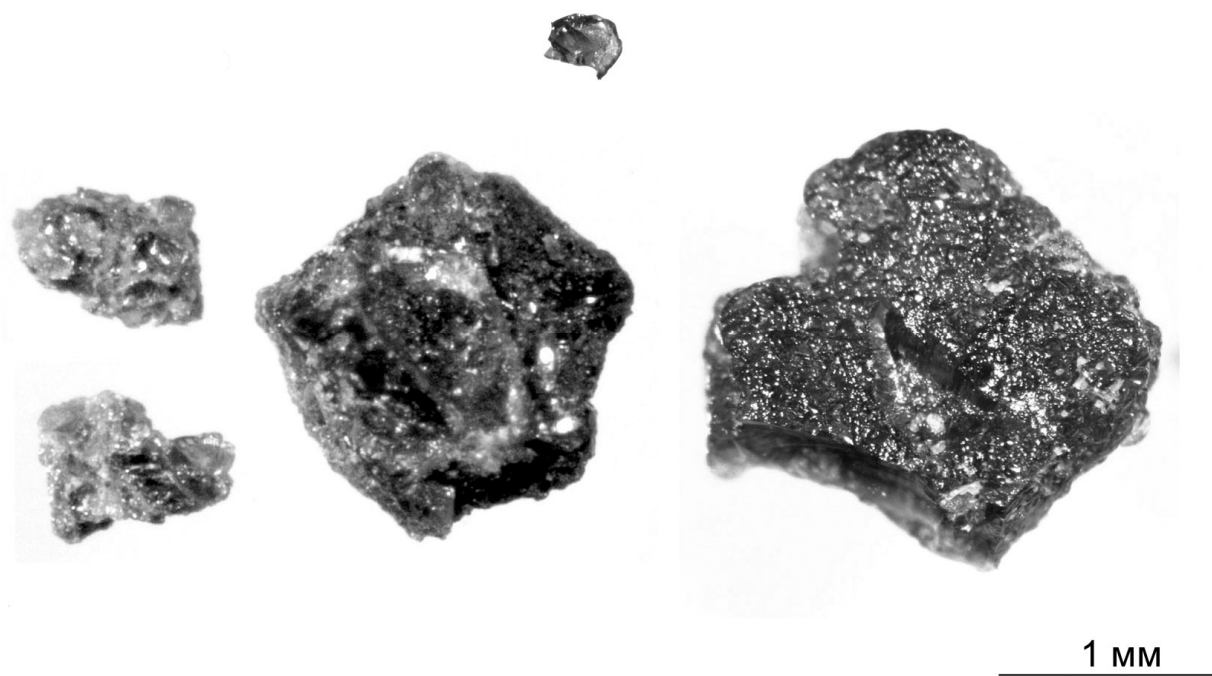


Fig. 2. Green garnet grains from kimberlites and placer of Nyurba pipe, the Nakyn field, Yakutia.

Top – garnet from kimberlites of Nyurba pipe. Bottom - green garnet from placer Nyurba, in the centre – intergrowth “garnet + chrome spinel”

The earlier data for the kimberlites from the Nakyn field (Nyurba, Botuobinsk, May pipes Markha body and pre-pipe dike) show no findings of green garnet [5, 6, 13, and other publications]. At the same time [6], describing garnets from the Nakyn field point out that «Among the analyzed garnet grains both from the pipes and veins there are no varieties corresponding to garnet of groups 7 and 8 showing a high share of the grossular mineral»

Table 2.

Chemical composition of green garnet grains from Nyurbinskaya pipe (wt. %).

Body samples	Placers			Kimber- lites	Probes from the kimberlites and/or placers tails											
	36/420-7 Grt Sp	24/340- 6 Grt	12/300- 3 Grt		080/480- 14.2 Grt	26/510- 439 Grt	3/6,0- 1 Grt	3/7,5- 1 Grt	3/7,5- 2 Grt	3/7,5- 3 Grt	3/7,5- 4 Grt	5/1,0- 1 Grt	5/1,0- 2 Grt	5/1,0- 3 Grt	5/5,0- 1 Grt	
Minerals	Grt	Grt	Grt	Grt	Grt	Grt	Grt	Grt	Grt	Grt	Grt	Grt	Grt	Grt		
SiO ₂	38,8	38,66	38,02	39,73	37,15	37,70	38,83	38,06	37,71	38,77	38,07	38,52	38,24	37,95		
TiO ₂	0,35	1,46	1,65	0,09	1,75	1,45	1,16	1,39	1,40	1,04	1,67	1,24	1,31	1,05		
Al ₂ O ₃	14,68	12,58	11,33	16,63	9,96	11,78	11,41	11,30	10,34	13,25	10,65	11,66	10,17	13,64		
Cr ₂ O ₃	9,63	11,25	12,67	7,49	13,72	11,29	13,44	13,30	14,17	11,18	12,91	12,42	13,77	10,58		
FeO	7,05	6,18	5,85	6,69	5,63	8,10	5,89	6,10	5,67	7,61	5,40	6,37	5,72	7,70		
MnO	0,46	0,49	0,47	0,41	0,41	0,54	0,47	0,45	0,43	0,48	0,37	0,43	0,37	0,51		
MgO	10,17	10,07	9,2	10,78	7,68	7,92	10,31	10,10	8,09	11,21	7,99	9,04	7,56	9,85		
CaO	18,06	18,67	20,16	17,34	22,87	20,57	17,75	18,32	21,57	16,20	21,93	19,50	22,31	18,00		
Na ₂ O	0,04	0,03	0,03	0,00	0,05	0,00	0,00	0,15	0,11	0,03	0,00	0,15	0,00	0,00		
Cymma	99,24	99,39	99,38	99,16	99,22	99,35	99,26	99,17	99,49	99,77	98,99	99,33	99,45	99,28		
Uvar, %	29,34	33,64	38,37	22,3	42,5	34,5	40,2	37,6	43,8	33,6	38,9	37,9	41,6	32,4		

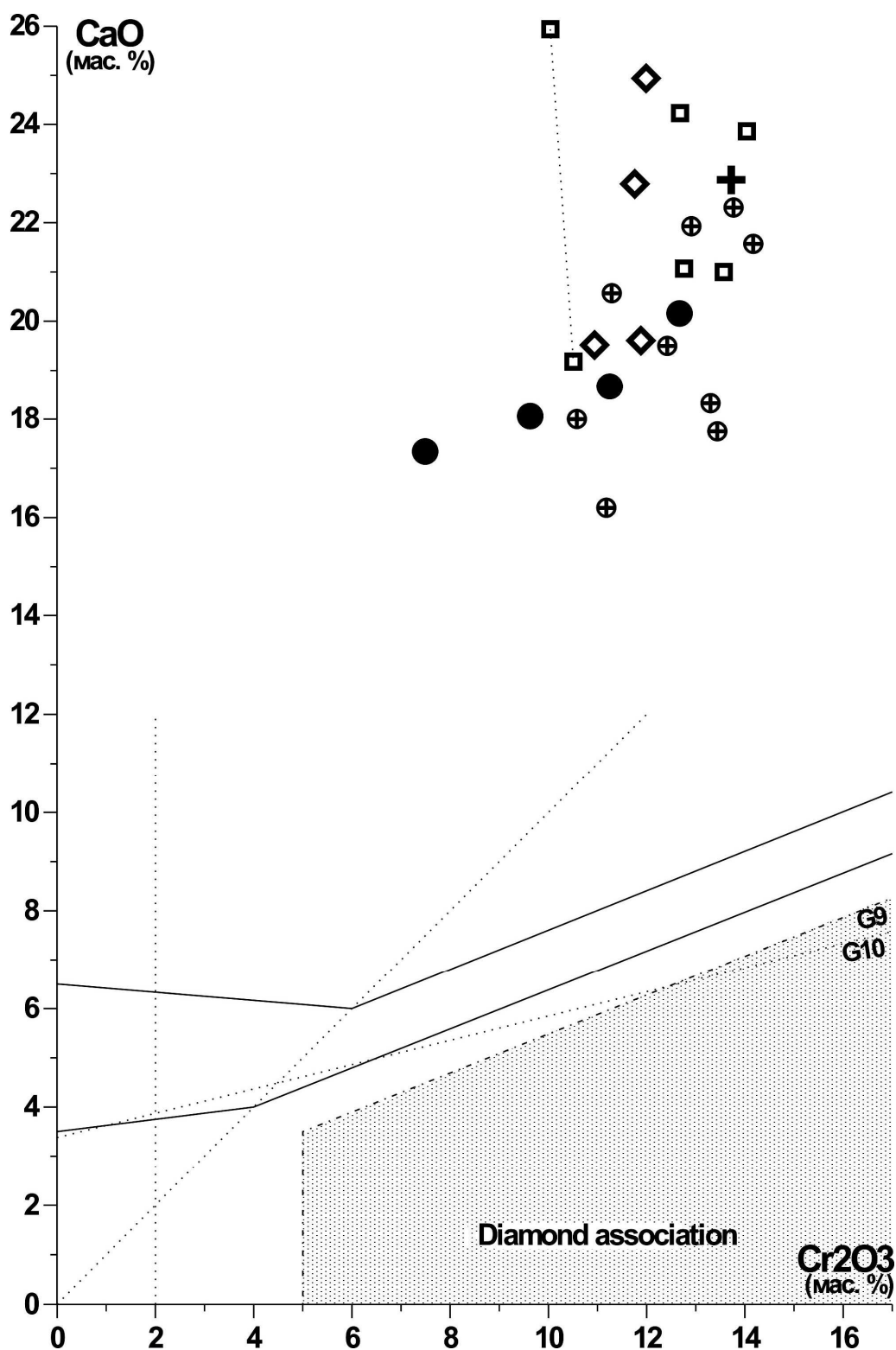


Fig. 3. Features of the chemical composition of garnets from Newlands dike, Nyurba pipe and placer (the diagram by [10]).

Legends: Newlands dike: 1 - our data, 2 - data from [20]; Nyurba pipe: 3 - kimberlites, 4 - placer, 5 - enrichment "tails" of kimberlites and placer.

(by classification of Dawson and Stephens, [21]). Their data show that «...1 garnet grain belonging to group 7 (*green garnet - C.M.C*) which is not available in samples of known bodies of the field has been found in Khanin site» - without any relation to a certain site, age and type of the collected samples. The composition of this garnet as a whole is similar to the composition of low-titanium garnet from the intergrowth with chromespinellid from the Dyakhtar unit, Nyurba placer.

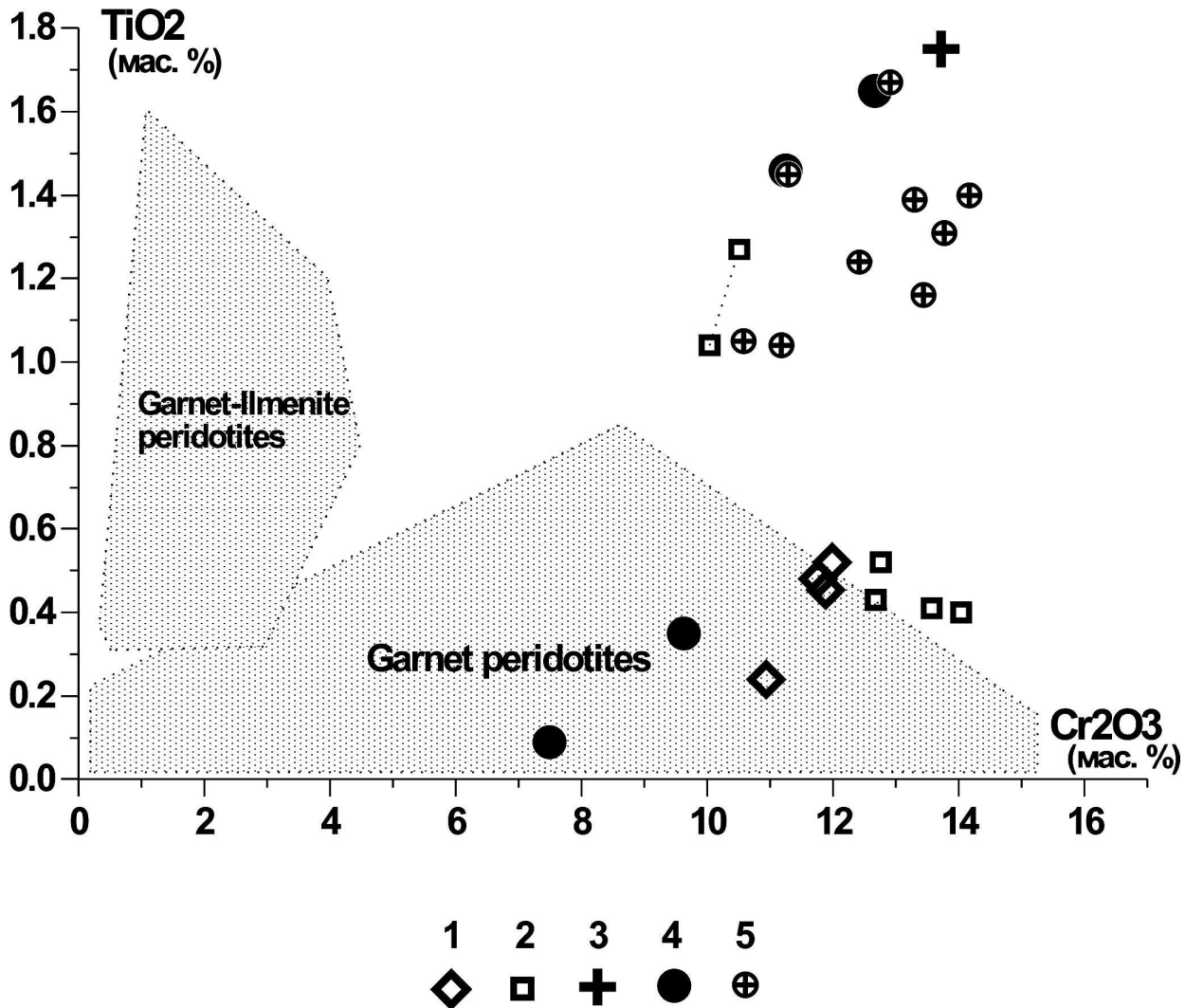


Fig. 4. Features of the chemical composition of the garnet from Newlands dike, Nyurba pipe and placer on Cr₂O₃ - TiO₂ plot.

Legends: Newlands dike: 1 - our data, 2 - data from [20]; Nyurba pipe: 3 - kimberlites, 4 - placer, 5 - enrichment "tails" of kimberlites and placer.

As a whole, by the chemical composition the studied garnets from kimberlites of Newlands dike form a quite isolated series (garnets of group 7 by [21]) with the share of the uvarovite and grossular components of 44,2 % as an average (35,8-62,8), and the share of the pyrope component of 35,8 % as an average (25,6-43,7 %). This series is characterized by the internal heterogeneity reflected primarily in titanium concentration (from 0,09 % to 1,75 % TiO₂), with prevalence of high-

titanium varieties in the pipe and placer Nyurba (with the broadest scatter in the garnet composition as a whole), and of medium-titanium varieties of green garnet in the Newlands dike.

The published data on the composition of green garnets from kimberlites all over the world [34; 37; 38; 14] show medium-titanium garnets (0,3-0,7 % TiO₂) are predominant, low-titanium varieties (0,1-0,3 % TiO₂) are less abundant and high-titanium prevailing in the Nyurba pipe (> 1 % TiO₂) are found only in one sample from Newlands dike [20] (see above). The heterogeneity of green garnets (in terms of the chemical composition) can suggest various and unstable conditions of formation of these garnets.

DISTRIBUTION OF RARE ELEMENTS IN GREEN GARNETS

Distribution of rare-earth elements in green garnets of the studied samples is rather indicative. The medium-titanium green garnets from Newlands dike demonstrate flat-like "sinusoidal" REE pattern with slightly lower medium REE (MREE) concentrations and significantly higher LREE contents (fig. 5A). Moreover, the low-titanium garnet from the sample NL-41 shows higher MREE concentrations (from Gd to Nd).

Only a low-titanium garnet from the intergrowth with chrome-spinellid (sample 36/420-7, the Nyurba pipe and placer (fig. 5B)) has a similar, "sinusoidal" REE distribution. At the same time high-titanium garnets show "the elevated-like" REE distribution, marked by higher LREE and MREE contents.

The trace element distribution (fig. 6) demonstrates that all green garnets exhibit decreased Ni, Co (and low-titanium garnets show lower Ga concentration as well), and the increased Sc contents. Moreover, the medium-titanium garnets are marked by significantly increased LREE and slightly higher Zr (to 43 ppm) contents. The high-titanium varieties show higher contents of both LREE and MREE, yttrium, titanium, but in particular Zr – (from 652 to 1042 ppm (!)), while low-titanium garners have Zr low (13 ppm) and increased LREE and MREE contents.

As a whole, a stable and obvious paragenesis of green garnets with olivine allows interpretation of rare elements distribution (Y, Zr, Ga, Ni) in garnets using well-known methods of temperature and pressure $T_{(Ni)}$, $P_{(Cr)}$ calculations and corresponding discrimination diagrams which show fields of garnet compositions of reference types of rocks and reference processes [17, 25-30]. The trace element distribution in green garnets has not been studied, and available discrimination diagrams have been obtained without taking into account the composition of green garnets.

The most informative elements for pyropes are: Ti, Zr, Y, Ga and Cr, Ni [17, 18, 25-30].

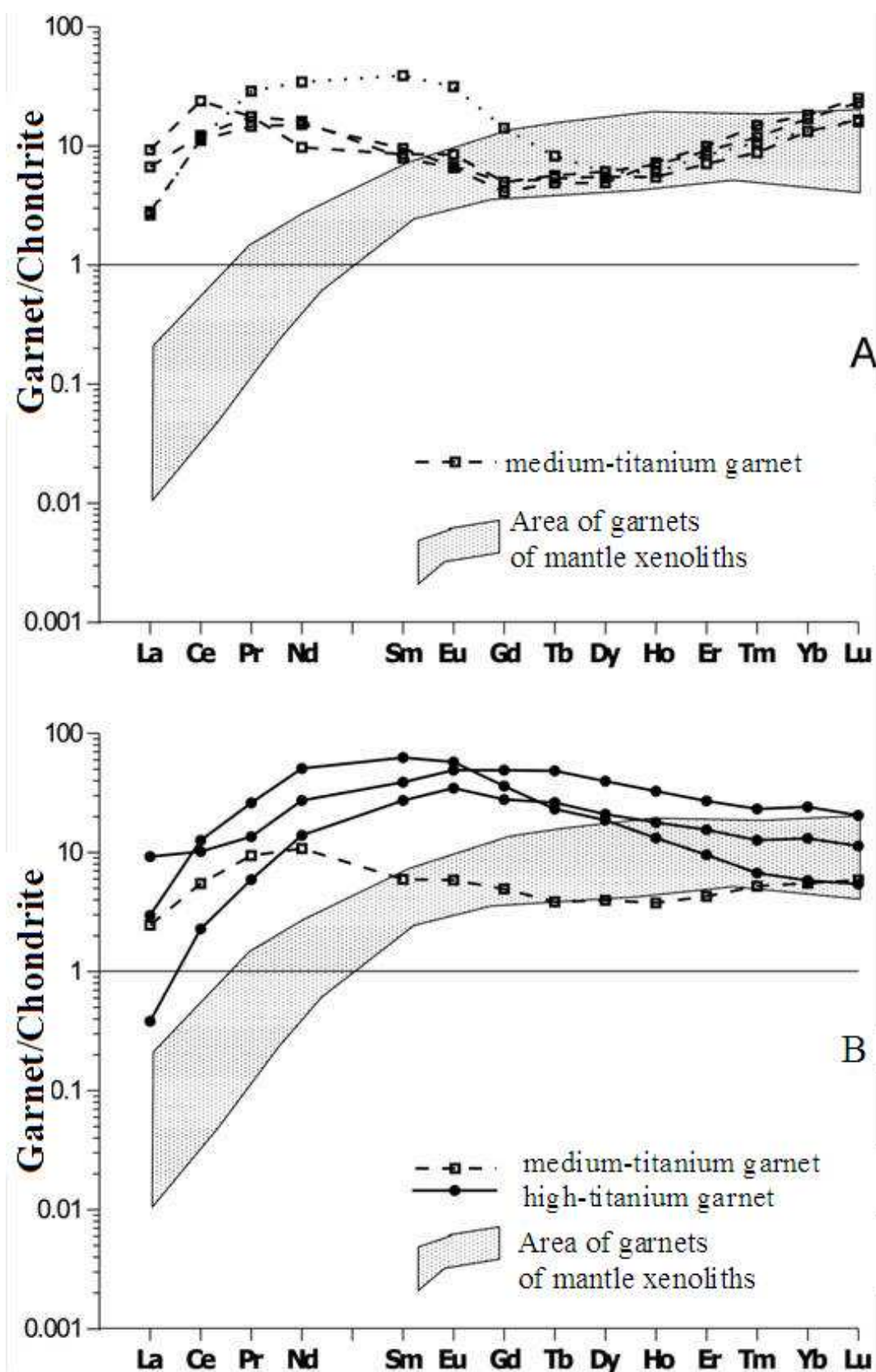


Fig. 5. Chondrite-normalized [16] REE distribution in green garnets.

A - from Newlands dike, B - kimberlites and placer of Nyurba pipe.

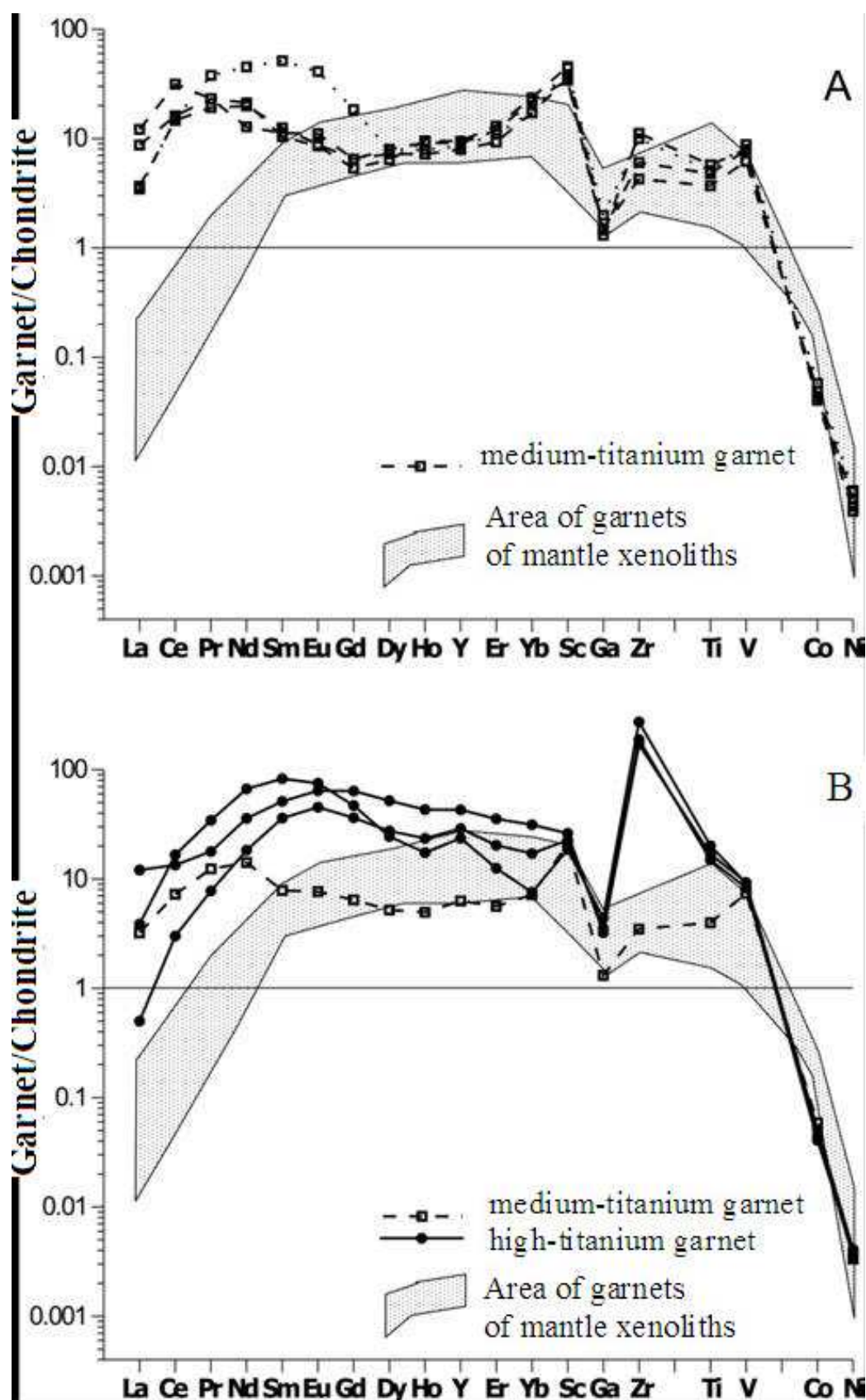


Fig. 6. Chondrite-normalized C1 [33] distribution of trace elements in green garnets. A - from Newlands dike, B - kimberlites and placer of Nyurba pipe.

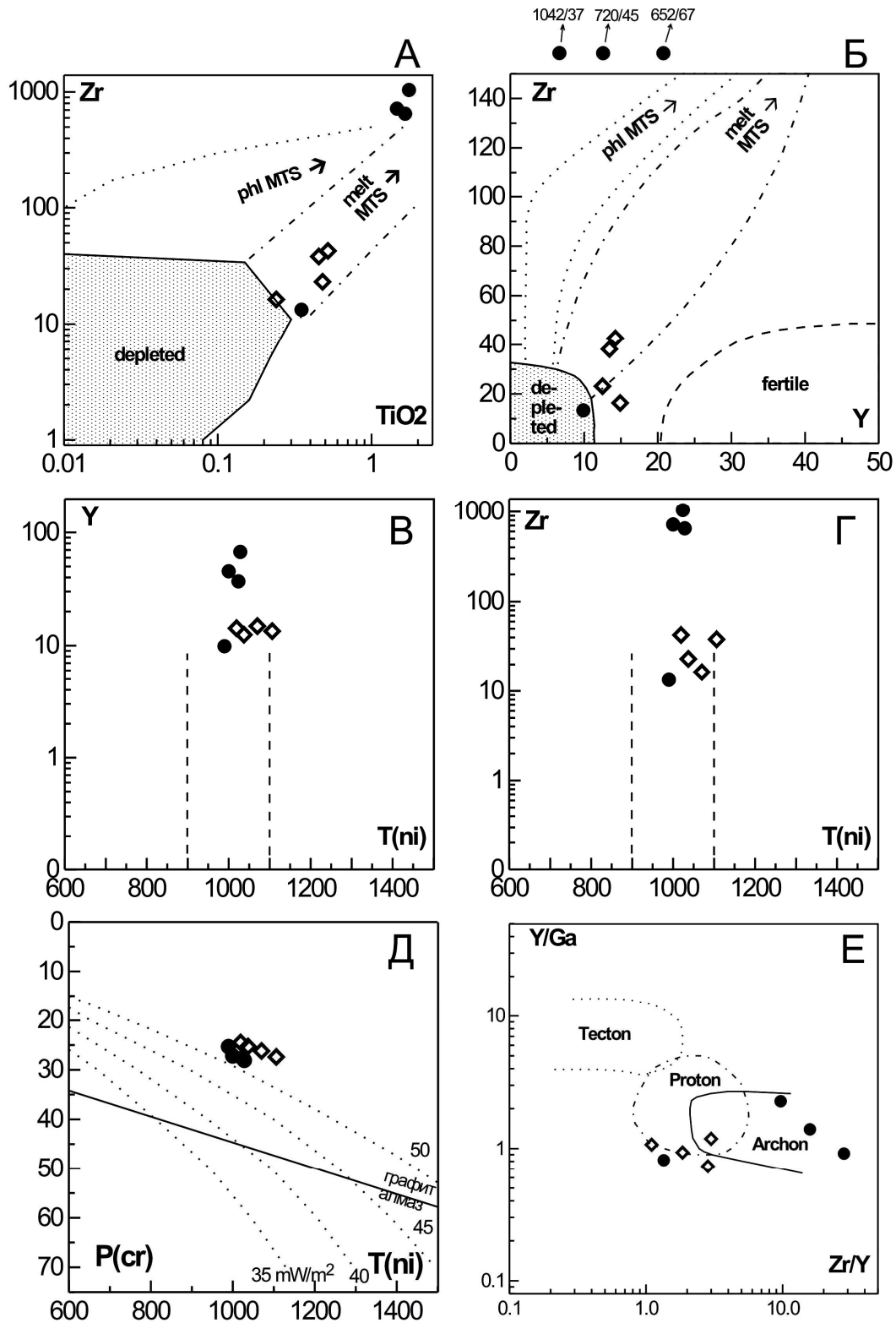


Fig. 7. Features of trace element distribution in green garnets from kimberlites of Newlands dike, Nyurba pipe and placer.

A - Zr (ppm) vs TiO_2 (wt. %); B Zr (ppm) vs Y (ppm); C - Y (ppm) vs $T_{(Ni)}$ °C; D - Zr (ppm) vs $T_{(Ni)}$ °C; E - $P_{(Cr)}$ (RG96P) vs $T_{(Ni)}$ °C (C99T); F – tectonics features from Zr/Y - Y/Ga distribution in garnets. Diagram from Griffin et al., [23; 28, 29]; Canil, [18].

As regard to various contents and ratios of trace elements we can distinguish the pyropes from “fertile” (primitive, non-depleted) mantle rocks, «deleted» rocks, as well as from rocks which underwent high-temperature” «melted» and low-temperature «phlogopite» mantle metasomatism. So, the pyropes from depleted mantle rocks show minimum concentrations of all incompatible elements while pyropes from fertile rocks demonstrate increased Y content. At the same time the pyropes from rocks, which underwent high-temperature mantle metasomatism due to the astenosphere melts exhibit the increased contents of incompatible elements: Zr, Ti, Y, Ga («melted metasomatism»), while the pyropes from rocks with the low-temperature, “phlogopite” mantle metasomatism demonstrate higher Zr content. At the same time they are marked by average concentrations of other incompatible elements (Ti, Y, Ga) and high Zr/Y value.

On diagram TiO_2 -Zr (fig. 7A) low - and medium-titanium green garnets are similar to those which were subjected to the weak and moderate melted metasomatism, while high-titanium green garnets lie beyond reference composition of garnets (due to high zirconium concentration) that can suggest a very high degree of influence of metasomatic processes. Moreover, it can indirectly indicate that green garnets could be directly produced from metasomatic process (during the infiltration, "obvious", "modal" metasomatism) while from available discrimination diagrams one can consider that the redistribution of trace elements in pyropes resulted from the diffusion "hidden" metasomatism. The interpretation of trace element distribution in pyropes (which is the additional tool for studying endogenous processes) provides more information, than the authors of this system presumed [17, 18, 25-30]. It usually happens when the method is well thought and reliable and the features revealed from this system are not artifacts, but the reality.

The same picture is shown on Y-Zr diagram (fig. 7B), on which the compositions of high-titanium green garnets lie outside the fields of influence of mantle metasomatism (owing to very high zirconium content).

Calculations of PT-conditions of garnet formation ($T_{(Ni)}$ °C, $P_{(Cr)}$ - Fig. 7G, D) show that on one hand they originate under T- conditions of «the diamond window» (900-1100°), and on the other hand they suggest moderate pressure of their formation (25-28 kbars) in the conditions of high heat flow (accordance of their parameters to conductive geotherm 52-55 mW/m²).

By the distribution of Y, Zr and Ga (fig. 7E) high-titanium garnets correspond to the “archone”, and low-titanium and medium-titanium garnets – to “proton” at the interface with “archone”.

OXYGEN ISOTOPE STUDIES OF MINERALS

We managed to analyze oxygen isotope composition in green garnets and olivines from very fresh xenoliths of garnet-bearing rocks, Newlands dike (table 1). All three studied garnets are depleted by heavy oxygen isotope ($\delta^{18}O = 4,05; 4,20; 4,25 \text{ ‰}$) that strongly distinguishes them from typical mantle rocks (mantle interval $5,37 \pm 0,36 \text{ ‰}$ by [32]). It is well visible on diagram by Taylor et al., [39]

(fig. 8).

Olivine from the sample NL-11 is characterized by the "light" isotope oxygen composition ($\delta^{18}\text{O} = 4,91 \text{ ‰}$). Though it is similar to mantle parameters, as compared to the garnet, it is not typical of mantle rocks. At the same time an olivine from "usual" garnet peridotite of Newlands dike has the oxygen isotope composition ($\delta^{18}\text{O} = 5,11 \text{ ‰}$) typical of mantle olivines ($\delta^{18}\text{O} = 5,22 \pm 0,22 \text{ ‰}$) [32].

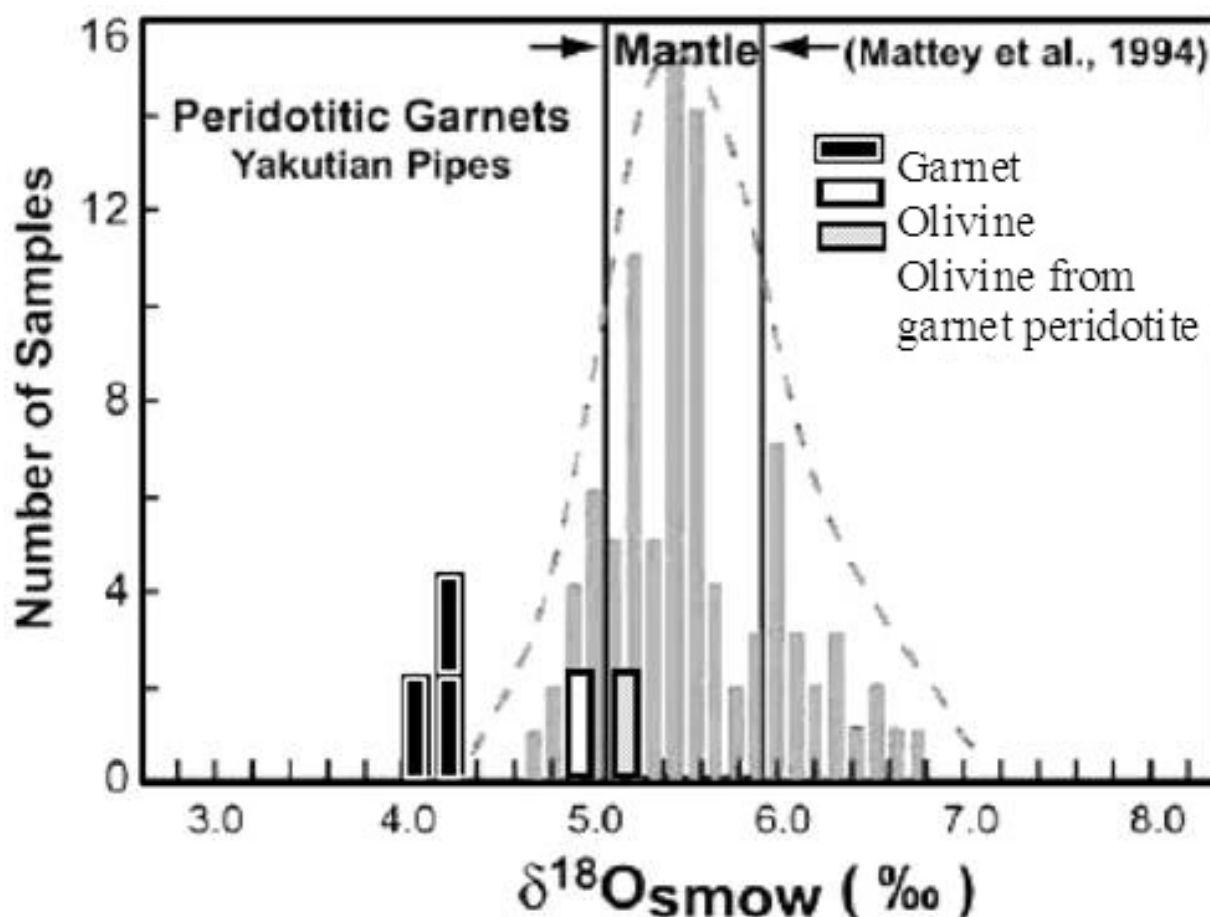


Fig. 8. Oxygen isotope composition of green garnets and olivines from samples of Newlands dike [29]

RB-SR AND SM-ND ISOTOPE COMPOSITIONS OF ROCKS

We managed to analyze Rb-Sr and Sm-Nd isotope compositions of the largest and almost unchanged «wehrlite» sample, but being olivine granitite proper (sample NL-11) (table 3).

A relatively "young" modeled age of the sample as regard to the depleted mantle (1,78 Ga) suggests the age of formation and of "wehrlite" to be is rather young i.e. Mesoproterozoic.

The age of the rock is 1200 Ma, the isotope composition of the mantle source is similar to BSE ($\epsilon\text{Nd} +0.01$, $\epsilon\text{Sr}-6.7$), and at quite probable age of 1500 Ma the

isotope composition of the mantle source of the sample corresponds to moderately depleted mantle ($\epsilon\text{Nd} +3,16$, $\epsilon\text{Sr}-34,2$) close to the mantle trend.

Table 3.

Sr-Nd-isotopic composition of “wehrlite” xenoliths from Newlands dike

Sample	HJI-11
Rb, ppm	20,56
Sr, ppm	112,5
$^{87}\text{Rb}/^{86}\text{Sr}$	0,5282
$^{87}\text{Sr}/^{86}\text{Sr}$	0,711689 \pm 6
Sm, ppm	1,797
Nd, ppm	9,408
$^{147}\text{Sm}/^{144}\text{Nd}$	0,1155
$^{143}\text{Nd}/^{144}\text{Nd}$	0,511999 \pm 9
T_{(Nd)DM}, млрд. лет	1,784

PT-PARAMETRES OF FORMATION OF ROCKS AND GARNET MACROCRYSTS

Studies of mineral parageneses of deep-seated rocks (gar+ol+sp) combined with investigations of garnet trace element composition provided PT-parameters of rock formation. Different methods were used.

PT-parameters of formation of separate green garnet grains were determined using the garnet composition: the temperature was defined via thermometer from Canil, [18] (C99T), and pressure via barometer Grutter, Latti and Menzies, 2006 (GLM06P).

Table 4 demonstrates that green garnets from Newlands dike and Nyurba pipe show similar PT-parameters: 1019-1106°C, 24,5-27,4 kbars and 990-1028°C, 25,3-28,1 kbars, accordingly. (Average values are much similar: 1058 and 1010° C, 25,9 and 27,1 kbars). The PT-parameters as a whole are confirmed by independent methods from mineral parageneses. The temperature of forming the paragenesis ol+gar in the sample NL-11 (O'Neill and Wood, 1979 - NW79T) is 1085 ° C that is quite comparable with 1019 ° C. At the same time for paragenesis ol+sp in the same sample NL-11 the pressure is almost the same 23,4 kbars (Finnerty and Boyd, 1978 - FB78P), but temperature (Ballhaus, Berry and Green, 1991 - BBG91T) is significantly lower – 805° C. A slightly wider scatter in values (but with similar differences) is found for the sample NL-21. It can suggest the non-equilibrium character of ol+sp+gar paragenesis in samples NL-11 and NL-21.

Table 4.

TP-parameters of formation of green garnets					
Paragenesis	T, C			P, кбар	
	Grt	Grt+Ol	Ol+Sp	Grt	Ol
Method	C99T	NW79T	BBG91T	GLT06P	FB78P
Sample	Dike Newlands				
HJI-11	1019	1084	805	24,5	23,4
HJI-21	1037	1240	856	25,3	29,7
HJI-31	1070			26,2	
HJI-41	1106			27,4	
Sample	pipe and placers Nyurbinskaya				
26/510-439	1024			27,7	
12/300-3	1028			28,1	
24/340-6	1000			27,2	
36/420-7	990			25,3	

Garnets on TP-diagram (fig. 9) form compact areas at medium depth in the upper mantle (80-90 km) and correspond to a very hot geotherm (Nyurba pipe and Newlands dike: 52 and 55 mW/m²).

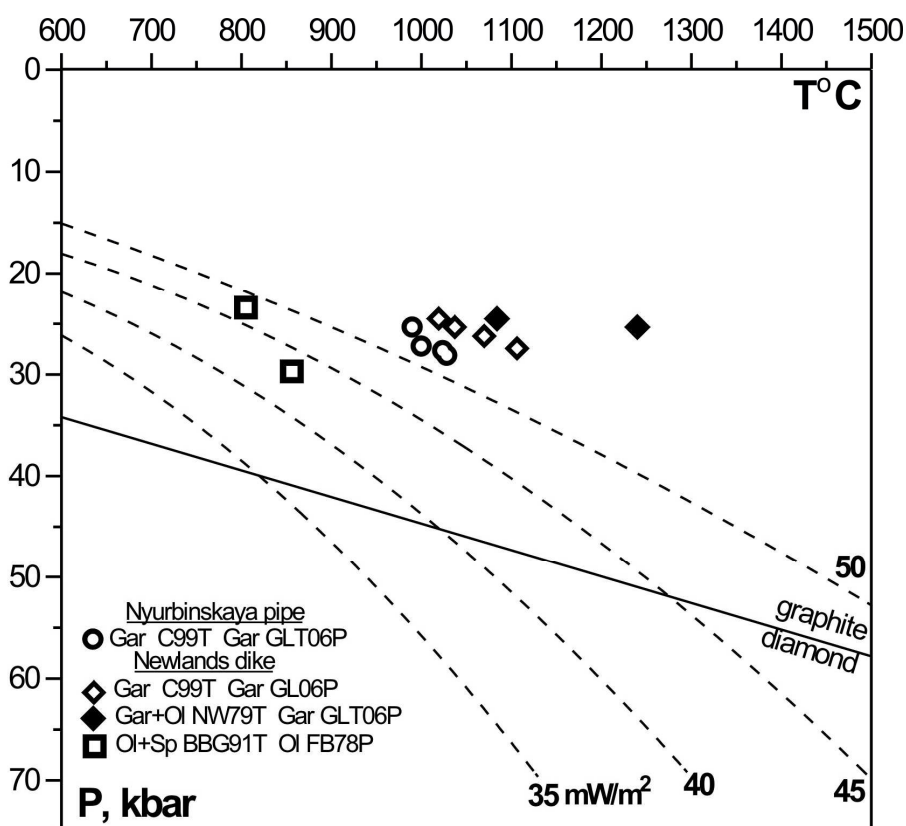


Fig. 9. TP-diagram of formation of green garnets from samples of Newlands dike, kimberlites and placer of Nyurba pipe.

DISCUSSION

Complex studies (including isotope-geochemical studies) of absolutely fresh mantle rocks containing green garnets found in kimberlites of Newlands dike as well as separate green garnet grains found in kimberlites and placer of Nyurba pipe, and their comparison helped to shed light on the origin of these exotic mantle «wehrlites».

Xenoliths of rocks with green garnet from kimberlites demonstrate a very changeable modal composition: from garnet-bearing rocks (to 70 % of garnet), through almost mono-olivine rocks with single small garnet inclusions, to «chromatic ores» (sp (60 %) + gar (30 %)) [14]; clinopyroxene in these xenoliths is practically absent (or at least very scarce). Textures of rocks containing green garnet are rather various - xenomorphic, poikilitic, in cases similar to panidiomorphic. Structures of rocks are also various: massive, schlieren, parallel-banded.

Green garnet grains in some samples from Newlands dike (fig. 1A) exhibit irregular contours, but the clear straight-like margins as though the garnet grew in free space due to the crystallization growth or metasomatic process. On the other hand, in the xenoliths from Zimnyaya pipe [14] «chromite forms almost continuous units which contain elongated garnet grains, contacts of the garnet with chromite are irregular».

«By some signs it is similar to schlieren-like inclusions of the chromite ores containing green garnet in ultramafic rocks of the Ural Mountains and in rocks from the Bushveld complex». Thus, [15] points out « ... a zonal distribution of inclusions of other minerals in green garnet grains from kimberlites, and also heterogeneous composition of its grains which in cases has a clear zonal structure». Heterogeneous structure and composition is found for the intergrowths of two garnet grains from the Newlands dike [20].

Green garnets from kimberlites show the increased LREE and MREE contents as well as higher Sc and in particular Zr. Though the chemical composition of green garnets and concentrations of trace elements are similar, the titanium content in garnets from different samples can differ in 20 times, and that of zirconium - even in 80 times (!), reaching very high values (from 0,09 to 1,75 % TiO₂ and from 13 to 1042 ppm Zr).

The oxygen isotope composition in green garnets ($\delta^{18}\text{O} = 4,05-4,25 \text{ ‰}$) and olivine ($\delta^{18}\text{O} = 4,91 \text{ ‰}$) is significantly different from mantle values. By these indicators the samples with green garnets from kimberlites are similar to the «layered gabbro» from the Semail complex, Oman [22], depleted in $\delta^{18}\text{O}$ in comparison with an average oceanic crust.

The age of rocks with green garnet is relatively young, most likely Mesoproterozoic ($T_{\text{NdDM}} = 1,78 \text{ Ga}$) that can be hardly typical for "usual" rocks of the mantle substratum.

The rocks with green garnet exhibit non-equilibrium character of ol+sp+gar paragenesis. They were produced at medium depth in the mantle (80-90 km) in the

conditions of a high heat flow (52-55 mW/m²), that can be related to the plume formation.

By these features, the rocks with green garnet from kimberlites are not «wehrlites», but most likely are metasomatic formations like uvarovite-chromite veins or schlieren at average depth in the upper mantle - similar to uvarovite-chromite veins of a metasomatic origin in the crustal serpentinites.

The metasomatic nature of uvarovite-containing deep-seated rocks can be confirmed by secant veins of obvious metasomatic origin containing fine-crystalline gar+phlog+sp aggregate in the sample NL-11 from Newlands dike, and by crystalline phlogopite-bearing vein-like inclusions in xenoliths from Zimnyaya pipe [14].

A specific formation of green garnets in kimberlites can be confirmed by the garnet distribution in kimberlites Mud Lake (Canada, Slave Craton). Fig.10 (diagram from Sobolev [10]) shows the fields of eclogite and peridotite garnets. Moreover, the composition of high-calcium and high-chromium (including green) garnets form absolutely special trend of composition change, that confirms a special way of formation of such garnets.

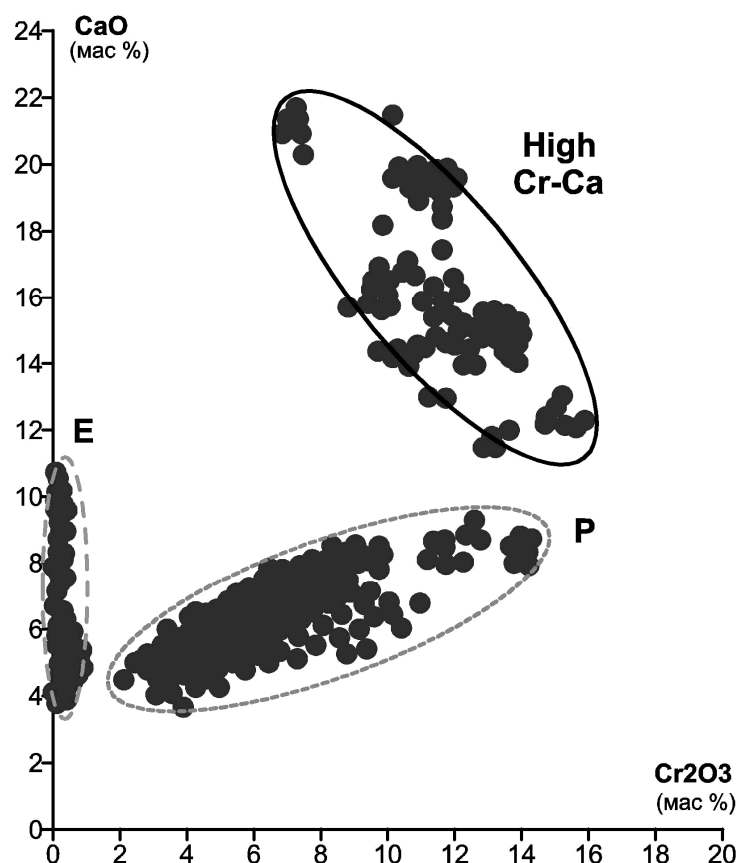


Fig. 10. Distribution of garnets in kimberlites of Mud Lake field (Canada, Slave Craton).

Eclogite-bearing garnets (E) and peridotites granites (P). The compositions of high-calcium (including green) garnets (high Cr-Ca) demonstrate a special location on the diagram and form absolutely special trend of composition.

THE CONCLUSIONS

Complex studies (including isotope-geochemical studies) of absolutely fresh mantle rocks containing green garnets found in kimberlites of Newlands dike as well as separate green garnet grains found in kimberlites and placer of Nyurba pipe, and their comparison helped to shed light on the origin of these exotic mantle «wehrlites».

Xenoliths of rocks with green garnet from kimberlites demonstrate a very changeable modal composition: from garnet-bearing rocks (to 70% of garnet), through almost mono-olivine rocks with single small garnet inclusions, to «chromatic ores» (sp (60 %) + gar (30 %)) [14]; clinopyroxene in these xenoliths is practically absent (or at least very scarce).

Textures of rocks containing green garnet are rather various - xenomorphic, poikilitic, in cases similar to panidiomorphic. Structures of rocks are also various: massive, schlieren, parallel-banded.

Green garnets from kimberlites demonstrate subidiomorphic and irregular shape, zonal distribution of other mineral and heterogeneous composition of grains which sometimes have a clear zonal structure.

Though the chemical composition of green garnets and concentrations of trace elements are similar, they show the increased LREE and MREE contents as well as higher Sc. Moreover, the titanium content in garnets from different samples can differ in 20 times, and that of zirconium - even in 80 times (!), reaching very high values (from 0,09 to 1,75 % TiO₂ and from 13 to 1042 ppm Zr).

The oxygen isotope composition in green garnets ($\delta^{18}\text{O} = 4,05-4,25 \text{ ‰}$) and olivine ($\delta^{18}\text{O} = 4,91 \text{ ‰}$) is significantly different from mantle values. By these indicators the samples with green garnets from kimberlites are similar to the «layered gabbro» from ophiolite complexes.

The age of rocks with a green garnet is relatively young, most likely Mesoproterozoic ($T_{\text{NdDM}} = 1,78 \text{ Ga}$) that can be hardly typical for "usual" rocks of the mantle substratum.

The rocks with green garnet exhibit non-equilibrium character of ol+sp+gar paragenesis. They were produced at medium depth in the mantle (80-90 km) in the conditions of a high heat flow (52-55 mW/m²), that can be related to the plume formation.

By these features, the rocks with green garnet from kimberlites are not «wehrlites», but most likely are metasomatic formations like uvarovite-chromite veins or schlieren at average depth in the upper mantle - similar to uvarovite-chromite veins of a metasomatic origin in the crustal serpentinites.

ACKNOWLEDGMENT

Authors are grateful to John Gyorni, the head of the geological excursion «Small Mines» at 7th International Kimberlite Conference to (the Cape Town University, Cape Town, the Republic of South Africa) and to Felix Vitoldovich Kaminsky (KM Diamond Exploration,

Vancouver, Canada) for the possibility to sample kimberlites of Newlands dike. The authors are thankful to Ilupin I.P., Bogomolov E.S., Kapitonov I.N., Antonov A.V., Tsepin A.I., Dubinina E.O. for the consultations on analytical methods and to Simakov I.K. for unique "PTQuick" software for calculation of PT-parameters:

REFERENCES

1. **Antonova T.A., Nikulin I.I.** The information of the garnets optical-spectroscopic characteristics from different types rocks of the Nakyn kimberlite field // In.: Problems of forecasting and searches of deposits of diamonds in the closed territories: Materials of the conference devoted to 40-anniversary YaNIGP TsNIGRI ALROSA Co. – Yakutsk: Publishing house YaNC SB RAS, 2008. p. 146-150 (in Russian).
2. **Bobrievich A.P., Ilupin I.P., Kozlov I.T. et al.** Petrography and mineralogy of the kimberlitic rocks from Yakutia, M., Nedra, 1964 (in Russian).
3. **Zinchuk N.N., Alyabjev S.G., Banzeruk V.I., Stegnitsky Yu.B., Rotman A.Ya., Egorov K.N., Koptil V.I.** Geology, material composition and diamondiferous kimberlites of the Nakyn field, Yakutia (on an example of Nyurbinskaya pipe). // Geology of diamond - the present and the future. Voronezh. 2005. p. 807-824 (in Russian).
4. **Zankovich N.S., Zinchuk N.N.** Petrographical-mineralogical characteristics kimberlitic rocks of different intrusion phases of Nakyn fields. // In: Problems of diamond geology and some ways of their decision. Voronezh. 2001. p. 54-72 (in Russian).
5. **Kornilova V.P., Fomin A.S., Zaytsev A.I.** New type of the diamondiferous kimberlitic rocks on the Siberian platform. // Regional geology and metallogeny.- 2001.- № 13-14.- p. 105-117 (in Russian).
6. **Kornilova V.P., Rogovoy V.V., Ivanov A.S.** Paragenetic associations of garnet from magmatic sources and panned sample aureoles of the Nakyn kimberlite field // In.: Problems of forecasting and searches of deposits of diamonds in the closed territories: Materials of the conference devoted to 40-anniversary YaNIGP TsNIGRI ALROSA Co. – Yakutsk: Publishing house YaNC SB RAS, 2008. p. 183-190 (in Russian).
7. **Kopylova M.G., Vishnevsky A.A., Ilupin I.P.** High-uvarovite garnet in chrome-diopside dissolution structures // Dokl. Akad. Nauk SSSR, 1992, Vol. 326, № 3, p. 516-520 (in Russian).
8. **Milashev V.A.** The term "kimberlite" and classification of the kimberlitic rocks // Geol. and Geophys., 1963, N 4, p.42-52 (in Russian).
9. **Pokhilenko N.P., Agashev A.M., Vavilov M.A., Sobolev N.V.** Petrological-geochemical characteristics of the kimberlites of especially deep origin, feature of their forecasting and prospecting, potential economic value // Geological aspects of a mineral base of "ALROSA" company, a modern condition, prospects, decisions. Additional materials. Mirny. 2003. p. 147-151 (in Russian).
10. **Sobolev N.V.** (1974) Deep-seated inclusions in kimberlites and a problem of composition of the upper mantle. - Novosibirsk, Nauka, 264 p (in Russian).
11. **Spetsius Z.V., Taylor L.A., Wally.** Geochemistry and $d^{18}O$ of the garnets from the diamondiferous xenoliths of Nyurbinskaya pipe //Proceedings of VI International Seminar «Deepseated magmatism, its sources and plumes: Irkutsk-Mirny. 2006. p. 71-95 (in Russian).
12. **Tarskih O.V., Spetsius Z.V.** Typomorphyc features of indicator minerals from Nyurbinskaya kimberlite pipes (Sredne-Marhinsky area, Yakutia)// In.: Problems of forecasting and searches of deposits of diamonds in the closed territories: Materials of the conference devoted to 40-anniversary YaNIGP TsNIGRI ALROSA Co. – Yakutsk: Publishing house YaNC SB RAS, 2008. p. 208-215 (in Russian).

13. **Tomshin M.D., Fomin A.C., Kornilova V.P., Cherny C.D., Yanigin Yu.T.** Features of magmatic formations Nakyn kimberlite fields of the Yakutia province // *Geol. and Geophys.*-1998.- Vol.39, № 12.- p. 1693-1703 (in Russian).
14. **Kharkiv A.D.** A find of the ore wehrlite xenoliths in “Zimnaya” kimberlite pipe (Verhne-Munsky diamondiferous region, Yakutia) // *Dokl. Akad. Nauk SSSR.* 252(3), (1978) p.181-184 (in Russian).
15. **Kharkiv A.D.** Undercrusts (protomagmatic) a stage of crystallization of kimberlite minerals and its connection with diamondiferous. // *News SA the USSR, Geol. series, № 1* (1975). P. 14-23 (in Russian).
16. **Boynton W.V.** Geochemistry of the rare earth elements: meteorite studies. In: Henderson P. (ed.), *Rare earth element geochemistry.* Elsevier, 1984, pp. 63-114.
17. **Canil D.** (1996) An experimental calibration of the nickel in garnet geothermometer with applications: reply. *Contrib Mineral Petrol* 124: 219±223
18. **Canil D.** (1999) The Ni-in-garnet geothermometer: calibration at natural abundances. *Contributions to Mineralogy and Petrology*, 136: 240–246.
19. **Cherny S.D., Fomin A.S., Yanygin Yu.T., Banzeruk V.I , Kornilova V.P.** (1998) Geology and composition of the Nakyn field kimberlite pipes and diamond properties (Yakutia) // 7-th IKC. Cape Town. Extended Abstracts. P. 9-10.
20. **Clarke D.B. and Carswell D.A.** (1977) Green garnets from the Newlands kimberlite, Cape Province, South Africa. // *Earth and Planetary Science Letters* 34. p. 30- 38.
21. **Dawson J.B. and Stephens W.E.** (1975) Statistical analysis of garnets from kimberlites and associated xenoliths. *Journal of Geology*, v. 83, p. 589-607.
22. **Gregory R.T. and Taylor H.P.** (1981) An oxygen isotope profile in a section of Cretaceous oceanic crust, Semail ophiolite Oman: evidence for d18O buffering of the jceans by deep (>5 km) seawater – hydrothermal circulation at mid-ocean ridges. *J. Geophys. Res.*, 86, 2737-2755.
23. **Griffin W.L., Jaques A.L., Sie S.H., Ryan C.G. Cousens D.R. and Suter G.F.** (1988) Conditions of diamond growth: a proton microprobe study of inclusions in West Australian diamonds. *Contrib. Mineral. Petrol.*, 99: 143-158.
24. **Griffin W.L., Cousens D.R., Ryan C.G., Sie S.H. and Suter G.F.** (1989a). Ni in chrome pyrope garnets: a new thermometer. *Contrib. Mineral. Petrol.*, 103: 199-203.
25. **Griffin W.L., Smith D., Boyd F.R., Cousens D.R., Ryan C.G., Sie S.H. and Suter G.F.,** (1989b). Trace element zoning in garnets from sheared mantle xenoliths. *Geochim. Cosmochim. Acta*, 53: 561-567.
26. **Griffin W.L., Sobolev N.V., Ryan C.G., Pokhilenko N.P., Win T.T. and Yefimov Y.** (1993) Trace elements in garnets and chromites: diamond formation in the Siberian lithosphere. *Lithos*, 29: 235-256.
27. **Griffin W.L., Ryan C.G., Gurney J.J., Sobolev N.V. and Win T.T.** (1994) Chromite macrocrysts in kimberlites and lamproites: geochemistry and origin. In: H.O.A. Meyer and O.H. Leonardos (Editors), *Kimberlites, Related Rocks and Mantle Xenoliths.* CPRM Spec. Publ. 1A/93, pp. 366-377.
28. **Griffin W.L., Ryan C.G.** (1995) Trace elements in indicator minerals: area selection and target evaluation in diamond exploration. *J Geochem Explor* 53: 311–337
29. **Griffin W.L., O'Reilly S.Y., Ryan C.G., Gaul O., Ionov D.** (1998) Secular variation in the composition of subcontinental lithospheric mantle. In: Braun, J., Dooley, J.C., Goleby, B.R., van der Hilst, R.D., Klootwijk, C.T. (Eds.) *Structure and Evolution of the Australian Continent.* *Geodynamycs* Vol. 26, American Geophysical Union, Washington, DC, pp 1-26.

30. **Griffin W.L., Ryan C.G., Kaminsky F.V., O'Reilly S.Y., Natapov L.M., Win T.T., Kinny P.D., Ilupin I.P.** (1999) The Siberian lithosphere traverse. Mantle terranes and the assembly of the Siberian craton. *Tectonophysics* 310, 1–35.
31. **Hornung G., Nixon P.H.** In: Lesotho kimberlites. Maferu: Lesotho Nat. Develop. Corp., 1973, p. 122-130.
32. **Mattey D., Lowry D., Macpherson C.** (1994). Oxygen isotope composition of mantle peridotite. *Earth Planet. Sci. Lett.* 128, 231-241.
33. **McDonough W.E., Sun S.S.** 1995. The composition of the Earth. *Chemical Geology* 120, 223-253.
34. **Nixon P.H., Griffin B.L., Davies G.R., Condliffe E.** Cr garnet indicators in Venezuela kumberkites and their bearing on the evolution of the Guyana craton. // *Proceedings of the Fifth IKC, Brazil, 1993.* P 376-387.
35. **Norman M.D., Pearson N.J., Sharma A., Griffin W.L.** (1996). Quantitative analysis of trace elements in geological materials by laser ablation ICPMS: instrumental operating conditions and calibration values of NIST glasses. *Geostand. Newsl.* 20, 247-261.
36. **Smith C.B., Gurney J.J., Skinner E.M.W., Clement C.R., Ebrahim N.** (1985). Geochemical character of Southern African kimberlites. A new approach based on isotopic contents. *Trans. Geol. Soc. S. Afr.* 88, 267-280
37. **Sobolev N.V., Lavrent'ev Yu.G., Pokhilenko N.P. and Usova L.V.** Chrome-rich garnets from the kimberlites of Yakutia and their paragenesis. // *Contrib. Mineral. Petrol.* 40 (1973) p. 39-50.
38. **Schulze D.J.** (1986) Green garnets from South Afrikan kimberlites and their relationship to wehrlites and crustal uwarowites. *Proceeding 4th IKC, Pert. V.* 2 p. 820-826.
39. **Taylor L.A., Spetsius Z.V., Wiesli R., Anand M., Promprated P., and Valley J.W.** (2003) The origin of mantle peridotites: crustal signatures from Yakutian kimberlites. 8th IKC. Victoria. Exstented Abstracts.

DEEP-SEATED XENOLITHS AND XENOCRYSTS FROM SYTYKANSKAYA PIPE: EVIDENCE FOR THE EVOLUTION OF THE MANTLE BENEATH ALAKIT, YAKUTIA

Ashchepkov I.V.¹, Vladykin N.V.², Ntaflos T.³, Logvinova A.M.¹, Yudin D.S.¹,
Karpenko M.A.⁴, Palesskiy V.S.¹, Khmel'nikova O.S.¹

¹*Institute of Geology and Mineralogy SD RAS, Koptyugave 3, Novosibirsk, Russian Federation*

²*Institute of Geochemistry SD RAS, Irkutsk, Russia*

³*University of Vienna, Austria*

⁴*Alrosa Stock Company, Mirny, Russia*

ABSTRACT

The concentrate from two phases of the kimberlite (breccia and porphyritic kimberlite) and about 130 xenoliths from the Sytykanskaya pipe of the Alakit field (Yakutia) were studied by EPMA and LAM ICP methods. Reconstructions of the PTX/ fO_2 mantle sections were made separately for the two phases. The porphyritic kimberlites and breccia show differences in the mineral compositions although the reconstructed mantle layering and pressure interval remains the same. For the porphyritic kimberlite the trends P- Fe# - CaO in garnet, fO_2 are sub-vertical while the xenocrysts from the breccia show stepped and curved trends possibly due to interaction with fluids. Minerals within xenoliths show the widest variation in all pressure intervals. PT points for the ilmenites which trace the magmatic system show splitting of the magmatic source into two levels at the pyroxenite lens (4GPa) [33, 38] accompanied by peridotite contamination and an increase in Cr in ilmenites. Two groups of metasomatites with Fe#Ol ~ 10-12% and 13-15% were created by the melts derived from protokimberlites and trace the mantle columns from the lithosphere base (Ilm-Gar-Cr diopside) to Moho becoming essentially pyroxenitic (Cr-diopside with Phl).

The first Opx-Gar-based mantle geotherm from the Alakit field has been constructed from 15 associations and is close to 35 mw/m² in the lower part of mantle section but deviates to high temperatures in the upper part of the mantle section. The oxidation state for the protokimberlite melts determined from ilmenites at the lithosphere base is higher than for the other pipes in the Alakit field Yakutian kimberlite province which probably accounts for the decrease in the diamond grade of this pipe.

The geochemistry of the minerals (garnets and clinopyroxenes) from breccias, metasomatic peridotite xenoliths and pyroxenites systematically differ. Cr-Diopside xenocrysts from the breccia were produced by the most differentiated melts and enriched protokimberlite or carbonatite; they show highly inclined nearly linear REE patterns and deep troughs of HFSE. The REE patterns for minerals of the metasomatic xenoliths are less inclined with lower La/Ce_n ratios and without troughs in spider diagrams. The garnets often show S-shaped patterns. Clinopyroxenes from the Cr websterites show different enrichments in REE highly inclined and more straight pattern and deep troughs in Ba and varying enrichment in Nb-Ta-U lower

then REE. Those with lower TRE reveal Zr-Hf dips. The clinopyroxenes from glimmerites reveal highest REE and dips in Pb. Garnets show also more straight line REE patterns with then in primitive melts Sr – Ba dips but varying Th-U Nb- Ta.

The ^{40}Ar - ^{39}Ar ages for micas from the Alakit field reveal three intervals for the metasomatism. The first (1154 Ma) relates to dispersed phlogopites found throughout the mantle column, and probably corresponds to the continental arc stage in the early stage of Rodinia. Veined highly alkaline and Ti-rich veins with richterite ~1015 Ma corresponds to the plume event within the Rodinia mantle. The ~600-550 Ma stagemarksthe final Rodinia break-up. The last one near 385 Ma is protokimberlite related.

Keywords: mantle, kimberlites, lithosphere, mantle xenoliths, xenocrysts, monomineral thermobarometry, pyropes, ilmenites, geochemistry.

INTRODUCTION

The Sytykanskaya kimberlite pipe is located near the boundary of the Daldyn and Alakite fields in the upper stretches of the Sytykan creek [5, 45, 52]. It is buried by dolerite sills that are ~ 60m in thickness. The pipe is built up from the two major phases: black porphyritic kimberlites and greenish grey autolithic breccia containing a huge amount of xenoliths. The kimberlite is now completely excavated and is lying near the pipe. The diamond grade is not very high compared with the other large pipes in the Alakit field but some large diamonds to 342 carats were discovered.

Among the kimberlites from Alakit field, the Sytykanskaya pipe is characterized by a large amount of deep-seated xenoliths which contain relics of fresh minerals, e.g. pyroxenes, garnets, olivines, micas, amphiboles, chromites, ilmenites and some other rare phases.

In this work we give the characteristics of the deep-seated xenoliths and xenocryst minerals from this pipe using mainly EPMA and ICP MS analyses and compare these results with the data for the concentrates from breccia and porphyritic kimberlites on the variation and TPX diagrams. The xenocrysts of porphyritic kimberlite breccia and the xenoliths were analyzed separately.

METHODS AND DATA

The minerals from the concentrates of breccia (500) and porphyritic kimberlites (400) were analyzed by EPMA. We also studied about 130 peridotite xenoliths of lherzolite, mainly the enriched harzburgite type, half of which contain veins with phlogopites and other minerals, and 9 pyroxenites and two eclogites. All of them were analyzed using a Camebax Micro microprobe using the methods described [21]. The most interesting xenoliths (5) were analyzed in detail in the University of Vienna.

Analyses of trace elements for three types of inclusions (xenocrysts from the breccia concentrate, metasomatic xenoliths and Gar websterites) were made by the LAM ICP MS methods using Finnigan Element mass spectrometer and laser ablation system Nd YAG: UV NewWave.

PETROGRAPHY

The percentage of xenolith types is given using the collection of about 250 xenoliths with corrections after A.Manakov [24]. Among the xenoliths are harzburgites (5 %) and slightly depleted garnet lherzolites (40 %), Sp lherzolites (15 %), garnet phlogopite-ilmenite veined xenoliths (20 %), dunites (4 %), garnet dunites (1 %), garnet pyroxenites with ilmenites and mica (7 %), and Phl-Ilm metasomatic veins (glimmerites) (8 %).

Most xenoliths contain phlogopite. It is found as sporadic grains dispersed in the rocks and also as micro- and macro-veins, commonly with Cr-diopsides and rarely garnet or chromite. Phlogopites commonly form coronas on garnets or together with pyroxenes totally replace garnets grains, forming symplectites. Veins of Ilm-Phl-Cr-diopsides form the stockworks in the peridotite matrix and cut through the large porphyroclasts of olivine and garnets. Some monomineralic ilmenite veins cut large garnet porphyroclasts. Rare fine-grained essentially olivine peridotites contain intergranular Ilm and ulvospinel grains as well as Cr-diopsides (Cr-Di) and garnet relics. They are relatively low temperature analogs of the deformed peridotites [1, 17]. The eclogite xenoliths which occur in other Yakutian kimberlite pipes [44, 45, 52] are rare; we collected only two, though some diamond-bearing eclogites were discovered in pipe [52] with kyanite also [20]. Several practically fresh garnet pyroxenites (websterites) which also contain mica and chromites, were discovered. Some of them contain significant amounts of graphite.

The megacryst association is represented mainly by ilmenite and pyrope garnets. Several large ilmenite nodules contain large monocrystals cemented by fine Ilm grains and, in the outer contact, these aggregates contain Cr-Di and olivines from the peridotites.

MINERALOGY

Pyrope compositions on the diagram for the breccia and xenoliths (fig. 1a) and porphyritic kimberlites and pyroxenites (fig. 1a) show similarity in the configuration of the clouds and clots of data points and close interval of Cr_2O_3 variations to 13%. The total amount of sub-Ca garnets [33, 36, 45, 46, 49] is higher in porphyritic kimberlites. The largest fraction of Ti-rich garnets plots in the part of the left diagrams, as well as CaO-rich garnets of pyroxenitic type and Fe-enriched from the metasomatites in the middle part of the diagram.

In the P-Fe# and P-CaO diagrams (figs. 7-9), the trends for garnets from the breccia are more curved, possibly due to metasomatic processes.

The Cr-diopsides on the variation diagrams (fig. 2) divide into three intervals according to FeO content. Most are the low-Fe type (1-2 % FeO) and come from enriched harzburgites and lherzolites with low contents of all admixtures

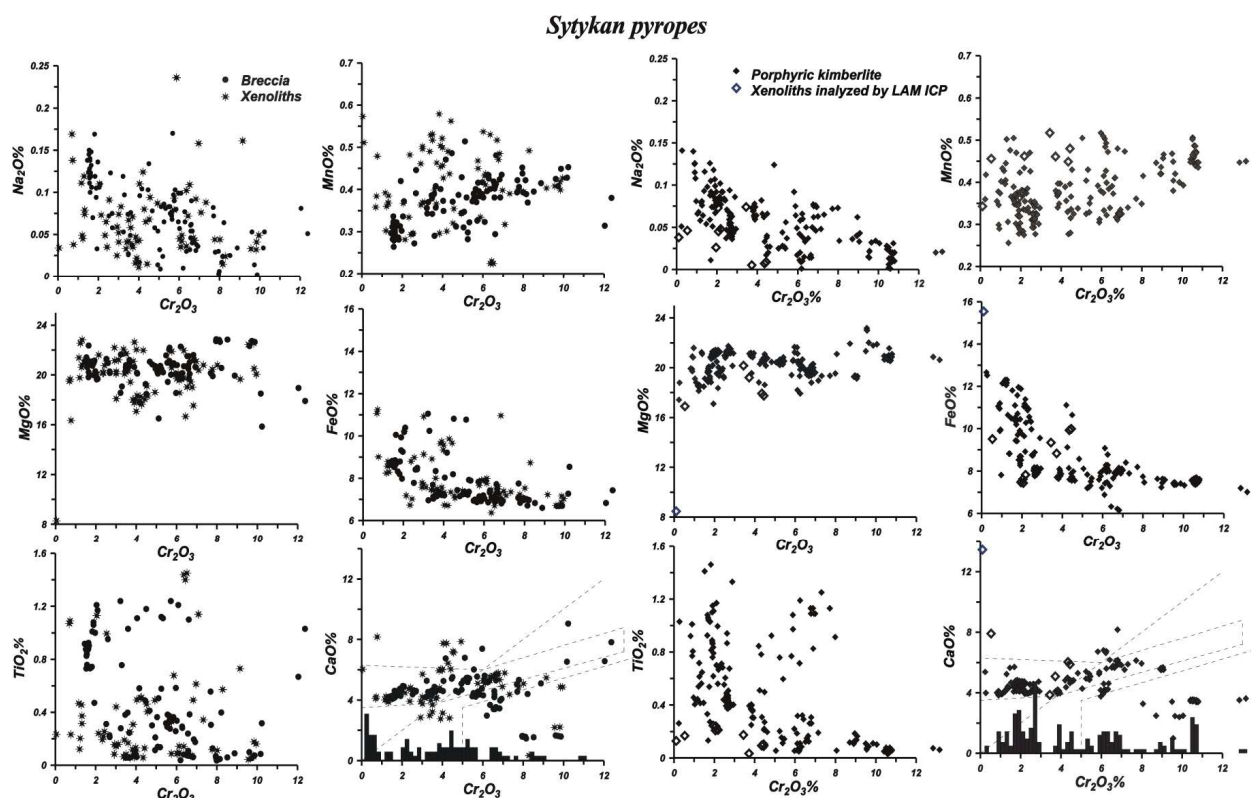


Fig. 1. Compositions of the pyropes (a) from breccia (b) and porphyritic kimberlites from Sytykansкая pipe.

In addition in (fig. 1a) the compositions of the analyzed xenoliths are shown, and on (fig. 1b) compositions of the veined metasomatites and pyroxenites analyzed by LAM ICP-MS, including Cr which slightly increases at the end of interval. The varieties showing greatest variability Na, Cr, Al, Ti are metasomatic Cr-Di from the middle part of diagram (2-3.5 % FeO). The highest values are from Cr-Di glimmerites with richterite. The Fe-rich part corresponds to the Ilm metasomatites. They form two branches with different contents of Na and Ti.

Chromites are represented mostly by Cr-rich varieties. The fraction of the varieties that locate within the diamond window [36, 45, 46] is higher in the breccia and slightly less in the porphyritic kimberlites. But some varieties are enriched in TiO_2 . The amount of such chromites is higher in the metasomatic xenoliths. The Al_2O_3 - Cr_2O_3 chromite plot does not show the common linear Cr-Al correlation but creates a cloud of points in the Cr-rich part due to the high degree of metasomatism. Only harzburgitic chromites form common Al_2O_3 - Cr_2O_3 trend.

Ilmenites from Sytykansкая reveal the greatest variations (fig. 4) and most complicated trends among those studied in the Yakutian province, showing wide variations in Cr and Al. For the ilmenites from the porphyritic kimberlite there are 4 levels of Cr_2O_3 enrichment, while in Daldyn region three levels are common [19]. The trend of ~ 0.5 is parallel to the TiO_2 and formed by the fraction of uncontaminated protokimberlite melts. The linear increase in this component from 2 to 3% relates to the stage of the formation of the melt channels in the mantle

column, which is followed by the permanent dissolution of associations containing chromite and Cr-diopsides.

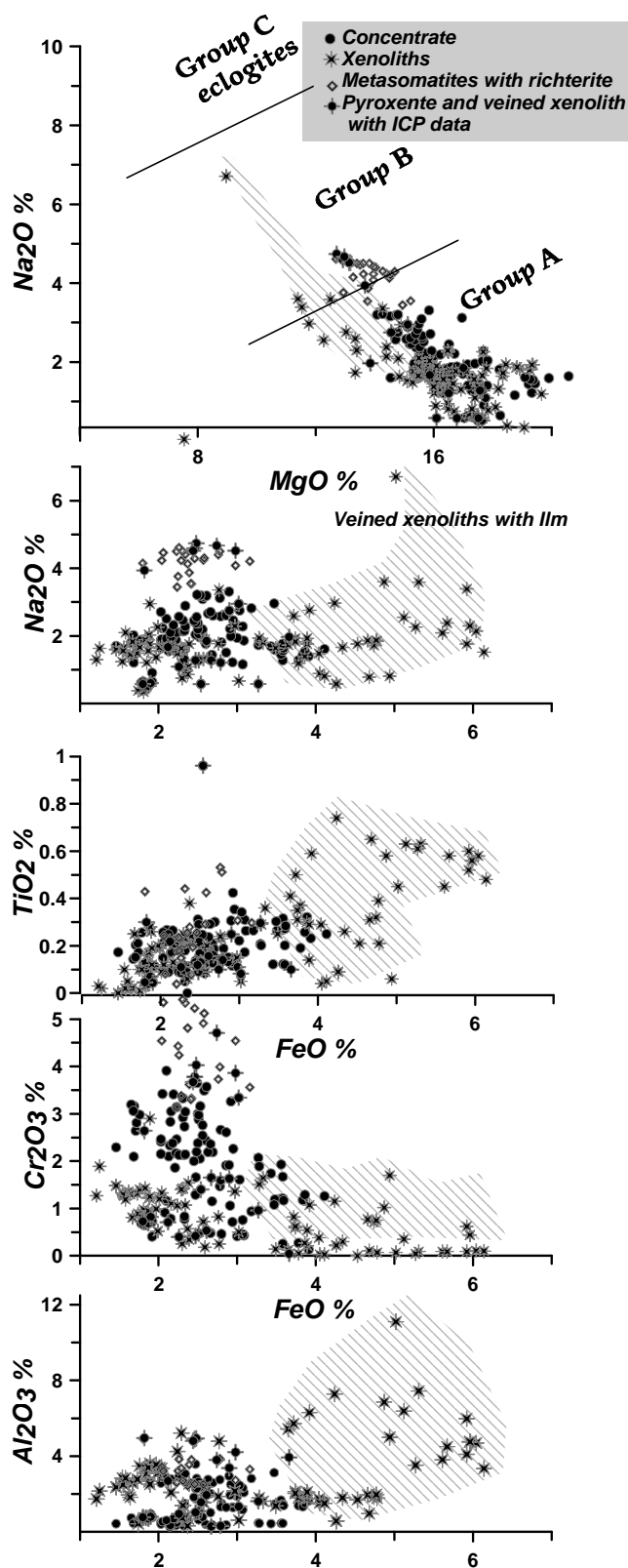


Fig. 2. Compositions of Cr-diopsides from breccia and porphyric kimberlites from Sytykanskaya pipe. The signs are the same.

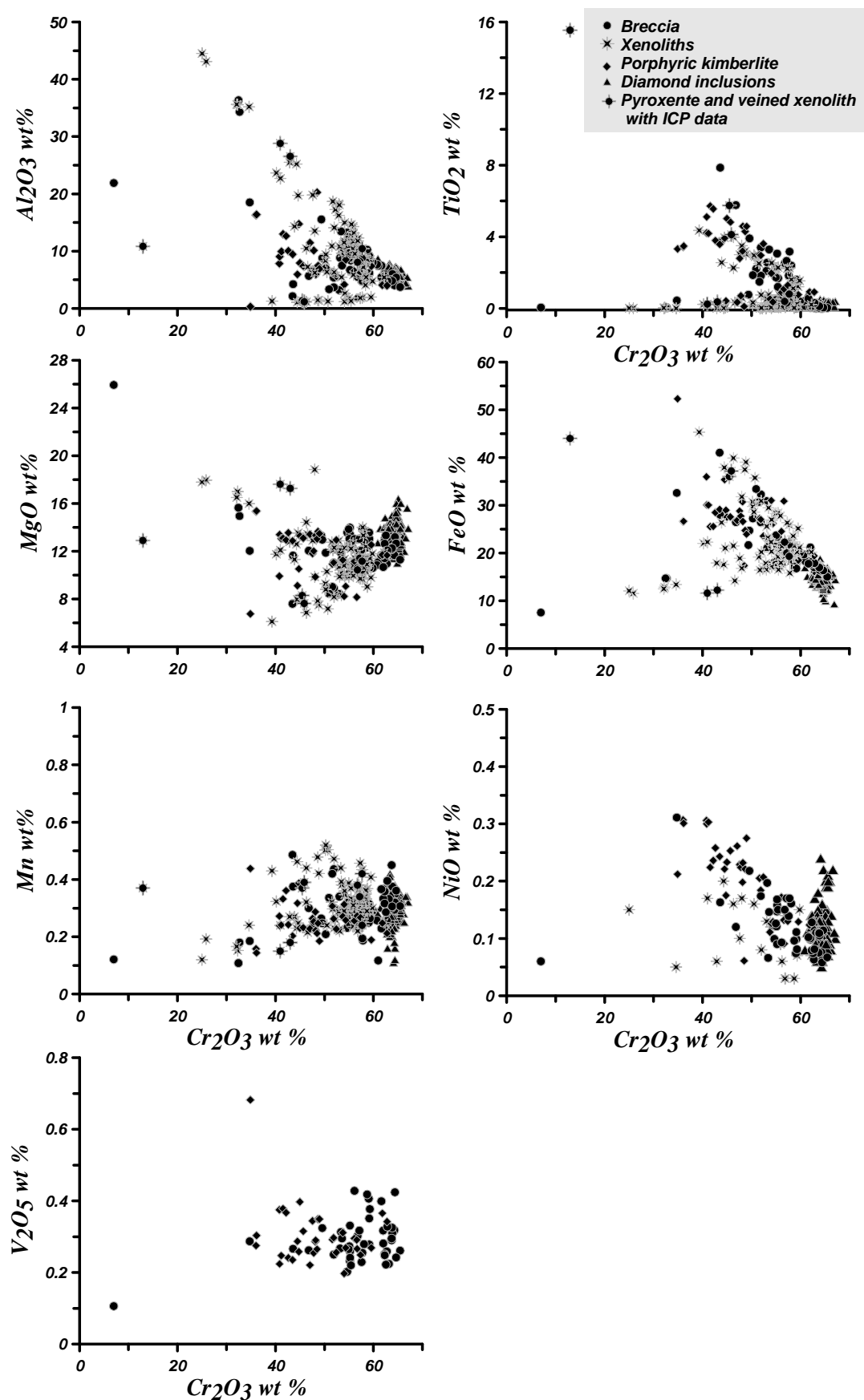


Fig.3. Compositions of chromites.

From breccia (a) and porphyric kimberlites (b) from Sytykanskaya pipe. The signs are the same.

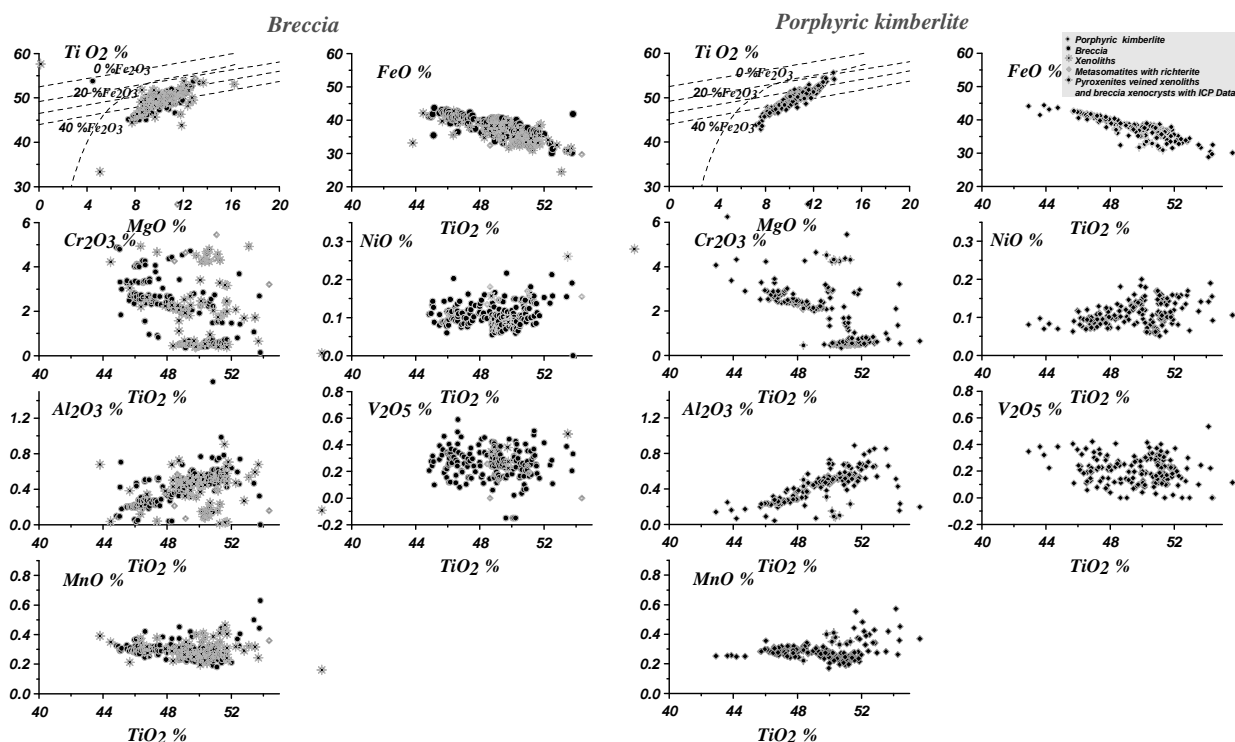


Fig.4. Compositions of ilmenites.

From breccia (a) and porphyric kimberlites (b) from Sytykanskaya pipe. The signs are the same.

A further two levels ~ 3.5 and 5% Cr_2O_3 in the middle part of the TiO_2 - Cr_2O_3 trends belong to the phlogopite-bearing metasomatites and glimmerite with richterites which have very high Cr contents. They are from the middle part of the mantle column and belong to the lower so-called pyroxenite lens [35]. In the low-Ti part of the trend, there are several levels of the Cr-enrichment as seen in many Alakit kimberlites.

This is quite different compared with the situation of the South Africa where Cr-enrichment is common for the low- and high-Mg ilmenite varieties. This was determined as Haggerty's parabola [14] and explained as a structural phenomenon. But in reality it is related to the metasomatites located in the upper and lower parts of the protokimberlite system.

The ilmenite trend from the kimberlite breccia and from xenoliths show very close configuration and division into the same levels but the trends are more dispersed. In group 1 (low-Cr), Cr decreases together with the TiO_2 . The MnO content is in general also decreasing.

Amphiboles. Amphiboles in the Sytykanskaya pipe were found in the veins with phlogopites and ilmenites. Only those found in alkaline glimmerites are richterite. Since they are not so high pressure as those obtained in the high pressure experiments at 7.0-9.0 GPa [18], they are the K-Na type of richterites which were obtained in experiments at 3 GPa [55]. Similar amphiboles were found in the harzburgites from Udachnaya pipe. Most amphiboles from veined xenoliths from Sytykanskaya are Cr-pargasite and one is pargasitic hornblende, similar to those

found in the northern parts of Yakutia. Only one ilmenite from the ilmenite-bearing vein reveals high Ti content.

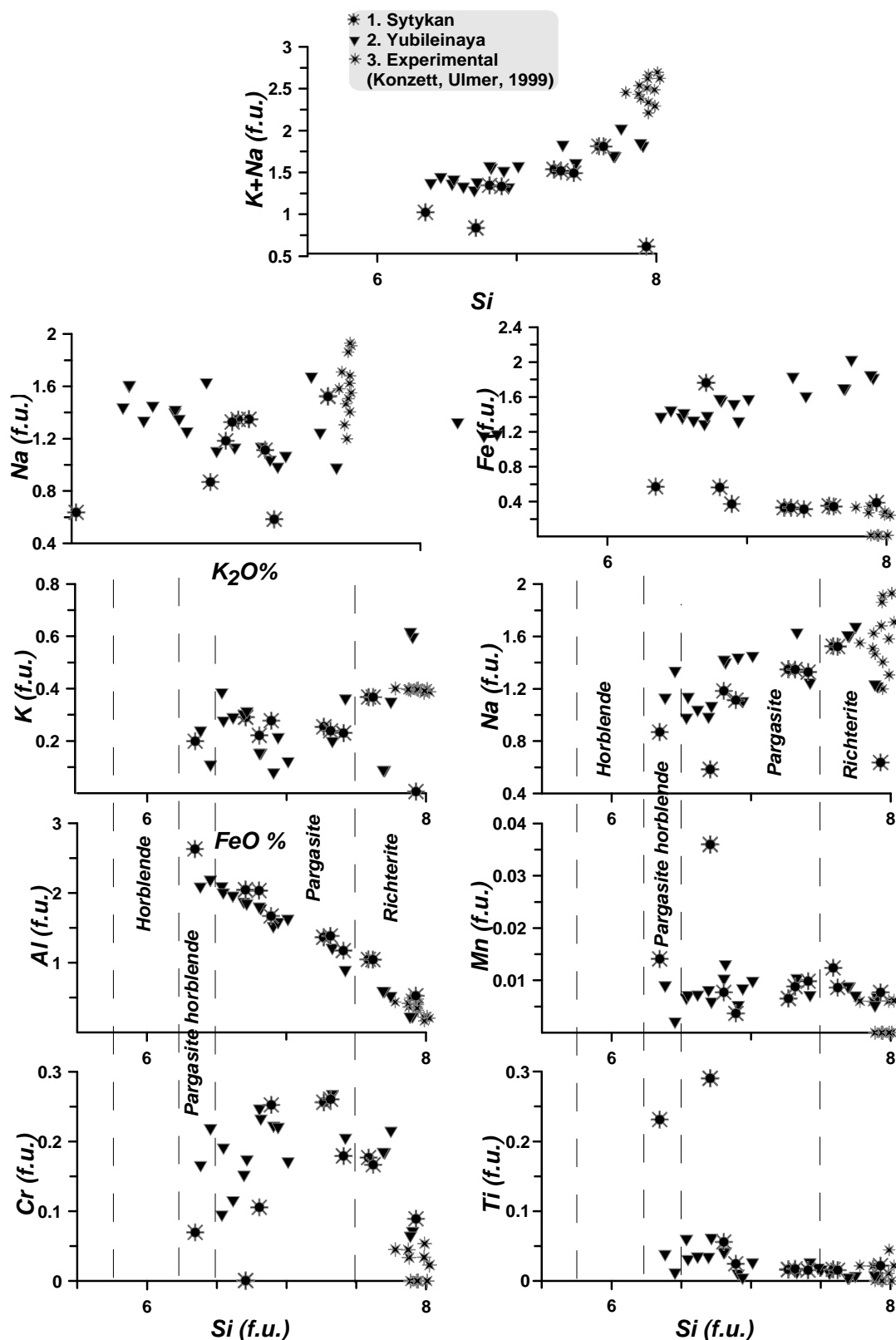


Fig.5. Compositions of amphiboles.

From breccia and mantle xenoliths from Sytykanskaya pipe. The signs are the same.

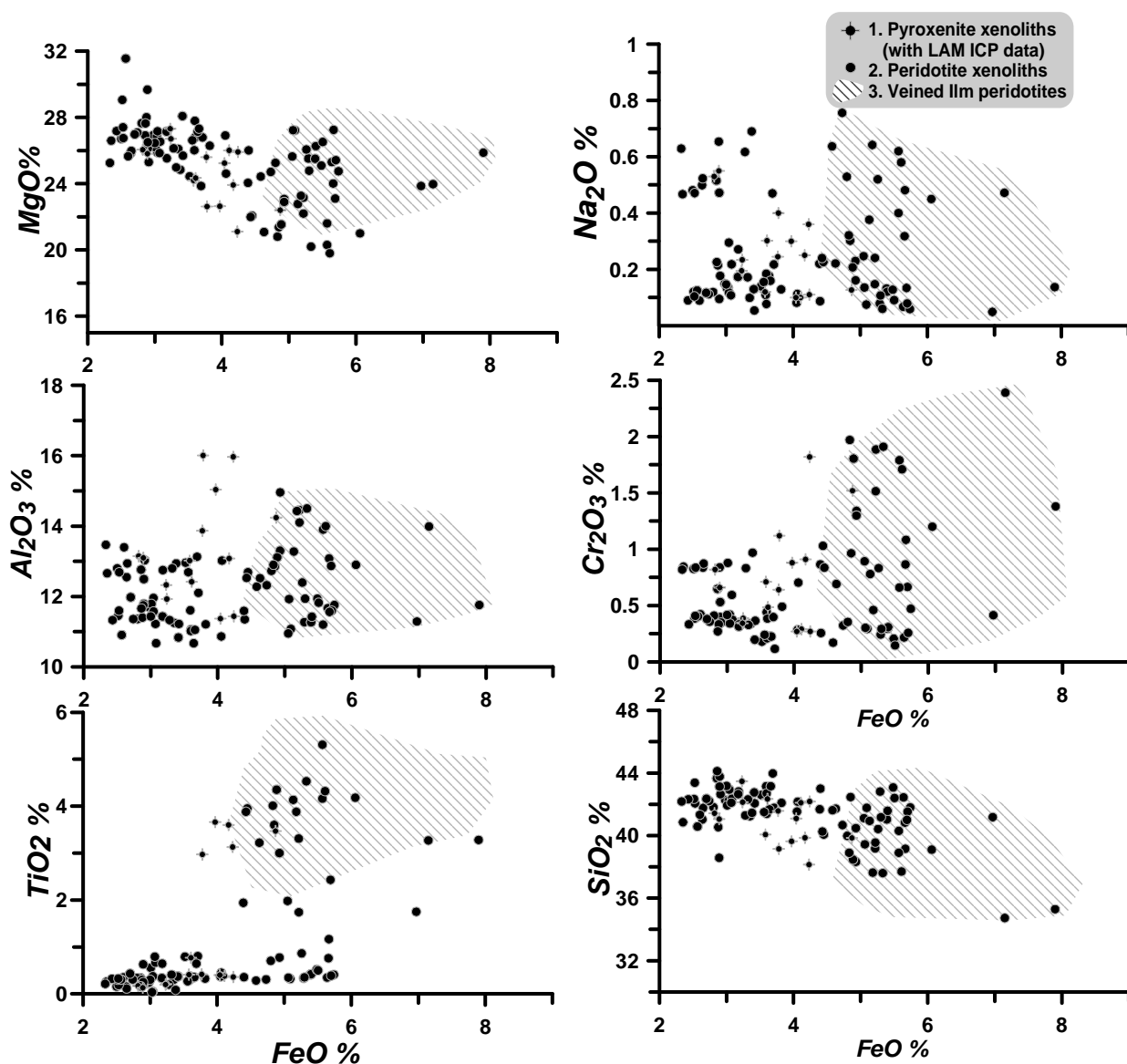


Fig.6. Compositions of phlogopites.

From breccia and mantle xenoliths from Sytykanskaya pipe. The signs are the same.

Phlogopites from Sytykanskaya xenoliths are highly variable in composition. For the low-Fe varieties two levels of the Cr₂O₃ enrichment are visible: 0.5 and 2% Cr₂O₃. Phlogopites with FeO > 4% and Cr₂O₃ close to 4-5 % are from the ilmenite-bearing veins. The Na₂O content is also up to 0.8 % being lower in the middle part of the trend and high for the ilmenite-bearing associations. In the middle part of the diagram the TiO₂ level is highest at 2-5 %. Variations with increasing admixtures in phlogopites are accompanied by a decrease in SiO₂. The rise of Ti, Na, Cr corresponds to the increase of the Al/(Al+Si) oreastonite component which corresponds to a pressure decrease [2, 26].

PTX DIAGRAMS AND VARIATION OF THE OXYGEN FUGACITY CONDITIONS

Separate PTX_fO₂ diagrams obtained for the xenocrysts from the breccia (fig. 7) and porphyritic kimberlite (fig. 8) give the opportunity to evaluate the sequence of events. Variations of PT conditions for garnet xenocrysts form a simple linear trend which is at 600°C at the level of the Moho and descends to 35 mW/m² geotherm at 6.5 GPa, where there is an inflection corresponding to the convective branch [11] formed by the high temperature trend for chromite and ilmenites.

Table 1.

Compositions of the major and trace element components for clinopyroxenes, phlogopites from the autolithic breccias from Sytykanskata pipe

Number	S079	S052	S053	S054	S055	S056	S068	S640	S068	S067	S053	STK14	STK24
Element	Clinopyroxenes											Phlogopites	
SiO ₂	54.21	54.36	53.32	53.92	54.31	54.89	54.29	54.81	54.55	54.83	54.82	40.67	37.63
TiO ₂	0.121	0.048	0.094	0.185	0.069	0.268	0.14	0.05	0.268	0.1	0.094	0.308	3.88
Al ₂ O ₃	0.618	2.83	0.71	2.83	2.69	3.27	4.25	2.82	1.59	0.94	0.71	12.32	14.43
Cr ₂ O ₃	2.26	3.01	2.61	0.788	3.35	0.681	3.51	3.37	4.09	3.53	2.61	0.323	0.46
FeO	2.22	2.18	2.04	3.25	1.9	4.3	2.07	2.31	2.39	2.36	2.04	4.73	5.18
MnO	0.067	0.1	0.046	0.068	0.101	0.142	0.075	0.086	0.102	0.062	0.046	0.035	0.063
MgO	16.06	14.27	15.63	14.67	13.93	17.57	13.22	13.92	14.75	14.86	15.63	24.71	23.27
CaO	21.24	18.96	21.2	20.3	18.55	14.69	16.96	18.12	17.64	19.84	21.2	0.044	0.052
Na ₂ O	1.84	3.06	1.82	2.24	3.22	2.65	4.04	3.38	3.3	2.43	1.82	0.756	0.642
K ₂ O	0.008	0.027	0.027	0.031	0.02	0.04	0.009	0	0.009	0.003	0.027	10.63	9.7
Total	98.644	98.845	97.497	98.282	98.14	98.501	98.564	98.866	98.689	98.955	98.997	94.526	95.307
Ba	3.67	0.59	7.60	0.66	15.71	12.24	0.68	0.97	0.97	6.31	0.29	21546	16128
La	1.72	8.80	9.34	3.25	16.39	45.02	31.01	38.98	45.26	116.82	5.97	3.60	0.59
Ce		35	29	13	36	114	106	136	178	299	11	6.72	1.69
Pr	0.8	5.9	4.7	2.0	5.0	15.2	11.2	14.1	18.2	34.9	1.5	0.79	0.32
Nd	4.5	28.3	23.7	9.2	22.1	66.1	44.5	52.8	65.1	131.7	5.4	5.22	2.96
Sm	1.05	5.72	5.18	1.87	4.28	12.25	8.00	9.81	11.81	20.73	0.44	2.58	0.90
Eu	0.39	1.64	1.55	0.53	1.11	3.44	2.48	3.03	3.34	6.00	0.12	0.60	0.30
Gd	1.11	4.28	4.18	1.38	3.78	10.36	5.89	6.77	7.82	13.81	0.3	0.44	0.47
Tb	0.14	0.43	0.43	0.14	0.45	1.10	0.66	0.77	0.87	1.56	0.03	0.03	0.06
Dy	0.84	2.05	1.97	0.60	1.88	4.92	2.87	3.48	3.64	6.33	0.13	0.12	0.18
Ho	0.14	0.29	0.28	0.09	0.31	0.68	0.37	0.45	0.47	0.91	0.02	0.03	0.03
Er	0.34	0.65	0.56	0.18	0.71	1.08	0.70	0.82	0.84	1.57	0.03	0.08	0.05
Tm	0.04	0.06	0.06	0.02	0.08	0.12	0.06	0.08	0.09	0.18	0.003	0.02	0.02
Yb	0.22	0.40	0.31	0.10	0.48	0.66	0.32	0.38	0.44	0.83	0.011	0.06	0.11
Lu	0.03	0.04	0.03	0.01	0.06	0.06	0.04	0.04	0.05	0.09	0.002	0.01	0.04
Hf	0.56	2.43	3.14	1.04	5.70	6.93	1.92	2.35	2.42	4.43	0.37	0.35	0.22
Ta	0.03	0.11	0.17	0.02	0.34	0.15	0.03	0.04	0.20	4.06	0.002	0.61	3.77
Pb	2.84	0.29	0.71	0.33	10.44	5.86	2.77	3.72	4.12	4.77	0.8	9.96	1.92
Th	0.09	0.10	0.62	0.03	1.07	2.43	1.76	2.37	2.32	10.06	0.46	10.58	4.44
U	0.06	0.03	0.18	0.01	0.82	0.28	0.35	0.53	0.50	1.01	0.02	0.34	0.53
Sc	20	47	45	15	196	186	109	143	144	199	12	42	21
V	182	155	376	187	348	1084	1236	1649	1637	1462	141	1897	634
Co	34	7	18	9	119	72	76	100	103	101	5	1023	490
Cu	5.46	0.18	6.56	1.05	52.71	16.51	2.53	6.42	2.16	11.66	0.3	33	18
Ni	434	114	317	126	2524	1014	957	1257	1253	1566	85	7548	4607
Rb	0.73	0.04	0.63	0.05	3.81	0.32	0.01	0.02	0.07	0.40	0.03	7.56	3.38
Sr	102	247	253	119	415	968	770	979	1042	1318	133	50	21
Y	3.35	7.02	6.25	2.05	7.71	15.80	9.11	10.54	11.46	19.87	0.36	568	587
Zr	4.47	35.1	41.3	13.8	115.9	143.7	52.4	64.6	75.5	148.6	3.19	49	43
Nb	0.26	0.73	2.24	0.18	3.57	3.04	1.30	1.78	5.29	168.22	0.03	4.3	69

Note: Major components were analyzed using microprobe CamebaxMicro, analyst O.S. Kmelnikova. TRE analyzes of minerals were obtained using LAM ICP method using Finnigan Element and laser system Nd YAG: UVNewWave, analyst S.V. Palessky.

Table 2.

Compositions of the major and trace element components for garnets and ilmenites from the autolithic breccias from Sytykanskata pipe.

Number	SG076	SG077	STK137	SG078	SG079	SG066	SG087	SG060	SG062	SG063	SG064	SI169	SI152	SI149	SI150	SI135	SI123
Element	Garnets											Ilmenites					
SiO2	41.08	41.73	39.55	41.82	42.07	40.1	41.64	40.13	41.89	42.1	41.82						
TiO2	0.581	0.074	1.74	0.335	0.045	0.317	0.578	1.03	0.227	1.08	0.301	45.68	48.27	52.16	51.17	52.42	50.67
Al2O3	19.12	16.5	14.10	18.87	17.88	14.69	18.42	12.07	21.26	19.83	19.87	0.198	0.301	0.788	0.561	0.704	0.527
Cr2O3	4.16	9.87	1.89	5.76	8.11	10.23	5.25	12.37	2.68	1.89	4.79	2.52	2.41	0.528	0.468	0.744	0.578
FeO	9.21	6.7	5.22	7.14	7.01	8.54	7.36	7.43	8.42	9.32	7.15	42.59	40.37	33.83	36.64	34.21	37.85
MnO	0.471	0.449	0.06	0.416	0.422	0.453	0.282	0.38	0.391	0.313	0.387	0.284	0.289	0.42	0.227	0.286	0.213
MgO	17.79	22.65	23.16	20.79	22.81	15.85	20.41	17.91	20.28	20.95	20.85	7.66	8.97	12.47	10.07	12.23	10.37
CaO	6.75	1.59	0.01	4.56	1.57	9.05	5.47	7.82	4.56	4.74	4.52	0.063	0.105	0.157	0.096	0.158	0.087
Na2O	0.10	0.00	0.24	0.09	0.02	0.05	0.07	0.05	0.08	0.09	0.06	0.406	0.118	0.198	0.207	0.151	0.157
K2O	0.02	0.02	9.95	0.02	0.02	0.02	0.02	0.03	0.01	0.02	0.02						
Total	99.28	99.58	95.91	99.79	99.96	99.3	99.5	99.21	99.8	100.33	99.75	99.41	100.84	100.54	99.44	100.9	100.45
Ba	4.44	3.14	22.82	7.27	0.91	1.93	3.06	0.03	0.12	2.16	4.07	12.24	405	0.22	0.001	0.15	0.02
La	0.97	0.11	1.70	0.73	0.10	0.71	0.13	0.02	0.06	0.59	0.37	4.53	17.59	0.130	0.008	0.011	0.012
Ce	0.56	0.82	6.56	2.78	1.04	2.74	1.30	0.12	0.47	2.08	1.45	9.31	28.98	0.827	0.015	0.023	0.078
Pr	0.23	0.44	0.82	0.38	0.23	0.49	0.17	0.03	0.07	0.56	0.18	1.28	2.12	0.049	0.006	0.002	0.008
Nd	3.13	4.06	4.76	1.69	1.93	2.75	1.04	0.29	0.35	4.04	1.47	5.72	9.13	0.256	0.057	0.009	0.049
Sm	1.22	1.42	0.80	0.46	1.50	0.98	0.86	0.29	0.12	0.90	1.37	0.67	1.13	0.072	0.026	0.007	0.016
Eu	0.53	0.31	0.17	0.09	0.62	0.39	0.06	0.17	0.06	0.20	0.55	0.13	0.29	0.016	0.007	0.003	0.003
Gd	2.51	0.65	0.47	0.24	2.57	1.32	0.14	0.60	0.24	0.57	2.93	0.24	0.61	0.058	0.014	0.024	0.021
Tb	0.83	0.07	0.04	0.02	0.50	0.15	0.04	0.16	0.09	0.09	0.66	0.03	0.09	0.007	0.004	0.004	0.009
Dy	6.93	0.40	0.15	0.07	3.79	0.53	0.31	1.35	1.02	1.13	5.71	0.15	0.39	0.040	0.041	0.029	0.021
Ho	2.10	0.07	0.03	0.02	0.92	0.08	0.10	0.37	0.34	0.38	1.35	0.03	0.05	0.008	0.013	0.005	0.003
Er	5.37	0.17	0.23	0.09	2.72	0.20	0.39	1.06	1.49	1.61	4.69	0.08	0.11	0.024	0.012	0.016	0.019
Tm	0.75	0.05	0.02	0.01	0.41	0.04	0.07	0.19	0.27	0.29	0.74	0.01	0.03	0.003	0.005	0.003	0.008
Yb	5.40	0.28	0.36	0.23	3.06	0.38	0.81	1.40	2.17	2.98	5.85	0.10	0.10	0.032	0.026	0.034	0.022
Lu	0.85	0.11	0.08	0.03	0.49	0.12	0.15	0.23	0.39	0.59	0.88	0.02	0.02	0.005	0.007	0.007	0.005
Hf	0.70	0.26	0.17	0.13	2.26	0.64	0.11	0.57	0.11	0.54	1.96	28	45	17	17	28	26
Ta	0.01	0.07	1.12	0.05	0.06	0.05	0.11	0.01	0.02	0.21	0.09	431	18	269	183	377	364
Pb	0.77	0.84	1.73	1.75	0.35	0.73	1.05	0.22	0.27	1.73	2.83	6.36	7.88	1.67	0.18	0.99	0.59
Th	0.04	0.27	0.47	0.30	0.02	0.12	0.03	0.003	0.02	0.15	0.05	0.25	1.33	0.01	0.005	0.002	0.001
U	0.02	0.04	8.84	0.04	0.03	0.07	0.05	0.01	0.02	0.10	0.11	0.34	0.87	0.08	0.04	0.05	0.04
Sc	108	107	15	8	143	259	136	42	125	463	156	64.4	14.0	32.5	31.7	40.7	39.7
V	217	102	2151	1412	476	628	435	74	386	778	371	2826	1466	2110	1809	1801	1840
Co	41	23	539	408	93	106	68	22	71	107	118	331	42	270	222	196	202
Cu	180	202	13	78	3.3	7.5	14.1	1.0	0.7	10.1	23.4	59	34	55	47	34	30
Ni	286	192	849	437	169	104	119	47	66	226	505	1370	329	1015	935	1030	1256
Rb	0.05	0.10	7.35	3.50	0.01	0.14	0.52	0.06	0.11	0.15	0.39	5.22	2.37	0.21	0.03	0.33	0.14
Sr	0.00	2.56	389	194.57	1.75	126.61	3.90	1.32	0.54	8.42	11.78	70.8	38.3	6.4	0.4	0.5	0.5
Y	2.8	1.9	6	3.7	22.6	1.9	2.6	8.9	10.5	11.1	36.3	5.75	14.80	0.22	0.16	0.11	0.11
Zr	58.5	32.0	54	34.8	80.0	36.7	4.6	19.3	2.9	17.1	70.3	408	601	417	417	760	764
Nb	2.71	2.03	14	1.70	0.58	0.69	1.26	0.05	0.31	1.74	0.72	3477	204	2005	1264	2708	2478

Such trends with a deviation from the conductive geotherms at the upper part [12, 38] are determined in the continental mantle of many regions worldwide [8, 37]. Deviations to the high-temperature region occurs at several levels, ranging from 6.5 to 3.5 GPa, which corresponds to interaction with the protokimberlites melts traced mainly by ilmenite PT points.

The lower part of the ilmenite trend is formed by the uncontaminated low-Cr varieties but in the upper part the Cr-content increases. However, at the level of 4.0 GPa, it is growing abruptly. In this interval the Fe-content of garnets is rising also and next at the level of 3.0 GPa. The PT estimates for chromite and ilmenite coincide in pressure, but chromites mark relatively lower temperature conditions. Probably the formation of this mineral occurs at the outer contacts of the protokimberlites. The CaO and FeO content in garnets are quite stable in certain pressure intervals and abruptly change near 5.0 GPa.

Most of the variations are found in the range of 4.0-5.0 GPa further above 4.0 GPa. Kinks in P-Fe# are observed near 3.2, 2.8 and 1.6 GPa. At the bottom of the chart, which presents the PTX estimates for inclusions in diamonds, there are 4 levels of CaO content which is rather stable in pressure intervals, which is very

unusual.

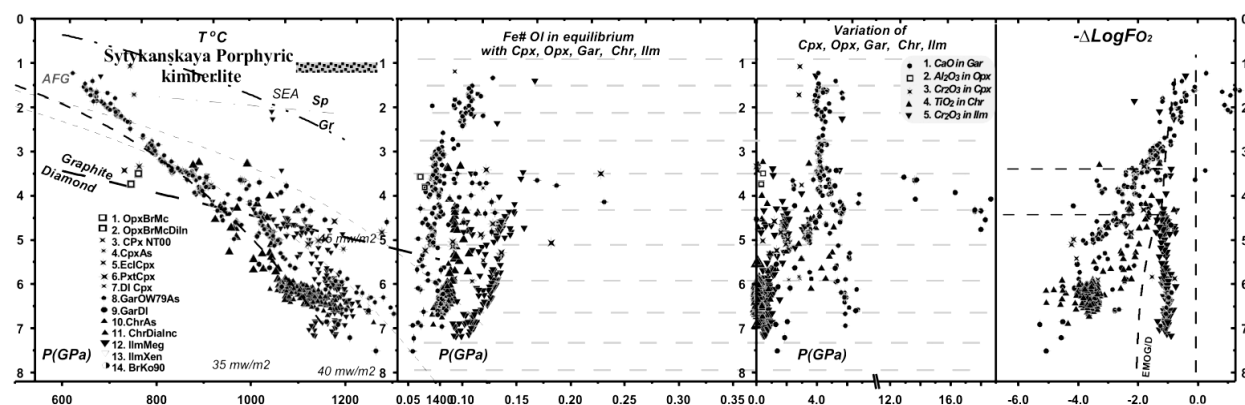


Fig. 7. $PT \times fO_2$ diagram for the concentrate from porphyritic kimberlite from Sytykanskaya pipe.

Signs: 1. Opx: $T^\circ C$ [10] - P (GPa)[28]. 2. The same for diamond inclusions. Cpx: 3. $T^\circ C$ - P (GPa) [29]; 4. $T^\circ C$ [29] modified [10] - P (GPa) [5]; 5. The same for eclogites; 6. The same for pyroxenites. 7. The same for diamond inclusions; Garnet (monomineral) 8. 9. $T^\circ C$ [31] - P (GPa) [5], 10. The same for diamond inclusions. Chromite 11. $T^\circ C$ [30] - P (GPa) [5]; 12. The same for diamond inclusions. 13. Ilmenite megacrysts $T^\circ C$ [27] - P (GPa) [5]; 14. The same for xenoliths; 15. $T^\circ C$ - P (GPa) [10]. The compositions of the diamond inclusions is taken from [22, 48-50]. The field for the diamond bearing associations after [27].

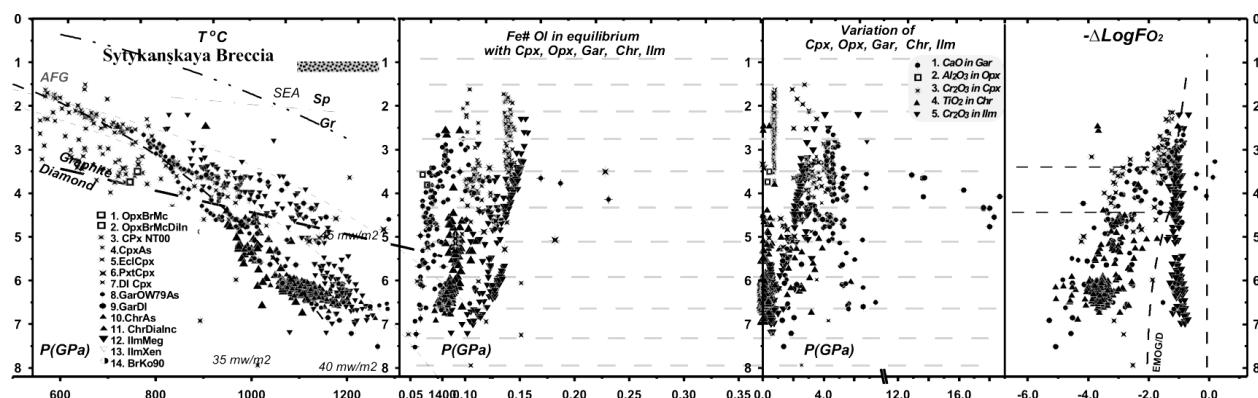


Fig. 8. $PT \times fO_2$ diagram for the concentrate from breccia from Sytykanskaya pipe.

The ilmenite P - fO_2 trend of Sytykanskaya reveals comparatively oxidized conditions, unlike for other mantle sections in Yakutia [5-9] where it usually traces the dividing line of the stability of carbonatite melt and diamond [53, 54]. The variations of oxidizing conditions defined for garnet and chromite are limited by this line on the left [27]. Above 4.0 GPa oxidizing conditions increase drastically, which corresponds to an increase of metasomatism under the influence of differentiating melt systems.

For the xenocrysts found in the breccia, which appears to be (but not obviously) formed after the porphyritic kimberlites, the general variation of the P - $Fe\#$ trends is similar. However, the diversity of linear and curved skew trend appears to be higher, probably due to the influence of several branched systems of the melts derived from kimberlites in different levels.

Table 3.

Compositions of the major components for amphiboles, phlogopites and rutiles from the autolithic breccias from Sytykanskata pipe.

Sample	Stk196	Stk196a	SytD018	SytD047	SytD018	SytD146	SytD163	S68	ST75	Stk35	ST250	
Compon	Richterites		Pargasites									Rutile
SiO ₂	51,89	52,4	48,88	54,08	49,88	49,97	46,79	46,95	42,31	42,1	0,018	
TiO ₂	0,15	0,14	0,146	0,197	0,146	0,154	0,488	0,217	2,05	0,38	98,1	
Al ₂ O ₃	6,08	6,09	7,79	3,05	7,79	7,91	11,36	9,44	14,88	11,37	0,027	
Cr ₂ O ₃	1,53	1,45	2,18	0,769	2,18	2,22	0,88	2,13	0,588	0,29	1,69	
FeO	2,88	2,82	2,67	3,16	2,67	2,66	4,43	2,97	4,55	4,11	0,127	
MnO	0,1	0,07	0,052	0,062	0,052	0,07	0,06	0,029	0,111	0,04	0	
MgO	21,23	21,2	20,29	14,53	20,29	19,7	18,16	20,25	17,78	26,01	0,039	
CaO	6,47	6,54	8,56	20,91	8,56	8,64	10,35	10,52	10,61	0	0,023	
Na ₂ O	5,38	5,4	4,68	2,24	4,68	4,68	4,02	3,83	2,99	0,1	0,056	
K ₂ O	1,97	1,98	1,34	0,034	1,34	1,26	1,14	1,45	1,04	10,67	0,001	
Total	97,68	98,09	96,588	99,032	97,588	97,264	97,678	97,786	96,909	95,07	100,081	
Sample	Stk196	Stk9	Stk167	Stk167a	ST 196I	ST 196I	ST 186I	ST 60I	ST 75	s104	Stk208	
Compon	Phlogopites										Rutile	
SiO ₂	41,43	41,06	39,15	39,86	42,14	43,47	38,14	41,58	39,85	42,34	0	
TiO ₂	0,17	0,41	2,97	3,6	0,211	0,199	3,13	0,414	3,47	0,768	95,58	
Al ₂ O ₃	13,15	13,02	16,01	13,08	11,93	12,33	15,97	13,87	14,24	12,42	0	
Cr ₂ O ₃	0,82	0,71	1,12	0,91	0,387	0,343	1,82	0,64	1,52	0,485	0,02	
FeO	2,82	3,58	3,78	4,17	3,24	3,23	4,23	3,77	4,87	3,61	0,082	
MnO	0,02	0,03	0,03	0,05	0,034	0,041	0,042	0,03	0,046	0,012	0	
MgO	26,05	24,19	22,62	23,92	26,71	27,32	21,11	25,6	22,4	24,34	0,016	
CaO	0	0,02	0	0,01	0,118	0,022	0,031	0,036	0,032	0,171	0	
Na ₂ O	0,53	0,12	0,4	0,25	0,234	0,195	0,36	0,245	0,127	0,302	0,022	
K ₂ O	9,57	10,8	10,06	9,28	9,57	9,09	7,82	9,02	9,85	10,28	0	
Total	94,56	93,94	96,14	95,13	94,574	96,24	92,653	95,205	96,405	94,728	95,72	

Actually protokimberlite melt formed two large isolated systems at two levels of the mantle column. The melts parental for ilmenites moved to the upper part to 4.5-3.5 GPa, becoming significantly enriched in Cr₂O₃. The CaO and FeO trends for garnet at each level have formed separate, often curvilinear, trends which seem to reflect the variation of the composition of the mantle of the substrate that is changing under the influence of the melts in the vein systems. The same linear trend with large often sub-horizontal variations can also be seen on the P-fO₂ diagrams. For the chromite oxidation stage variations are similar to those from the porphyritic kimberlites but the amount of chromites in the deepest levels is higher.

Clinopyroxenes from the breccia reveal mostly low pressure conditions. Clinopyroxenes with Fe#Ol ~ 15 % are close in Fe# to the most Fe-rich varieties of ilmenites which were formed from the latest and most fractionated derivatives of protokimberlite systems that after the crystallization of ilmenite-diopside systems created significant amounts of diopside -phlogopite veins at the top of the mantle section. Associations with (Fe#Ol ~ 11-12) were formed by another more magnesian system that created polymineral clinopyroxene-garnet-ilmenite associations.

PTX diagrams for the xenoliths (fig. 9) show a different configuration of trends and clusters in P-Fe#, X diagrams for some minerals, reflecting variations of polymineral peridotite associations. The widest variations are defined near the pyroxenite lens [5, 9, 33, 39]. Veins with phlogopite, ilmenites and richterites were formed here as well as the websterites with graphite and phlogopite. The most Fe#Ol rich metasomatic clinopyroxenes, ilmenite and phlogopites occur in the middle part of the section. The most Cr-rich varieties of clinopyroxene are located at 3.0 GPa.

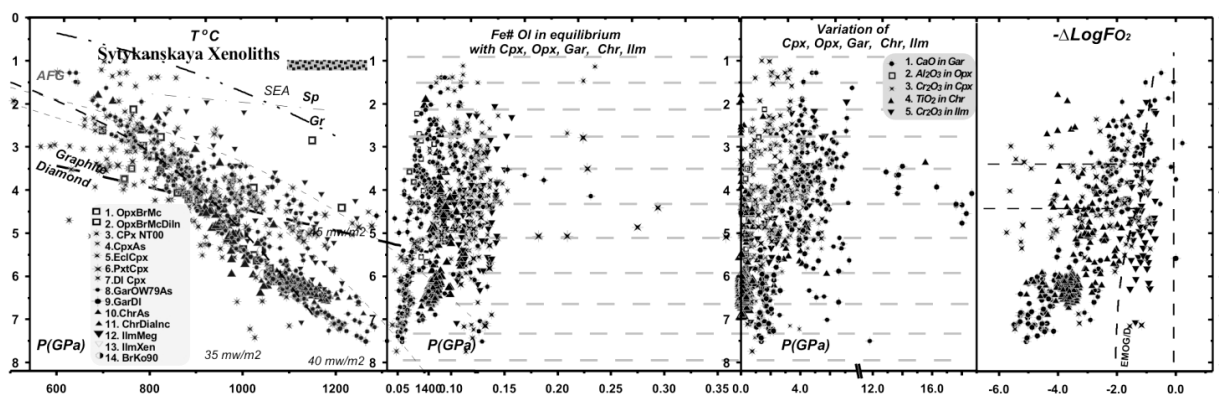


Fig. 9. $PT \times FO_2$ diagram for the concentrate from breccia from Sytykanskaya pipe.

PT conditions for the most commonly used thermobarometry for 15 associations [11] nearly repeat the garnet geotherm from 6.5 to 2.0 GPa. This is the first polymineral geotherm for the mantle in the Alakit field. The PT estimates based on clinopyroxenes [5, 7, 29] give somewhat similar but broader range, reflecting high-temperature and low-temperature branches. The combined geotherms give step deviation to 35 mw/m^2 conductive branch similar to those for mantle beneath Udachnaya [17]. Clinopyroxene geotherms for Sytykanskaya are similar to those beneath the Daldyn field, and quite different from those determined for the mantle beneath Yubileynaya pipe [4].

Some variations in the high-temperature part of the diagram near ~ 3.5 and 4.0 GPa corresponds to the metasomatites, thus marking the positions of the fluid-saturated melts. The highest temperature conditions are defined by orthopyroxenes and ilmenites and clinopyroxene diamond inclusions which could be formed from protokimberlite derivatives.

Almost linear trends of Fe# for the pyroxenes of chromite in the middle part of the mantle columns correspond to the three types of evolving magmatic system responsible for the existence of at least three separate types of metasomatites. Most ferrous 14-15 Fe#Ol for the Cpx and Ilm at depths of 5.5-6.5 GPa and above. Two varieties with Fe#Ol 11 and 12,5 % were generated within the 5.5 to 3.7 GPa interval.

Two garnet-pyroxene-chromite sub-trends between Fe#Ol - 6-9 % show the primary layering in the mantle. In the lower part of the mantle column, mantle inclusions create an evolving Fe-trend from the garnets to chromite diamond

inclusions.

Higher values are local trends. Variation of CaO for the garnets from xenoliths is higher than for xenocrysts. Variations of Cr-clinopyroxene of the xenoliths are also higher and varying in each level of the mantle column. Very wide variations of oxidizing conditions are characteristic for the pyroxenes and garnets in each level of the P-fO₂ for xenoliths.

VARIATIONS OF TRACE ELEMENTS IN XENOLITH MINERALS

Rare earth element patterns were analyzed for three types of samples including xenocrysts from the breccia, metasomatic xenoliths, and for xenolith of glimmerites with amphiboles close to richterites and websterites with graphite.

There are systematic variations for TRE in each group. For Cr-diopsides from the breccia (fig. 10) very high La/Yb_n ratios are characteristic and relatively linear spectra with La/Ce_n>1 which corresponds to very low melting degrees which can occur only in volatile-rich systems. They also reveal deep Ta-Nb and less pronounced Zr minima, which corresponds to co-precipitation of ilmenite and rutile. The most enriched spectrum has La ~500 C1 and has no minimum of high field strength (HFSE) components, probably was derived from the most fractionated fluid-saturated enriched melt close to carbonatites. Pyroxene with rounded REE spectrum "humped" in the left part belong to the common peridotites [8, 9, 17] from the melts formed at ~ 0.75-1 % melting degree which have not undergone interactions with metasomatic agents.

Garnets reveal also flattened REE distributions without essential HFSE and as usual are dominated by the HREE. Some garnets have S-shaped spectra. But sharp dips in Sr and high Pb, U peaks which are common in lithospheric mantle peridotite [17] were not found. They reveal elevated Ba, Th, U contents and even Ta, Nb, which is common for fertilization by the carbonatite melts [8, 9, 28] unlike to crustal derived melts [25].

There are two types of ilmenite REE patterns. The first one shows flattened patterns, typical for the most Mg-rich ilmenites [11]. The other type reveals highly inclined patterns, enriched in LREE in different degrees which are characteristic of the ilmenites derived from the differentiated protokimberlite melts and from the metasomatitic veins with garnets. All of them have HFSE maxima and enrichment in Y which increase along with the level of REE.

Clinopyroxenes from the metasomatic peridotites (fig. 11) are also characterized by the slightly lower inclination of REE patterns and La/Ce_n and La/Pr_n<1 as a rule. This means that the melting degrees for the parental melts are

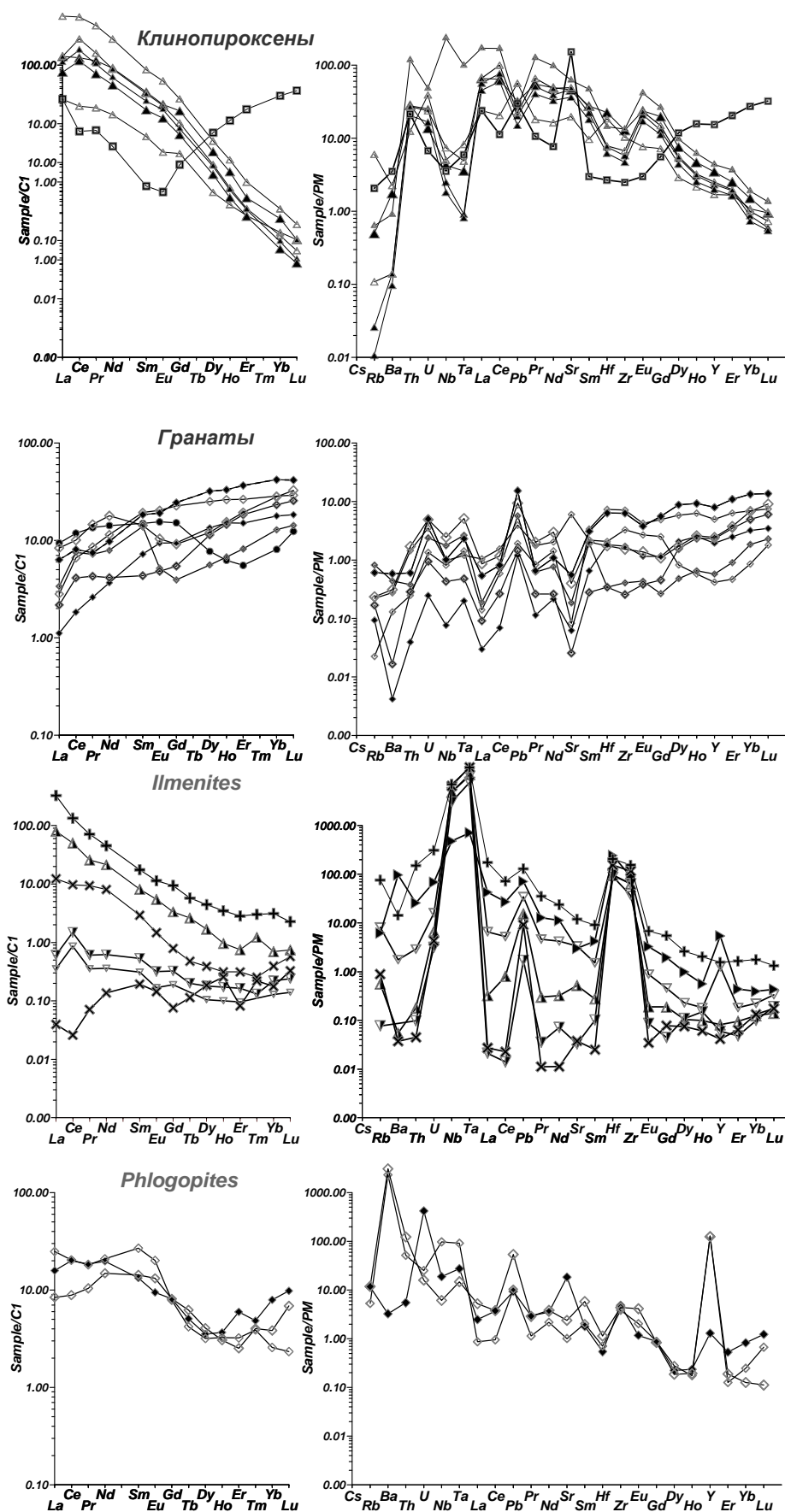


Fig. 10. REE and TRE spider diagrams for the minerals from concentrates breccia of Sytykanskaya pipe.

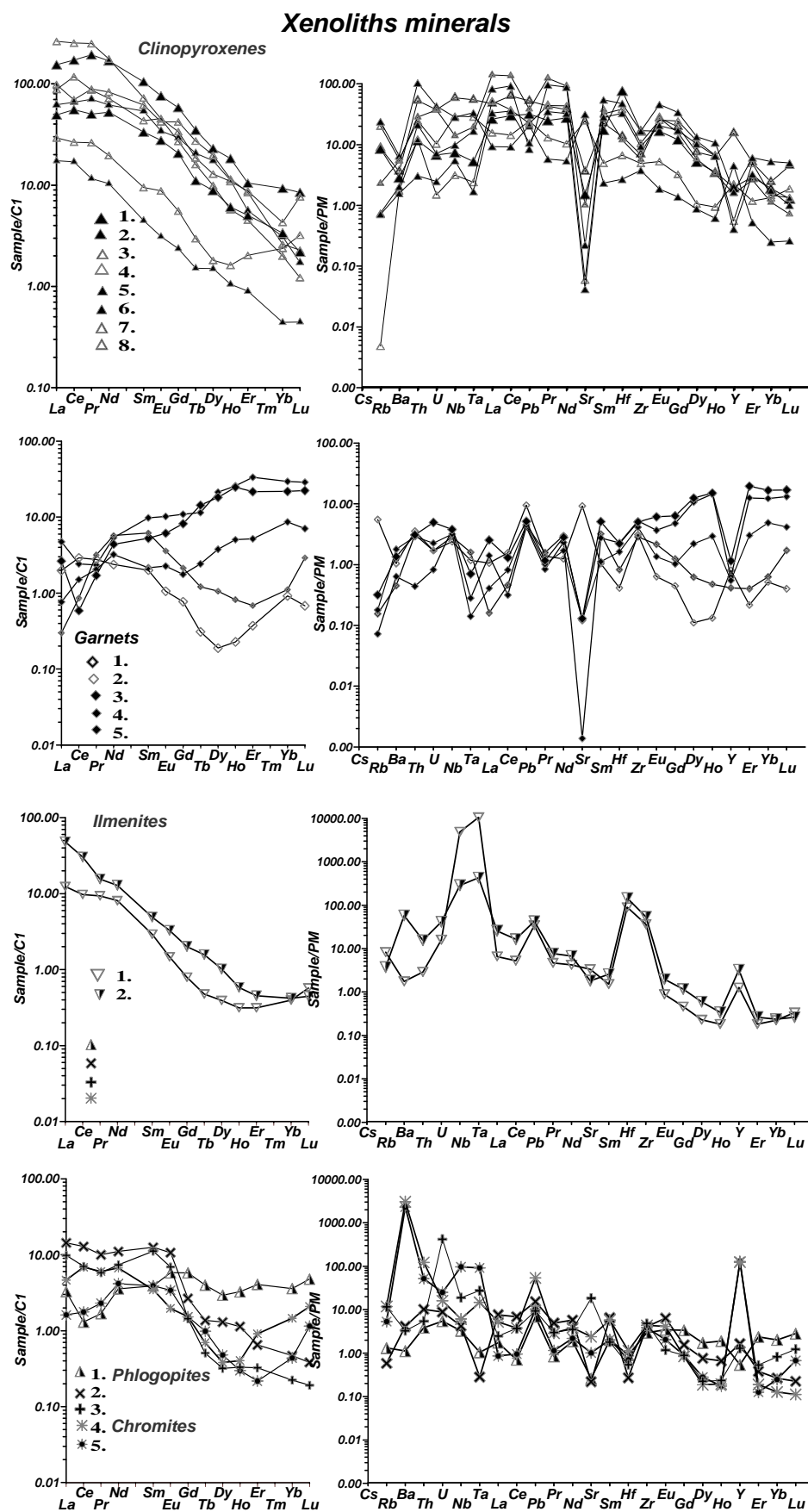


Fig. 11. REE and TRE spider diagrams for the minerals from metasomatic xenoliths of Sytykanskaya pipe.

higher than for the previous group, and the Gar/Cpx ratios in the rocks are lower. The lack of essential U maxima which are a relic subduction sign but some elevated LILE components are a result of the metasomatism. The level of depletion of the Zr is quite high, that is more typical for H₂O than for carbonatite type of metasomatism. For many of the analyzed garnets, especially from the deep part of the mantle column, the deep troughs of MREE or S-spectra are found, that are probably evidence for the primary harzburgitic nature or back arc - dunite associations.

Ilmenites from xenoliths are characterized by inclined REE patterns and HFSE peaks slightly lower than the ilmenites of the first group with the low REE content. The difference between the Ta-Nb and Zr-Hf is also smaller, compared with the megacrystalline ilmenites.

Phlogopites have characteristic patterns that resemble those for clinopyroxenes due to the high inclination of Gd/Yb_n. But the LREE part is flattened. This is typical of phlogopite patterns from peridotites in picrite basalts from the Vitim plateau [6]. The spectra with the cut hump in the left part are results of crystallization from melts which had already crystallized clinopyroxenes with patterns that are humped in the LREE part.

Cr-Diopside xenocrysts from the breccia were produced by the most differentiated melts and enriched protokimberlite or carbonatite; they show highly inclined nearly linear REE patterns and deep troughs of HFSE. The REE patterns for minerals of the metasomatic xenoliths are less inclined with lower La/Ce_n ratios and without troughs in spider diagrams. The garnets often show S-shaped patterns.

Clinopyroxenes from the Cr websterites show different enrichments in REE highly inclined and more straight pattern and deep troughs in Ba and varying enrichment in Nb-Ta-U lower than REE. Those with lower TRE reveal Zr-Hf dips. The clinopyroxenes from glimmerites reveal highest REE and dips in Pb. Garnets show also more straight line REE patterns with then in primitive melts Sr – Ba dips but varying Th-U Nb- Ta. Thus series of clinopyroxenes from garnet pyroxenites (fig. 12) with graphites reveal in general cognate origin possibly formed by the different melting degree accompanied by the melt differentiation and precipitation of the minor ilmenites and rutile. An the original possibly was produced by the hybridization with Ti – bearing eclogites revealing also the straight-line REE patterns for garnets and pyroxenes with the inflections [9]

So the pyroxenes from pyroxenites Sytykanskaya pipe correspond to a lower melting degree taking place in volatile-saturated systems lower than for Cr-diopsides from Vitim plateau [11], which were created from 1 % melts of primitive mantle. The left part reveals some variation which is likely caused by LREE fractional crystallization of clinopyroxene or AFC process.

For the clinopyroxenes from metasomatic vein Stk167 (fig. 12), the elevated levels of LREE and flattened LMREE part are similar to the phlogopites. The HREE part of the pattern is also is concave. The convex REE tendencies are characteristic for the final crystallization of melts that precipitated phases with

convex REE distributions. Such patterns are common for the phlogopites. Phlogopite in this same vein shows a more pronounced tilt in HREE and the

Pyroxenites

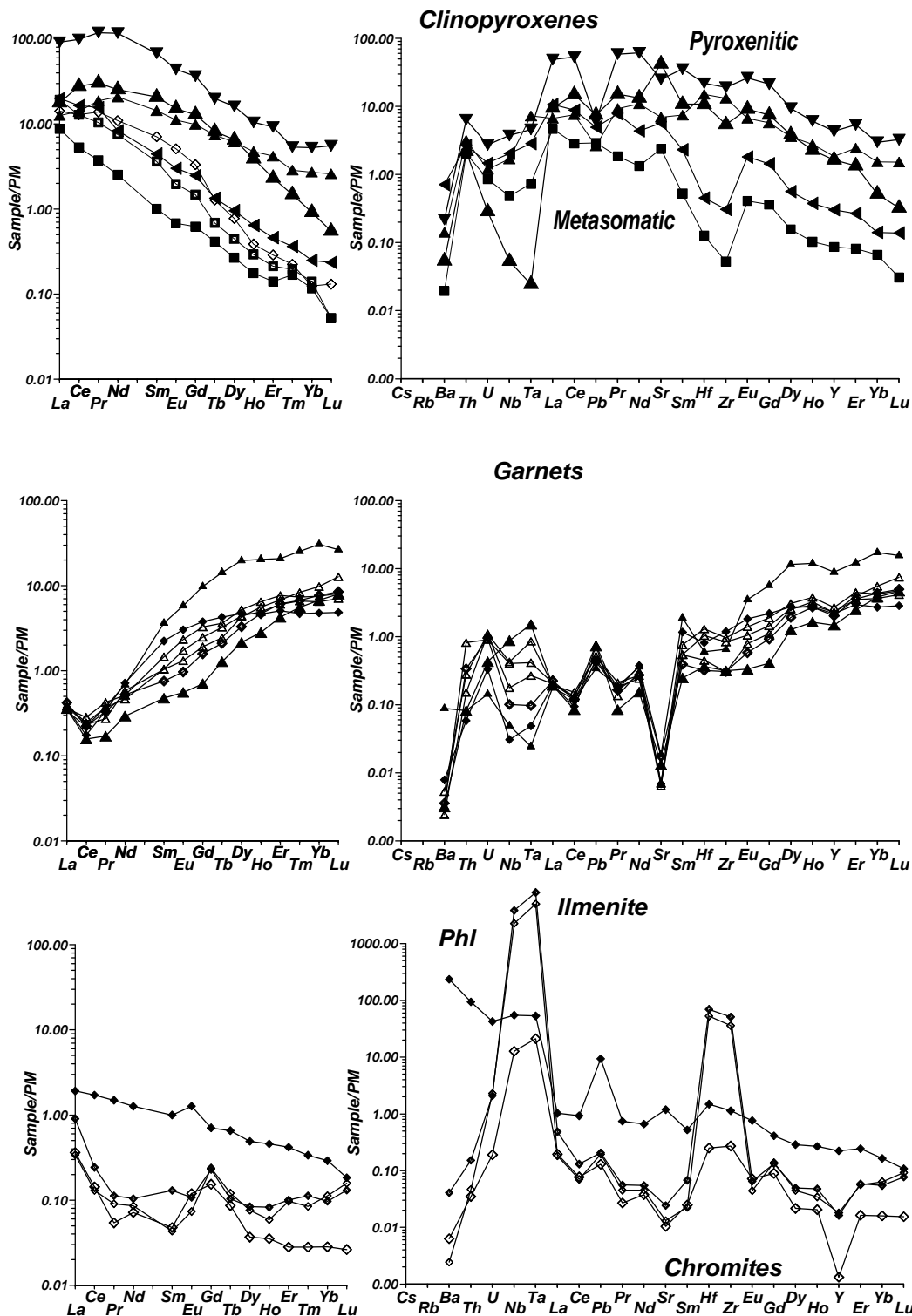


Fig. 12. REE and TRE spider diagrams for the minerals from pyroxenite xenoliths and richterite bearing glimmerites from Sytykanskaya pipe.

LMREE. As with most phlogopites, it is characterized by a high concentration of Ba. The TRE spiderdiagrams for minerals from the websterites reveal minima in Ba, Sr, Pb. But metasomatites reveal elevated incompatible element levels especially in Rb and Ba.

Garnets from the pyroxenites show rounded convex REE patterns with the hump and maximum in Dy. They are characterized by deep troughs of Ba, Sr, Pb (Pb minimum is not typical for garnets), a small dip in Zr and quite high levels of U, Ta, Nb. Garnets from metasomatites show a concave HMREE part of the pattern which is common for harzburgites from Udachnaya and other pipes [8, 17]. Metasomatites and pyroxenites show similar signs of metasomatism with elevated HFSE components which commonly mark the carbonatite-related metasomatism [16]. The glimmerites with richterites reflect the fluid-rich conditions with the essential LILE enrichments. But the lack of Sr, Pb, U anomalies probably shows that peridotite did not undergo fluid flux from a subducted slab subjected to the typical oceanic metasomatism.

⁴⁰AR-³⁹AR AGES OF PHLOGOPITES

Comparing with the phlogopite ages of mantle peridotites in the Daldyn field that mainly refer to Archean events, magmatic and metasomatic events in the Alakit region refer to the middle and late Proterozoic events and the Proterozoic-Phanerozoic boundary. One of the most ancient of the ⁴⁰Ar-³⁹Ar ages in the mantle of Alakit is given by xenocrysts from Amakinskaya pipe (1154 Ma). Ti- and alkali-rich veins with richterites in the Sytykanskaya pipe give 1015 Ma (integrated 879 Ma) (fig. 13). Several phlogopite xenocrysts from other pipes in the Alakit field are close to 600-530 Ma. The latest event at 382 Ma is close to the beginning of the Late Devonian plume event. Similar ages are also noted in other isotopic systems [13, 32, 43, 44]. As a rule it is divided from the main kimberlite appearance of the kimberlite by an interval of about 25-30 Ma.

DISCUSSION

ANCIENT METASOMATISM

⁴⁰Ar-³⁹Ar age suggests that there were ancient metasomatites like in mantle columns beneath Udachnaya pipe [35] which appears to be associated mainly with water-bearing highly alkaline melts, and relatively young metasomites which were produced by differentiated carbonatite-type melts. The first is probably characterized by back-arc melts with relatively high Ba, Sr, Pb, Sr, K-Na. In our case the scattered phlogopites suggest the influence of K-rich fluids which may have taken place in the marginal continental environment which should be accompanied the lamproite magmatism. But absence of HFSE anomalies means relatively reduced conditions. Formation of websterites with phlogopite and graphite which are complementary to the ancient metasomatites with the elevated U, Ta, Nb and LILE elements should refer to this time. But there is no such

depletion though the sinusoidal garnet REE patterns are quite common. Relatively low alkalinity and Fe# is characteristic for the pyroxenes from this stage. The abundance of carbon may be sign of typical subduction processes but graphite oxygen isotope values close to average mantle values.

This type of metasomatite is in the low-Fe part of the variation diagram. Judging by the abundance of S-type garnets, almost the entire lithospheric mantle column under the Sytykanskaya pipe was subjected to large-scale phlogopite metasomatism. The formation of highly alkaline and Ti metasomatic veins with richterite ~1015 Ma ago refers to large-scale plume-related melt percolation in the lithospheric mantle of Rodinia [42]. Similarly in South Africa phlogopite metasomatism in mantle corresponding to 1100 Ma is associated with the plume-generated Bushveld intrusion [15].

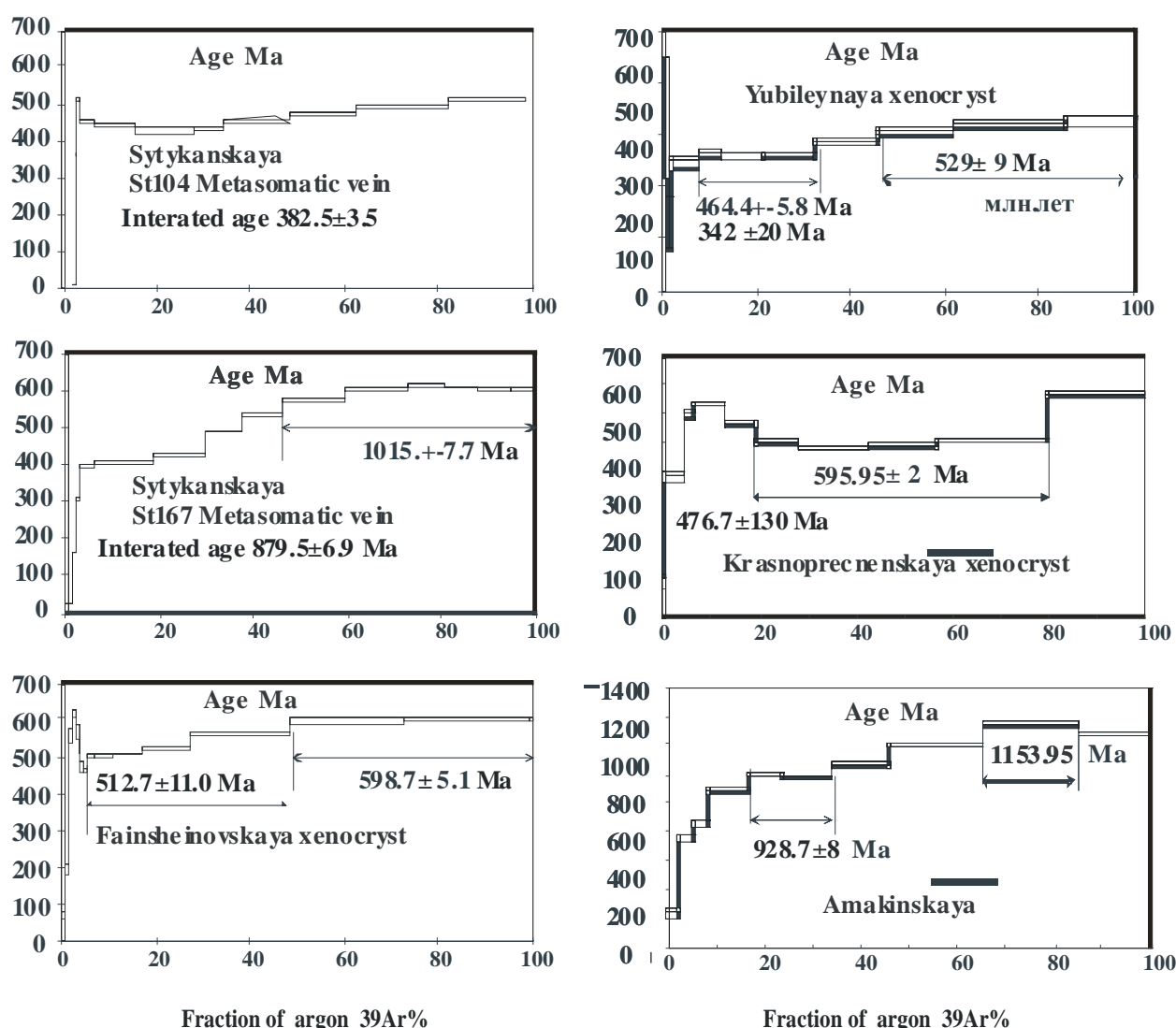


Fig. 13. Ages of the phlogopites received by ^{40}Ar - ^{39}Ar method for the xenoliths of Sytykanskaya pipe in comparison with the ages for the xenocrysts from Alakite kimberlite pipes.

The largest event shown in the lithosphere under many Alakit pipes occurred

~ 600-550 Ma ago, close to the Proterozoic-Phanerozoic boundary. Such an event is close to the time of mellilite carbonatite magmatism in the Sayan Foothills and the Baikal are [59]. This should correspond to the Ti-rich carbonatite-type metasomatism

PROTOKIMBERLITE STAGE

High-Fe and Ti metasomatic ilmenite veins are related to the protokimberlite melts. The amount of ilmenites in the pipe is rather high. It seems that protokimberlite melts could dissolve early metasomatites in the base of the mantle column. According to some works, an essentially oxide liquid could form a separate phase due to immiscibility with the silicate melt [12] and, apparently, form an intrusive phase. Almost monomineralic ilmenite veinlets in peridotites cut the large porphyroclasts of garnets in some xenoliths.

Furthermore, metasomatites related to the ilmenites are much more ferrous than usual peridotites. The influence of ilmenite metasomatism appears in the xenoliths sufficiently widely, although scattered Phl metasomatism dominates. It is not clear to what extent the protokimberlitic melts influenced the lithospheric mantle. Did they cause changes only near the conducting channels or was it more widespread? An answer could be given by the study of xenoliths of other small pipes of this field.

The time gap of 25-30 Ma between the beginning of plume activity and mantle metasomatism and appearance of major kimberlitic explosions is documented also by other isotopic systems [43]. However, it is not possible to discount the presence of excess argon, which can produce a more ancient age, measured only by the ^{40}Ar - ^{39}Ar method. However, the dating of kimberlite by this method gives acceptable results [1].

INFLUENCE OF MANTLE METASOMATISM ON DIAMOND GRADE

Among the diamond inclusions of Sytykanskaya pipe, chromites dominate [24, 45, 52] as in many other pipes from the Alakit field [49, 50]. Another widely distributed group is sub-Ca pyropes. In a subordinate quantity, the high-temperature Cr-pyroxene, apparently related to the proto-kimberlite, and usual Fe-enriched Cr-diopsides from metasomatites are found. Sub-calcic pyropes [45, 46, 36] undoubtedly came from the ancient giant-grained dunites [34], which form veins and lenses in the lithospheric mantle. The age of such garnets by analogy with others may be 3-2.7 billion years [23]. The chromite diamond inclusions form an individual group. They are not very frequently associated with the pyropes and differ in PT conditions. It seems that they are closer in conditions to the ilmenites and some high-temperature and relatively ferrous pyropes. The giant-grained dunite veins with pyropes [34] and chromites have a different genesis; however, they both served as conductors of melts. Chromite dunites could be formed with

the participation of the high-temperature fluid-rich melts, which, as a rule, relate to a separate stage of the protokimberlitic process. Thus, if this is correct, then a particularly large part of the diamonds of the Sytykanskaya pipe and Alakit field as a whole is connected with the protokimberlite stage. From other side the presence of the highly depleted substratum in the lower part of the lithospheric mantle is also a contributory factor for an increased diamond grade.

However, judging by the oxidation states for the ilmenites, proto-kimberlitic melts beneath the Sytykanskaya pipes were strongly oxidized, by 1 log unit higher than the diamond stability line [27, 53, 54]. This possibly served as the reason for the dissolution of many diamonds.

The work is supported by RBRF grants 05-05-64718, 03-05-64146; 08-05-00524; 11-05-00060; 11-05-91060-PICS and joint research projects of IGM SB RAS and ALROSA Stock company 77-2, 65-03, 02-05. Many thanks to Prof. Hilary Downes for the corrections of the text.

REFERENCES

1. **Agashev A.M., Pokhilenko N.P., Tolstov A.V., Polyanchko N.P., Mal'kovets V.G., Sobolev N.V.** (2004) New data on age of kimberlites from Yakutian kimberlite province. // Doklady Earth sciences RAN 399 (1):95–99.
2. **Arai S.** Pressure-temperature dependent compositional variation of phlogopitic micas in upper mantle peridotites. // Contributions Mineralogy and Petrology. 1984 v.87 pp. 260-264.
3. **Artemieva I M.** The continental lithosphere: Reconciling thermal, seismic, and petrologic data // Lithos 2009. V.109 (1), pp. 23-46.
4. **Ashchepkov I.V., Vladykin N.V., Nikolaeva I.V., Palessky S. V., Logvinova A.M., Saprykin A.I., Khmel'nikova O. S., Anoshin G.N.** Mineralogy and Geochemistry of Mantle Inclusions and Mantle Column Structure of the Yubileynaya Kimberlite Pipe, Alakit Field, Yakutia. // Doklady of RAS ESS. 2004. v.395 (4), pp. 517–523.
5. **Ashchepkov I.V., Pokhilenko N.P., Vladykin N.V., Logvinova A.M., Kostrovitsky S.I., Afanasiev V.P., Pokhilenko L.N., Kuligin S.S., Malygina L.V., Alymova N.V., Khmelnikova O.S., Palessky S.V., Nikolaeva I.V., Karpenko M.A., Stagnitsky Y.B.** Structure and evolution of the lithospheric mantle beneath Siberian craton, thermobarometric study // Tectonophysics. 2010, v. 485, pp.17-41.
6. **Ashchepkov I.V., André L., Downes H., Belyatsky B.A.** Pyroxenites and megacrysts from Vitim picrite-basalts (Russia): Polybaric fractionation of rising melts in the mantle? // Journal of Asian Earth Sciences, 2011 v. 42, pp. 14-37.
7. **Ashchepkov I.V., Rotman A.Y., Somov S.V., Afanasiev V.P., Downes H., Logvinova A.M., Nossyko S. Shimupi J., Palessky S.V., Khmelnikova O.S., Vladykin N.V.** Composition and thermal structure of the lithospheric mantle beneath kimberlite pipes from the Catoca cluster, Angola. // Tectonophysics, 2012. v.530–531, pp. 128-151.
8. **Ashchepkov I.V., Vladykin N.V., Ntaflos T., Downes H., Mitchel R., Smelov A.P. Rotman A.Ya, Stegnitsky Yu., Smarov G.P, Makovchuk I. V., Nigmatulina E.N., Khmelnikova O.S.** Regularities of the mantle lithosphere structure and formation beneath Siberian craton in comparison with other cratons // Gondwana Research 2013a.v. 23, pp. 4-24.
9. **Ashchepkov I.V., Ntaflos T., Kuligin S.S., Malygina E.V., Agashev A.M., Logvinova A.M., Mityukhin S.I., Alymova N.V., Vladykin N.V., Palessky S.V., Khmelnikova O.S.** Deep-Seated Xenoliths from the Brown Breccia of the Udachnaya Pipe, Siberia // D. G. Pearson et al. (eds.), Proceedings of 10th International Kimberlite Conference, V1,

- Special Issue of the Journal of the Geological Society of India, 2013b. pp. 59-74.
10. **Brey G.P., Kohler T.** Geothermobarometry in four-phase lherzolites. II. New thermobarometers, and practical assessment of existing thermobarometers // *J. Petrol* 1990. V. 31. P. 1353-1378.
 11. **Boyd F.R., Pokhilenko N.P., Pearson D.G., Mertzman S.A., Sobolev N.V., Finger L.W.** Composition of the Siberian cratonic mantle: evidence from Udachnaya peridotite xenoliths. // *Contributions to Mineralogy and Petrology* 1997, 128, 2-3. 228-246.
 12. **Dawson J. B.** Kimberlites and their xenoliths. Springer-Verlag, Berlin. 1980. 252p.
 13. **Griffin W. L., Ryan C. G., Kaminsky F. V., O'Reilly S. Y., Natapov L. M., Win T. T., Kinny P.D., Ilupin I. P.** The Siberian lithosphere traverse: Mantle terranes and the assembly of the Siberian Craton // *Tectonophysics*, 1999. v.310, pp.1-35
 14. **Haggerty S.E.** The chemistry and genesis of opaque minerals in kimberlite // *Physics and chemistry of the Earth*. New York. 1975. V. 9. P. 227-243.
 15. **Hopp J., Trierloff M., Brey G.P., Woodland A.B., Simon N.S.C., Wijbrans J.R., Siebel W., Reitter E.** $^{40}\text{Ar}/^{39}\text{Ar}$ -ages of phlogopite in mantle xenoliths from South African kimberlites: Evidence for metasomatic mantle impregnation during the Kibaran orogenic cycle // *Lithos*, 2008, v. 106, pp. 351-364.
 16. **Howarth G.H., Barry P.H., Pernet-Fisher J.F., Baziotisa I.P., Pokhilenko N.P., Pokhilenko L.N., Bodnar R.J., Taylor L.A.** Superplume Metasomatism: Evidence from Siberian mantle xenoliths // *Lithos*. 2014. doi: 10.1016/j.lithos.2013.09.006.
 17. **Ionov D.A., Doucet L.S., Ashchepkov I.V.** Composition of the Lithospheric Mantle in the Siberian Craton: New Constraints from Fresh Peridotites in the Udachnaya-East Kimberlite // *Journal of Petrology*, 2010. v.51, pp. 2177-2210.
 18. **Konzett J., Ulmer P.** The Stability of Hydrous Potassic Phases in Lherzolititic Mantle - an Experimental Study to 9.5 GPa in Simplified and Natural Bulk Compositions // *Journal of Petrology* 1999 v.40, pp. 629–652.
 19. **Kostrovitsky S.I., Alymova N.V., Yakovlev D.A., Serov I.V., Ivanov A.S., Serov V.P.** Specific features of picroilmenite composition in various diamondiferous fields of the Yakutian province // *Doklady Earth Sciences*. 2006, v.406, pp 19-23.
 20. **Koptil' V.I., Las'ko E.E., Serenko V.P.** Diamond kyanite eclogites from Sytykanskaya kimberlite pipe –first finding in USA // *Doklady Earth Sciences*. 1975. v. 225. № 4. pp 924–927.
 21. **Lavrent'ev Yu.G., Usova, L.V. Kuznetsova A.I., Letov S.V.** X-ray spectral quant metric microanalysis of the most important minerals of kimberlites // *Russian Geology and Geophysics*, 1987, 48 (5) pp. 75–81.
 22. **Logvinova A.M., Taylor L.A., Floss C., Sobolev N.V.** Geochemistry of multiple diamond inclusions of harzburgitic garnets as examined in situ. *International // Geology Review*. 2005, 47, 1223-1233.
 23. **Logvinova A.M., Ashchepkov I.V.** Diamond inclusions and eclogites thermobarometry, Siberia. *Goldschmidt Conference Abstracts // Geochimica et Cosmochimica Acta*. Special Supplement. 2008b. 72. 16S, A567.
 24. **Malkovets V.G., Griffin W.L., Pearson N.J., Rezvukhin D.I., O'Reilly S.Y., Pokhilenko N.P., Garanin V.K., Spetsius Z.V., Litasov K.D.** Late metasomatic addition of garnet to the SCLM: Os-isotope evidence // *Goldschmidt Conference Abstracts*. 2012 p. 1315.
 25. **Manakov A.V., 2001.** Material models of the upper mantle of Yakutian diamond-bearing province // *Herald of the Voronezh University*. 2001 v.11, pp. 46-54 (in russian).
 26. **Marchesi C., Garrido C.J., Bosch D., Bodinier J.-L., Gervilla F., Hidas K.** Mantle refertilization by melts of crustal-derived garnet pyroxenite: Evidence from the Ronda peridotite massif, southern Spain // *Earth and Planetary Science Letters*, 2013. 362, 66-75.

27. **Mitchell R.H.** Kimberlites, Orangeites, and Related Rocks. 1995, pp 1-90.
28. **McCammion C.A., Griffin W.L., Shee S.R., O'Neill H.S.C.** Oxidation during metasomatism in ultramafic xenoliths from the Wesselton kimberlite, South Africa: implications for the survival of diamond // *Contrib. Mineral. and Petrol.* - 2001. - Vol. 141. - N 3. - P. 287-296.
29. **McGregor I.D.** The system MgO- SiO₂-Al₂O₃: solubility of Al₂O₃ in enstatite for spinel and garnet peridotite compositions // *Am. Miner.* 1974. V. 59. P. 110-119.
30. **Nimis P., Taylor W.** 2000. Single clinopyroxene thermobarometry for garnet peridotites. Part I. Calibration and testing of a Cr-in-Cpx barometer and an enstatite-in-Cpx thermometer. *Contributions to Mineralogy and Petrology* 139, 541-554.
31. **O'Neill H. St. C. & Wall V. J.** The olivine orthopyroxene-spinel oxygen geobarometer, the nickel precipitation curve, and the oxygen fugacity of the Earth's upper mantle // *Journal of Petrology* 1987.v28, pp.1169-1191.
32. **O'Neill H.St.C., Wood B.J.** An experimental study of Fe-Mg- partitioning between garnet and olivine and its calibration as a geothermometer // *Contrib Mineral Petrol.* 1979. v. 70; pp. 5970.
33. **Pearson D.G.** 1999. The age of continental roots. *Lithos*, 48, 171-194.
34. **Pearson D.G., Kelley S.P., Pokhilenko N.P. and Boyd F.R.** Laser ⁴⁰Ar/³⁹Ar analyses of phlogopites from southern African and Siberian kimberlites and their xenoliths: constraints on eruption ages, melt degassing and mantle volatile composition // *Russian Geology and Geophysics.* 1997. V. 38. P. 106-117.
35. **Pokhilenko N. P., Sobolev N.V., Kuligin S. S., Shimizu N.** Peculiarities of distribution of pyroxenite paragenesis garnets in Yakutian kimberlites and some aspects of the evolution of the Siberian craton lithospheric mantle // *Proceedings of the VII International Kimberlite Conference. The P.H. Nixon volume.* 1999. P. 690-707.
36. **Pokhilenko N.P., Pearson D.G., Boyd F.R., Sobolev N.V.** 1991. Megacrystalline dunites: sources of Siberian diamonds. *Carnegie Institute Washington. Yearbook.* 90, 11-18.
37. **Pokhilenko L.N., Alifirova T.A., Yudin D.S.** ⁴⁰AR/³⁹AR dating of phlogopite of mantle xenoliths from kimberlite pipes of Yakutia: evidence for deep ancient metasomatism of the Siberian platform // *10th International Kimberlite Conference (Bangalore, India, 6-11 February, 2012): Long Abstracts.* Bangalore, 2012. P. 57.
38. **Pokhilenko N.P., Sobolev N.V.** Mineralogical criteria for kimberlite diamond grade // *Kimberlites of Yakutia: Field guide book: Sixth International Kimberlite Conference.* Novosibirsk, 1995. P. 79-81.
39. **Rudnick R.L., McDonough W.F., O'Connell R.J.,** 1998. Thermal structure, thickness and composition of continental lithosphere // *Chemical Geology* 145, 395-411.
40. **Reimers L.F., Pokhilenko N.P., Yefimova E.S., Sobolev N.V.** Ultramafic Mantle Assemblages from Sytykanskaya Kimberlite Pipe (Yakutia) *Seventh International Kimberlite Conference, Cape Town, April 1998: Extended Abstracts, Cape Town (1998),* pp. 730–732.
41. **Roden M.F., Patiño-Douce A.E., Jagoutz E., Laz'ko E.E.,** 2006. High pressure petrogenesis of Mg-rich garnet pyroxenites from Mir kimberlite, Russia // *Lithos*, 90/1-2, 77-91.
42. **Rodionov A S , Amshinsky., Pokhilenko N P.** 1988. Ilmenite – Pyrope wehrlite – a new type of kimberlite xenoliths paragenesis. // *Russian Geol. Geophys.* 19/7. 53-57.
43. **Rodionov A.S., Sobolev N.V., Pokhilenko N.P., Suddaby P., Amshinsky A.N.,** 1991. Ilmenite-bearing peridotites and megacrysts from Dalnaya kimberlite pipe, Yakutia // *Fifth International Kimberlite Conference: Extended abstracts, United States,* 339-341.

44. **Santosh M., Maruyama S., Yamamoto A.** 2009. The making and breaking of supercontinents: Some speculations based on superplumes, super downwelling and the role of tectosphere. // *Gondwana Research* 15, 324-341.
45. **Smelov A.P., Zaitsev A.I.** The Age and Localization of Kimberlite Magmatism in the Yakutian Kimberlite Province: Constraints from Isotope Geochronology—An Overview. D. G. Pearson et al. (eds.), *Proceedings of 10th International Kimberlite Conference, Volume 1, Special Issue of the Journal of the Geological Society of India*, 2013. pp. 225-234.
46. **Snyder G.A., Taylor L.A., Crozaz G., Halliday A.N., Beard B.L, Sobolev V.N., Sobolev N.V.** The origin of Yakutian eclogite xenoliths // *Journal of Petrology*.1997. v. 38. pp. 85-113.
47. **Sobolev N.V.**, 1977. Deep-Seated Inclusions in Kimberlites and the Problem of the Composition of the Mantle // *Amer. Geophys. Union, Washington, DC*.279 p.
48. **Sobolev N.V., Lavrentev Y.G., Pokhilenko N.P., Usova L.V.** Chrome-Rich Garnets from the Kimberlites of Yakutia and Their Parageneses // *Contributions to Mineralogy and Petrology*, 1973, 40, N 1, 39-52.
49. **Sobolev N. V., Pokhilenko N. V., Efimova E.S.** 1984. Xenoliths of diamond bearing peridotites in kimberlites and problem of the diamond origin. *Russian Geology and Geophysics*, 25/12, 63-80.
50. **Sobolev N.V., Logvinova A.M., Efimova E.S.** 2009. Syngenetic phlogopite inclusions in kimberlite-hosted diamonds: implications for role of volatiles in diamond formation. *Russian Geology and Geophysics* 50, 1234–1248.
51. **Sobolev N.V., Logvinova A.M., Zedgenizov D.A., Yefimova E.S., Taylor L.A., Promprated P., Koptil V.I., Zinchuk N.N.** Mineral Inclusions in Diamonds from Komsomolskaya and Krasnopresnenskaya Pipes, Yakutia: Evidence for Deep Lithospheric Heterogeneities in Siberian Craton // 8th International Kimberlite conference, Victoria, BC, Canada, June 22-27th, 2003: Extended Abstracts, 2003, FLA_0141.
52. **Sobolev N.V, Logvinova A.M, Zedgenizov D.A, Seryotkin Y.V., Yefimova E.S., Floss C., Taylor L.A.** 2004. Mineral inclusions in microdiamonds and macrodiamonds from kimberlites of Yakutia: a comparative study // *Lithos*, 77, 225–242.
53. **Solovieva L.V., Egorov K.N., Markova M.E., Kharkiv A.D., Popolitov K.E., Barankevich V.G.** 1997. Mantle metasomatism and melting in deep-seated xenoliths from the Udachnaya pipe, their possible relationship with diamond and kimberlite formation. *Russian Geology and Geophysics*. 38/1, 172- 193.
54. **Spetsius Z.V., Serenko V.P.** 1990. Composition of the continental mantle and low crustbeneath the Siberian platform / Moscow, Nauka.271 p.
55. **Stagno V., Frost D.J.** Carbon speciation in the asthenosphere: experimental measurements of the redox conditions at which carbonate - bearing melts coexist with graphite or diamond in peridotite assemblages // *Earth Planet. Sci. Lett.* 2010, v.300, pp.72–84.
56. **Stagno V., Ojwang D.O., McCammon C.A. Frost D.J.** The oxidation state of the mantle and the extraction of carbon from Earth’s interior // *Nature*. 2013 v. 493 pp.84-88.
57. **Sweeney R.J., Thompson A. B., Ulmer P.** 1993. Melting experiments were performed on a natural mica-amphibole-rutile-ilmenite-clinopyroxene (MARID) sample from the Kaapvaal mantle lithosphere (AJE137) at 20 to 35 kbar and 800 to 1450°C // *Contributions to Mineralogy and Petrology* (1993).
58. **Taylor L.A., Anand M.** 2004. Diamonds: time capsules from the Siberian Mantle // *Chemie der Erde*. 64, 1-74.
59. **Taylor W.R., Kammerman M., Hamilton R.** New thermometer and oxygen fugacity sensor calibrations for ilmenite and chromian spinel-bearing peridotitic assemblages // 7th International Kimberlite Conference.Extended abstracts. Cape town. 1998. Pp.891-901.

60. **Tappe S., Foley S.F., Jenner G.A., Heaman L.M., Kjarsgaard B. A., Romer R. L., Stracke A., Joyce N., Hoefs J.** 2006. Genesis of ultramafic lamprophyres and carbonatites at Aillik Bay, Labrador: a consequence of incipient lithospheric thinning beneath the North Atlantic craton // *Journal of Petrology* 47, 1261–1315.
61. **Travin A.V., Aschepkov I.V., Udin D., Prostyakov K.** Laser and stepwise-heating $^{40}\text{Ar}/^{39}\text{Ar}$ dating of kimberlite-like rocks from Sayan Foothills and peripheral part of the Siberian platform // *Geochimica et Cosmochimica Acta. Special Supplement*. 2002.v 66. - № 15A. - . A783.